Universidad Autónoma de Madrid

Programa de Doctorado en Biociencias Moleculares

IMPACT OF COX7A2L IN THE BIOGENESIS OF HUMAN MITOCHONDRIAL RESPIRATORY CHAIN SUPERCOMPLEXES

Tesis Doctoral

Teresa Lobo Jarne

Madrid 2018

DEPARTAMENTO DE BIOQUÍMICA

FACULTAD DE MEDICINA

UNIVERSIDAD AUTÓNOMA DE MADRID

IMPACT OF COX7A2L IN THE BIOGENESIS OF HUMAN MITOCHONDRIAL RESPIRATORY CHAIN SUPERCOMPLEXES

Memoria presentada por la Licenciada en Biotecnología

Teresa Lobo Jarne

para optar al grado de Doctor por la Universidad Autónoma de Madrid

Directora de Tesis:

Dra. Cristina Ugalde Bilbao

Instituto de Investigación Hospital 12 de Octubre (i+12)

DEPARTAMENTO DE BIOQUÍMICA

FACULTAD DE MEDICINA

UNIVERSIDAD AUTÓNOMA DE MADRID

Doña **Cristina Ugalde Bilbao**, Doctora en Ciencias, como Directora de Tesis,

CERTIFICA:

Que Doña Teresa Lobo Jarne, con DNI 72996109-C, licenciada en Biotecnología, ha realizado bajo mi dirección en el Instituto de Investigación Hospital 12 de Octubre (i+12) de Madrid, el trabajo titulado:

IMPACT OF COX7A2L IN THE BIOGENESIS OF HUMAN MITOCHONDRIAL RESPIRATORY CHAIN SUPERCOMPLEXES

Una vez supervisado el trabajo, considero que cumple con éxito todos los requisitos necesarios en cuanto a originalidad y calidad para ser presentado como Tesis Doctoral con el objeto de optar al título de Doctor por la Universidad Autónoma de Madrid.

Madrid, a 25 de Enero del 2018

Dra. Cristina Ugalde Bilbao
Directora de Tesis
Laboratorio de Enfermedades Raras: Mitocondriales y Neuromusculares
Instituto de Investigación Hospital 12 de Octubre (i+12)
Avenida de Córdoba s/n
28041 Madrid

Esta tesis doctoral ha sido realizada gracias a la concesión de una ayuda del Instituto de Investigación Hospital 12 de Octubre (i+12) para la incorporación de becarios a proyectos de investigación; de un Contrato de Formación en Investigación del Fondo de Investigaciones Sanitarias / Instituto de Salud Carlos III / fondos FEDER asignado a Doña Teresa Lobo Jarne con cargo al proyecto de investigación FIS 14-00209; así como por el proyecto del *National Institute of General Medical Sciences* (NIGMS-NIH, número 1R01GM105781-01) concedidos a la Dra. Cristina Ugalde Bilbao.

A todos los que eché de menos, en especial a mis padres y a mi hermana

AGRADECIMIENTOS

Este trabajo no hubiera sido posible sin el interés y ánimo de muchas personas. A todos, gracias de corazón.

Gracias a mi directora de tesis, la Dra. Cristina Ugalde Bilbao, por haberme dado la oportunidad de realizar mi doctorado en su grupo de investigación. Y por la formación científica que me ha brindado.

Gracias al director del grupo de *Enfermedades Raras, Mitocondriales y Neuromusculares* el Dr. Miguel Ángel Casanueva y al director de la institución el Dr. Joaquín Arenas Barbero, por su cercanía y apoyo y por permitirme formar parte del Instituto de Investigación del Hospital 12 de Octubre de Madrid.

Gracias a la Dra. María Morán y al Dr. Francisco Martínez, por su disposición a contestarme a las tantas preguntas experimentales y teóricas durante todo este tiempo y siempre con una sonrisa.

Gracias a la Dra. Esther Gallardo, por su eficaz ayuda en la tutorización de este trabajo y por los buenos consejos que me ha dado.

Gracias a Alberto Blázquez, por su ayuda con los análisis genéticos y a Inés García, por su ayuda proteómica con buen sentido del humor.

Gracias a Pilar, Vicky, Sara y Charo, por sus buenos consejos tanto profesionales como personales. Sin ellas el laboratorio no sería lo mismo.

Gracias a Pablo, Adrián y Guille, por las charlas de pasillo y de cultivos celulares.

Gracias a Miguel, Dani, Vero, Patri, Javi y Gabriel, por sacarme una sonrisa cuando la he necesitado. Por los geniales momentos en el laboratorio, en la cafetería y fuera del trabajo.

Gracias a Xandra, Gaba y Elena, por acogerme, escucharme, apoyarme y consolarme. Ellas han estado en los grandes momentos, en tantas risas, anécdotas y confesiones. Porque las fiestitas, las cañas, las películas y las charlas de ciencia y no-ciencia en el laboratorio hicieron el día a día mucho más fácil.

Gracias a Laura, por todo lo que ha hecho por mí. Por las horas midiendo cadena respiratoria mitocondrial que se recompensaban con cines domingueros. Porque siempre ha estado para mí en cualquier circunstancia, amiga y consejera, dentro y fuera del laboratorio. Porque ella y David me han adoptado a la madrileña, y han hecho que mi experiencia en la gran ciudad haya sido genial. Gracias de todo corazón, porque me llevo dos grandes amigos.

Gracias a Ana, por su sincera amistad. Por su sentido del humor, su capacidad de trabajo y su ayuda cuando la he necesitado, tanto experimental como personal.

Gracias a Alberto y Rafa, esos monstruos monstruosos. Gracias por estar ahí siempre, serenos y guardianes. Por su enorme ayuda experimental, por aguantar mi organización de laboratorio y por sus palabras de consuelo, alegría y templanza siempre que las he necesitado. En especial a Rafa por las discusiones científicas, las hipótesis, las estrategias experimentales y toda su valiosa ayuda en el desarrollo de este trabajo.

Gracias a David, por enseñarme durante mi primer año de tesis, por darme el testigo de la *blue-native*, por escuchar y entender y por seguir compartiendo buenos momentos. Y a Javi, también por escucharme.

Gracias a la Dra. Erika Fernández-Vizarra, por su confianza en mí cuando era una estudiante de máster. Porque aquel año fue estupendo y aprendí mucho.

Gracias al Dr. Antoni Barrientos y a todo su equipo del laboratorio de *Mitochondrial Biogenesis in Health, Disease and Aging* de la Universidad de Miami, por haberme acogido tan bien en su grupo y haberme enseñado nuevas técnicas experimentales y una forma diferente de trabajar en un laboratorio de investigación.

Gracias a Marta, el destino nos volvió a unir. Gracias por todas las tardes de cañas sin alcohol con limón, de paseos, de Malasaña, de compras y de teatros. Por haber sido mi confidente, porque "en la calle pasábamos las horas… has estado ahí por encima de todas las cosas". Y a Alfonso, por su gran interés por mi trabajo.

Gracias a Carolina y Ana, por ser las mejores compañeras de piso que una puede tener. Gracias por ayudarme siempre que lo he necesitado.

Gracias a Marina, por llevarme una vez a la semana a un mundo melódico lleno de notas, acordes y arpegios, donde las pipetas se sustituían por guitarras.

Gracias a mis círculas, a Yoli, Ana M, Diana, Ana G, Mariaje y Belén, por apoyarme en cualquier circunstancia. Juntas desde los inicios biotec y desde cualquier punto del mundo. Gracias por los consejos, confidencias y desahogos circulares; los vídeos, correos y skype circulares; las fiestas, celebraciones y viajes circulares; las alegrías, risas y lloros circulares. Y gracias a los círculos Jordi N, Miguel, Jordi P y Tomás por animarme siempre y porque sin ellos el círculo no sería del todo circular.

Gracias a Guillermo y Diana, por haber estado conmigo desde el principio. Porque para mí, Zaragoza son ellos. Y pase el tiempo que pase, están para escucharme.

Gracias a toda mi familia, por su apoyo, ánimo y empuje en el desarrollo de este doctorado. En especial a mi tío Adolfo y a mi tito Antonio, por siempre preguntarme por mi tesis y darme buenos consejos. Y a mi yayo, por ser tan curioso y siempre estar dispuesto a aprender cosas de "aquello llamado mitocondria". Estés donde estés, gracias yayo.

Gracias a Romà, por ser paciente y comprensivo. Porque me conoce y me entiende, porque ha vivido esta tesis como si fuera suya. Gracias por animarme siempre, ser mi más sincero confidente y por haber hecho mucho más fácil esta aventura. Y gracias a su familia también, por su interés y ánimo en todo momento.

Gracias a mi hermana Laura, por su gran ayuda en la maquetación y en la revisión gramatical de este trabajo. Por ser mi cómplice en cada nueva experiencia y por escucharme siempre. Gracias por darle el toque divertido, musical y artístico a mi vida.

Gracias a mis padres Manuel y Maruxa, porque a ellos les debo todo. Gracias por vuestro apoyo, exigencia, dedicación y cariño en cada nueva etapa. Por todos los buenos consejos que me dais, por enseñarme tanto y siempre estar para mí.

SUMMARY / RESUMEN

Mitochondrial respiratory chain (MRC) complexes I, III and IV are associated in large supramolecular structures termed supercomplexes (SCs) and respirasomes, whose biogenesis and functional and pathophysiological relevance remain unclear. Such superstructures originate interdependences between the individual OXPHOS complexes, with major biomedical implications for the diagnosis of mitochondrial disorders because combined deficiencies of these complexes can be attributed to a genetic defect of a single MRC complex. Furthermore, the functional implication of the mitochondrial protein COX7A2L / COX7RP / SCAFI in the biogenesis of SCs is a subject of intense and controversial debate. To elucidate the role of COX7A2L in the structural organization of human MRC, blue native electrophoresis, proteomic analyses and *COX7A2L* downregulation assays were performed in control and mutant transmitochondrial cybrids lacking one of each MRC complexes. Our results showed that human COX7A2L binds primarily to the SC-unbound complex III dimer ($CIII_2$) and to a minor extent to free complex IV, to specifically promote the stabilization of the SC III_2+IV without affecting the respirasomes formation. Further analyses in TALEN-mediated *COX7A2L* knockout (*COX7A2L*-KO) HEK293T cells demonstrated that the lack of COX7A2L prevents SC III_2+IV formation without affecting *de novo* complex IV biogenesis, enhances the biogenetic rates of $CIII_2$, and delays the formation of the complex III-containing respirasomes that, nonetheless, accumulate to control steady-state levels. Functional substrate competition assays revealed that, upon the induction of complex I deficiency, *COX7A2L*-KO cells significantly favour electron flux through complex II. Altogether, our data suggest that COX7A2L establishes a regulatory checkpoint for the biogenesis of $CIII_2$ and complex III-containing SCs that limits succinate oxidation when complex I activity is compromised, and that independent regulatory mechanisms co-exist for the biogenesis of SC III_2+IV and the respirasomes.

The primary role of COX7A2L in the biogenesis of complex III-related MRC structures was confirmed through comparative analyses of the assembly and composition of human SCs between control cells and two mutant cybrids lacking complex IV due to pathogenic nonsense mutations in the COX1 and COX2 subunits, respectively. In the absence of complex IV, three different bands corresponding to fully-assembled SC I+III_2 were identified, which also contained COX7A2L. Surprisingly, two of these SC I+III_2 bands showed the presence of specific complex IV subunits that regularly take part in late steps of complex IV assembly. Reversible inhibition of mitochondrial translation demonstrated that the biogenesis of COX7A2L-containing SC I+III_2 is completed prior to the stepwise association of complex IV subunits. Radioactive pulse-chase analyses additionally showed that the insertion of COX subunits is essential to stabilize the COX7A2L-containing SC I+III_2. Our results thus reveal the existence of alternative COX assembly lines for the synthesis of free- versus SC-associated complex IV.

Los complejos I, III y IV (CI, CIII, CIV) de la cadena respiratoria mitocondrial (CRM) están asociados en estructuras supramoleculares denominadas supercomplejos (SCs) y respirasomas, cuya biogénesis y relevancia tanto funcional como fisiopatológica todavía no están claras. Estas superestructuras originan interdependencias entre los complejos individuales del sistema OXPHOS, lo que conlleva importantes implicaciones para el diagnóstico de las patologías mitocondriales. Ello se debe a que algunos déficits enzimáticos combinados de los complejos de la CRM se pueden atribuir a mutaciones en genes estructurales de un solo complejo. Además, existe un debate intenso y controvertido sobre el papel de la proteína mitocondrial COX7A2L / COX7RP / SCAFI en la función y biogénesis de los SCs. Para dilucidar el papel de COX7A2L en la organización estructural de la CRM en humanos, se realizaron análisis bioquímicos y proteómicos sobre cíbridos transmitocondriales control y mutantes carentes de uno de los complejos de la CRM, así como ensayos de silenciamiento del ARN mensajero de *COX7A2L*. Los resultados demostraron que COX7A2L se une principalmente al dímero del complejo III ($CIII_2$) y en menor medida al CIV, para promover específicamente la estabilización del SC III_2+IV sin afectar a la formación del respirasoma. El estudio se extendió a células HEK293T carentes de COX7A2L (*COX7A2L*-KO), creadas en el laboratorio mediante la tecnología TALEN. La ausencia de COX7A2L impide la formación del SC III_2+IV sin afectar a la biogénesis *de novo* del CIV; además, promueve un aumento tanto en la cinética de ensamblaje como en los niveles estacionarios del $CIII_2$, al tiempo que retrasa la formación de los SCs que contienen al CIII (que no obstante, alcanzan los niveles estacionarios del control). Ensayos funcionales de competición de sustratos revelaron que en las células *COX7A2L*-KO aumenta significativamente el flujo de electrones desde el CII al $CIII_2$ al inducir un déficit parcial en la actividad del CI. En conclusión, COX7A2L establecería un punto de control de la biogénesis del $CIII_2$ y de los SCs que contienen al CIII, lo cual limitaría la oxidación del succinato cuando la actividad enzimática del CI está disminuida. Asimismo, estos datos muestran la coexistencia de mecanismos reguladores independientes en la biogénesis del SC III_2+IV y de los respirasomas.

La función principal de COX7A2L sobre la biogénesis del CIII se confirmó mediante análisis del ensamblaje y composición de los SCs en cíbridos humanos control y mutantes sin CIV debido a mutaciones patogénicas en las subunidades COX1 y COX2. En ausencia del CIV, se identificaron tres bandas correspondientes a diferentes especies del SC I+III_2 que también contienen a COX7A2L; de ellas, dos bandas mostraron la presencia de subunidades COX específicas del ensamblaje tardío del CIV. Este trabajo demuestra que la formación del SC I+III_2 ocurre antes de la asociación gradual de las subunidades del CIV, las cuales son esenciales para estabilizar dicha estructura y revela la existencia de líneas de ensamblaje alternativas para la síntesis del CIV en su forma individual o asociada a los SCs.

INDEX

ABBREVIATIONS

1D-BN-PAGE First non-denaturing dimension of the blue native gel electrophoresis

2D-BN/SDS-PAGE Second denaturing dimension of the blue native gel electrophoresis

ADNc Complementary DNA

ADNg Genomic DNA

ADNn Nuclear DNA

ATP Adenosine 5'-triphosphate

BN-PAGE Blue native polyacrylamide gel electrophoresis

BSA Bovine serum albumin

CI Complex I or NADH dehydrogenase:ubiquinone oxidoreductase

CII Complex II or succinate:ubiquinone oxidoreductase

CIII Complex III or ubiquinol:cytochrome *c* oxidoreductase or cytochrome *bc1* complex

$CIII_2$ Complex III dimer

CIV Complex IV or cytochrome *c* oxidase

CIV_2 Complex IV dimer

CV Complex V or ATP synthase

CID Collision induced dissociation

CMV Cytomegalovirus

CO-IP Co-immunoprecipitation

CoQ Coenzyme Q or ubiquinone

COX Complex IV or Cytochrome c oxidase

CS Citrate synthase

CYBRID Cytoplasmic hybrid

CYTB Cytochrome *b*

Cyt *c* Cytochrome *c*

DAB 3.3'-diamidobenzidine tetrahydrochloride

DCPIP 2,6-dichlorophenol indophenol

DIG Digitonin

DMEM Dulbecco's Modified Eagle Medium

DMSO Dimethyl sulfoxide

DQ Decyl ubiquinone

DQH_2 Decyl ubiquinol

DTNB 5,5'-dithiobis 2-nitrobenzoic acid

EDTA Ethylene diamine tetra acetic acid

FAD^+ Flavin adenine dinucleotide, oxidized

$FADH_2$ Flavin adenine dinucleotide, reduced

FBS Fetal bovine serum

FDR False discovery rate

Fe-S Iron-sulphur cluster

GFP Green fluorescent protein

HA Human influenza hemagglutinin

HRP Horseradish Peroxidase

IGA *In-Gel* Activity

IMM Inner mitochondrial membrane

IMS Intermembrane space

IP Immunoprecipitate

KCN Potassium cyanide

kDa KiloDalton

LC-MS Liquid Chromatography – Mass Spectrometry

LM Lauryl maltoside

MS Mass Spectrometry

MITRAC Mitochondrial translation regulation assembly intermediate of cytochrome *c* oxidase

MRC Mitochondrial respiratory chain

mtDNA Mitochondrial DNA

Myc Gene *c-myc* -derived Tag

NAD^+ Nicotinamide adenine dinucleotide, oxidized

NADH Nicotinamide adenine dinucleotide, reduced

NTB Nitro tetrazolium Blue

OMM Outer mitochondrial membrane

OXPHOS Oxidative phosphorylation system

PBS Phosphate buffered saline

PCR Polymerase chain reaction

Q Ubiquinone

QH_2 Ubiquinol

RISP Rieske iron-sulphur protein

rRNA Ribosomic RNA

ROS Reactive oxygen species

RVD Repeat variable di-residues

SC Supercomplex

SD Standard deviation

SDS Sodium dodecyl sulphate

SDS-PAGE Sodium dodecyl sulphate-polyacrylamide gel electrophoresis

siCOX7A2L Silencing of the *COX7A2L* mRNA

siNDUFB8 Silencing of the *NDUFB8* mRNA

SN Supernatant

SQR Succinate: ubiquinone oxidoreductase

TALEN Transcriptor activator-like effector nuclease

TIM Translocase of the inner membrane

tRNA Transfer RNA

TXRD Texas Red conjugated

VDAC Voltage-Dependent Anion Channel

INTRODUCTION

1. Mitochondria: overall features of a unique organelle

Mitochondria are cytoplasmic organelles of eukaryotic cells that take part in a variety of cellular metabolic functions. These capsule-shaped organelles are divided by an outer membrane (OMM) and an inner membrane (IMM), which are composed of phospholipid bilayers and proteins. Together, they create two separate compartments: the internal matrix and the intermembrane space (IMS). The outer membrane encloses the entire organelle and contains multiple copies of integral membrane proteins that allow ions and small molecules (of 5000 Da or less) to freely diffuse between cytosol and mitochondria (Alberts et al., 2007). The inner membrane contains numerous carriers and translocases that mediate transport and membrane insertion of precursor proteins into mitochondria (Neupert, 2015).

The main mitochondrial role is the production of adenosine 5'-triphosphate (ATP), the key energy source of the cell, through the aerobic substrate oxidation carried out by the oxidative phosphorylation (OXPHOS) system (Reid et al., 1966). The OXPHOS system is embedded in the lipid bilayer of the IMM and it is composed of five multiprotein enzyme complexes and two mobile electron carriers (Figure 1). The first four enzyme complexes (CI-CIV) comprise the mitochondrial respiratory chain (MRC), which facilitates electron transfer from reducing equivalents to molecular oxygen. During oxidative phosphorylation, organic nutrients are catabolized into small electron donor molecules, $NADH_2$ and $FADH_2$, which transfer the electrons to CI and CII, respectively. CoQ uptakes the electrons from both sources, transferring them to dimeric CIII ($CIII_2$), then to cyt *c* and finally to CIV, that yields the electrons to molecular oxygen. This electron flux is coupled to a proton pump from the matrix to the intermembrane space through complexes I, III and IV, generating an electrochemical gradient across the IMM that provides the necessary free energy for the ATP synthase (complex V, CV) to synthesize ATP.

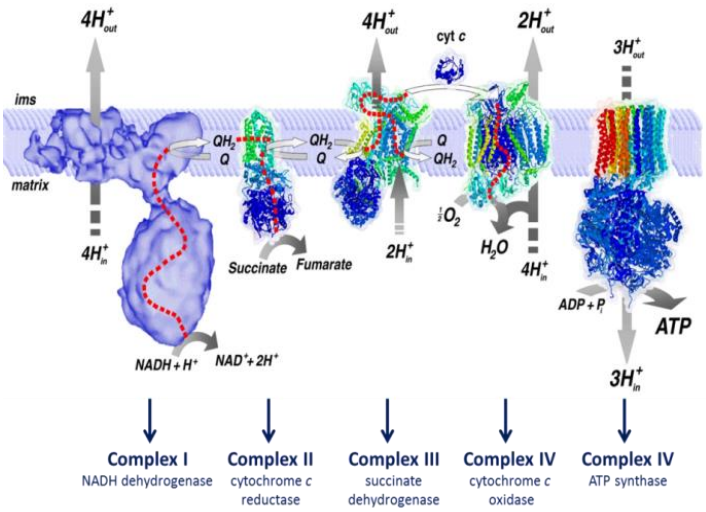

Figure 1.The oxidative phosphorylation (OXPHOS) system. All complexes are represented as monomers. cyt *c*: cytochrome *c*; Q: ubiquinone; QH_2: ubiquinol; ims: intermembrane space. Adapted from (Nijtmans et al., 2004).

Mitochondria contain a separate autonomously replicating DNA genome, the mitochondrial DNA (mtDNA), a closed-circular double-stranded DNA molecule formed by a heavy (H) strand and a light (L) strand, which contains 16.569-base pairs (Anderson et al., 1981; Andrews et al., 1999) and which is replicated within the organelle matrix (Clayton, 1991). Mammalian mtDNA encodes 37 genes: 24 components of the mitochondrial translational machinery (22 tRNAs and 2 rRNAs, 12S and 16S), and 13 structural proteins of four out of the five mitochondrial OXPHOS complexes. Thereby, due to its limited coding capacity, the mitochondrial genome requires to coordinate with the nuclear genome, which encodes the remainder OXPHOS subunits as well as the factors involved in the regulation of mtDNA gene expression, replication and maintenance (Garesse and Vallejo, 2001). Despite the small size of the mitochondrial genome, mtDNA mutations are an important cause of uniparental inherited metabolic disease. Mitochondrial genetics have an important feature due to the polyploid nature of its genome (up to several mtDNA copies per cell), homoplasmy and heteroplasmy. Homoplasmy is the existence of identical mtDNA copies within a cell and heteroplasmy is the mixture of two or more mitochondrial genotypes. The value of these terms gains relevance when considering pathogenic mtDNA mutations, where some affect all copies of the mitochondrial genome (homoplasmic mutations) whereas others are only present in some copies of the mitochondrial genome (heteroplasmic mutations) (Taylor and Turnbull, 2005). Experimental evidence in the cellular distribution of both mutated and wild-type mtDNA in muscle determined a ”threshold level” of any mtDNA mutation that is required to cause a biochemical defect, and hence the clinical expression of the disease (Sciacco et al., 1994).

2. Mitochondrial respiratory chain

In the late 50s, the redox enzymes and prosthetic groups responsible for the classic mitochondrial electron transfer chain were defined (Chance and Williams, 1955), followed by their reconstitution in the early 60s (Hatefi et al., 1962). The overall MRC activity was postulated as a sequential transfer of electrons between four major multi-enzymatic complexes that carry out cellular respiration (Figure 1): NADH dehydrogenase:ubiquinone oxidoreductase (complex I, CI), succinate:ubiquinone oxidoreductase (complex II, CII), ubiquinol:cytochrome *c* oxidoreductase or cytochrome *bc1* complex (complex III, CIII), and cytochrome *c* oxidase (complex IV, CIV). In addition, the electron transfer is ensured by the diffusion of two mobile electron carriers: the lipophilic ubiquinone, also designated as coenzyme Q (CoQ, Q), embedded in the membrane lipid bilayer, and the hydrophilic heme

protein cytochrome *c* (cyt *c*) located on the external surface of the IMM (Kröger and Klingenberg, 1973; Margoliash et al., 1973).

2.1. COMPLEX I

Complex I (CI) or NADH dehydrogenase:ubiquinone oxidoreductase is the largest enzyme of the OXPHOS system. It catalyses the transfer of two electrons from NADH to ubiquinone coupled to the translocation of four protons across the membrane, and it is an important generation site of mitochondrial reactive oxygen species (Barja, 1999; Cadenas et al., 1977; Genova et al., 2001; Herrero and Barja, 2000; Kussmaul and Hirst, 2006) (further described in section 5.3). Mammalian CI has 45 subunits encoded by 44 genes, among which 14 are the core subunits (7 of them encoded by mtDNA) that are highly conserved from bacteria to human, and the remainder 31 are supernumerary subunits (Baradaran et al., 2013; Carroll et al., 2003; Efremov et al., 2010; Fiedorczuk et al., 2016; Letts, Degliesposti, et al., 2016; Stroud et al., 2016; Vinothkumar et al., 2014; Zhu et al., 2016; Zickermann et al., 2015). All the subunits are resolved within the L-shaped arrangement consisting of two arms: a hydrophilic peripheral arm projecting into the matrix, and a hydrophobic membrane arm, embedded in the IMM (Berrisford and Sazanov, 2009; Efremov and Sazanov, 2011; Hunte et al., 2010; Sazanov and Hinchliffe, 2006). The complex can be divided into three structurally and functionally defined modules (Guerrero-Castillo et al., 2017; Hunte et al., 2010; Zhu et al., 2015) (Figure 2): the matrix arm N-module, which preserves the entire path for NADH oxidation and it is composed by three core subunits (NDUFS1, NDUFV1 and NDUFV2); the quinone-binding Q module, which accommodates the Fe-S clusters that transfer electrons to ubiquinone and it is composed by four core subunits (NDUFS2, NDUFS3, NDUFS7 and NDUFS8); and the P-module in the membrane arm that is subdivided in two parts: proximal (P_P) and distal (P_D), which is responsible for proton pumping and it is composed by seven highly hydrophobic mtDNA-encoded subunits (ND1-6 and ND4L).

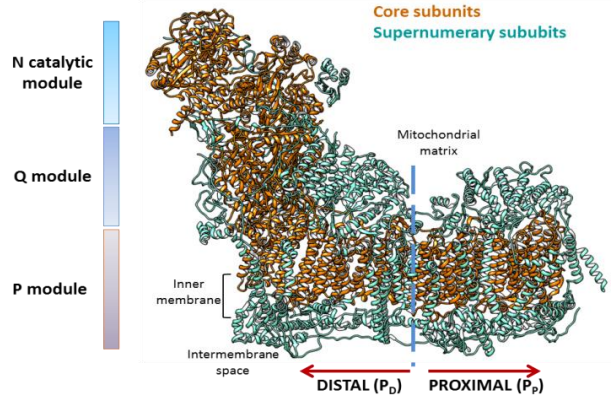

Figure 2. High-resolved structure of human mitochondrial complex I. CI is divided in three functional modules. The P module is subdivided in the distal and proximal membrane arms. In total, 14 core subunits (orange) and 31 supernumerary subunits (cyan) form the entire structure. The figure was created using the 5XTH.pdb structure (Guo et al., 2017).

Due to its size, L-shaped asymmetry, membrane-bound location and multi-component structure, mammalian CI has proved difficult to crystallize. However, the past five years have been distinguished by fascinating breakthroughs in the understanding of the complete CI structure (Figure 2). The 3.4, 3.7, and 3.7 Å of the matrix arm, membrane arm, and overall CI maps (Fiedorczuk et al., 2016; Zhu et al., 2016) respectively, allowed building up all the 45 subunits into the human CI structure (Guo et al., 2017). The structural observations of the entire human CI was found consistent with the previous conclusions from the cryoEM maps of the bovine (Zhu et al., 2016) and ovine (Fiedorczuk et al., 2016) highly-resolved CI. The stoichiometry of proton translocation, considered historically to be four in bacteria and yeast (Baradaran et al., 2013; Galkin et al., 2006) has been recently corroborated in mammals (Jones et al., 2017). Moreover, depending on its catalytic status (e.g. such as during hypoxia) mammalian CI exists in different "active" or "de-active" states (Babot et al., 2014; Dröse et al., 2016; Galkin et al., 2009). Wide studies have provided insights into the biosynthesis of mammalian CI as a stepwise assembly process (Antonicka et al., 2003; Guerrero-Castillo et al., 2017; Lazarou et al., 2007; Perales-Clemente et al., 2010; Ugalde et al., 2004; Vartak et al., 2015; Vogel et al., 2007) addressed by sub-modules that could be either part of membrane-associated or matrix-associated subcomplexes (Dieteren et al., 2008) (Figure 3). Importantly, CI enzyme deficiency is the most frequent mitochondrial disorder and presents with a diverse range of clinical manifestations associated with mutations in both mitochondrial and nuclear-encoded subunits or assembly factors (Nouws et al., 2012; Valsecchi et al., 2009).

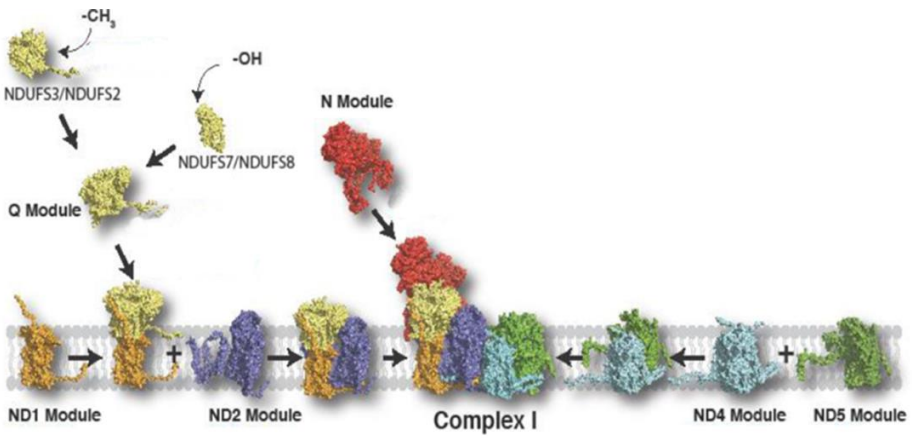

Figure 3. The assembly pathway of mitochondrial complex I. CI subunits assemble into discrete modules before joining to form the functional complex in associations with complexes III and IV. The Q module integrates with the ND1 module and further associates with the ND2 module. The ND4 and ND5 modules associate together followed by integration with the Q/ND1/ND2 modules to form a late stage intermediate comprised of the Q-module and the completed membrane arm of CI. The N-module then associates with this late stage intermediate to form the fully assembled complex. Adapted from (Formosa et al., 2017).

2.2. COMPLEX II

Complex II or succinate:ubiquinone oxidoreductase, the smallest enzyme of the MRC, couples the oxidation of succinate to fumarate in the mitochondrial matrix, with the reduction of ubiquinone (Q) in the membrane. Despite its function in the MRC, complex II plays its main functional role as a succinate dehydrogenase in the Krebs cycle (Lenaz and Genova, 2010). Eukaryotic CII is composed of four subunits (SDHA, SDHB, SDHC and SDHD) encoded by the nuclear genome. The crystal structure of mammalian CII purified from porcine (Sun et al., 2005) and avian (Huang et al., 2006) heart revealed a hydrophilic head (or catalytic domain) that protrudes into the matrix and a hydrophobic tail (or membrane anchor domain) that is embedded within the IMM, with a short segment projecting into the soluble IMS (Sun et al., 2005). The two core subunits, SDHA and SDHB, form the catalytic domain and contain the redox cofactors; SDHA contains the FAD and the binding site for succinate and SDHB contains the three iron-sulphur (Fe/S) centres that mediate electron transfer to ubiquinone. The membrane domain encloses the other two subunits, SDHC and SDHD, which contain the *heme* group, another succinate binding site and the transmembrane helices that hold the complex to the IMM (Sun et al., 2005; Yankovskaya, 2003). Besides the two protons generated from the oxidation of succinate, another two protons are required for the full ubiquinone reduction, thereby with no net proton translocation. Four assembly factors (SDHAF-1 to 4) have been reported to play a role in the stepwise assembly of holo-CII; briefly, following the flavination of SDHA through SDHAF2 and other putative factors (Bezawork-Geleta et al., 2016; Hao et al., 2009; Huang et al., 2013; Kounosu, 2014), the chaperone-like assembly factor SDHAF4 binds to SDHA to reduce auto-oxidation (Van Vranken et al., 2014). The insertion of [Fe–S] clusters into SDHB requires the assembly factor SDHAF1 and later SDHAF3 (Bezawork-Geleta et al., 2014; Ghezzi et al., 2009; Maio et al., 2016; Na et al., 2014) to protect the system from oxidative damage. Little is known about the biogenesis of the SDHC and SDHD subunits and the heme group insertion, to form the complete holoenyme (Bezawork-Geleta et al., 2017).

2.3. COMPLEX III

Complex III, cytochrome *bc1* complex or ubiquinol:cytochrome c oxidoreductase catalyzes the transfer of electrons from ubiquinol (reduced coenzyme Q) to cyt *c* and it link this redox reaction to translocation of protons across the membrane. The CIII structures from several species including yeast, chicken and bovine have been crystallized, and solved to atomic resolution (Hunte et al., 2000; Iwata, 1998; Xia D et al., 1994). Recent highly-resolved human CIII has been also first described (Guo et al., 2017). This structure of ~480 kDa is a symmetrical homodimer that contains three core protein subunits with redox prosthetic groups:

cytochrome *b* (MTCYB), which contains a low-potential (b_L) and a high-potential (b_H) heme *b* moieties as prosthetic groups; cytochrome *c*1 (CYC1), containing a c-type heme group; and the Rieske protein (UQCRFS1 or RISP) with a 2Fe-2S cluster. Another eight supernumerary subunits (UQCRC1, UQCRC2, UQCRH, UQCRB, UQCRQ, Subunit 9, UQCR10 and UQCR11) conform the entity (Schägger et al., 1986; Xia et al., 2013), and possibly function in the structural stability and regulation of the coordinated activity of the dimeric enzyme. The so-called Q-cycle theory is the most accepted hypothesis describing the molecular mechanism of electron transfer and proton translocation through CIII (Mitchell, 1975; Zhang et al., 1998).

$CIII_2$ assembly studies in yeast models (Atkinson et al., 2011; Cui et al., 2012; Gruschke et al., 2012; Smith et al., 2012; Wagener et al., 2011; Zara et al., 2004, 2009a), as well as on $CIII_2$-associated human disease models (Fernández-Vizarra and Zeviani, 2015) have provided some insight into the intriguing assembly pathway of the complex (Figure 4), although more research is needed to unravel its biogenesis.

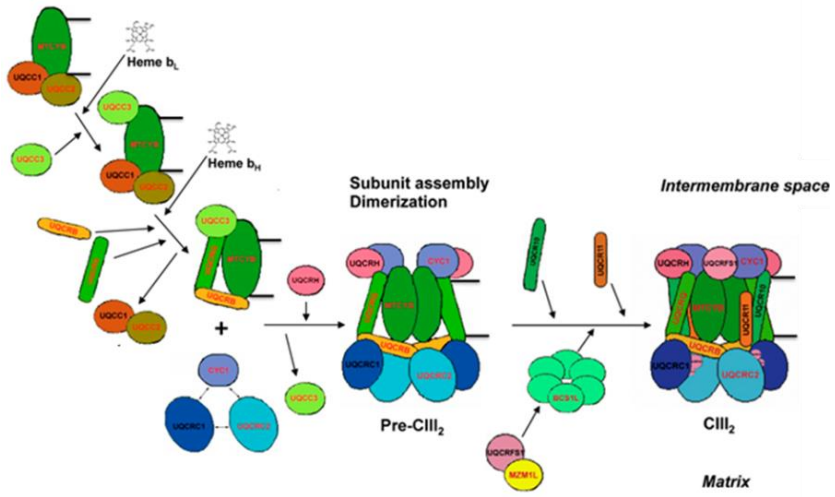

Figure 4. Mitochondrial $CIII_2$ assembly pathway. The biogenesis of $CIII_2$ involves a dynamic multi-step process considered to be similar to that in yeast. After the formation of an early intermediate composed of subunits MTCYB+UQCRB+UQCRQ, an additional sub-assembly containing UQCRC1, UQCRC2, and CYC1 is incorporated, followed by UQCRH and later UQCR10, to form the pre-complex III (pre-$CIII_2$). At this point, the complex is already dimeric (Fernandez-Vizarra et al., 2007). Finally, UQCRFS1 is translocated from the matrix into the inner mitochondrial membrane and it is incorporated into pre-$CIII_2$. In the matrix, UQCRFS1 is bound and stabilized by MZM1L (Sánchez et al., 2013). Finally the last subunit (UQCR11) joins the nascent complex, so that assembly is completed. Adapted from (Bottani et al., 2017; Fernández-Vizarra and Zeviani, 2015).

2.4. COMPLEX IV

Complex IV (CIV), or cytochrome c oxidase (COX), catalyses the complete reduction of molecular oxygen to water and promotes the translocation of two protons across the IMM. Mammalian COX is a multimeric enzyme that comprises 14 subunits, three of which (MT-CO1

or COX1, MT-CO2 or COX2 and MT-CO3 or COX3) are encoded by the mtDNA and form the hydrophobic catalytic core embedded in the IMM. The remainder subunits (COX4, COX5A, COX5B, COX7A, COX6C, COX7C, COX6B, COX6A, COX7B, COX8 and NDUFA4), are encoded in the nuclear DNA and they may be involved in the stabilization of the dimeric state of the oxidase, in the modulation of its catalytic activity and in its protection from oxidative damage (Fontanesi et al., 2008; Timón-Gómez et al., 2017). The COX1 and COX2 subunits harbour the redox centres: COX1 harbours a heme a centre and a binuclear heme a3-copper (CuB) centre, and COX2 contains a dinuclear copper center (CuA). The first crystal structure of the enzyme was resolved from bovine heart (Tsukihara et al., 1995; Yoshikawa et al., 1998), data that represented a real step forward in the understanding of the function and biogenesis of the complex. Recent highly-resolved human CIV has been also described for the first time (Guo et al., 2017).

Over the last 50 years, experimental data in yeast models have shed light into the CIV assembly pathway (McStay et al., 2013), gathering useful information to be compared with the biogenesis of mammalian CIV (Dennerlein and Rehling, 2015; Nijtmans et al., 1998; Soto et al., 2012; Vidoni et al., 2017). However, due to the specific features of mammalian CIV, such as the presence of tissue-specific isoforms or the more than 30 COX assembly factors involved in its biogenesis among others, numerous hypotheses and models have been proposed for the assembly of mammalian CIV (Vidoni et al. 2017; Timón-Gómez et al. 2017) (Figure 5).

Around 75% of the CIV enzyme deficiencies originate from mutations in nuclear-encoded subunits (Blázquez et al., 2016), although mutations on the mtDNA-encoded subunits have also been described leading to a wide range of clinical features (Barrientos et al., 2002).

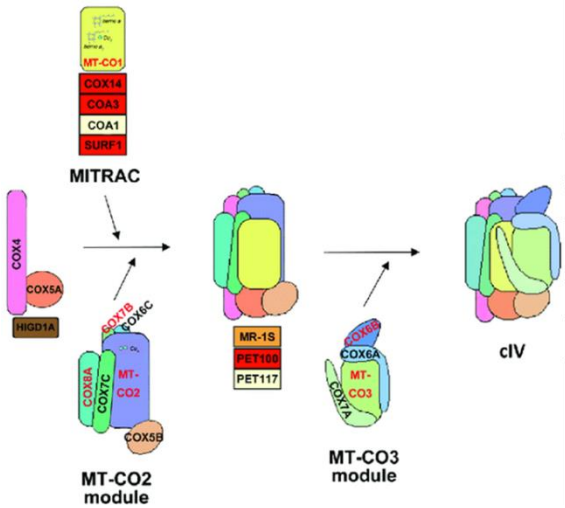

Figure 5. Mitochondrial CIV assembly pathway. Model for the biogenesis of monomeric CIV. The catalytic core subunits (MT-CO1, MT-CO2 and MT-CO3) form subassembly modules with other subunits and assembly factors prior to their incorporation in the main pathway. Proteins whose genes have been found mutated in mitochondrial disorders are displayed in red. Adapted from (Vidoni et al., 2017).

3. Models for the structural organization of the respiratory chain

Despite the well-known functional relevance of the respiratory chain, the structural organization of its components remains unclear.

3.1. SOLID-STATE MODEL

The pioneering spectrophotometric studies of Chance and Williams represented the MRC as a solid state assembly of prosthetic groups that carry out sequential redox reactions in a protein matrix (Chance and Williams, 1955). The evidences in favour of this "rigid" or "solid-state model" were based on the isolation of CI-CIII and CII-CIII active units in a stoichiometric molar ratio of 1:1 during intermediate purification steps of the individual enzymes, that were interpreted as secondary enzymatically active complexes (Fowler and Hatefi, 1961); and on the reconstitution of a "repeating unit of electron transfer" containing all MRC complexes from bovine heart mitochondria (Blair, 1967). This model implied the notion of permanently-bound CoQ to the MRC units. Accordingly, vesicle reconstitution experiments showed stoichiometric associations between CI and $CIII_2$ at high protein concentrations with no exchange between free and bound ubiquinone, i.e., no 'CoQ-pool' behaviour (Ragan and Heron, 1978). Only when sufficient lipid was added the CoQ-pool behaviour was restored, but this was interpreted as the movement of complex-associated CoQ rather than of free CoQ (Heron et al., 1978). Later studies in *Saccharomyces cerevisiae* provided evidence that CoQ and cyt *c* only diffused freely along the membrane upon the addition of chaotropic agents, suggesting that the respiratory chain in yeast also behaves as one functional unit that at least comprises complexes III and IV with bound CoQ and cyt *c* (Boumans et al., 1998).

3.2. LIQUID-STATE MODEL

The general vision gradually evolved into a "random collision", "fluid" or "liquid-state" model, proposed by Hackenbrock and co-workers, that pictured all membrane proteins and redox components that catalyse electron transport and ATP synthesis in constant and independent diffusional motion, where electron transfer takes place through diffusion-based collisions among the redox partners (Höchli and Hackenbrock, 1976). Evidence in favour of the "liquid-state model" arose from kinetic analyses proposing not only that electron transfer in the CoQ and cyt *c* regions obeyed a pool behaviour in mammalian mitochondria, but also that it followed saturation kinetics with regards to CoQ and cyt *c* concentrations (Gupte and Hackenbrock, 1988; Kröger and Klingenberg, 1973). Furthermore, enzymatic activities were retained upon isolation of the individual OXPHOS complexes (Hatefi et al., 1962) and the use of fluorescent antibodies against $CIII_2$ and CIV caused independent aggregation of these

complexes, suggesting that they diffuse laterally in the membrane plane independent of one another (Höchli et al., 1985).

3.3. DYNAMIC AGGREGATE OR PLASTICITY MODEL

The two previous models were proposed for the way in which MRC components interact to accomplish a maximal-efficient electron transfer, representing extreme examples where intermediate modes of operation are feasible. Alternative studies by Ferguson-Miller and collaborators that analysed the role of lateral diffusion of cyt *c* in electron transfer within native mitochondrial membranes, gave rise to the "dynamic aggregate" model (Hochman et al., 1982). In this model, a dynamic equilibrium exists between freely diffusing and associated-forms of the MRC components, all active in electron transfer. This new representation of the respiratory chain reconciled the two classical models, as it incorporated transient aggregates as well as free lateral diffusion of redox components to account for the electron transport rates. The reversible formation of specific MRC aggregates additionally offered a mechanism for localized proton flow and the possibility of regulating the direction and efficiency of electron transfer (Ferguson-Miller et al., 1986; Hochman et al., 1985). This idea was disregarded in favour of the "fluid" model until new data from two groups, based on the use of blue native polyacrylamide gel electrophoresis (BN-PAGE) developed by Schägger and collaborators, showed the co-existence of individual MRC complexes together with their inter-associations in supramolecular assemblies that were termed supercomplexes (SCs) (Cruciat et al., 2000; Schägger and Pfeiffer, 2000). Experimental evidences demonstrated that SCs are evolutionarily conserved stable structures in both prokaryotes and eukaryotes, and not random associations of MRC complexes (Chaban et al., 2014; Melo and Teixeira, 2016), and recent high-resolution cryo-electron microscopy (cryo-EM) analyses showed the detailed structural architecture of mammalian respiratory SCs (Guo et al., 2017; Letts, Fiedorczuk, et al., 2016; Sousa et al., 2016; Wu et al., 2016) (Figure 6). The coexistence of individual MRC complexes and SCs thus supports the principles of the "dynamic aggregate" model, which was lately renamed as the "plasticity" model by Enríquez and co-workers (Acín-Pérez et al., 2008; Acin-Perez and Enriquez, 2014). In its current form, this model proposes that the switch between freely moving MRC complexes to fixed SCs would optimize electron flux from different substrates (NADH and $FADH_2$), adapting the efficiency of the respiratory chain to changes in cellular metabolism via partitioned CoQ and cyt *c* pools (Lapuente-Brun et al., 2013).

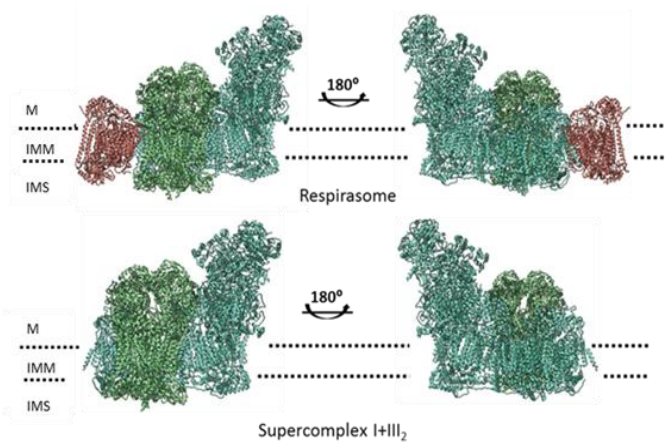

Figure 6. Architectures of human supercomplexes. Side views along the membrane from the loose respirasome or SC I+III_2+IV_1 (top) and SC I+III_2 (bottom), according to the 5XTH structure in the PDB database proposed by (Guo et al., 2017). The structural models of CI, $CIII_2$, and CIV are coloured in salmon, turquoise, and navy blue, respectively. The transmembrane region is indicated by two dashed lines. M, matrix; IMM, inner mitochondrial membrane; IMS, intermembrane space.

4. Structural architectures of the respiratory chain supercomplexes

4.1. TYPES OF RESPIRATORY CHAIN SUPERCOMPLEXES

The notion of "supercomplexes" first appeared upon the observations of preferential associations between bacterial MRC complexes (Berry and Trumpower, 1985; Sone et al., 1987). Respiratory chain SCs of different compositions and stoichiometries were later reported by means of BN-PAGE analyses of mitochondrial fractions solubilized with the mild detergent digitonin. This method allows the retention of labile supramolecular assemblies of membrane protein complexes that would otherwise be dissociated. The solubilization of OXPHOS complexes from yeast and bovine heart mitochondria using varying digitonin-to-protein ratios and subsequent BN-PAGE allowed to separate assorted types of stoichiometric associations of complexes I, III and IV within the molecular mass range from ~750 to ~2100 kDa, in an overall 1:3:6 stoichiometry (Schägger and Pfeiffer, 2001). Additional BN-PAGE, single-particle electron microscopy (EM) and cryo-electron tomography studies, consistently reported specific associations between CI, $CIII_2$ and CIV in a wide range of organisms (Chaban et al., 2014). It is worth mentioning that for a long time, many researchers attributed the appearance of SCs on BN-PAGE gels to protein aggregation as a consequence of detergent solubilization. However, the migrations of these bands in the gels are consistently reproducible, as shown by many different laboratories in the last 17 years, and well-defined structures from these bands extracted from the gels are now available.

The composition and abundance of the respiratory chain SCs may vary among organisms and tissues depending on the metabolic and physiological conditions (Cogliati et al., 2013; Dencher et al., 2007; Greggio et al., 2017; Helbig et al., 2009; Jang et al., 2017; Lapuente-Brun et al., 2013; Ramírez-Aguilar et al., 2011; Rosca et al., 2008; Schägger and Pfeiffer, 2000),

as well as on the lipid content of the IMM (Böttinger et al., 2012; Pfeiffer et al., 2003; Tasseva et al., 2013; Zhang et al., 2002). In most CI-containing eukaryotes, CI primarily interacts with $CIII_2$ and CIV to form the most abundant SC, $I+III_2+IV_1$, to which additional CIV monomers are added to form SCs $I+III_2+IV_{2-4}$. These structures are known as the respirasomes (Schägger and Pfeiffer, 2000), since they contain all the components required to transfer electrons from NADH to molecular oxygen. Additionally, CI associates with $CIII_2$ to form SC $I+III_2$; and $CIII_2$ binds one to two CIV monomers to assemble SCs III_2+IV_{1-2}. In mammals, most CI, ~40-50% of $CIII_2$ and ~20-30% of CIV are localized in the largest SCs $I+III_2$ and $I+III_2+IV_{1-4}$ (Figure 7). $CIII_2$ and CIV may also interact to form SC III_2+IV_1 that scarcely represents 5-10% of the total MRC structures (Moreno-Lastres et al., 2012; Schägger and Pfeiffer, 2001). In higher plants mitochondria, CIV-containing SCs are barely detectable, and SC $I+III_2$ is the predominant macrostructure (Dudkina et al., 2005). In *Saccharomyces*, which lacks CI, two bands of ~750 and ~1000 kDa corresponding to SCs III_2+IV_1 and III_2+IV_2, respectively, are predominant (Cruciat et al., 2000; Schägger and Pfeiffer, 2000). These variations in the relative abundance of SCs may reflect different stoichiometries of CI, $CIII_2$ and CIV among organisms.

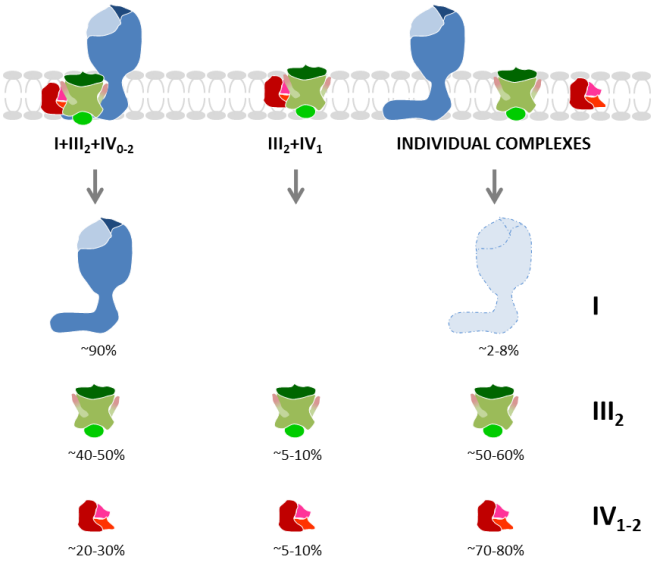

Figure 7. Distribution of human respiratory chain complexes and supercomplexes. Most CI (blue), ~half of $CIII_2$ (green) and ~20-30% of CIV (red) are localized in the respirasome ($I+III_2+IV_{0-1}$). SC III_2+IV_1 represent ~5% of the total amount of MRC structures, as well as CIV dimers (IV_2). Free CI (light blue) requires being associated in SCs to minimize destabilization and ROS generation.

Regarding CII and CV, these enzymes form oligomers that do not interact with complexes I, III and IV under normal physiological conditions (Dudkina et al., 2011; Moreno-Lastres et al., 2012; Muster et al., 2010; Quarato et al., 2011; Schäfer et al., 2006; Schägger and Pfeiffer, 2000, 2001). Based on the differential solubilisation of MRC complexes and SCs on BN-PAGE, a higher organization level of SCs in "respiratory strings" was proposed for mammals and yeast (Wittig, Carrozzo, et al., 2006), where respirasomes would be interconnected by CIV tetramers at regular intervals, thus generating linear assemblies of respiratory SCs. The

observation of CI dimers (CI_2) in *Yarrowia lipolytica* (Nubel et al., 2009) redefined this model as "respiratory patches" generated by the interactions between two CI monomers within adjacent respiratory strings. An alternative model for plants based on single-particle EM, proposed the repetition of $I_2III_2IV_2$ units into a respiratory string mediated by the interaction of two neighbouring CIV through a dimeric interface (Bultema et al., 2009), which differed from the previous model by the lower abundance of CIV copies. In this regard, recent structural analyses in HEK293 cells have shown the arrangement of the MRC complexes in a novel circular structure termed the megacomplex (MC) $I_2+III_2+IV_2$ (Guo et al., 2017), where $CIII_2$ forms a central core surrounded by two copies each of CI and CIV. Guo et al. also hypothesized that in emergency conditions, CII could join the megacomplex molecular machine creating the MC $I_2+II_2+III_2+IV_2$, to provide a most effective pathway to release the high-energy electrons.

The structural and functional characterization of the SCs among different species would benefit very much from *in situ* studies without disrupting the mitochondrial membranes with detergents; for example, using fluorescence life-time imaging, as recently published (Rieger et al., 2017).

4.2. SUPERCOMPLEXES $I+III_2$ AND III_2+IV_{1-2}

The first structure of SC $I+III_2$ from *Arabidopsis thaliana* mitochondria was determined at 18Å resolution (Dudkina et al., 2005), revealing the lateral association of $CIII_2$ to the membrane-embedded distal part of CI. However, the lack of an atomic CI structure failed to decipher the precise subunit interactions within this SC. Recently, the architecture of the mammalian SC $I+III_2$ was resolved at high resolution in human (Guo et al., 2017) (Figure 6), ovine (Letts, Fiedorczuk, et al., 2016) and bovine (Sousa et al., 2016). In these structures, contacts between CI and $CIII_2$ were similar to the ones detected for SC $I+III_2+IV_1$ (described in Section 4.3).

A pseudo-atomic model at 15Å resolution of yeast SC III_2+IV_{1-2} (Heinemeyer et al., 2007) revealed that $CIII_2$ is attached to the convex side of two CIV monomers, leaving the opposite interfaces open for CIV dimerization. Cardiolipin and phosphatidylethanolamine lipids were identified at the $CIII_2$-CIV interface. This structure also revealed cyt *c* bound to $CIII_2$, which moves and rotates within a distance of 40Å (~4 nm) to mediate electron transfer between $CIII_2$ and CIV. Later studies based on 3D-cryo-EM maps specified the distance between the cyt *c* binding sites of $CIII_2$ and CIV as ~6nm, considered to be sufficiently short to enable the channelling of cyt *c* between these complexes (Mileykovskaya et al., 2012), although this was previously refuted (Trouillard et al., 2011). The yeast $CIII_2$ subunits cytochrome *b* (MT-CYB), cytochrome c_1 (CYC1), Qcr6 (Hinge protein or UQCRH), Qcr7 (UQCRQ), Qcr8 (UQCRB) and Qcr9 (UQCR10) were identified at the $CIII_2$-CIV interface, as well as the CIV subunits CoxI (COX1),

CoxII (COX2), CoxIII (COX3), CoxV (COX4), CoxVIIa (COX6C), CoxVII (COX7A) and CoxVIII (COX7C) (Heinemeyer et al., 2007). However, direct evidence supporting precise subunit interactions was missing. Due to its low relative abundance, SCs III_2+IV_{1-2} from higher organisms await structural characterization.

4.3. RESPIRASOME OR SUPERCOMPLEX I+III_2+IV_1

In mammalian mitochondria, I+III_2+IV_1 is the most abundant SC. The first 3D maps of bovine heart SC I+III_2+IV_1 (Althoff et al., 2011; Dudkina et al., 2011; Schäfer et al., 2006, 2007) revealed the lateral binding of $CIII_2$ to the middle part of the CI membrane arm, with CIV positioned in the distal tip of CI while laterally interacting with $CIII_2$, and cardiolipin molecules filling the gaps between the transmembrane domains at the interfaces between the individual complexes (Althoff et al., 2011; Dudkina et al., 2011). The recent characterization of the atomic structure of mammalian CI by cryo-EM (Fiedorczuk et al., 2016; Zhu et al., 2016) represented a major step forward that enabled to obtain high-resolution projection maps of the mammalian respirasomes (Gu et al., 2016; Guo et al., 2017; Letts, Fiedorczuk, et al., 2016; Sousa et al., 2016; Wu et al., 2016) (Figure 6). Yang and collaborators solved the conformation of porcine SC I+III_2+IV_1 (Gu et al., 2016; Wu et al., 2016), where CIV would loosely bind CI and $CIII_2$. In addition, Letts et al. (Letts, Fiedorczuk, et al., 2016) distinguished two architectures for the ovine respirasome, a major “tight” and a minor “loose” conformations, where CIV would contact both CI and $CIII_2$ within the tight form, but only CI within the loose form. Sousa et al. also resolved two classes of SC I+III_2+IV_1 in bovine (Sousa et al., 2016). The tight form of the ovine respirasome was essentially identical to the bovine respirasome class 1. However, the bovine respirasome class 2 differed in the conformational flexibility of $CIII_2$, as this rotates by 25º relative to CI while CIV remains unchanged. The bovine respirasome additionally showed clear density in one of the two membrane extrinsic iron-sulphur domains of $CIII_2$, suggesting that only one CIII monomer would be active (Sousa et al., 2016). The heterogeneity among these structures deserves further consideration (Milenkovic et al., 2017), as it could reflect the existence of independent structural entities resulting from the dynamic association and dissociation of the MRC complexes in response to, eg., tissue-specific phospholipid environments or ROS levels.

The respirasome-bound CI is more compact than free CI due to its associations with $CIII_2$ and CIV (Fiedorczuk et al., 2016; Zhu et al., 2016). Although several interaction points exist between CI, $CIII_2$ and CIV, the most extensive and stable interactions take place between CI supernumerary subunits (absent in bacteria) and $CIII_2$ at two major points: CI subunits NDUFA11 (B14.7 in bovine) and NDUFB4 (B15) directly interact with $CIII_2$ subunit UQCRQ at the

matrix and inner membrane interface, and CI subunits NDUFB4 and NDUFB9 (B22) bind $CIII_2$ subunits UQCRC1 and UQCRFS1 in the matrix (Letts, Fiedorczuk, et al., 2016; Wu et al., 2016). Another important interaction occurs between CI subunit NDUFB7 (B18) and subunit UQCRH on $CIII_2$. Both subunits contain disulphide bonds, suggesting that redox regulation might modulate the interactions between MRC complexes (Letts, Fiedorczuk, et al., 2016). Since the long helix of NDUFB7 is poised at the interface of the three complexes, it may also interact with CIV through the COX7A and COX8B subunits at the intermembrane space and inner membrane interface (Letts, Fiedorczuk, et al., 2016; Wu et al., 2016). CIV is less tightly bound to the respirasomes and major contacts differ among structures, reflecting its varying location. There is a close association of CIV subunit COX7C and ND5 on CI, as well as an interaction of COX7A on CIV with $CIII_2$ subunits UQCR11, UQCRC1 and UQCRB at the matrix and inner membrane interface (Letts, Fiedorczuk, et al., 2016; Wu et al., 2016). This interaction between $CIII_2$ and IV seems to swing away in the loose respirasome form, where only COX7A would contact CI through subunit ND5 (Letts, Fiedorczuk, et al., 2016).

4.4. Effect of cardiolipin on the stabilization of supercomplexes

Supporting the idea that phospholipids mediate protein–protein interactions in the IMM, cardiolipin molecules were detected within yeast SCs III_2+IV_{1-2} (Mileykovskaya et al., 2012), where they stabilize these structures (Pfeiffer et al., 2003; Zhang et al., 2002). Moreover, studies in lymphocytes from patients with Barth syndrome, a mitochondrial disorder in which cardiolipin levels are drastically reduced due to mutations affecting Tafazzin (an enzyme involved in cardiolipin maturation), revealed the specific destabilization of SC I+III_2+IV_1 (McKenzie et al., 2006). A pluripotent stem cell model system of this disorder later confirmed the role of cardiolipin content for SCs stabilization (Dudek et al., 2013). Consistent with these observations, the atomic structure of the respirasome revealed clear gaps between CI, $CIII_2$ and CIV that were occupied by cardiolipin molecules to further stabilize the respirasome (Althoff et al., 2011; Wu et al., 2016). Although cardiolipin is considered to stabilize SCs, phosphatidylethanolamine, another phospholipid of the inner membrane, seems to exert the opposite effect (Böttinger et al., 2012).

5. Function of respiratory chain supercomplexes

5.1. Catalytic enhancement of the electron flux through substrate channelling

The arrangement into SCs was initially proposed to maximize the efficiency of the electron flux across the MRC (Schägger and Pfeiffer, 2000). Indeed, spectrophotometric assays of the MRC activities of isolated SCs from bovine heart mitochondria showed that CI in SC I+III_2 displays

about half the activity of that in SC I+III_2+IV_1, suggesting that the full respirasome was the most active unit (Schäfer et al., 2006). Substrate channelling was proposed as a possible mechanism to explain the increased rates of electron transfer within SCs based on flux control analyses of the MRC complexes in bovine heart mitochondria (Blanchi et al., 2004). The authors suggested that CI and $CIII_2$ behave as a single enzymatic unit, where electron transfer through CoQ is accomplished by channelling between the two redox enzymes without following a pool behaviour, in agreement with other reports in yeast (Boumans et al., 1998) and bovine mitochondria (Ragan and Heron, 1978). Following studies that analysed the roles of CoQ and cyt *c* in the attenuation of $CIII_2$ and CIV pharmacological inhibition on the respiratory flux supported the dynamic compartmentalization of the respiratory substrates (Benard et al., 2008), as well as studies based in the competition of substrates for NADH and succinate oxidation (Lapuente-Brun et al., 2013). The proposal that SCs may provide distinct electron translocation pathways through the partition of CoQ into different pools to mediate metabolic adaptation (Lapuente-Brun et al., 2013), was questioned by kinetic and flux control studies showing that the metabolic pathways for NADH and succinate oxidation comprise different CoQ redox steady states, but communicate and converge on a single non-partitioned CoQ pool (Blaza et al., 2014; Milenkovic et al., 2017). It has also been argued that the cyt *c* pool is equally compartmentalized (Lapuente-Brun et al., 2013), but studies monitoring the reduction potential of CIII upon addition of NADH, succinate or both (Blaza et al., 2014), evidenced against cyt *c* partitioning. In agreement, time-resolved spectroscopic analysis of cyt *c* oxidation in intact yeast cells showed that cyt *c* is not trapped within SCs and, therefore, there are no restrictions that limit its diffusion (Trouillard et al., 2011). Moreover, the respirasome structures showed no evidence of a protein-mediated substrate channel connecting the CoQ binding sites of CI and $CIII_2$ (Letts, Fiedorczuk, et al., 2016), since both active sites are open to the membrane and separated by 10 nm, as also evidenced for cyt *c*, in agreement with previous studies that questioned substrate channelling based on the distances between the substrates binding sites on SCs (Dudkina et al., 2011). Therefore, the function of a direct catalytic role for mitochondrial SCs remains questionable (Milenkovic et al., 2017).

5.2. ASSEMBLY AND STABILITY OF COMPLEX I

Experimental evidence accumulated on respiratory chain disease models, suggests that the formation of mammalian SCs confer stability to their individual components, and most particularly to CI. The first description of a patient with progressive exercise intolerance due to a nonsense mutation in the $CIII_2$ subunit gene *MT-CYB* associated with a combined enzyme deficiency of complexes I and III (Lamantea et al., 2002), was followed by a more extensive

study showing that genetic alterations leading to a loss of $CIII_2$ prevented respirasome formation and led to the secondary loss of CI (Schägger et al., 2004). Further studies confirmed that not only the structural integrity of $CIII_2$ (Acín-Pérez et al., 2004), but also that of CIV (Diaz et al., 2006; Hornig-Do et al., 2012; Li et al., 2007), were essential to maintain the stability of mammalian CI. Despite these evidences, ostensible CI functional alterations are relatively infrequent to most patients presenting with $CIII_2$ or CIV enzyme deficiencies (Fernández-Vizarra and Zeviani, 2015; Rak et al., 2016), indicating that only severe structural alterations of these two complexes induce a parallel CI dysfunction. On the contrary, a dramatic decrease in CI levels does not generally lead to $CIII_2$ and CIV functional defects in mammals (Schägger et al., 2004). In agreement, the depletion of 28 different CI accessory subunits in human HEK293T cells showed a loss of SCs I+III_2 and I+III_2+IV_1 with no alterations in the steady-state levels of $CIII_2$ or CIV (Stroud et al., 2016). However, the fact that CI is purified and remains active in its free form adds to the debate whether CI stability may rely on additional molecular mechanisms, like alterations in the mitochondrial membrane potential (Quarato et al., 2011) or ROS levels. In this regard, the absence of respirasomes due to the lack of cyt *c* (Vempati et al., 2009), $CIII_2$ or CIV induced reverse electron transport from reduced CoQ to CI, triggering local superoxide generation and CI degradation (Guarás et al., 2016).

5.3. MODULATION OF ROS PRODUCTION

Because CI and $CIII_2$ constitute the main redox centres responsible for oxygen reduction to superoxide (Genova et al., 2001; Sun and Trumpower, 2003), it has been hypothesized that their arrangement into SCs could minimize ROS production. Measurements in bovine heart mitochondria provided the first demonstration that the disruption of SC I+III_2 enhanced the generation of superoxide from CI (Maranzana et al., 2013), and a direct correlation between ROS levels and CI dissociated from SCs was established in neurons and astrocytes (Lopez-Fabuel et al., 2016). According to the ovine respirasome structure (Letts, Fiedorczuk, et al., 2016), the two CoQ binding cavities on $CIII_2$ are arranged in such way that the symmetry of $CIII_2$ is broken, and this asymmetry could limit ROS production at the expense of maximal activity. Although decreased ROS production may be a functional consequence of SCs, oxygen levels can also modulate the assembly of these superstructures and the efficiency of mitochondrial respiration. For instance, during prolonged hypoxia, potato mitochondria showed a rearrangement of CI from SC I+III_2 to its free form (Ramírez-Aguilar et al., 2011). Or studies in mouse fibroblasts lacking the Rieske Fe-S protein of $CIII_2$ showed that enhanced ROS disrupted SCs and produced a deleterious effect on the stability of complexes I and IV (Diaz et al., 2012). One way the cells adapt to hypoxic conditions is by building a more efficient respiratory chain

through CIV, a key enzyme composed of oxygen-regulated subunit isoforms in yeast and mammals (Aras et al., 2013; Cogliati et al., 2016; Liu and Barrientos, 2012). Variations in oxygen levels may thus affect the assembly state of CIV and its incorporation into respirasomes. Aging, a fundamental biological process that affects all eukaryotic lives, is generally attributed to increased oxidative damage induced by ROS, and this is usually accompanied by a decay of SCs levels (Frenzel et al., 2010).

6. Biogenesis of respiratory chain supercomplexes

6.1. The respirasome assembly pathway

The precise mechanisms that regulate the biosynthesis of mammalian mitochondrial SCs remain unsolved and two models have been proposed to explain the association of CI with complexes III and IV (Guerrero-Castillo et al., 2017; Moreno-Lastres et al., 2012). The first model (Figure 8) proposes that CI gets fully-assembled prior to its binding to SCs. Time-course incorporation analyses of the 13 radiolabelled mitochondrial-encoded polypeptides into complexes and SCs showed the existence of a temporal gap between the formation of the complexes and their co-localization in SCs, suggesting that SCs originate by the direct association of single preassembled complexes (Acín-Pérez et al., 2008). Recent proteomic studies based on BN-PAGE and complexome profiling of CI intermediates upon mitochondrial translation inhibition with chloramphenicol, agreed that CI was independently assembled before SC formation (Guerrero-Castillo et al., 2017).

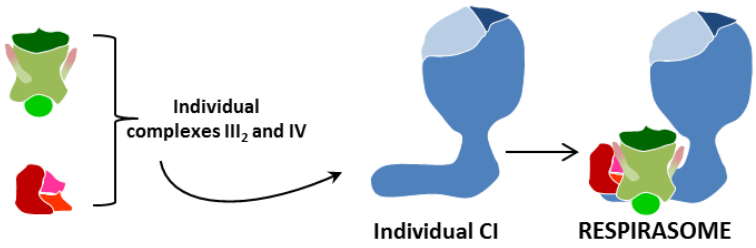

Figure 8. Respirasome biogenesis through direct association of fully assembled respiratory chain complexes. This model proposes that the mammalian respirasome ($I+III_2+IV_1$) originates by the direct association of single preassembled CI (blue), $CIII_2$ (green) and CIV (red).

The possibility that the formation of the respirasome could be achieved instead through a coordinated association of submodules and free subunits was supported by the observation in *Neurospora crassa* that the assembly of SC $I+III_2$ occurs before the individual CI is formed (Marques et al., 2007), and by studies showing that, in mitochondria from patients with chronically reduced CIV levels, newly-imported COX subunits preferentially integrate into

SCs (Kovářová et al., 2012; Lazarou et al., 2009). In accordance with this idea and previously to this work, our group analyzed the formation of SC assembly intermediates by reversibly depleting control cell lines of OXPHOS complexes by long treatment with doxycycline, a reversible inhibitor of mitochondrial translation. Results led to propose a second model (Figure 9) that involves the sequential binding of subcomplexes from $CIII_2$ and CIV to an almost complete CI scaffold that lacks the N catalytic module, which would be incorporated at the end of the assembly process to ensure the activation of the respirasome once all the essential structural components are present (Moreno-Lastres et al., 2012).

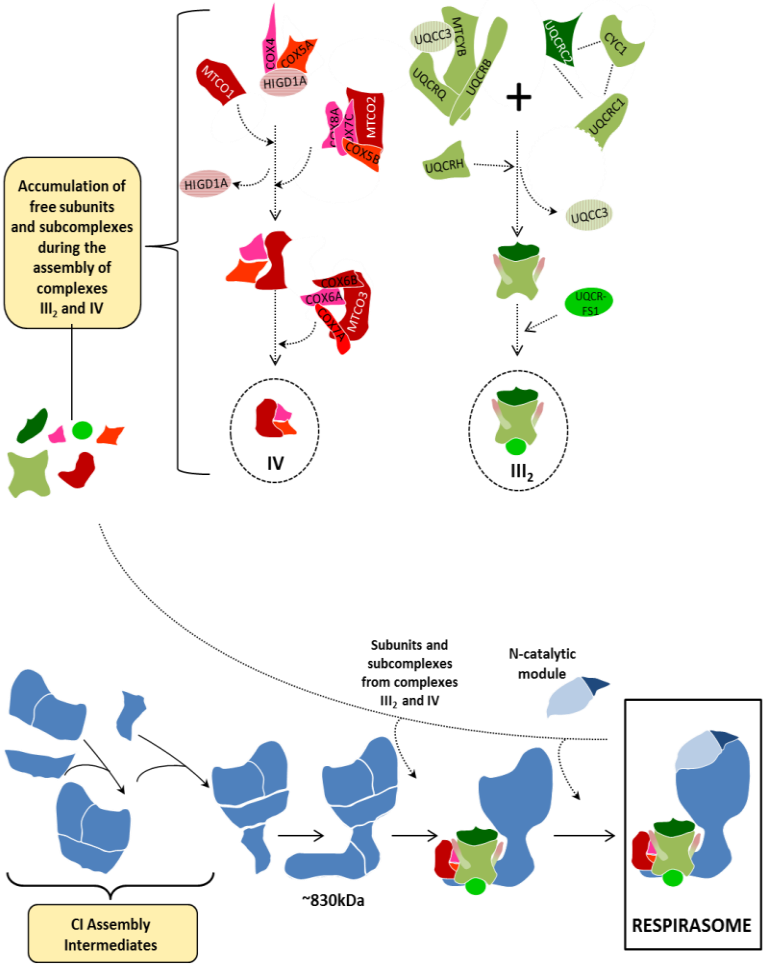

Figure 9. Respirasome biogenesis through the stepwise association of partially assembled respiratory chain complexes and submodules. This model proposes the sequential and coordinated association of submodules and free subunits from $CIII_2$ (green) and CIV (red) to a CI-scaffold (blue) that lacks the N catalytic module, which is incorporated at the latest assembly stage to ensure respirasome activation in the presence of all the necessary structural components. The assembly pathways of individual $CIII_2$ and CIV are depicted according to stablished models, and SC III_2+IV_1 is formed independently of the respirasomes. Supercomplex assembly factors COX7A2L and HIGD2A are marked in green/red.

6.2. SUPERCOMPLEX ASSEMBLY FACTORS

An important issue is the regulatory function that chaperones or assembly factors play on the assembly of SCs and respirasomes. In this regard, the two protein types defined as SC assembly factors, COX7A2L and the RCFs, are the best-studied ones.

6.2.1. COX7A2L/COX7RP/SCAFI

An interesting debate concerns the regulatory role of the protein COX7A2L/COX7RP in the formation and stabilization of mitochondrial SCs. Cox7a2l was first reported in mice to be present in the respirasomes and SC III_2+IV_1 but not in $CIII_2$ or free CIV, therefore constituting the first SC-specific assembly factor that was renamed SCAFI (Lapuente-Brun et al., 2013). The authors discovered that certain wild-type mouse strains widely used in biological research were homozygous for a 6 bp deletion in the *Cox7a2l* gene and expressed a short, unstable Cox7a2l isoform that failed to support CIV association into SCs, thereby promoting differences in mitochondrial respiration rates and ATP production. The authors proposed that Cox7a2l was a SC-specific assembly factor that aids CIV integration into SCs to adapt respirasomes formation and mitochondrial function to metabolic variations (Barrientos and Ugalde, 2013; Lapuente-Brun et al., 2013). This hypothesis was challenged by a depth characterization in isolated heart and liver mitochondria from control mouse strains that contained either the full-length *Cox7a2l* gene (i.e., CD1 mice) or the variant with the 6-bp deletion (i.e.,C57BL/6J, C57BL/6N, and BALB/c mice), that demonstrated that all mice had normal formation of respirasomes and normal respiratory chain function, thus showing that the truncated version of the *Cox7a2l* gene does not impact the bioenergetic capacity *in vivo* (Mourier, Matic, et al., 2014). This observation was conclusively supported by other studies (Davoudi et al., 2016; Ikeda et al., 2013; Jha et al., 2016; Sun et al., 2016; Williams et al., 2016).

Variations observed among tissues in the relative distribution of BN-PAGE bands above the canonical respirasome (SC I+III_2+IV_1) in mice strains bearing the short Cox7a2l isoform (Davoudi et al., 2016; Jha et al., 2016; Williams et al., 2016), opened the possibility that the assembly of specific SCs could be regulated in a tissue-specific manner. Interestingly, the short Cox7a2l isoform in C57BL/6 mice induced tissue-specific differences in the levels of the larger respirasomes I+III_2+IV_{2-4}, which were less abundant in liver than in heart mitochondria (Williams et al., 2016). The canonical respirasome (I+III_2+IV_1) was observed in the heart and skeletal muscle of mice expressing the short Cox7a2l isoform but not in the liver (Cogliati et al., 2016), whereas other studies observed its presence in the liver of mice expressing the short Cox7a2l isoform (Jha et al., 2016; Mourier, Matic, et al., 2014; Williams et al., 2016) (Table 1). The high sequence similarity between Cox7a2l and tissue-specific isoforms of the CIV subunit Cox7a, led to speculate that Cox7a2l may replace Cox7a within SCs, acting as a bridge to stabilize the interaction between $CIII_2$ and CIV (Letts, Fiedorczuk, et al., 2016). Mass spectrometric analyses of SCs from CD1 mice mitochondria (that express the long Cox7a2l isoform), revealed that the Cox7a2 subunit was present almost exclusively in CIV_{1-2}, whereas Cox7a2l was present in SCs III_2+IV and I+III_2+IV_{1-4} (Cogliati et al., 2016).

Table 1. Literature overview on the SCs organization reported in the C57BL/6 mouse strain harbouring the short COX7A2L isoform.

Study	Mouse Tissue	Respirasome $I+III_2+IV_n$	SC III_2+IV_1
Lapuente-Brun et al., 2013	Liver	-	-
Ikdea et al., 2013	Sk. Muscle	+	nd
Mourier et al., 2013	Heart/liver	+	-
Jha et al., 2016	Liver	+	-
Williams et al., 2016	Liver/heart	+	-
Cogliati et al., 2016	Heart/sk. Muscle	+	-
Cogliati et al., 2016	Liver/kidney/brain	-	-

+: present; -: absent; nd: not determined.

6.2.2. Respiratory complex factor 1, RCF1

Three independent groups identified the respiratory complex factor Rcf1 that belongs to the conserved *hypoxia induced gene 1* (Hig1) protein family and that controls the formation and stabilization of yeast SC III_2+IV_{1-2} (Chen et al., 2012; Strogolova et al., 2012; Vukotic et al., 2012). Rcf1 deletion yeast mutants (*Rcf1Δ*) resulted in defective CIV activity, decreased SC III_2+IV_{1-2} levels and increased ROS production (Chen et al., 2012; Vukotic et al., 2012). Latest studies showed that Rcf1 interacts with CIV to regulate late stages of its assembly process (Garlich et al., 2017), suggesting that it functions in the assembly of individual CIV rather than playing a direct role in SC III_2+IV_{1-2}. Rcf1 eukaryotic homologs include two variants, *HIGD1A* and *HIGD2A*, that display the broadest expression pattern in mammals (Chen et al., 2012). Whereas *HIGD1A* was shown to bind CIV in early assembly stages (Römpler et al., 2016), and to upregulate CIV activity under hypoxic cellular stress (Hayashi et al., 2015), *HIGD2A* knockdown caused the depletion of SC III_2+IV_1 and of CIV-containing bands above the SC $I+III_2+IV_1$ without altering free CIV levels (Chen et al., 2012), suggestive of a true SC stabilizing role.

HYPOTHESIS AND GOALS

Mitochondrial respiratory chain complexes associate in larger structures named supercomplexes (SCs) and respirasomes. The functional relevance of these respirasomes and intermediate supercomplexes, such as SC I+III_2 and SC III_2+IV, is currently under intense debate and remain to be fully determined. These entities are thought to offer functional and structural advantages to the system, including the stabilization and prevention of degradation of the component enzymes. In this regard, MRC organization in SCs is biomedically relevant because disease-causing genetic defects affecting only one MRC complex often cause alterations in the assembly and stability of other complexes. Hence, structural interdependences exist among MRC complexes, yet to be fully understood. High-resolution cryo-electron microscopic structures of mammalian SCs became recently available, only to heighten the intrigue of trying to understand how are they assembled and how their dynamics is regulated. Therefore, a controversial question on the field of mitochondrial membrane biogenesis is how respirasomes biosynthesis is regulated and which players are involved in controlling this process. Regarding the role of SC assembly factors, recent relevant studies have highlighted opposing roles for the COX7A2L / COX7RP / SCAFI protein in the formation and function of the mitochondrial SCs and respirasomes.

Based on previous studies of the pathways and chaperones that regulate the biosynthesis of macromolecular enzymatic oxidative phosphorylation complexes, the main purpose of this work has been to address how the biogenesis of human mitochondrial SCs is regulated and to clarify the role of the COX7A2L assembly factor in this process. In particular, the goals have been:

1. To functionally characterize COX7A2L and to shed light on the regulatory role that this protein plays in the biosynthetic process of human mitochondrial SCs and respirasomes.

2. To gain insight into the mechanisms that regulate the structural interdependences among respiratory chain complexes in human cell lines depleted of one MRC complex, by studying the alterations and specific accumulations of assembly intermediates, which will allow elaborating a more detailed map of the biosynthetic pathway of SCs.

EXPERIMENTAL PROCEDURES

1. Human cell lines

1.1. TRANSMITOCHONDRIAL CYBRIDS

To better understand how genetic defects in mtDNA-encoded OXPHOS subunits affect the regulation of the OXPHOS system *in vivo*, cytoplasmic hybrid (cybrid) cell lines have proved to be a valuable tool. Cybrids allow studying the pathogenic mechanisms associated to mtDNA mutations (King and Attardi, 1989), due to the expression of a specific mtDNA within cells with a fixed nuclear background. Cybrids are generated using a cell line that has been completely depleted of mtDNA by long-term exposure to ethidium bromide, termed *rho zero* (ρ^0) (Hayashi et al., 1991; King and Attardi, 1989). These cells can be repopulated with enucleated cytoplasts or platelets containing either functional mitochondria or pathogenic mtDNA (Chomyn et al., 1994; King and Attardi, 1989) and therefore, the studied cells differ only in their mtDNA genotype.

The cybrid cell lines used in this study were generated through the fusion of ρ^0 cells with enucleated fibroblasts isolated from patient's blood that contained the mtDNA mutation of interest in the presence of polyethylene glycol, as described elsewhere (King and Attardi, 1989). Specifically, four cybrids cell lines were used that presented MRC enzymatic defects due to homoplasmic mutations in the mtDNA:

- A CI-deficient (CI-KD [knockdown]) cell line which harbours a homoplasmic m.4681T > C mutation in the *MT-ND2* subunit gene that leads to a severe CI assembly defect due to a p.L71P substitution (Ugalde et al., 2007).
- A CIII mutant (CIII-KO) cell line which contains a homoplasmic 4-bp deletion in the *MT-CYB* gene affecting the *de novo* synthesis of cytochrome *b* (Rana et al., 2000).
- A CIV mutant cell line (CIV-KO or COX1Δ) that lacks holo-COX due to the homoplasmic m.6930G > A transition in the *MT-COI* gene, that creates a stop codon that results in a predicted loss of the last 170 amino acids of the COX1 polypeptide (Bruno et al., 1999).
- A CIV mutant cell line (COX2Δ) that lacks holo-COX due to the homoplasmic m.7896 G>A nonsense mutation in the *MT-COII* gene, which presumably causes a loss of 123 amino acids at the C-terminus of COX2 (Campos et al., 2001).

Besides, the cell line from human osteosarcoma 143B-TK$^-$ was used as an experimental control, as well as the human embryonic kidney HEK293T cell line (CRL-3216), obtained from ATCC.

1.2. STABLE HEK293T-DERIVED CELL LINES

- *COX7A2L*- knockout (KO) clone 1 and clone 2 (*COX7A2L* -KO1 and *COX7A2L*-KO2), created in HEK293T cells using TALEN vectors and described in section 1.2.1.
- Reconstituted *COX7A2L*-KO clone 1 and clone 2 and control HEK293T cells, shown in Table 2 and described in section 1.2.2.

1.2.1. TALEN constructs and generation of gene COX7A2L knockout cell lines

To analyse the specific function of COX7A2L, stable human knockout (KO) lines were created in control HEK293T cells using the TALEN (Transcriptor activator-like effector nucleases) strategy, a widely used technology for precise and efficient gene editing in live cells. TALEN is based on a class of proteins derived from transcription activator–like effector or TALE proteins (Romer et al., 2007; Schornack et al., 2006). TALEs are highly specific DNA-binding proteins that feature an array of 33 or 34-amino acid repeats. Each repeat is highly conserved, with the exception of the so-called repeat variable di-residues (RVDs) at amino acid positions 12 and 13 (Figure 10A). The RVDs determine the DNA sequence to which the TALE will bind, meaning that the structure of the DNA-binding domain can be manipulated to produce a protein domain that binds specifically to any DNA sequence of interest in the genome (Boch et al., 2009; Moscou and Bogdanove, 2009). These TALEs can be fused to the catalytic domain from a DNA nuclease, FokI, to generate a transcription activator-like effector nuclease, TALEN, capable of precisely targeting DNA manipulation (Figure 10B). The resulting TALEN constructs combine high specificity and activity, effectively generating engineered sequence-specific nucleases that bind and cleave DNA sequences only at pre-selected sites.

The activity of the TALEN system involves two steps. First, a double-strand break is introduced into eukaryotic DNA in the region of the spacer sequence separating the TALEN recognition sites. Second, the cell's ability to resolve the double-break via one of two well-conserved repair pathways is harnessed to generate a modification of choice at that genomic location. In the absence of a homologous donor DNA, the break is repaired by non-homologous end joining that mediates deletions or insertions of several nucleotides in the target site and, as one of the results, knockout due to reading frame mutations and stop codon formation. This sequence-targeting technology is known to function in a variety of host systems, including bacteria, yeast, plants, insects, zebrafish, and mammals.

The TALEN constructs used in this work were obtained from Thermo Fisher Scientific. The left and right TALENs were designed to bind the TGGGCGTCATGTACTACAA and the GCAGAAGTTGGCAGGAGCA DNA sequences, respectively, at the human *COX7A2L* locus. Both

vectors were transformed in NEB 5-alpha Competent *E.coli* High Efficiency Kit (Invitrogen) and amplified using PureLinkTM HiPure Plasmid Filter Midiprep Kit (Invitrogen), according to the manufacturer's instructions. For TALENs transfection HEK293T cells were transfected three times, with three-day intervals, with 10 µl of Lipofectamine™ (Thermo Fisher Scientific) mixed with 4 µg of vector DNA in OPTIMEM-I media (Gibco) according to the manufacturer's instructions.

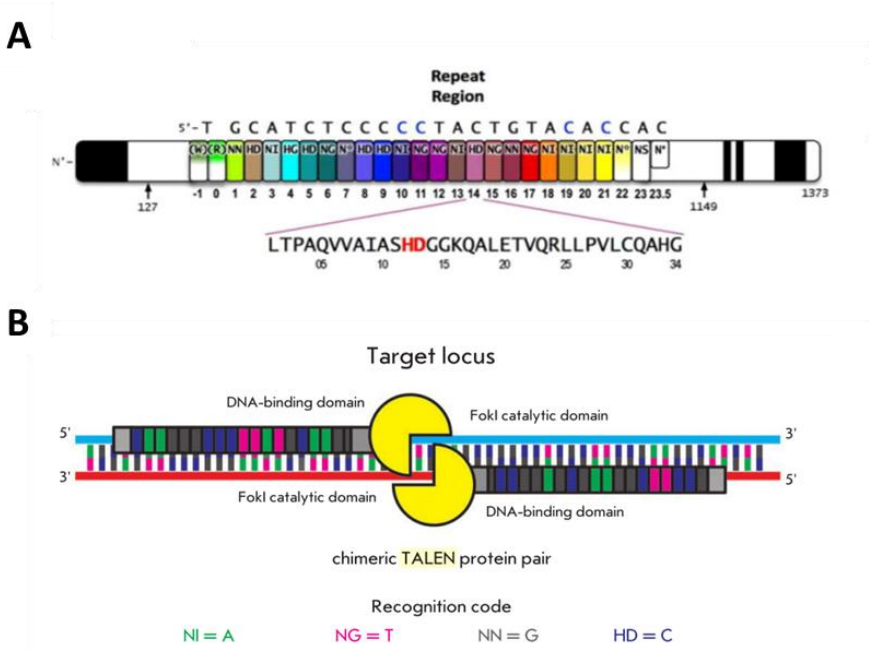

Figure 10. Scheme for TALEN proteins. **(A)** Example of a TAL effector containing the sequence of a representative repeat region is shown; RVD residues (HD) that recognize cytosines are in red. Modified from (Mak et al., 2013). **(B)** TALENs work as pairs of monomers and their binding sites are chosen so that they are located on opposite DNA strands of the target DNA sequence and are separated by a spacer sequence (12–25 bp), distance sufficient for dimerization of the FokI catalytic domains. Dimerized FokI introduces a double-strand break into DNA. Two amino acid residues in the monomer are responsible for binding. The recognition code (single-letter annotation is used to designate amino acid residues) is shown (Nemudryi et al., 2014).

After eight days single cells were isolated using Fluorescence Activated Cell Sorting (FACS) and the surviving colonies screened by immunoblotting against COX7A2L. To sequence the selected clones, *COX7A2L*-KO clones 1 and 2 were first amplified by polymerase chain reaction (PCR) from isolated HEK293T cDNA with the forward primer 5'-aagttaggcgatcttcgggc-3' and with the reverse primer 5' gctcggacatgagaagtggc-3'. Secondly, the PCR-amplified DNA fragments were purified according to the Wizard® Genomic DNA Purification Kit (Promega) and cloned directly into a sequencing vector, following the TOPO® TA Cloning® Kit for Sequencing (Invitrogen) procedure. Finally, the cloning reaction product was transformed in

NEB 5-alpha competent *E.coli* (Invitrogen) cells, amplified with the PureLinkTM HiPure Plasmid Filter Midiprep Kit (Invitrogen), and validated by sequencing with the M13 Reverse primer.

1.2.2. Plasmids and reconstitution of COX7A2L-KOs with the long and short-version of COX7A2L gene

The wild-type (long) version of COX7A2L will be herein designated as COX7A2L, unless otherwise indicated. Due to the natural resistance of HEK293T cells to the antibiotic neomycin, COX7A2L was subcloned from the commercial vector pCMV6-COX7A2L-Myc-DDK-Neo (Origene, PS100001) with neomycin resistance, to the pCMV6-AEntry-Hygro plasmid (Origene, PS100024) , with hygromycin resistance, using the *Sfa*AI and *Mss*I sites. Briefly, 100 µl of the digestion reaction of both plasmids were separated in an agarose gel electrophoresis. The digested DNA-bands were purified using the Wizard® Genomic DNA Purification Kit (Promega) and subsequently ligated using the T4 DNA Ligase (NEB) according to manufacturer's instructions. 1 µl of the ligation reaction was transformed in NEB 5-alpha competent *E.coli* cells (Invitrogen), amplified with the PureLinkTM HiPure Plasmid Filter Midiprep Kit (Invitrogen) and validated by sequencing with the VP1.5 primer 5'-ggactttccaaaatgtcg3'.

The short version of mouse Cox7a2l comprises an *in-frame* 6 base pairs deletion that leads to the absence of 2 amino acids (V72 and P73) (Lapuente-Brun et al., 2013). To generate the short variant form of human COX7A2L (herein designated as COX7A2L^{short}), the Q5® Site-Directed Mutagenesis Kit from NEB was used. ~ 20 ng of template DNA extracted from HEK293T cells were used, along with the primers GTTTTTCCAGAAAGCTGATGGT (forward) and GCCTCGTTTCAGGTAGAC (reverse), designed to flank the region to be deleted. After exponential amplification and the treatment with kinase and ligase, 5 µl of the reaction were transformed in NEB 5-alpha competent *E.coli* cells (Invitrogen), using the pCMV6-A-Entry-Hygro plasmid (Origene, PS100024), according to the manufacturer's instructions. Further sequencing of the pCMV6-COX7A2Lshort-Hygro using the VP1.5 primer 5'-ggactttccaaaatgtcg3' confirmed the correct cloning.

Stable cell lines were established by transfection of WT HEK293T cells and *COX7A2L*-KO clones 1 and 2 in a six well plate with 10 µl of Lipofectamine 2000 (Invitrogen), mixed with either the long-COX7A2L-Myc-DDK-Hygro or the short-COX7A2L-Myc-DDK-Hygro plasmids in OPTIMEM-I media (Gibco). Two days after transfection, the media was supplemented with 200 µg/ml of hygromycin and drug selection was maintained for at least 1 month. After drug removal, the stable cell lines were screened by immunoblotting against COX7A2L.

Table 2. Stable cell lines created in the laboratory.

Background Cell Line		
HEK293T	***COX7A2L*-KO1**	***COX7A2L*-KO2**
HEK293T + EV	*COX7A2L*-KO1 + EV	*COX7A2L*-KO2 + EV
HEK293T + COX7A2L	*COX7A2L*-KO1 + COX7A2L	*COX7A2L*-KO2 + COX7A2L
HEL293T + COX7A2L^{short}	*COX7A2L*-KO1 + COX7A2L^{short}	*COX7A2L*-KO2 + COX7A2L^{short}

Three different cells were used to transfect plasmids and to create the indicated stable cell lines. **KO1**: knockout clone 1; **KO2**: knockout clone 2; **EV**: empty vector; **COX7A2L:** pCMV6-COX7A2L-Hygro plasmid; **COX7A2L^{short}:** pCMV6-COX7A2Lshort-Hygro plasmid.

2. Mitochondrial samples provided by other research groups

- Isolated mitochondrial extracts from HeLa cells, either transduced with the empty pWPXLd-ires-PuroR vector or stably overexpressing hemagglutinin (HA)-tagged LYRM7 / MZM1L (MZM1L-HA), generated as previously described (Sánchez et al., 2013) were kindly provided by Dr. Erika Fernández-Vizarra.
- Isolated heart mitochondria from the following mice models (Mourier, Matic, et al., 2014) were kindly provided by Dr. Nils Göran Larsson:
  - Wild-type CD1 mice, which express high levels of the long COX7A2L protein isoform of 113 amino acids.
  - Wild-type C57BL/6J and C57BL/6N mice, which express low levels of a shorter and unstable COX7A2L protein isoform of 111 amino acids.
  - Mutant *LrpprKO* mice, CIV-conditional knockout mice with C57BL/6N genetic background, generated as previously described (Ruzzenente et al., 2012).

3. Reagents, solutions and buffers

Commonly used solutions and buffers used in this work were performed according to the descriptions detailed in (Sambrook and Russell, 2001). The compositions of the specific media and reagents used are detailed in each experimental procedure section or in the corresponding bibliography.

4. Cell culture

Cells were cultured at 37°C in DMEM (*Dulbecco's Modified Eagle Medium*, Life Technologies) supplemented with 4.5 g/L glucose, 10% fetal bovine serum (FBS), 2 mM L-glutamine, 1 mM sodium pyruvate, and 100 U/ml of penicillin/streptomycin antibiotics (Lonza). In the case of

the cybrids, 50 µg/ml of uridine (Lonza) were also added to the medium. Culture vessels were used to subculture the adherent mammalian cells.

To cryopreserve the cultured cells, the adherent cells were washed in PBS, dettached with trypsin-EDTA (0.2 mg/ml trypsin, 0.22 mg/ml EDTA) (Lonza) and centrifuged for 5 minutes at 1500 rpm at 4°C. Subsequently, cells were resuspended in 1 ml of the freezing solution, containing 10% of the cryoprotective agent dimethyl sulfoxide (DMSO) in DMEM culture medium, transferred to cryovials (Thermo Fisher Scientific) into a CoolCell (at room temperature, with 2-propanol) and put into a -80°C freezer. After approximately 24 hours, the cryovials were transferred into liquid nitrogen for long term storage. Frozen cell lines were rapidly thawed by placing the cryovials in a 37°C water bath and subsequently transferred into a culture vessel.

5. Reversible inhibition of mitochondrial translation (Doxycycline assay)

Doxycycline is a specific reversible inhibitor of mitochondrial translation when used at low concentrations in the culture media, and it allows to synchronously resume the translation of coding mitochondrial proteins once removed from the medium (Van den Bogert et al., 1988). Doxycycline treatment has proven to be a successful strategy to follow the accumulation of newly synthesized MRC complexes and their further association in SCs (Moreno-Lastres et al., 2012; Ugalde et al., 2004). In this work, 15 mg/ml doxycycline was added to the culture medium. Cells were grown in exponential conditions and harvested at different time points (Figure 11) after the drug removal. Samples were then processed according to the experimental assays and stored until use.

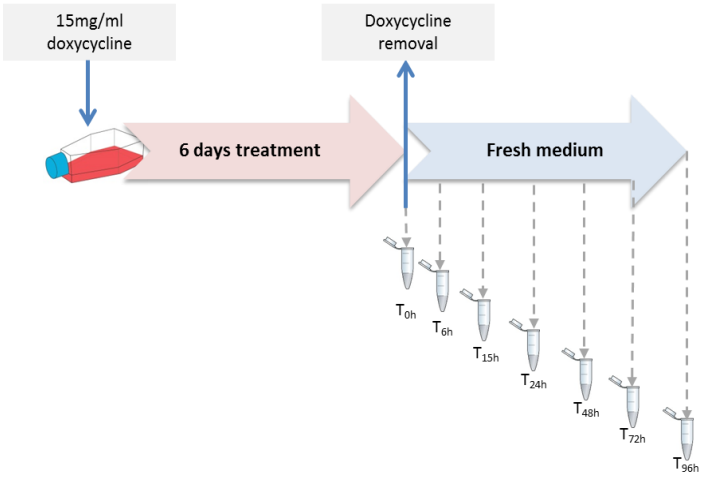

Figure 11. Reversible inhibition of mitochondrial translation with doxycycline. Upon 6 days of doxycycline treatment (T_{0h}), the drug was removed and cells were grown in fresh medium and harvested at different time points (hours) after doxycycline removal (T_{6h} to T_{96h}).

6. Functional characterization of the mitochondrial respiratory chain

6.1. RESPIRATORY CHAIN ENZYME ACTIVITIES

The respiratory chain enzyme activities from complexes I, II, III and IV were measured for 3 minutes at 37°C using a DU-650 spectrophotometer (Beckman) with minor variations relative to established methods (Medja et al., 2009). Values were expressed relative to the citrate synthase (CS) activity. Schematic examples of the enzyme activity measurements of the MRC complexes are shown in Figure 12.

6.1.1. Sample Preparation

Whole cell extracts were prepared from 15 x10^6 cells resuspended in 400-700 µl of Mannitol buffer (225 nM mannitol, 75 mM sucrose, 10mM Tris-HCl, 01 M EDTA at pH 7.2). Cells were lysed by sonication and protein concentration was measured using the MicroBCA Protein Assay kit (Pierce). All samples were set to a final concentration of 3 µg/ml prior to enzyme activity measurements.

6.1.2. Enzyme activities of CI-CIV and citrate synthase

In brief, CI enzyme activity was measured by following the decrease of NADH absorbance at 340 nm that results from NADH oxidation. 20 µg of the cellular homogenates were dissolved in the reaction medium containing 500 mM of phosphate buffer at pH 7.5, 50 mg/ml of BSA, and 25 mM of decilubiquinone as the electrons acceptor.

CII activity was measured by following the increase of absorbance at 600 nm resulting from the reduction of 2,6-dichlorophenol-indophenol (DCPIP). 20 µg of the cellular homogenates were added to the reaction medium containing 500 mM of phosphate buffer at pH 7.5, 5 mM of DCPIP, 10 mM of potassium cyanide (KCN), 0.2 % BSA-EDTA and 200 mM of succinate as the electrons donor.

CIII activity was measured by following by the increase in cytochrome *c* absorbance at 550 nm which results from cytochrome *c* reduction. 20 µg of the cellular homogenates were added to the reaction medium containing 500 mM of phosphate buffer at pH 7.5, 1 mM of cytochrome *c*, 10 mM of KCN, 50 mM of EDTA, 5.5 % of Tween-20 and 10 mM of decylubiquinol as the electrons donor.

CIV activity was measured by following the decrease in absorbance at 550 nm resulting from the oxidation of reduced cytochrome *c,* which acts as the electrons donor. 40 µg of the

cell homogenates were added to the reaction medium containing 100 µM of cyrochrome *c* (Reduced 90-95%) in 50 mM phosphate buffer at pH 7.0.

The citrate synthase (CS) activity, an enzyme of the tricarboxylic acids cycle, was used to normalize the respiratory chain enzyme activities. CS activity was measured by following the increase in absorbance at 412 nm that results from the reduction of DTNB (5,5'-dithiobis 2-nitrobenzoic acid), for 3 minutes at 37°C. 40 µg of cellular homogenates were added to the reaction medium containing 1 mM of Tris-HCl at pH 8.1, 10% of Triton X-100, 5 mM DTNB in 95% ethanol, 10 mM of acetyl coenzyme A and 10 mM of oxaloacetate as the electrons donor.

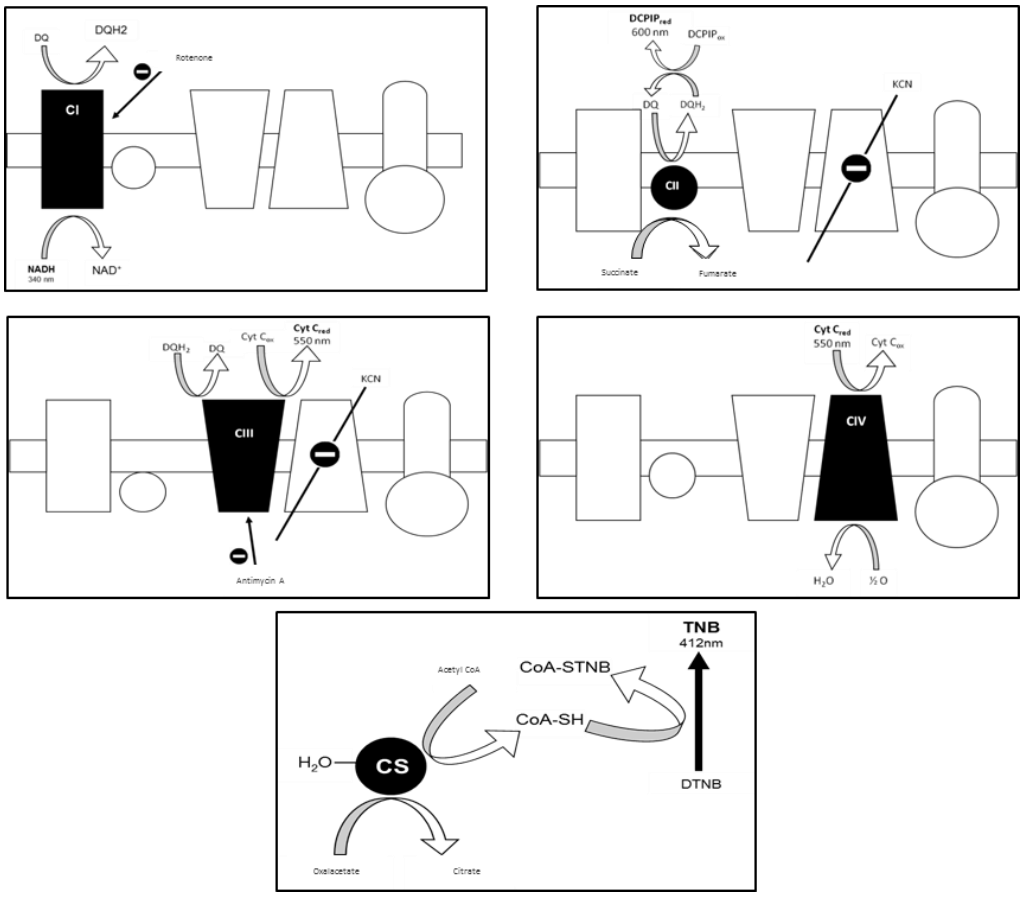

Figure 12. Graphical scheme of the respiratory chain enzyme activities. *Up and left:* CI enzyme activity; *Up and right:* CII enzyme activity; *Middle and left:* CIII enzyme activity; *Middle and right:* CIV enzyme activity; *Down*: CS activity.

6.2. CELL RESPIRATION MEASURED BY SEAHORSE ANALYZER

Oxygen consumption rates were measured in 143B cells and transmitochondrial cybrids using an XF24 Extracellular Flux Analyzer (Seahorse Bioscience). The day before the experiment, around 9.0 ×10^4 143B cells per well were plated in order to obtain a total amount of 150-200 µg protein per well on the day of the experiment. The cells were previously incubated with

either scrambled or specific COX7A2L siRNAs for 24 hours. As controls for the oxygen consumption measurements in siRNA-treated cells, around 5.0 ×10^3 143B cells and 1.0 ×10^4 CI-KD cells (CI defective mutant cybrids) per well were plated two days before the experiment, from which 150-200 µg protein per well were obtained on the day of the experiment. The cells were then incubated for 1 hour in unbuffered DMEM supplemented with 1 g/l glucose, 1 mM sodium pyruvate and 2 mM glutamine at 37°C in a CO_2-free incubator. Respiration was calculated after the addition of mitochondrial inhibitors rotenone and antimycin at 1 µM final concentration. In all experiments, the protein concentration in each well was determined using the Pierce BCA Protein Assay Kit (Thermo Fisher Scientific) after cell lysis in extraction buffer, and was used to calibrate the oxygen consumption data.

6.3. CELL RESPIRATION MEASURED BY POLAROGRAPHY

Endogenous cell respiration was measured polarographically at 37°C using a Clark-type electrode from Hansatech Instruments (Norfolk, UK). Substrate-driven respiration was assayed in digitonin-permeabilized cultured cells as reported (Barrientos et al., 2009). Briefly, trypsinized cells were washed with permeabilized-cell respiration buffer (PRB) containing 0.3 M mannitol, 10 mM KCl, 5 mM $MgCl_2$, 0.5 mM EDTA, 0.5 mM EGTA, 1 mg/ml BSA and 10 mM KH_3PO_4 (pH 7.4). Cells were resuspended at ~4 × 10^6 cells/ml in 1.5 ml of the same buffer air equilibrated at 37 °C and supplemented with 10 units of hexokinase and 2 mM ADP. 1 ml of cell suspension was immediately placed into the polarography chamber to measure endogenous respiration. Subsequently, digitonin was added at the optimal concentration (60 µg/10^6 HEK293T cells). The respiration measurements in permeabilized cells were then started by addition to the chamber of site I substrates (5 mM glutamate and 5 mM malate) to monitor their oxidation, followed by addition of site II substrates (5 mM succinate) to explore substrate competition. The order of the substrate addition did not influence the respiratory rates measured. In each case, the respiration was uncoupled by adding 18 µM FCCCP and subsequently inhibited with 240 µM KCN.

7. Indirect immunofluorescence

Cells were fixed with 4% paraformaldehyde for 15 minutes, permeabilized for 15 minutes with 0.1% Triton X-100, and incubated for 1 hour in blocking buffer containing 10% goat serum. Coverslips were incubated with an antibody against monoclonal complex V α subunit and a Texas Red-conjugated anti-mouse secondary antibody (Abcam). Coverslips were rinsed and

mounted in ProLong Gold antifade reagent (Molecular Probes) on glass slides, and cells were viewed with a Zeiss LSM 510 Meta confocal microscope and a 63x Plan-Apochromat oil inmersion objective (NA, 1.42). Sequential scanning of green and red channels was performed to avoid bleed-through effect. Cells were imaged randomly with 0.5- to 1.0-µm slices and 1,024- x 1,024-pixels resolution. For colocalization analysis, the ''Merge channels'' plugin from the ImageJ 1.48v software was used.

8. COX7A2L transient overexpression

Vectors pCMV6-Entry (C-terminal Myc-DDK-tagged), pCMV6-COX7A2L-Myc-DDK, pCMV6-AC-GFP and pCMV6-AC-COX7A2L-GFP were purchased from Origene (catalogue numbers PS100001, RC202697, PS100010 and RG202697, respectively), transformed in One Shot TOP10 chemically competent *E.coli* cells (Invitrogen) and amplified using PureLinkTM HiPure Plasmid Filter Midiprep Kit (Invitrogen), according to the manufacturer's instructions. For DNA transfection, 143B cells cultured in serum-free medium were transfected for 48 hours with 10 µg of plasmid DNA using 40 µl of FuGENE® HD Transfection Reagent (Promega), and alternatively, HEK293T cells were transfected with LipofectaminTM (Thermo Fisher Scientific) according to the manufacturer's instructions. Cells were harvested and processed according to each experimental assay requirements.

9. *COX7A2L* siRNAs Transfection

For siRNAs transfection, 143B cells and COX1Δ mutant cybrids were plated in 10 ml of DMEM supplemented with 10% FBS in 10-cm dishes with a cell density of $7.8x10^5$ cells per plate. The next day, cells were transfected with two mixed *COX7A2L* siRNAs (references SASI_Hs01_00081409 and SASI_Hs02_00338185, Sigma Aldrich) in the presence of 52 µl X-treme GENE siRNA Transfection Reagent (Roche) to achieve a final concentration of 0.15 µM siRNA in a total volume of 10 ml per plate. The negative control used was MISSION® siRNA Universal Negative Control (Sigma Aldrich). Cells were incubated at 37 ºC in a CO_2 incubator for 48 hours prior to experimental analyses.

10. *NDUFB8* siRNAs Transfection

For siRNAs transfection, wild-type HEK293T cells and *COX7A2L*-KO clones 1 and 2 were plated in 10 ml of DMEM supplemented with 10% FBS in 10-cm dishes with a cell density of $7.8x10^5$ cells per plate. The next day, cells were transfected with 4µg of two mixed *NDUFB8* siRNAs

(references SASI_Hs01_00049514 and SASI_Hs02_00338754, Sigma Aldrich) that targeted *NDUFB8* mRNA (reference sequence NM_005004) in the presence of 52 µl X-treme GENE siRNA Transfection Reagent (Roche) to achieve a final concentration of 0.15 µM siRNA in a total volume of 10 ml per plate. Cells were incubated at 37 ºC in a CO_2 incubator for 48 hours prior to experimental analyses.

11. Mitochondrial protein synthesis

Mitochondrial protein synthesis was determined by pulse-labelling in 80% confluent cells, as described by (Leary and Sasarman, 2009) with some adaptations. Cybrids were grown in a six-well plates pre-coated for 1 hour at room temperature with 0.1 mg/ml collagen in PBS to increase cell adherence. Cells were washed twice in PBS and incubated 20 minutes in DMEM devoid of methionine. Then, the media was supplemented with 100 µg/mL emetine for 10 minutes to inhibit cytoplasmic protein synthesis, followed by the addition of 10 µLCi of [^{35}S]-methionine and incubation for 2 hours pulse time. For pulse samples, after incubation cells were washed one time with PBS and collected. For chase samples, cells were washed twice with PBS and incubated in complete media for the indicated chase time. Cells were then harvested by trypsinization and mitochondria- enriched fractions were prepared for 2D-BN/SDS-PAGE as previously described (section 16.2). After electrophoresis, the gel was transferred to a nitrocellulose membrane and exposed to a film.

12. Purification of Whole Cell and Mitochondrial protein extracts

12.1. WHOLE CELL EXTRACTS

Cells were cultured until an approximately 70% confluent in a 175 cm^2 vessel, harvested with trypsin, washed twice with phosphate-buffered saline (PBS), and resuspended in 1 ml of cold phosphate-buffered saline (PBS). After 5 minutes centrifugation at 1500 rpm at 4°C, whole cell extracts were solubilised in HEPES buffer (20 mM HEPES NaOH pH 7.4; 150 mM NaCl; 10% glycerol, 1% Triton X-100) with 1x mammalian protease inhibitor cocktail (Roche). After 30 minutes on ice, extracts were cleared by 10 minutes centrifugation at 13000 rpm at 4°C. The protein concentration in the supernatant was determined using the MicroBCA Protein Assay Kit (Pierce) according to the manufacturer's instructions. After quantification, the supernatant was mixed with an equal volume of Laemmli 2X commercial solution (BioRad) containing 5% β-mercaptoethanol (Sigma). The samples were then boiled at 95°C for 10 minutes and stored at -20°C until use.

12.2. MITOCHONDRIA-ENRICHED FRACTIONS

Mitochondria-enriched fractions were isolated from cell cultures, as previously described with minor modifications (Nijtmans, 2002). Briefly, cells were cultured until an approximately 70% confluent, harvested with trypsin, washed twice with PBS, and resuspended in 100 µl PBS plus 100 µl of digitonin solubilized in PBS (4mg/ml). The cell solution was kept on ice for 10 minutes to dissolve the membranes. 1 ml of cold PBS was added to the cells, which were spun for 10 min at 10000 rpm at 4^{o}C. The supernatant was removed, the pellet washed once more in 1ml cold PBS, and the protein concentration was determined using the MicroBCA protein assay kit (Pierce). After quantification, the supernatant was mixed with an equal volume of Laemmli 2X commercial solution (BioRad) containing 5% β-mercaptoethanol (Sigma). The samples were then boiled at 95^{o}C for 10 minutes and stored at -20°C until use.

12.3. MITOCHONDRIAL ISOLATION

Mitochondria from human cells were isolated from at least ten 80–100% confluent 175 cm^2 flasks as described previously (Enríquez and Attardi, 1996). Briefly, the cells were resuspended in ice-cold T-K-Mg buffer (10 mM Tris–HCl, 10 mM KCl, 0.15 mM $MgCl_2$, pH 7.0) and disrupted with 10 strokes in a homogenizer (Kimble/ Kontes, Vineland, NJ, USA). Using a 1 M sucrose solution, the homogenate was brought to a final concentration of 0.25 M sucrose and a postnuclear supernatant was obtained by centrifugation of the samples twice for 3 minutes at 1500 g. Mitochondria were pelleted by centrifugation for 10 minutes at 8000 g and resuspended in 0.6 M Sorbitol 10 mM Hepes pH 7.4. Samples were stored at -80°C until use.

13. Immunoprecipitation

Co-immunoprecipitation (CO-IP) is a technique used to analyze protein-protein interactions. The goal is to know which proteins interact with the protein of interest. 1 mg of mitochondrial protein from HEK293T-transduced cells was solubilized in 600 ml of 4 g/g digitonin-to-protein buffer, as for BN electrophoresis (BNE) analyses. After centrifugation for 30 minutes at 13000 rpm at 4^{o}C, 50 mg supernatant was separated as the input fraction. The remaining supernatant was co-immunoprecipitated in resin spin columns (Pierce CoIP Kit, Thermo Fisher Scientific), in which 15 mg antibodies against DDK-tag (Oncogene), CORE2, or COX1 (Abcam) had been previously immobilized. The mixture was gently incubated overnight at 4^{o}C in a rotating shaker and centrifuged at 1000 g for 1 minute to separate the flow through fraction. The column was washed three times with lysis buffer containing 1% NP-40, and proteins were eluted. The

immunoprecipitate was divided in three aliquots, treated with 53 µl of loading sample buffer, and heated at 95°C for 5 minutes prior to loading.

14. SDS-PAGE Electrophoresis

For denaturing electrophoresis, 20–60 µg of whole cell or mitochondrial protein extracts were separated by sodium dodecyl sulfate-polyacrylamide gel electrophoresis (SDS–PAGE) in the Laemmli buffer system (Laemmli, 1970) using 0.2 M Tris-HCl buffer (pH 8.9) as anode buffer and 0.1 M Bis-Tris buffer, 0.1 M Tricine (pH 8.2) and 0.1% SDS as cathode buffer.

15. Western-blot

After electrophoresis, proteins were transferred to a PROTAN nitrocellulose membrane (GE Healthcare) at 30 V and at room temperature overnight, or at 90 V for 90 minutes at 4°C. The membranes were then incubated in blocking solution (0.1% Tween-20 and 5% skimmed powder milk in PBS) either for 14-16 hours at 4°C, or for 2 hours at room temperature. After blocking, the membranes were hybridized with specific primary antibodies (section 16, Table 3). They were then washed three times with 0.1% Tween-20 in PBS and incubated with the corresponding secondary antibody at a 1: 2000 dilution (section 16, Table 4). Both primary and secondary antibodies were prepared in 0.1% Tween-20 solution and 2.5% skimmed powder milk in PBS. After incubation with the secondary antibody, each membrane was washed three times with 0.1% Tween-20 in PBS, and then revealed using the ECL plus Western Blotting Detection System (GE Healthcare) in a ChemiDoc™ MP imaging apparatus (BioRad), following the manufacturer's instructions. Quantification of the chemiluminiscent signals was performed using the image analysis program ImageJv.1.45g (Wayne Rasband, NIH).

16. Blue Native Electrophoresis and In-Gel Activity (IGA) assays

Blue native polyacrylamide gel electrophoresis (BN-PAGE) is a method for the isolation of native protein complexes. In the first dimension, separation of the complexes under non-denaturing conditions occurs according to their molecular mass, and in the second dimension, where electrophoresis is performed under denaturing conditions, the individual subunits of the complexes are resolved and individually separated again on the basis of their molecular mass (Figure 13A).

16.1. SAMPLES PREPARATION FOR BN-PAGE

To extract mitochondrial proteins in native conditions, mitochondria extracts (previously explained in sections 11.1 and 11.2), were pelleted and solubilized in 200 µl buffer containing 1.5 M aminocaproic acid and 50 mM Bis-Tris (pH 7.0). To optimize solubilization conditions, protein-to-digitonin concentrations between 1-40 g/g were used; upon optimization, a protein-to-digitonin concentration of 4 g/g was used unless otherwise indicated. In some experiments, lauryl maltoside (LM) was used instead at 1%. Solubilized samples were incubated on ice for 15 minutes and centrifuged for 30 minutes at 13000 rpm at 4°C, and the supernatant was combined with 20 µl of sample buffer (750 mM aminocaproic acid, 50 mM Bis-Tris, 0.5 mM EDTA, 5% Serva Blue G-250) prior to loading.

16.2. BIDIMENSIONAL BLUE NATIVE ELECTROPHORESIS (2D-BN/SDS-PAGE)

For the first dimension electrophoresis (1D-BN-PAGE), precast NativePAGE™ 3-12% Bis-Tris Protein Gels (Thermo Fisher Scientific) were loaded with 60-80 µg of mitochondrial protein extracts as previously described (Nijtmans, 2002), using 50 mM Bis-Tris as the anode buffer and 15 mM Bis-Tris, 50 mM tricine, 0.02% Serva Blue G-250 as the cathode buffer. After electrophoresis, proteins were transferred to a PROTAN nitrocellulose membrane (Schleicher & Schuell) at 30 V overnight and probed with specific antibodies. Duplicate gels were further used to perform either IGA assays (described in section 16.3) or second-dimension electrophoresis.

The second dimension electrophoresis (2D-BN/SDS-PAGE) was performed following previously described methods (Nijtmans, 2002). Briefly, a 1D-BN-PAGE lane was cut out with a razorblade and placed on a small glass plate. The lane was incubated with a dissociating solution (01% SDS and 1% β -mercaptoethanol) for one hour at room temperature. Excess dissociating solution was drained away using a filter paper. The gel strip was placed at the top of the glass plate (Figure 13B) and the gel sandwich was further assembled. A 10% SDS-PAGE resolving gel was first cast, followed by casting of a 4% stacking gel around the gel strip. After polymerization, electrophoresis started using 0.2 M Tris-HCl buffer (pH 8.9) as the anode buffer and 0.1 M Bis-Tris buffer, 0.1 M Tricine (pH 8.2) and 0.1% SDS as the cathode buffer. Then proteins were transferred to nitrocellulose membranes, as described in section 14, and probed with specific antibodies.

16.3. IN-GEL ACTIVITY (IGA) ASSAYS

In this work, two different IGA assays were used:

For the complex I-IGA assay, gels were incubated for 2 hours at room temperature with the following solutions: 2 mM Tris-HCl, pH 7.4, 0.1 mg/ml NADH, and 2.5 mg/ml NTB (nitrotetrazolium blue). Gels were washed in distilled water, scanned and photographed immediately.

For the complex IV-IGA assay, gels were incubated for 48 hours at 37°C with the following solutions: 5 mg 3.3'-diamidobenzidine tetrahydrochloride (DAB) dissolved in 9 ml phosphate buffer (0.05 M, pH 7.4), 1 nM catalase (20 g /mL), 10 mg cytochrome c, and 750 mg sucrose). Gels were washed in distilled water, scanned and photographed immediately.

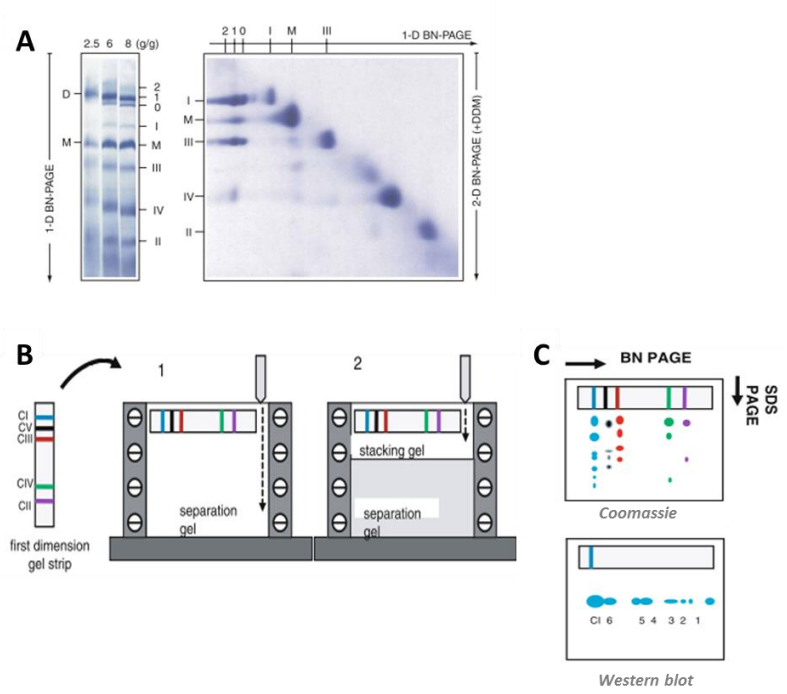

Figure 13. Blue native gel electrophoresis. (A) Example of a visualised separation of supramolecular assemblies of OXPHOS complexes by 1D-BN-PAGE using different concentrations of digitonin, and subsequent identification of their constituent individual complexes by 2D-BN/SDS-PAGE (Wittig, Braun, et al., 2006). I, II, III and IV refer to MRC complexes I–IV. 0, 1 and 2 indicate respiratory chain SCs containing monomeric CI, dimeric CIII, and zero (0), one (1) or two (2) copies of CIV, respectively. **(B)** Schematic representation of a second dimension gel casting followed by electrophoresis. The first dimension gel strip is turned 90° on top of the sandwich (1) and after polymerization of the resolving gel, the stacking gel is poured around the gel strip (2). **(C)** After electrophoresis, possible subassemblies are observed by *coomasie* staining or immunoblotting. The arrows indicate the direction of the first and second dimension. The individual subunits of the hypothetical red complex are resolved on the basis of their molecular mass. CI-CV: MRC complexes I to V. Modified from (Calvaruso et al., 2008).

17. Antibodies

The main technical features of the primary and secondary antibodies used in this work are detailed in Tables 3 and 4, respectively.

Table 3. Primary antibodies used in this work.

ANTIBODY	MOLECULAR WEIGHT	ORIGIN	MANUFACTURER	USE AND DILUTION
CI- NDUFA9	39 kDa	Mouse	Abcam	WB 1:1000
CI- NDUFB3	12 kDa	Mouse	Santa Cruz	WB 1:500
CI- NDUFB6	18 kDa	Mouse	Abcam	WB 1:1000
CI- NDUFB8	20 kDa	Mouse	Abcam	WB 1:1000
CI- NDUFS1	75 kDa	Rabbit	Gentex	WB 1:1000
CI- NDUFS2	49 kDa	Mouse	Abcam	WB 1:1000
CI- NDUFV2	24 kDa	Rabbit	Sigma	WB 1:1000
CII- SDHA	70 kDa	Mouse	Abcam	WB 1:10000
CII- SDHAB	30 kDa	Rabbit	Abcam	WB 1:1000
CIII-CORE2	48 kDa	Mouse	Abcam	IP/WB 1:2000
CIII- CYC1	35 kDa	Rabbit	Abcam	WB 1:1000
CIII- RISP	25 kDa	Mouse	Santa Cruz	WB 1:600
CIII- UQCRB	14 kDa	Rabbit	Proteintech	WB 1:500
CIII- UQCRQ	10 kDa	Rabbit	Sigma	WB 1:500
CIV- COX1	37 kDa	Mouse	Abcam	IP/WB 1:1000
CIV- COX2	24 kDa	Mouse	Abcam	WB 1:1000
CIV- COX4	16 kDa	Mouse	Abcam	WB 1:2000
CIV- COX5A	14 kDa	Mouse	Abcam	WB 1:1000
CIV- COX5B	14 kDa	Mouse	Santa Cruz	WB 1:1000
CIV- COX6C	9 kDa	Mouse	Abcam	WB 1:1000
CV- ATP synthase subunit alpha	50 kDa	Mouse	Abcam	IF 1:1000
COX7A2L	12 kDa	Mouse	Proteintech	WB 1:500

COX7A2L	12 kDa	Rabbit	Proteintech	WB 1:500
VDAC	39 kDa	Mouse	Abcam	WB 1:5000
β-actin	43 kDa	Mouse	Sigma	WB 1:5000
HA	*Tag*	Mouse	Roche	WB 1:1000
Myc	*Tag*	Mouse	Origene	IP/WB 1:1000
Turbo GFP	*Tag*	Mouse	Origene	IF/WB 1:1000

The table indicates the proteins that are targeted by the antibodies, their apparent molecular weights on SDS-PAGE, the animal origin of the antibodies, the manufacturer company from which the antibodies were purchased, their experimental utility and the dilutions used. CI-CV: Mitochondrial OXPHOS complexes I to V; WB: Western blot; IF: Immunofluorescence; IP: Immunoprecipitation.

Table 4. Secondary antibodies used in this work.

ANTIBODY	ORIGIN	ATTACHED TO	MANUFACTURER	USE AND DILUTION
Mouse Anti-IgG	Goat	Peroxidase	ThermoFisher	WB 1:2000
Rabbit Anti-IgG	Goat	Peroxidase	ThermoFisher	WB 1:2000
TXRD mouse anti-IgG2b	Goat	Texas Red	Molecular probes	IF 1:1000

The table indicates the secondary antibodies used, the animal origin of the antibodies, the fluorophore or enzyme to which antibodies are coupled, the manufacturer company from which the antibodies were purchased, as well as their experimental utility and the dilutions used. WB: Western blot; IF: Immunofluorescence.

18. Protein identification by liquid chromatography coupled to tandem mass spectrometry

Gel bands of interest were excised from blue native gels. All samples were reduced by adding 10 mM DTT for 30 minutes at 37°C and alkylated with 55 mM iodacetamide during 20 minutes in the dark. Next, digestion was performed by adding recombinant sequencing grade Trypsin (Roche) 1:20 (w/w) overnight at 37°C. The produced peptides were cleaned up with Omix tips (Agilent technologies), eluted with 80% ACN in 0.1% TFA, dried in a Speed-vac and resuspended in 0.1% formic acid.

To identify proteins, the resulting tryptic peptide mixtures were analyzed by nano-liquid chromatography coupled to mass spectrometry. Peptides were loaded onto a C18-A1 ASY-Column 2 cm precolumn (Thermo Fisher Scientific) and then eluted onto a Biosphere C18

analytic column (C18, inner diameter 75 µm, 15 µm long, 3 µm particle size) (NanoSeparations) and separated using a 150 min gradient from 0-45% Buffer B (Buffer A: 0.1% formic acid/2% ACN; Buffer B: 0.1% formic acid in ACN) at a flow-rate of 250 nL/min on a nanoEasy HPLC (Proxeon) coupled to a nanoelectrospay ion source (Proxeon). Mass spectra were acquired on the LTQ-Orbitrap Velos (Thermo Scientific) in the positive ion mode. Full-scan MS spectra (m/z 400-1800) were acquired in the Orbitrap at a resolution of 60,000 at m/z 400 and the 15 most intense ions were selected for collision induced dissociation (CID) fragmentation in the LTQ with a normalized collision energy of 35%. Precursor ion charge state screening and monoisotopic precursor selection were enabled. Singly charged ions and unassigned charge states were rejected. Dynamic exclusion was enabled with a repeat count of 1 and exclusion duration of 45 seconds.

Peptide identification from raw data (MS/MS spectra) was carried out using a licensed version of search engine MASCOT 2.3.0 through Proteome Discoverer Software 1.2.0.208 (Thermo Fisher Scientific). Database search was performed against a Uniprot- SwissProt with taxonomy restriction to Human (date 2012/12/11; 20233 sequences). The following parameters were used for the searches: tryptic cleavage after Arg and Lys, up to two missed cleavage sites allowed, tolerances of 10 ppm for precursor ions and 0.8 Da for MS/MS fragment ions. Oxidation of Methionine was selected as dynamic modification and carbamidomethylation of Cysteine as fixed modification. Search against decoy database (integrated decoy approach in MASCOT) was used for FDR calculation and this filter was applied to MASCOT results. The acceptance criteria for proteins identification were FDR < 1% and at least one peptide identified with high confidence (CI>95%).

19. Statistical data analysis

Unless indicated, all experiments were performed at least in triplicate and results were presented as mean ± standard deviation (SD) relative to either absolute values or percentages of the control. Statistical *p* values were obtained by application of the Mann-Whitney *U* test using the SPSS v21.0 program. $p < 0.05$ was considered to be significant.

RESULTS

CHAPTER 1. COX7A2L IS A MITOCHONDRIAL COMPLEX III BINDING PROTEIN THAT STABILIZES THE III_2+IV SUPERCOMPLEX WITHOUT AFFECTING RESPIRASOME FORMATION

1. Human COX7A2L co-localizes with respiratory chain complex III and IV and CIII-containing SCs

In humans, only one COX7A2L protein of 114 amino acids has been reported in the NCBI Gene database ([Gene ID: 9167] http://www.ncbi.nlm.nih.gov/gene/9167). The analysis of the distribution pattern of COX7A2L in relation to free MRC complexes and SCs was performed by BN-PAGE, followed by western blot, in digitonin-solubilized mitochondria from control 143B cells and in mutant cybrids lacking CI (CI-KD), CIII (CIII-KO) and CIV (CIV-KO) (Figure 14A and 14B). In controls, COX7A2L co-localized not only with SC III_2+IV and the respirasomes (SC I+III_2+IV_n), as previously described in murine models (Lapuente-Brun et al., 2013; Williams et al., 2016), but also with SC I+III_2, the CIII dimer ($CIII_2$) and monomeric CIV. The CI-KD cybrids showed a strong reduction in the levels of SC I+III_2+IV_n, SC III_2+IV and curiously, of monomeric CIV. Consistently, the amounts of COX7A2L within those structures were also reduced in the CI-defective cells compared with the controls. Lack of CIII (CIII-KO) caused the complete disruption of SC I+III_2+IV_n and SC III_2+IV, accompanied by increased levels of monomeric CIV and CIV oligomers. Only a minor residual COX7A2L signal co-migrating with free CIV was seen at the longest exposures (Figure 14C), suggesting that the lack of CIII profoundly affects the stability of COX7A2L and its binding to CIV. The CIV-KO cybrids showed the disappearance of monomeric CIV, SC III_2+IV, and SC I+III_2+IV_n, accompanied by an accumulation of SC I+III_2 and $CIII_2$. Interestingly, COX7A2L retained the ability to bind SC I+III_2 and $CIII_2$ in the absence of CIV, whereas very small amounts of COX7A2L were bound to CIV in the absence of CIII. In addition, a dramatic reduction in COX7A2L levels, comparable to that of the CIII structural subunits, was observed in the CIII-KO mutant cybrids (Figure 15). On the contrary, a slight reduction in COX7A2L levels was observed in the CIV-KO mutant, whereas no differences were observed in the CI-KD mutant, compared with the control 143B cells (Figure 15).

The presence of COX7A2L in $CIII_2$, SC I+III_2, and I+III_2+IV_n was further confirmed by high-resolution nano-LC/ESI-MS (nano-liquid chromatography/electrospray ionization-mass spectrometry) proteomics analysis. The excised blue native gel bands corresponding to SC I+III_2+IV_n in 143B cells and to SC I+III_2 and $CIII_2$ in the CIV-KO cybrids (Figure 16A) revealed the presence of the unique peptide corresponding to the COX7A2L protein (Figure 16B). This result confirmed the BNE-PAGE analyses.

Altogether, these results suggest that, in human cells, COX7A2L preferentially associates with $CIII_2$ and CIII-containing structures, and only to a minor extent with free CIV, suggesting that COX7A2L principally behaves as a CIII interactor rather than an assembly factor exclusive to CIV-containing SCs (Lapuente-Brun et al., 2013).

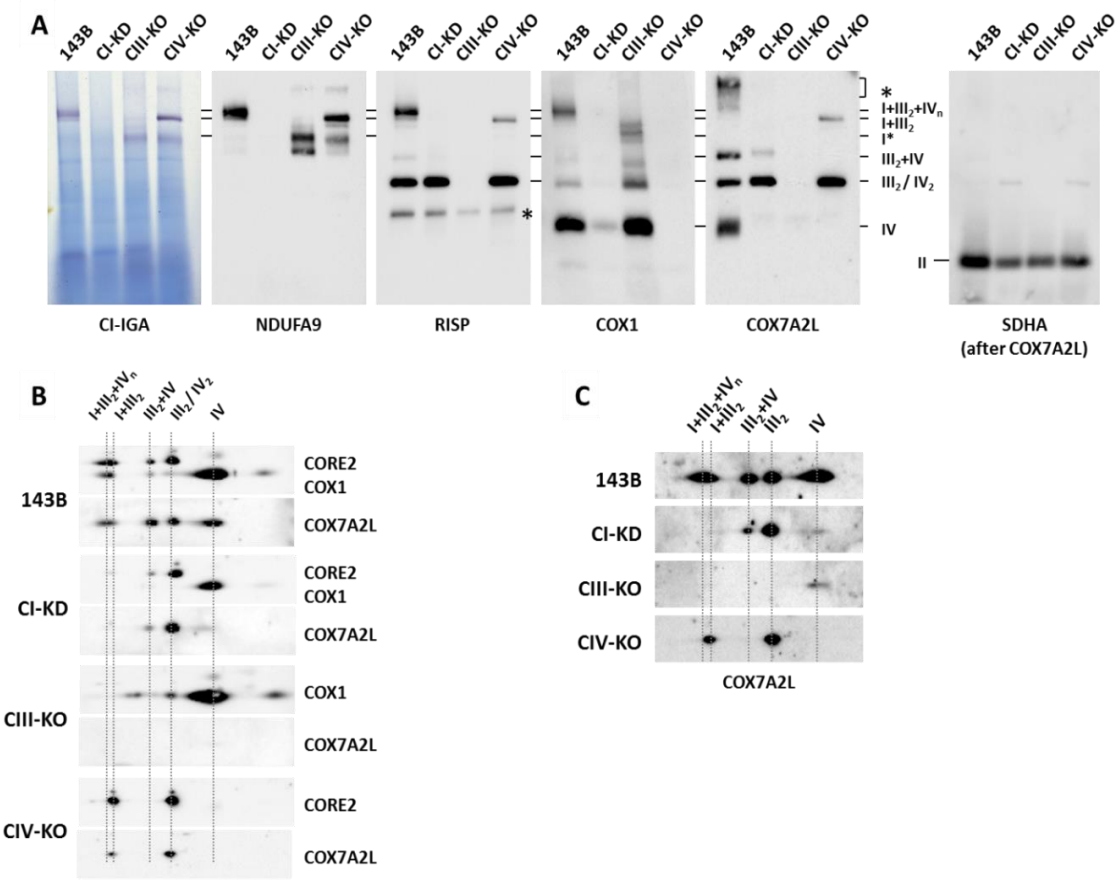

Figure 14. COX7A2L comigrates with respiratory chain supercomplexes and free complexes III and IV. Mitochondria from control 143B cells and mutant cybrids were extracted with a digitonin:protein ratio of 4 g:1 g and analyzed by BN-PAGE, followed either **(A)** by CI *in gel* activity (IGA) assay and western-blot or alternatively, **(B)** by 2D-BN/SDS-PAGE and immunoblotting with antibodies raised against human COX7A2L and the indicated OXPHOS subunits. **(C)** 2D-BN/SDS-PAGE analysis of COX7A2L distribution in control and mutant cybrids at long exposure times. $I+III_2+IV_n$, SC containing CI, CIII and CIV; $I+III_2$, SC containing CI and CIII; III_2+IV, SC containing CIII and CIV; I*, CI-containing structure; III_2, complex III dimer; IV, complex IV; IV_2, complex IV dimer; II, complex II. CIV-KO (COX1Δ cybrid).

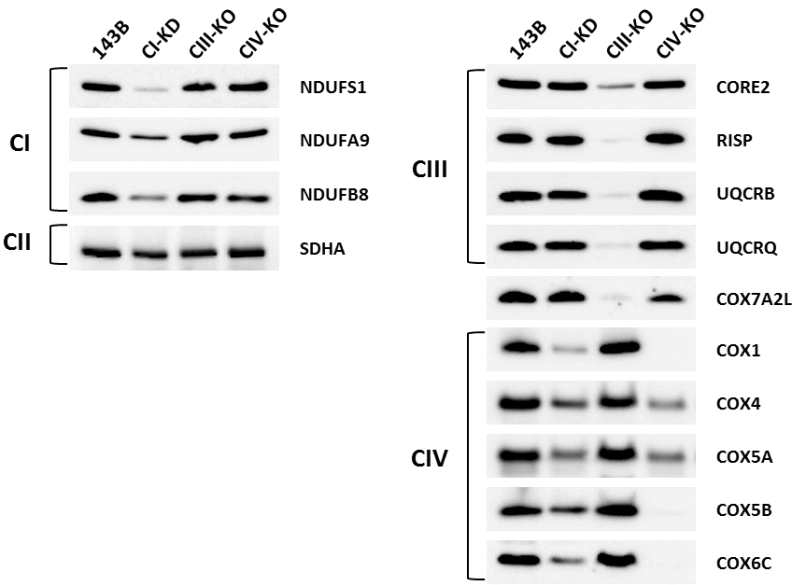

Figure 15. Comparison of the steady-state levels of MRC subunits and COX7A2L. Mitochondrial lysates from control 143B cells and mutant cybrids were analyzed by SDS-PAGE and western blot with the indicated antibodies that target COX7A2L and subunits from MRC complexes I, II, III and IV.

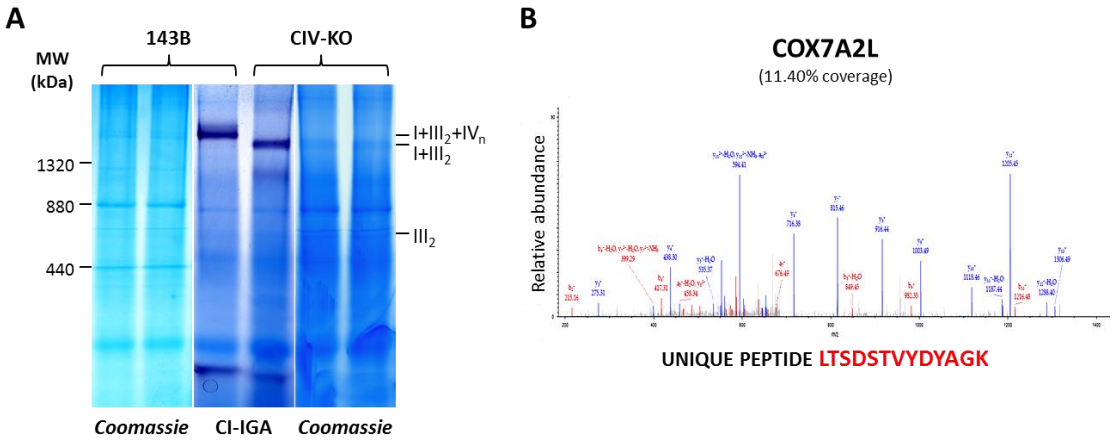

Figure 16. Proteomics for the identification of COX7A2L within MRC structures. (A) BN-PAGE and CI-IGA analysis of control 143B cells and CIV-KO mutant cybrids. After coomassie staining, the SC $I+III_2+IV_1$ band was excised from the control lane, and the bands corresponding to SC $I+III_2$ and $CIII_2$ were excised from the CIV-KO lane and subsequently analyzed by LC coupled to tandem MS (MS/MS). **(B)** MS/MS spectra from the doubly charged COX7A2L tryptic peptide unambiguously detected by LC-ESI/MS in two independent experiments per sample. The amino acids sequence of the identified COX7A2L unique peptide is highlighted in red. The most intense signals on the MS/MS spectra correspond to the main fragmentation series (b-amino and y-carboxy). Doubly charged fragments are marked with superscript 2+. $I+III_2+IV_n$, SC containing CI, CIII, and CIV; $I+III_2$, SC containing CI and CIII; III_2+IV, SC containing CIII and CIV; III_2, CIII dimer; MW, molecular weight.

2. Overexpressed COX7A2L is imported into Mitochondria and incorporated into MRC complexes and SCs, without significantly enhanced SC formation

To confirm the mitochondrial localization of human COX7A2L, control 143B cells were transfected with a construct expressing COX7A2L with a C-terminal GFP-tag, yielding a product of ~39.3 kDa (Figure 17A). COX7A2L-GFP was effectively overexpressed by ~15-fold relative to the endogenous COX7A2L. Subsequent confocal microscopy showed co-localization of COX7A2L-GFP with the ATP synthase (complex V), thus confirming the mitochondrial localization of the fusion protein (Figure 17B).

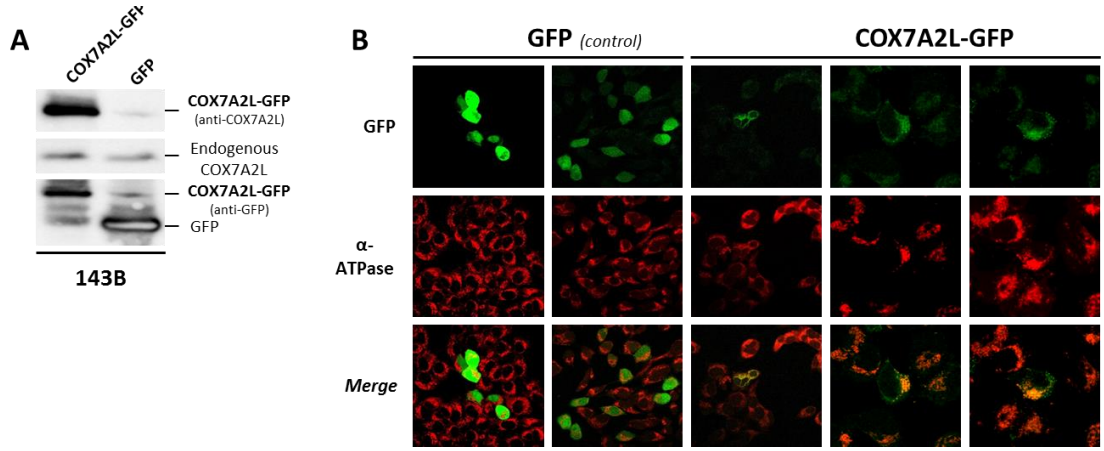

Figure 17. Tagged-COX7A2L is efficiently overexpressed in 143B cells and imported into the mitochondria. (A) Western blot analysis of the over expressed COX7A2L-GFP or GFP-empty constructs in 143B cells. **(B)** Confocal microscopy of 143B cells transiently transfected with the COX7A2L-GFP construct and with the empty-GFP vector used as a control. Upper images show the fluorescent GFP signal. Middle images show the mitochondrial network using an antibody against the ATP synthase alpha subunit. Lower images show the merge between the two signals.

Next, to examine the mitochondrial distribution of exogenous COX7A2L and the effect of COX7A2L overexpression on the assembly of the OXPHOS system, transfected exogenous COX7A2L followed by BNE-PAGE analysis was performed in the control 143B cells. To this end, 143B cells were transfected with the MYC-DDK-tagged COX7A2L construct, yielding a product of ~16.2 kDa (Figure 18A). COX7A2L-MYC-DDK was overexpressed by ~2-fold. BN-PAGE analyses confirmed the co-migration of exogenous COX7A2L with $CIII_2$, monomeric CIV, SC III_2+IV, and the respirasomes in digitonin-solubilized mitochondria (Figures 18B and 18C). In order to compare the different structures in which exogenous COX7A2L was incorporated, antibodies against CI subunit NDUFS1, CIII subunit CORE2 and CIV subunit COX5B were determined in parallel, thus showing that COX7A2L, with both tags, is efficiently incorporated into MRC complexes and SCs (Figure 18B and 18C).

Densitometry analyses of OXPHOS subunit distribution showed that the overexpression of tagged-COX7A2L induced no significant increase in the amounts of CIII- and CIV- containing structures (Figure 18D).

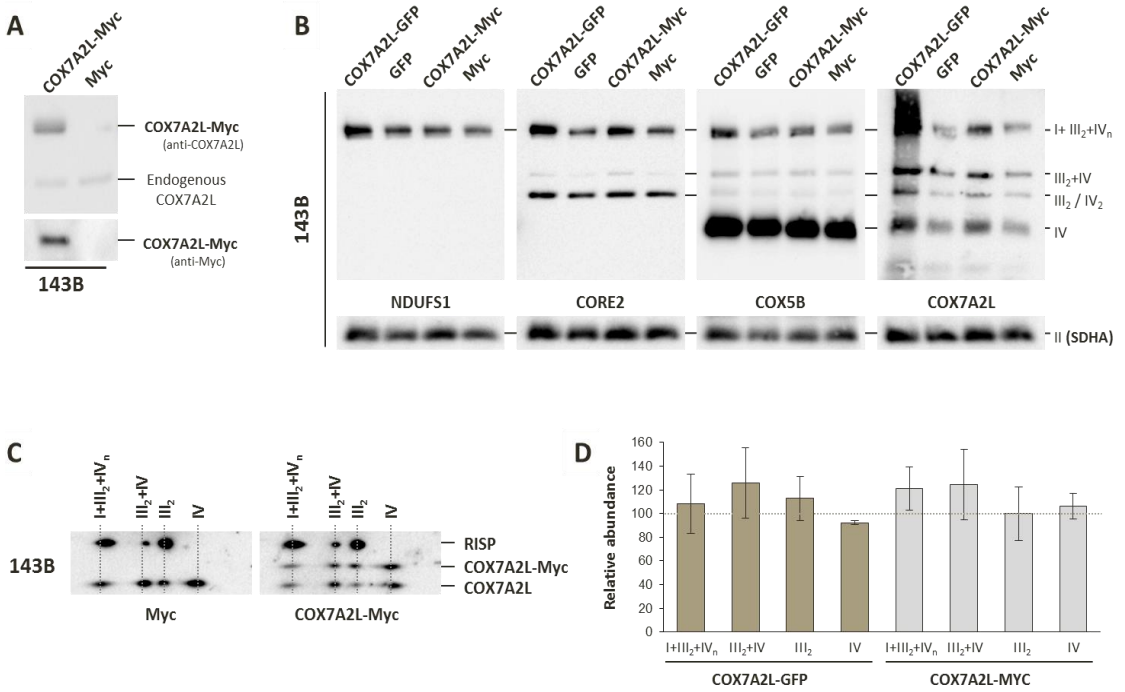

Figure 18. Overexpressed COX7A2L localizes to mitochondria with minor effects on the levels of MRC complexes and SCs. (A) Western blot analysis of the overexpressed COX7A2L-MYC-DDK construct and its corresponding empty vector (Myc) in control 143B cells. **(B)** 1D-BN-PAGE and **(C)** 2D-BN/SDS-PAGE analyses of 143B cells transiently transfected with either the COX7A2L-GFP or COX7A2L-MYC-DDK constructs and with their corresponding empty vectors. Membranes were incubated with antibodies raised against COX7A2L and the indicated OXPHOS subunits. **(D)** Densitometry analysis of the MRC complexes and SCs in 143B cells transfected with both COX7A2L-tagged constructs. The optical densities of immunoreactive bands that had not reached saturation levels were measured with the ChemiDoc MP Image Analyzer software package (Biorad). The antibody signals within the same structures were quantified; the mean values were normalized by CII and expressed as percentages of the cells transfected with the empty vectors (horizontal bar). Values represent the means ± SD from four independent experiments. $I+III_2+IV_n$, SC containing CI, CIII and CIV; $I+III_2$, SC containing CI and CIII; III_2+IV, SC containing CIII and CIV; III_2, complex III dimer; IV, complex IV; IV_2, complex IV dimer; II, complex II.

To further validate these results, the same analysis was extended to wild-type human embryonic kidney (HEK293T) cells, transfected with either the MYC-DDK-tagged COX7A2L construct or with the MYC-DDK tag alone. In HEK293T cells, COX7A2L-MYC-DDK was effectively overexpressed by ~10-fold, relative to endogenous COX7A2L (Figure 19A), and co-migrated with $CIII_2$, monomeric CIV, SC III_2+IV, and the respirasomes (SC $I+III_2+IV_n$), as observed by BN-

PAGE analysis (Figure 19B). Overexpression of tagged-COX7A2L in HEK293T cells did not alter the levels of MRC complexes or SCs.

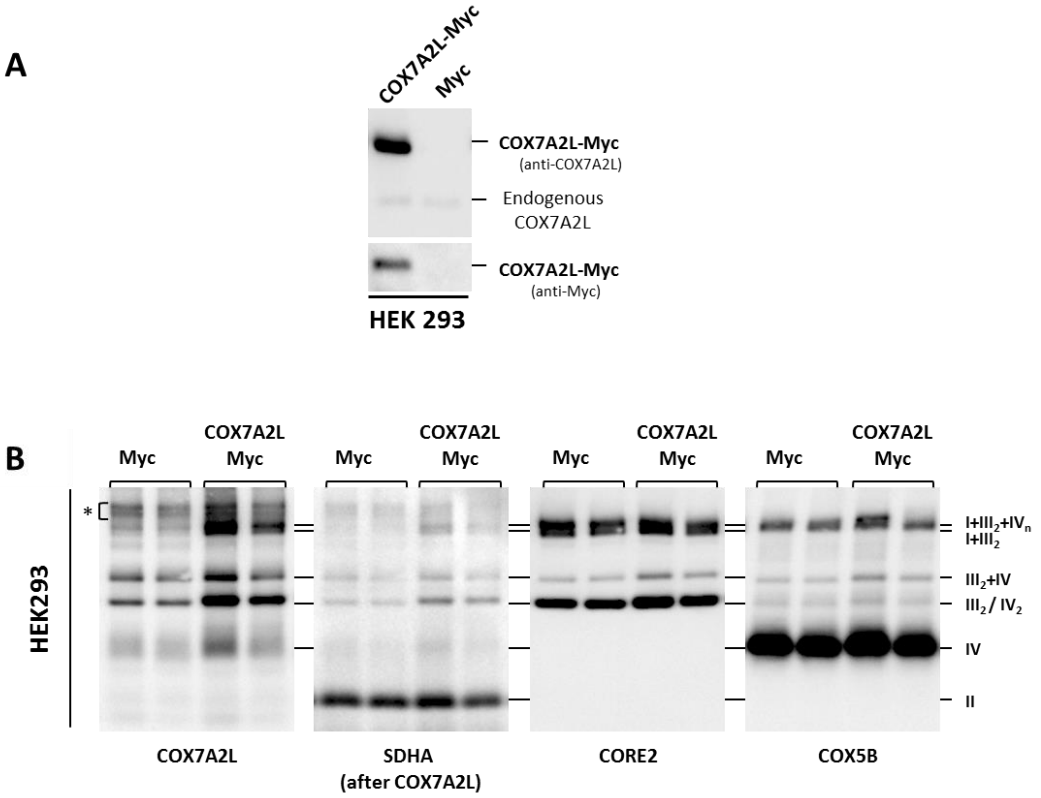

Figure 19. Overexpressed COX7A2L in HEK293T cells does not affect the levels of MRC complexes or SCs. (A) Western blot analysis of the overexpressed COX7A2L-MYC-DDK construct and its corresponding empty vector (Myc) in HEK293T cells. **(B)** BN-PAGE followed by western-blot analyses of control HEK293T cells transiently transfected either with the COX7A2L-MYC-DDK construct, or with the MYC-empty vector. Membranes were incubated with antibodies raised against COX7A2L and the indicated OXPHOS subunits. Two independent transfection experiments per experimental condition are shown on the same gel. Asterisks indicate unspecific signals that do not appear on 2D-BN/SDS-PAGE gels (see Figure 18C). $I+III_2+IV_n$, SC containing CI, CIII and CIV; $I+III_2$, SC containing CI and CIII; III_2+IV, SC containing CIII and CIV; III_2, complex III dimer; IV, complex IV; IV_2, complex IV dimer; II, complex II.

3. Overexpressed COX7A2L binds to CIII and CIV

To test whether the COX7A2L co-localization with MRC CIII and CIV was due to a direct physical interaction, co-immunoprecipitation assays were performed in digitonin-solubilized mitochondrial lysates from HEK293T cells transfected with either the COX7A2L-MYC-DDK construct or with the empty vector (Figure 20A). Immunoprecipitation with an anti-DDK antibody specifically pulled down the tagged-COX7A2L protein in cells overexpressing COX7A2L-MYC-DDK. In addition, the CIII subunits CORE1, CORE2, CYC1, RISP, and UQCRQ and the CIV subunits COX1, COX4, COX5B, and COX6C were detected in the co-immunoprecipitate (coIP). The CI subunits NDUFA9 and NDUFS1 were barely detectable, and CII was not detected in the coIP samples. When reverse immunoprecipitation assays were performed using antibodies against CORE2 (Figure 20B) or COX1 (Figure 20C) proteins, both the tagged and the endogenous COX7A2L proteins were successfully pulled down. Importantly, immunoprecipitation with CORE2 (but not with COX1) pulled down the endogenous COX7A2L protein in cells transfected with the empty vector (Figures 20B and 20C). These results suggest that COX7A2L physically interacts with CIII and CIV but it presents a higher affinity for CIII.

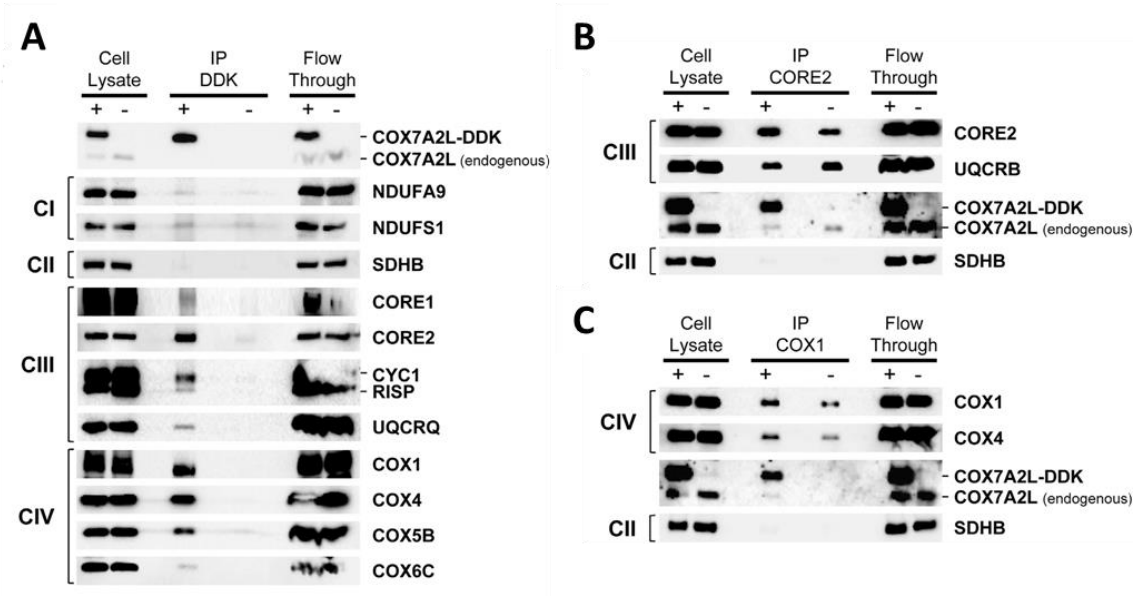

Figure 20. COX7A2L physically binds to CIII and CIV. (A) COX7A2L co-immunoprecipitation assay. Digitonin-solubilized mitochondrial extracts (4 g digitonin/1 g protein) from HEK293T cells transiently transfected with either the COX7A2L-MYC-DDK construct (+) or with the empty vector (-) were immunoprecipitated using an anti-DDK antibody. The same digitonin-solubilized mitochondrial extracts were used for reverse co-immunoprecipitation using antibodies against **(B)** CORE2 or **(C)** COX1. Samples were subsequently analyzed by SDS-PAGE and western blot with the indicated antibodies. IP, immunoprecipitate.

4. Endogenous COX7A2L associates with respiratory chain CIII and CIV and with SCs during their assembly process

Once the structural relationship between COX7A2L and the MRC complexes and SCs was confirmed, our next step was to analyze the assembly kinetics of COX7A2L into those structures by using doxycycline-induced reversible inhibition of mitochondrial translation in control 143B cells (Moreno-Lastres et al., 2012). Doxycycline was removed from cell-culture media after 6 days of treatment, and samples were collected at different time points (0, 6, 15, 24, 48, 72, and 96 hours). To follow the integration of endogenous COX7A2L into newly assembled CIII, CIV, and SCs, digitonin-solubilized mitochondria were separated by 2D-BN/SDS-PAGE and subsequently analyzed by western blot using antibodies that recognize COX7A2L and CORE2 (CIII), RISP (CIII), and COX5A (CIV) (Figure 21A). Signals from at least three independent experiments were quantified by densitometry and normalized to CII levels, and values were expressed relative to the levels in untreated cells (SS) (Figure 21B-E). After 6 days of doxycycline treatment (time 0 hours, 0h), there was a drastic decrease (80%–95%) in the levels of $CIII_2$, CIV, SC III_2+IV, and SC I+III_2+IV_n, as well as in the levels of COX7A2L that co-localizes with these structures. The CII levels remained normal after doxycycline treatment, as expected (Moreno-Lastres et al., 2012), because this complex lacks mtDNA encoded subunits. Once mitochondrial translation resumed (times 6 to 96 hours, 6h-96h) a gradual increase in the levels of the COX7A2L protein that co-localized with $CIII_2$ was observed. The incorporation of COX7A2L into $CIII_2$ occurred in parallel to the insertion of the CORE2 subunit, which forms a partially-assembled pre-CIII prior to the incorporation of RISP (Figure 21B). In contrast, CIV levels increased prior to the binding of COX7A2L (Figure 21C). Moreover, COX7A2L was incorporated into SC III_2+IV in parallel with the CORE2 and COX5A subunits, but again prior to the integration of RISP in this structure (Figure 21D). The incorporation of COX7A2L into the respirasomes occurred in parallel with CORE2 and COX5A, and earlier than the integration of RISP (Figure 21E).

In order to compare the assembly rates of COX7A2L within the different structures, the densitometric values corresponding to the accumulation of COX7A2L in $CIII_2$, CIV, SC III_2+IV and SC I+III_2+IV were drew together (Figure 22A and 22B). Interestingly, once COX7A2L had bound to CIV, there was a simultaneous accumulation of COX7A2L within CIV and SC III_2+IV.

Altogether, these results suggest that COX7A2L associates with $CIII_2$ during its assembly course, that it binds to CIV once this complex is fully assembled, and that it is incorporated into SC III_2+IV and SC I+III_2+IV_n before their formation is completed.

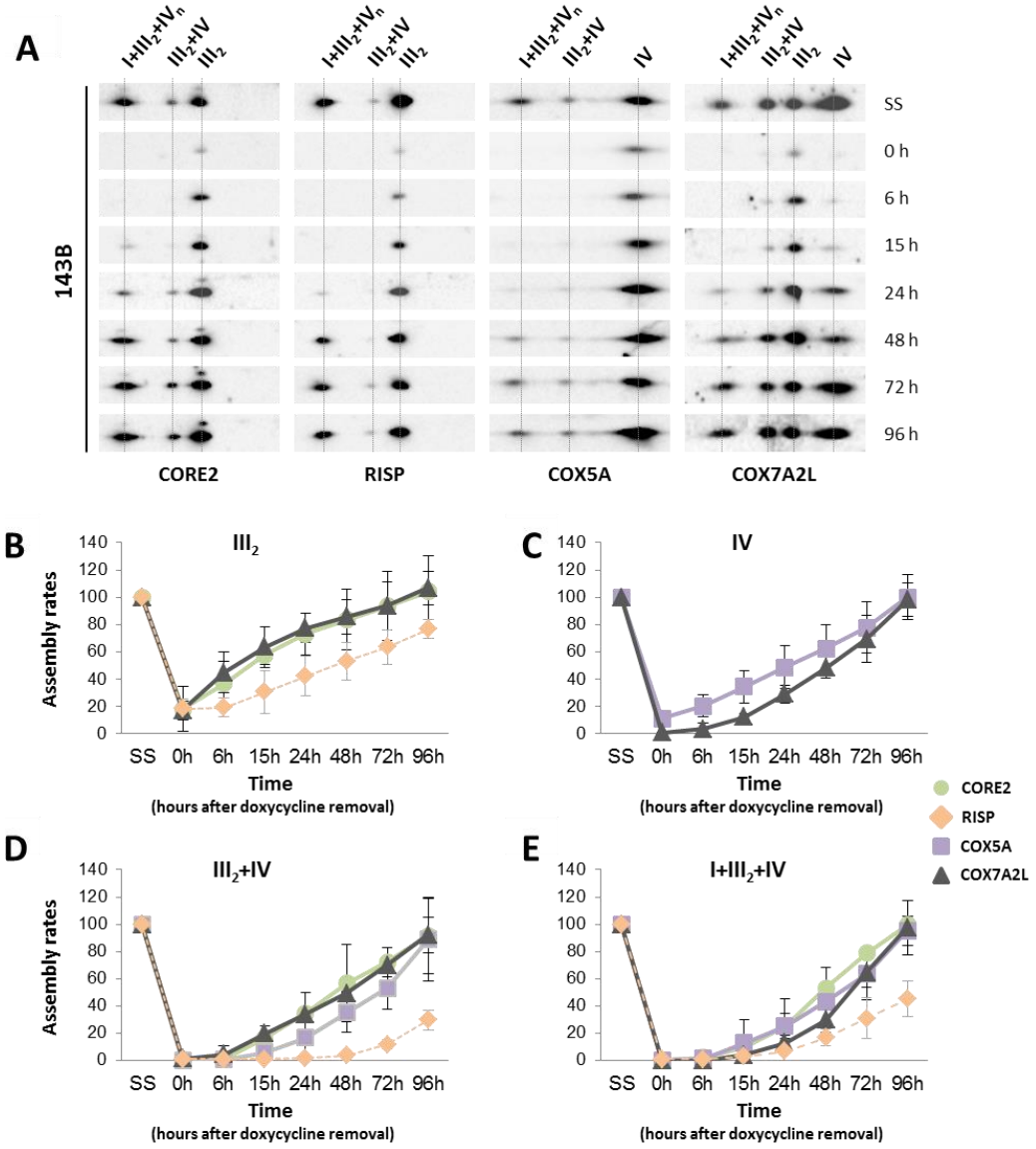

Figure 21. Comparison of the assembly kinetics of COX7A2L, CORE2, RISP and COX5A in CIII- and CIV-containing structures. (A) Mitochondria from doxycycline-treated 143B cells were extracted with a digitonin:protein ratio of 4 g:1 g and analyzed by 2D BN/SDS-PAGE and western blot with the indicated antibodies. **(B-E)** Densitometric profiles representing the incorporation rates of COX7A2L into $CIII_2$, CIV, SC III_2+IV and SC I+III_2+IV_n relative to the CIII subunits RISP and CORE2 and to the CIV subunit COX5A. The signals from three independent experiments were quantified and normalized by CII. Time point values are expressed as percentages of the untreated cells (SS) and indicated as means ± SD. I+III_2+IV_n, SC containing CI, CIII, and CIV; III_2+IV, SC containing CIII and CIV; III_2, CIII dimer; IV, CIV.

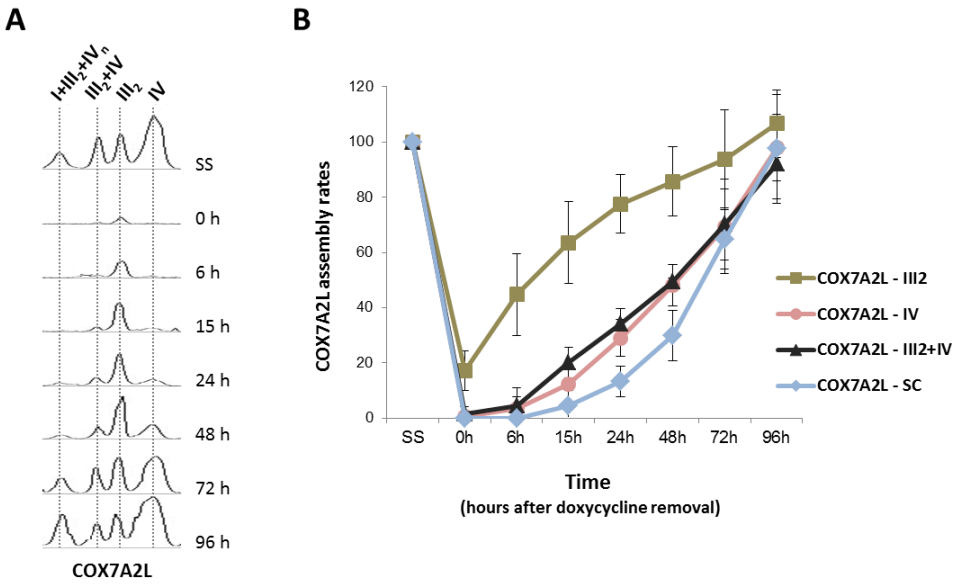

Figure 22. Assembly kinetics of COX7A2L in CIII- and CIV- containing structures. (A) Densitometric profiles representing the assembly progress of COX7A2L in CIII- and CIV- containing structures. **(B)** Mean incorporation rates of COX7A2L into CIII- and CIV- containing structures. The signals from three independent experiments were quantified and normalized by CII. Time point values are expressed as percentages of the untreated cells (SS) and indicated as means ± SD. I+III_2+IV_n, SC containing CI, CIII, and CIV; III_2+IV, SC containing CIII and CIV; III_2, CIII dimer; IV, CIV.

5. COX7A2L associates with CIII and SC III_2+IV prior to the insertion of the RISP catalytic subunit

In the reported CIII assembly models, incorporation of CORE2 allows the formation of a non-functional intermediate called pre-CIII, which contains CORE2 and the rest of the CIII subunits except RISP and the smallest subunit (Qcr10 in yeast, UQCR11 in mammals), which are incorporated at a later assembly stage (Fernández-Vizarra and Zeviani, 2015; Smith et al., 2012). This late assembly step is promoted by LYRM7/MZM1L, an assembly factor that binds RISP to stabilize it prior to its incorporation into CIII. HeLa cells that stably overexpress hemagglutinin (HA)- tagged MZM1L showed sequestering of RISP in a small subcomplex, thereby preventing CIII maturation (Sánchez et al., 2013).

Doxycycline experiments suggested that human COX7A2L could be a component of pre-CIII, as this protein gets incorporated into CIII in parallel with the CORE2 subunit but before the incorporation of RISP (Figure 21B). To confirm this hypothesis, the COX7A2L distribution was analyzed by 1D-BN-PAGE in digitonin-solubilized mitochondria isolated from HeLa cells overexpressing MZM1L (Figure 23). As observed by CI *in-gel* activity (IGA) assay, MZM1L overexpression induced a decrease in the levels and activity of the respirasomes (SC I+III_2+IV_n),

as well as an accumulation of CI- containing structures (Figure 23A). The levels of the RISP subunit were strongly decreased in the respirasomes, in SC III_2+IV, and in $CIII_2$, and there was a parallel accumulation of RISP in a small subcomplex that also contains MZM1L-HA (Sánchez et al., 2013) (Figure 23B). Upon MZM1L/LYRM7 overexpression, CORE2 and COX7A2L co-segregated with pre-SC III_2+IV and pre-CIII. Altogether, these results confirm that COX7A2L associates with pre-CIII before the incorporation of RISP takes place.

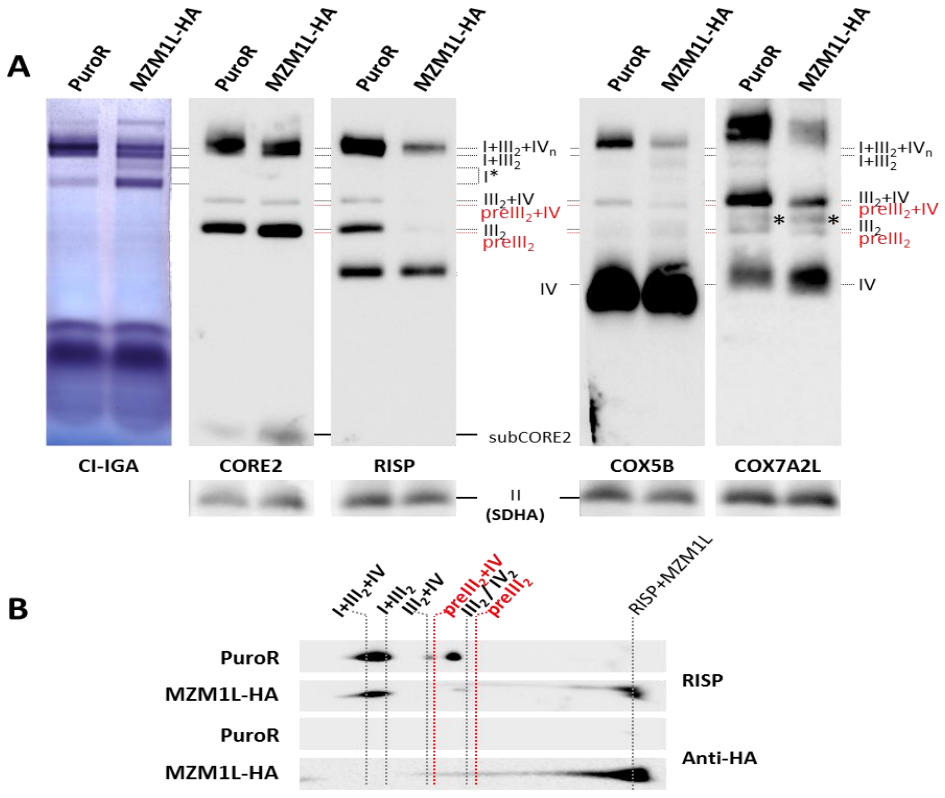

Figure 23. COX7A2L binds to CIII assembly intermediates. (A) Digitonin-solubilized mitochondrial extracts (4 g digitonin/1 g protein) from HeLa cells transduced with the MZM1L-HA construct or with the empty vector (PuroR) were analyzed by BN-PAGE and CI-IGA assays or, alternatively, by western blot and immunodetection. Asterisks indicate unspecific signals that do not appear on 2D BN/SDS-PAGE gels. **(B)** Subsequent 2D-BN/SDS-PAGE and western blot analyses were performed with antibodies against RISP and the HA epitope. $I+III_2+IV_n$, SC containing CI, CIII, and CIV; $I+III_2$, SC containing CI and CIII; I*, CI-containing structure; III_2+IV, SC containing CIII and CIV; pre-III_2+IV, SC containing pre-CIII and CIV; III_2, CIII dimer; pre-III_2, pre-CIII lacking the RISP subunit; IV, CIV; IV_2, CIV dimer; II, CII. Subcomplexes that contain CORE2 and COX1 are indicated as subCORE2 and subCOX1, respectively. The association of RISP and MZM1L is indicated as RISP+MZM1L.

6. COX7A2L downregulation causes SC III_2+IV disassembly without altering respirasome stability

In order to investigate if COXA2L exerted a possible role on the biogenesis of the OXPHOS structures, transient knockdown (KD) of COX7A2L was carried out using a mix of two small interfering RNAs (siRNAs) targeting exons 2 and 3 of *COX7A2L* mRNA. The *COX7A2L*-KD efficiency was analyzed by SDS-PAGE of whole-cell protein extracts from control 143B cells and COX1Δ (CIV-KO) mutant cybrids (Figure 24A). *COX7A2L* RNAi effectively knocked down the COX7A2L protein by 80% in the 143B cells and by 74% in the CIV-KO mutant, compared with cells transfected with unspecific scrambled siRNAs (C- in Figure 24A and 24B). Next, the effects of *COX7A2L* silencing on the assembly of the OXPHOS system were analyzed by BN-PAGE in combination with CI-IGA and western blot analyses of mitochondrial-enriched fractions from 143B and CIV-KO cells (Figure 24C). Upon *COX7A2L*-KD, there was a significant decrease in the signals of COX7A2L that co-localized with $CIII_2$, monomeric CIV, and SCs III_2+IV, I+III_2, and I+III_2+IV_n. Despite the severe drop in COX7A2L levels, only a specific reduction in the levels of SC III_2+IV was observed in the 143B cells, whereas CI activity and the levels of free OXPHOS complexes and the respirasomes were normal.

To gain deeper insight into the nature of SC III_2+IV disruption in 143B cells, 2D-BN/SDS-PAGE and western blot analyses were carried out with antibodies against CORE2 (CIII), RISP (CIII), COX1 (CIV), and COX5B (CIV) (Figure 25A). Densitometric quantification from five independent experiments (Figures 25B-E) showed that *COX7A2L*-KD specifically led to a significant decrease in the levels of the four analyzed MRC subunits within SC III_2+IV, but not in the remainder CIII- and CIV-containing structures. Moreover, *COX7A2L* silencing did not result in a clear accumulation of intermediates smaller than $CIII_2$ and CIV, suggesting that their assembly and/or stability are not disturbed.

In agreement with these results, *COX7A2L*-KD in the CIV-KO mutant cybrids produced no significant alterations in the levels of $CIII_2$ or SC I+III_2 (Figures 26A-C).

Altogether, our results suggest that COX7A2L has a specific role in the stabilization of SC III_2+IV.

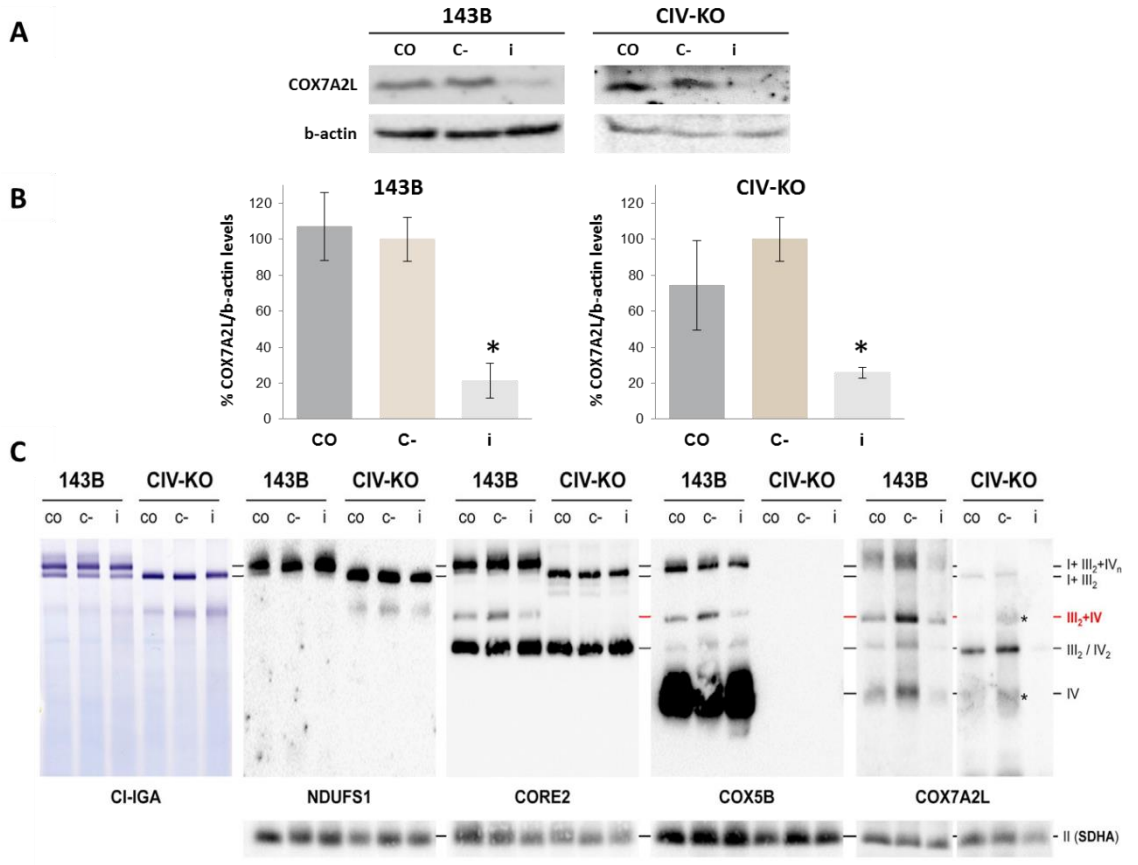

Figure 24. *COX7A2L* knock-down in human cells specifically decreases the levels of SC III_2+IV. (A) To characterize the functional role of COX7A2L in the OXPHOS system, silencing assays were performed with a mix of two *COX7A2L* siRNAs in control 143B cells as well as in mutant cybrids lacking complex IV (CIV-KO). Upon two rounds of transfection and silencing for 48 hours, cells were collected and whole cell extracts were analyzed by SDS-PAGE and western blot using antibodies targeted against COX7A2L and β-actin as a loading control. **(B)** The COX7A2L signals from five independent siRNA silencing experiments were quantified, normalized by β-actin and expressed as the percentages relative to the cells transfected with the scramble siRNA (C-). **(C)** Mitochondria from untreated (CO), mock-transfected (C), and *COX7A2L* siRNA-transfected (i) 143B cells and CIV-KO mutants were extracted with a digitonin:protein ratio of 4 g:1 g and analyzed by BN-PAGE, followed by CI-IGA assays, or alternatively, by western blot and immunodetection with the indicated antibodies. Asterisks indicate unspecific signals that do not appear on 2D-BN/SDS-PAGE gels. I+III_2+IV_n, SC containing CI, CIII and CIV; I+III_2, SC containing CI and CIII; III_2+IV, SC containing CIII and CIV; III_2, complex III dimer; IV, complex IV; IV_2, complex IV dimer; II, complex II; CO, cells only treated with the transfection reagent; C-, cells transfected with a scrambled siRNA; i, cells transfected with a combination of two specific *COX7A2L* siRNAs.

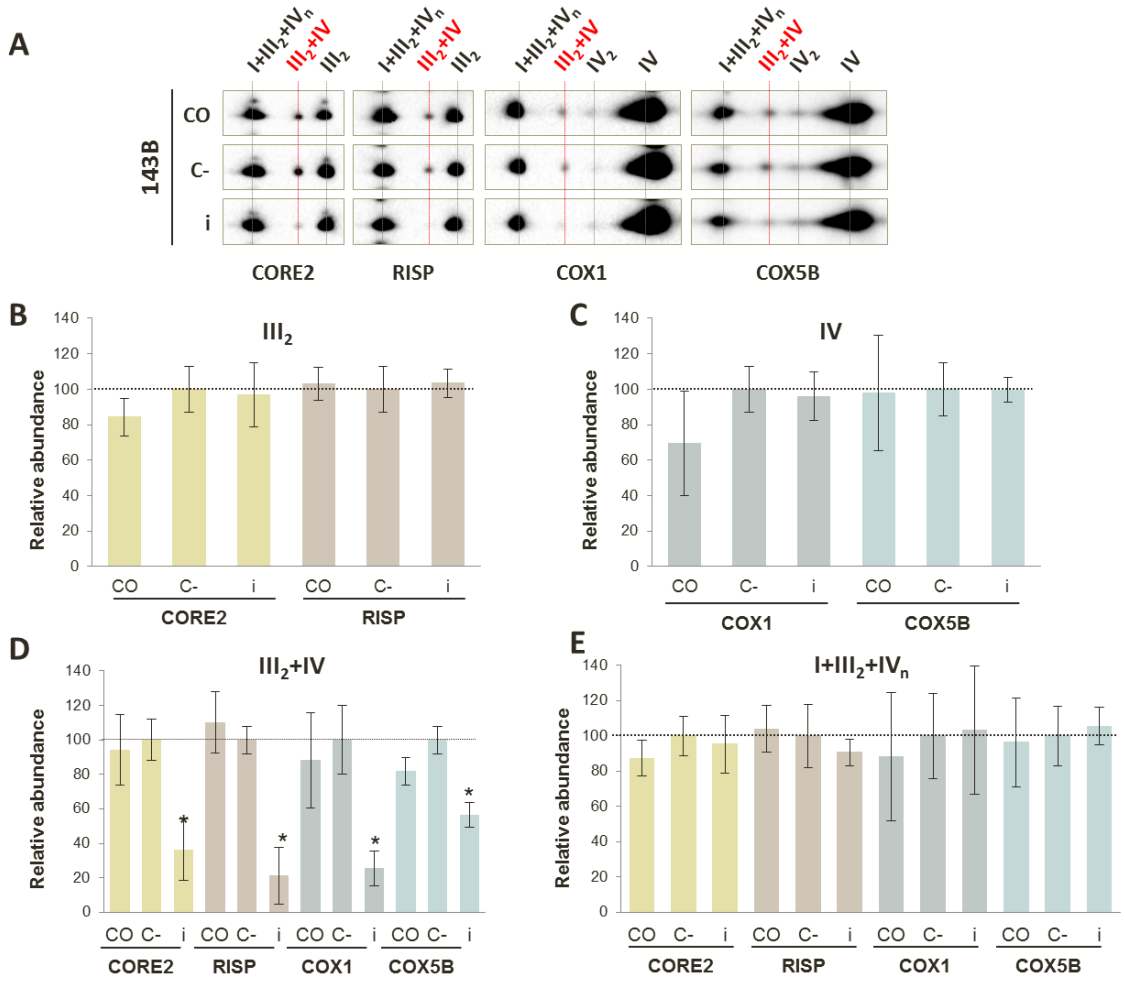

Figure 25. *COX7A2L* downregulation in 143B cells specifically decreases the levels of SC III_2+IV without affecting respirasome biogenesis. (A) Mitochondria from untreated (CO), mock-transfected (C), and *COX7A2L* siRNA-transfected (i) 143B cells were extracted with a digitonin:protein ratio of 4 g:1 g and analyzed by 2D-BN/SDS-PAGE followed by western blot analyses and immunodetection with the indicated antibodies. To address the relative amounts of **(B)** $CIII_2$, **(C)** CIV, **(D)** SC III_2+IV and **(E)** SC $I+III_2+IV_n$ in 143B cells upon *COX7A2L* silencing, the optical densities of immunoreactive bands that had not reached saturation levels were measured with the ImageLab™ software of the ChemiDoc™ MP Image Analyzer (Biorad). The signals from each antibody within the different structures were quantified, normalized by CII, and indicated as means ± SD from five independent siRNA experiments. Values are expressed as percentages of the cells transfected with scramble RNA (C, horizontal bar). $I+III_2+IV_n$, SC containing CI, CIII, and CIV; $I+III_2$, SC containing CI and CIII; III_2+IV, SC containing CIII and CIV; III_2, CIII dimer; IV, CIV; IV_2, CIV dimer; II, CII. *$p < 0.05$, Mann-Whitney *U* test.

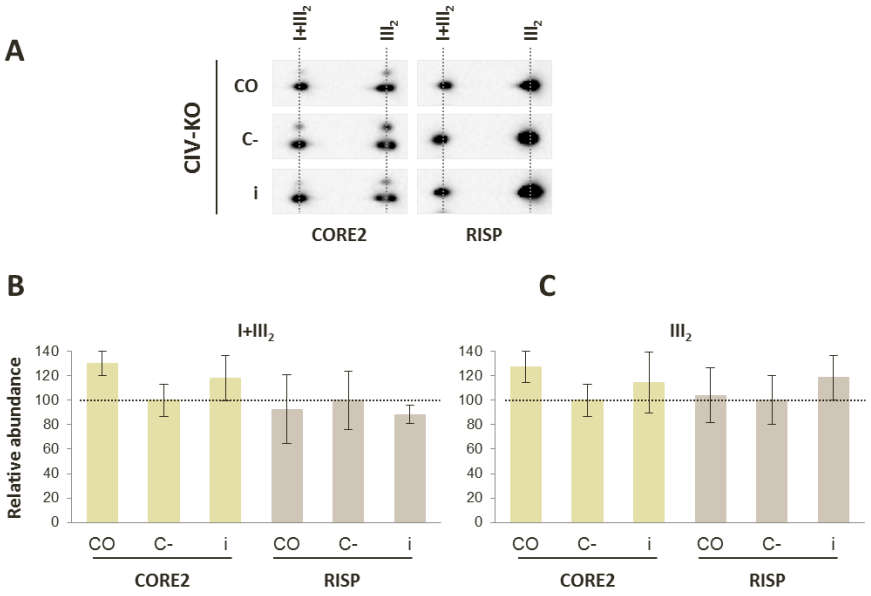

Figure 26. *COX7A2L* down regulation in CIV-KO mutant cybrids does not alter the biogenesis of OXPHOS structures. (A) Mitochondria from untreated (CO), mock-transfected (C), and *COX7A2L* siRNA-transfected (i) CIV-KO cells were extracted with a digitonin:protein ratio of 4 g:1 g and analyzed by 2D-BN/SDS-PAGE followed by western blot analyses and inmunodetection with CIII subunits CORE2 and RISP. To address the relative amounts of **(B)** $CIII_2$ and **(C)** SC $I+III_2$ in the CIV-KO mutants upon *COX7A2L* silencing, the signals from each antibody within these structures were quantified, normalized by CII, and indicated as means ± SD from three independent siRNA experiments. Numerical values are expressed as percentages of the signals obtained for each antibody in cells transfected with the scramble RNA (C-, represented as a horizontal bar). $I+III_2$, SC containing CI and CIII; III_2, CIII dimer.

7. COX7A2L downregulation does not affect the respiratory chain function

To further investigate the possible effect of COX7A2L on the MRC function, oxygen consumption rates (OCRs) were measured in 143B cells, yielding no significant differences between *COX7A2L*-silenced cells and cells transfected with scrambled siRNAs (Figure 27A). In contrast, mitochondrial respiration was drastically reduced in the CI-KD cybrids (used as an internal experimental control) that retained SC III_2+IV but showed minimal levels of CI and the respirasomes, in comparison with 143B cells (Figure 27B). Respiratory chain activities measured in *COX7A2L*-silenced 143B cells were also comparable to the activities in control cells (Figure 27C). These results show that a substantial loss of COX7A2L and SC III_2+IV has no significant impact on MRC function in human cultured cells.

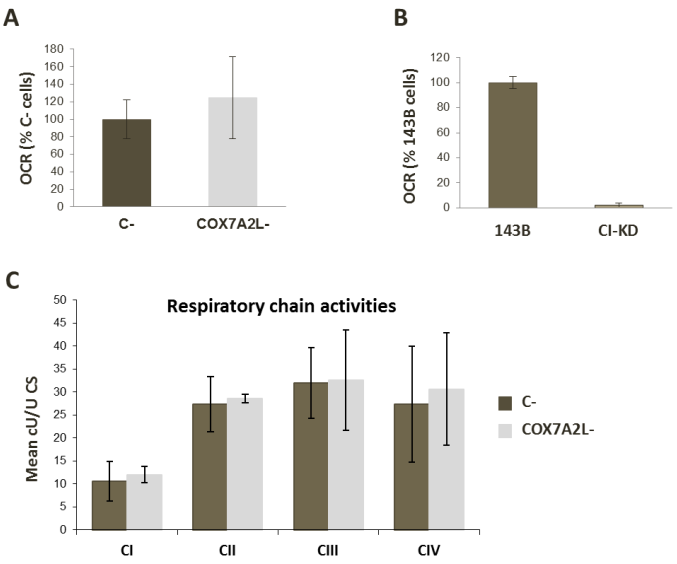

Figure 27. *COX7A2L* down regulation does not affect mitochondrial function. (A) Oxygen consumption rates (OCR) measured in 143B cells respiring in 1 g/l glucose-containing medium that were previously transfected either with a scrambled siRNA (C-, negative control), or with a combination of two specific *COX7A2L* siRNAs (COX7A2L-). Ten measurements per sample were performed each time in three independent experiments. Data are expressed as the mean± standard deviation of the percentages of the negative control. **(B)** Oxygen consumption rates (OCR) measured in control 143B cells and CI-defective mutant cybrids (CI-KD) respiring in 1 g/l glucose-containing medium. Five measurements per sample were performed each time in two independent experiments. Data are expressed as the mean± range of the percentages of the control 143B cells. OCR values were calculated in pmol O_2.min^{-1}.µg $protein^{-1}$ in all experiments. **(C)** Spectrophotometric measurements of the individual activities of MRC complexes I to IV (CI-CIV) in 143B cells transfected either with a scrambled siRNA (C-), or with a mix of two specific *COX7A2L* siRNAs (COX7A2L-). Enzyme activities are expressed as cU/U citrate synthase (CS).

8. Mouse Cox7a2l is essential for SC III_2+IV formation

Finally, in order to shed light on the contradictory conclusions regarding Cox7a2l function in murine models (Ikeda et al., 2013; Lapuente-Brun et al., 2013; Mourier, Matic, et al., 2014; Williams et al., 2016), several experiments using isolated heart mitochondria from CD1 and C57BL/6 mouse strains were carried out. First, the Cox7a2l levels relative to OXPHOS subunits were analyzed by western blot in CD1 mice versus C57BL/6J, C57BL/6N (Lrpprc wt) and *Lrpcc* KO mice (Figure 28A). The CD1 mice express high levels of a 113-amino acids Cox7a2l protein isoform (long Cox7a2l), whereas C57BL/6 mice express low levels of a shorter and unstable Cox7a2l protein isoform of 111 amino acids (short Cox7a2l). CI, CIII and CIV subunits were present at similar levels in all wild-type CD1, C57BL/6J, and C57BL/6N mouse strains. However, the levels of Cox7a2l and CIII subunits were slightly increased in the CIV-deficient conditional *Lrpprc* KO mice compared with their wild-type littermates, all of them maintained on the

C57BL/6N genetic background (Mourier, Ruzzenente, et al., 2014). These data suggest that COX7A2L, as well as CIII, is stabilized in the *Lrpprc* KO mice possibly as a response to the severe CIV deficiency. BN-PAGE followed by IGA assays (Figure 28B) and 2D-BN/SDS-PAGE analysis (Figure 28C) of digitonin-solubilized heart mitochondria from CD1, C57BL/6 and *Lrppc* KO mice confirmed similar activities of the respirasomes in all the wild-type strains (Figure 28B) and a strong reduction of CIV activity in the *Lrppc* KO mice compared to littermate controls. Analysis of the COX7A2L distribution in CD1 mice (Figure 28C) showed its preferential co-segregation with monomeric CIV, SC III_2+IV and the respirasomes and, to a minor extent, with $CIII_2$. In the wild-type C57BL/6 mice, however, COX7A2L was mostly found in CIII-containing structures (Figure 28C). These data suggest that the reduction in COX7A2L levels mostly hampers the binding of COX7A2L to CIV, which, nevertheless, only provoked the disappearance of SC III_2+IV without affecting the levels of monomeric CIV and the respirasomes, or the enzymatic activities of the MRC complexes (Figure 28B and 28C). Next, DDM-solubilized mouse heart mitochondria was examined, a condition in which respirasomes are disrupted (Figure 28D). The co-segregation between COX7A2L and monomeric CIV was totally lost, suggesting that their interaction is, indeed, labile. In CD1 mice, both COX7A2L and the CIII subunit CORE2 co-localized with dimeric CIII and SC III_2+IV, whereas in C57BL/6 mice, both proteins only were present in $CIII_2$.

To test whether the respirasome stability depends on COX7A2L levels, heart mitochondria from CD1 and C57BL/6J mice were exposed to increasing amounts of the detergent digitonin, followed by 1D-BN-PAGE analysis (Figure 29). Respirasome levels and MRC organization were comparable between both mouse strains at low digitonin-to-protein ratios. Even under the most stringent detergent conditions, respirasomes were still detectable in the C57BL/6J mice, albeit at slightly lower levels than those in the CD1 mice. Noteworthy, SCs from both mouse strains reorganized in different ways upon increasing digitonin concentrations, and some respirasome bands appeared to be more stable in C57BL/6J than in CD1 mice and vice versa. Altogether, these data indicate that COX7A2L is essential for SC III_2+IV stability but dispensable for the respirasomes formation and maintenance.

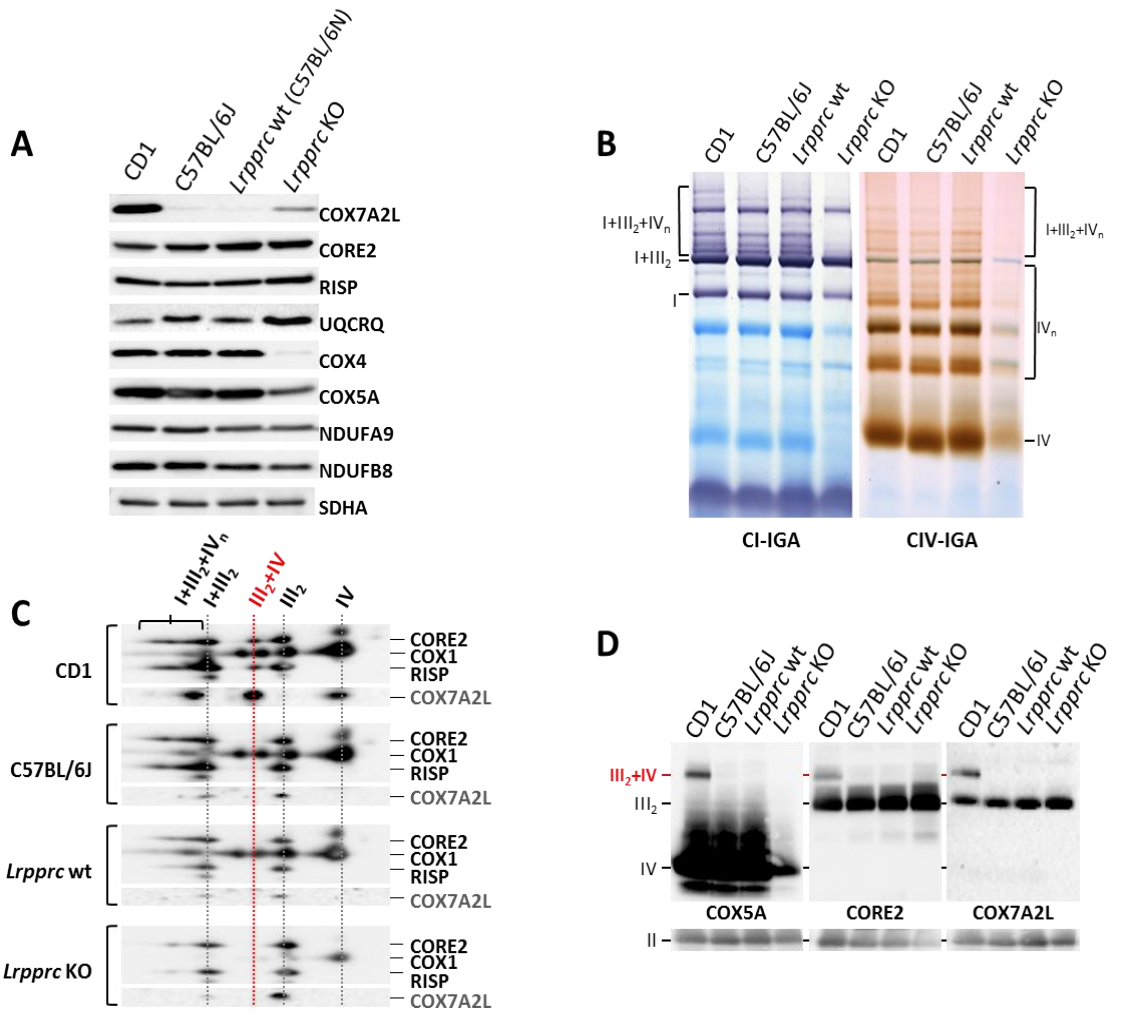

Figure 28. Mouse Cox7a2l is required for SC III_2+IV assembly. (A) Heart mitochondrial extracts from CD1 and C57BL/6J mouse strains, and from control littermates (*Lrpprc* wt) and *Lrpprc* deficient mice (*Lrpprc* KO) with a C57BL/6N genetic background, were analyzed by western blot with antibodies raised against COX7A2L and the indicated OXPHOS subunits. **(B)** Supramolecular organization of the respiratory chain in heart mitochondria from wild-type (wt) CD1, C57BL/6J, and C57BL/6N (*Lrpprc* wt) mouse strains, as well as from *Lrpprc*-deficient (KO) mice. Mitochondria were extracted with a digitonin:protein ratio of 4 g:1 g and analyzed by 1D-BN-PAGE, followed by CI and CIV-IGA assays, or by **(C)** 2D-BN/SDS-PAGE analyses followed by western blot and immunodetection with antibodies against COX7A2L and the indicated OXPHOS subunits. **(D)** Mitochondrial samples were solubilized with 2% DDM, which disrupts respirasomes and CIV oligomers but maintains SC III_2+IV and free complexes, and were next analyzed by BN-PAGE followed by western blot and immunodetection with the indicated antibodies. $I+III_2+IV_n$, SC containing CI, CIII, and CIV; $I+III_2$, SC containing CI and CIII; III_2+IV, SC containing CIII and CIV; III_2, CIII dimer; IV, monomeric CIV; IV_n, CIV oligomers.

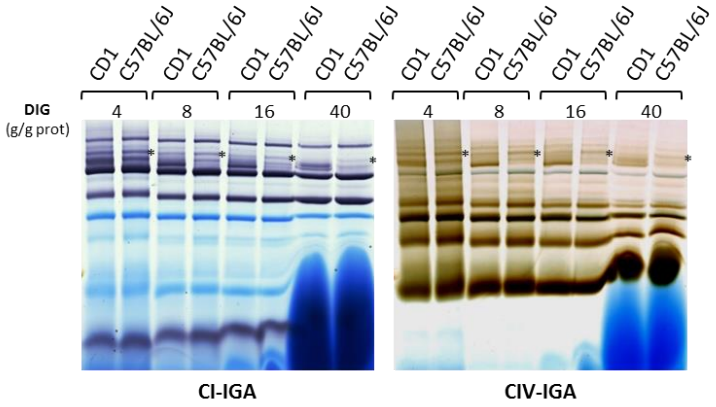

Figure 29. The lack of Cox7a2l does not affect the stability of the respirasomes in mice heart mitochondria. Heart mitochondria from CD1 and C57BL/6J mouse strains were extracted with increasing ratios of digitonin to mitochondrial protein (ranging from 4 to 40 g/g) and analyzed by 1D-BN-PAGE followed by CI-IGA or CIV-IGA assays. Asterisks indicate the presence of respirasome bands that are more stable in the mitochondria from C57BL/6J mice.

CHAPTER 2. MITOCHONDRIAL COX7A2L REGULATES THE BIOENERGETIC RATES OF DIMERIC COMPLEX III AND OF COMPLEX III-CONTAINING SUPERCOMPLEXES TO FINE TUNE SUCCINATE OXIDATION

1. TALEN-mediated generation of *COX7A2L* knockout (KO) cell lines

All our previous results indicated that COX7A2L preferentially interacts with mitochondrial $CIII_2$ and, to a minor extent, with monomeric CIV to promote the stabilization of SC III_2+IV in both mice and humans. However, COX7A2L would have no determinant role in the biogenesis, stabilization, or function of the free OXPHOS complexes or in the formation of the respirasomes I+III_2+IV_{0-2}. The experimental approach used in human cell lines consisted on the transient silencing of the expression of *COX7A2L* mRNA, which still yielded low levels of the COX7A2L protein and therefore, results were not fully conclusive.

To further determine the requirement of human COX7A2L for the formation and function of respiratory chain SCs, stable human *COX7A2L* knockout (KO) HEK293T cell lines were created using the TALEN gene editing approach (Christian et al., 2010; Li et al., 2011). A TALEN pair was designed to target a region within the first exon of the *COX7A2L* gene immediately downstream the start codon (Figure 30A). HEK293T cells were co-transfected with the TALEN pair and subsequently, single clones were isolated by size cell sorting and analyzed for out-of-frame mutations leading to COX7A2L protein loss. More than 100 clones were screened by immunoblotting from cell extracts using a specific anti-COX7A2L antibody. Five promising candidates were selected, that completely lacked the COX7A2L protein (Figure 30B). The *COX7A2L* gene was sequenced in two of these clones and found to carry KO mutations. Clone KO1 (C2E11) is homozygous and clone KO2 (C1C3) is compound heterozygous, both carrying *COX7A2L* alleles with short deletions involving the start codon and leading to the complete absence of COX7A2L (Figure 30C).

2. *COX7A2L*-KO cells display absence of SC III_2+IV with normal respirasome levels and increased $CIII_2$ levels and activity

To analyze the pattern of supramolecular assemblies of MRC complexes resulting from the total absence of COX7A2L in human cells, mitochondria-enriched fractions from wild type HEK293T (WT), KO1 and KO2 clones were analyzed by BN-PAGE followed by CI-*in gel* activity (IGA) assays and immunoblotting (Figure 31A). Subsequently, 2D-BN/SDS-PAGE was performed to analyze in detail the pattern of SCs in *COX7A2L*-KO cells and the co-localization of COX7A2L with all MRC structures in WT cells (Figure 31B). As previously observed in silenced COX7A2L cells, the total absence of COX7A2L led to the disappearance of the SC III_2+IV, whereas the respirasomes were detected in the *COX7A2L*-KO clones at levels similar to the WT. However some SCs larger than the respirasome I+III_2+IV_1 (indicated with an asterisk), occasionally appeared to be at lower levels in some experiments. These observations suggest that these

MRC structures assemble in the absence of COX7AL, but might be more labile than in WT mitochondria. Although our previous results suggested that COX7A2L associates with pre-$CIII_2$ before the incorporation of the RISP subunit (Figures 21 and 23), RISP assembly was not affected in *COX7A2L*-KO cells as it was detected in $CIII_2$, and in SCs $I+III_2$ and $I+III_2+IV_{1-n}$. However, the accumulation of $CIII_2$ was significantly increased by 2-3-fold in the absence of COX7A2L (Figure 31C). In agreement, spectrophotometric measurements of MRC enzyme activities showed that CIII activity was specifically enhanced by 20-40% in the KOs (Figure 31D), consistent with the accumulation of $CIII_2$ in these cells.

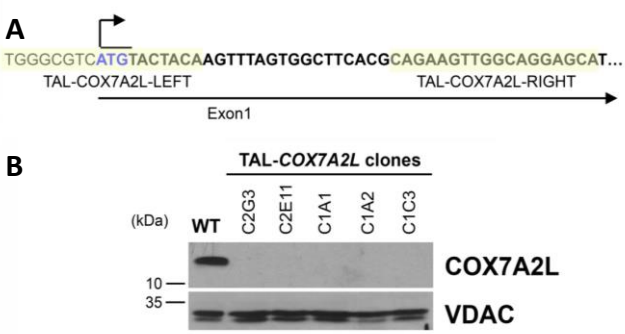

C

	TAL Clones	*COX7A2L* Genotype	DNA	Protein
KO1	C2E11	Mut. Homo	c.-1_13del	p.0
KO2	C1C3	C. Hetero	c.-1_8del/ c.-11_8del	p.0/ p.0

Figure 30. TALEN-mediated generation of *COX7A2L*-KO clones in HEK293T cells. (A) Schematic representation of the first exon of the *COX7A2L* locus and the sequences of the recognition sites of the two TALEN pairs. **(B)** Immunoblot analysis of the steady state levels of COX7A2L in HEK293T (WT) and TALEN-transfected HEK293T cell lines. VDAC was used as a loading control. **(C)** *COX7A2L* alleles in TAL-*COX7A2L* clones. The DNA numbering refers to the coding sequence (c.) and the protein (p.) number to the predicted full polypeptide (den Dunnen and Antonarakis, 2000). C: compound; Mut: mutant; Hetero: heterozygous; Homo: homozygous; del: deletion; -: position before starting ATG.

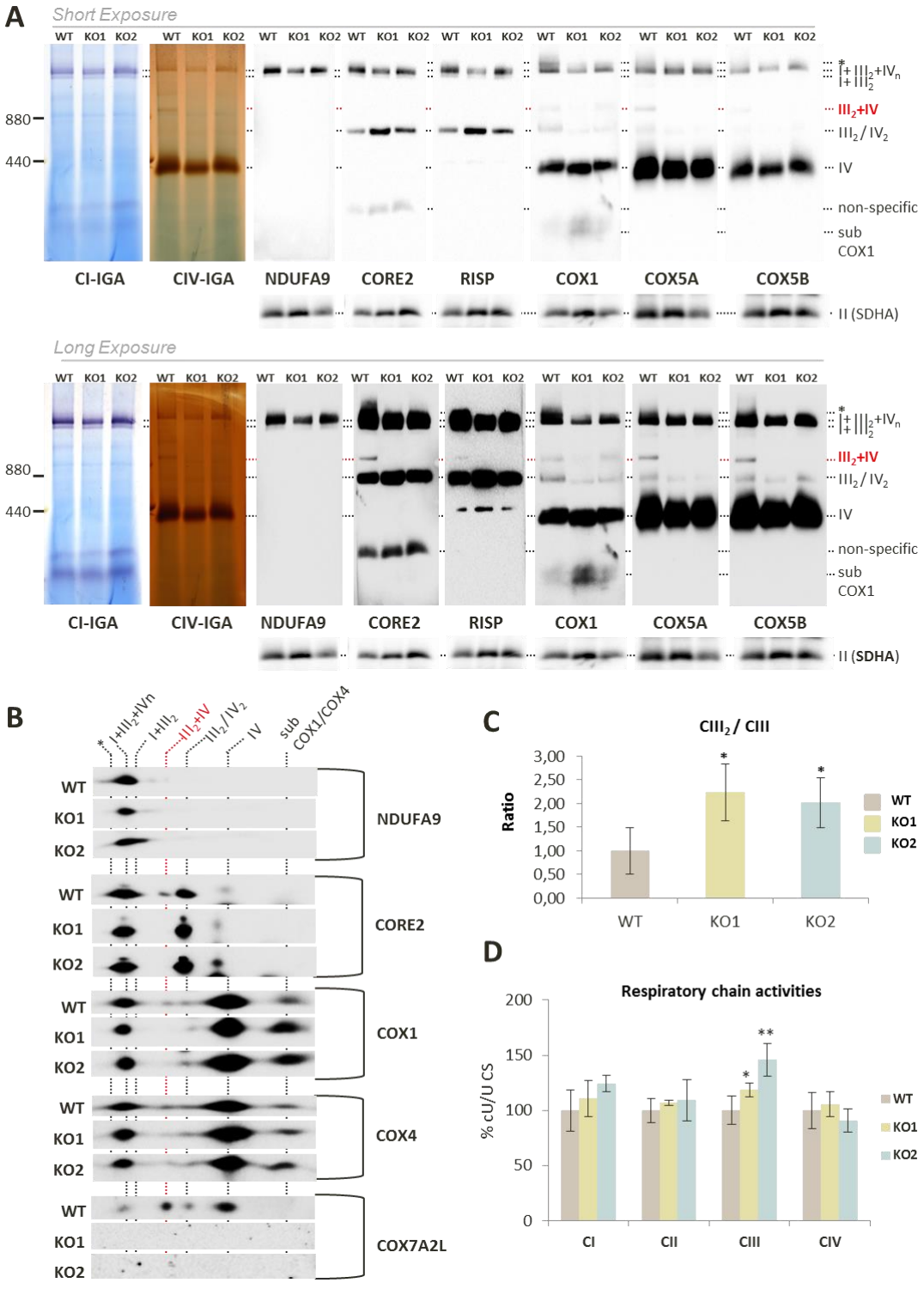

Figure 31. COX7A2L-KO cells display absence of SC III_2+IV with normal respirasome levels and altered accumulation of $CIII_2$. (A) Mitochondria extracted with a digitonin:protein ratio of 4:1 (g/g) and analyzed by 1D-BN-PAGE, followed by CI- and CIV-IGA assays, or alternatively, by immunoblotting using the indicated antibodies. Short and long exposures of the immunoblotting are shown. **(B)** Subsequent 2D-BN/SDS-PAGE and immunoblot analyses were performed with antibodies against COX7A2L and the indicated OXPHOS subunits. **(C)** To address the relative amount of $CIII_2$ in *COX7A2L*-KO cells, the signals from the CORE2 antibody from four BN-PAGE experiments were quantified by densitometry, normalized

by CII and indicated as mean ± SD. **(D)** Spectrophotometric measurements of the individual activities of MRC complexes I to IV (CI-CIV) in WT and *COX7A2L*-KO cells. Enzyme activities are expressed as cU/U citrate synthase (CS). Error bars represent the mean ± SD of four repetitions. **P* < 0.05, ***P* < 0.01. $I+III_2+IV_n$, SCs containing CI, $CIII_2$ and CIV; $I+III_2$, SC containing CI and $CIII_2$; III_2+IV, SC containing $CIII_2$ and CIV; III_2, complex III dimer ($CIII_2$); IV, complex IV; IV_2, complex IV dimer (CIV_2); II, complex II. Subcomplexes that contain COX1 and COX4 are indicated. Apparent subcomplexes that contain CORE2 are antibody artifacts that disappear in 2D-BN/SDS-PAGE gels.

3. The absence of COX7A2L does not affect the stability of the respirasomes

To assess whether the stability of the respirasomes depends on COX7A2L, mitochondria-enriched fractions from WT and *COX7A2L*-KO cells were exposed to varying concentrations of digitonin and the extracts were analyzed by BN-PAGE followed by CI- and CIV-IGAs or immunoblotting (Figures 32 and 33). Stringent SCs extraction conditions using increasing (4-40 mg/mg) digitonin-to-protein ratios (Figure 32) led to a parallel disintegration of the respirasomes (SCs $I+III_2+IV_{1-2}$) and consequent accumulation of SC $I+III_2$ and free CI in both cell types. Only when an extremely harsh 40 mg/mg digitonin:protein ratio was used, the respirasomes were slightly more unstable in *COX7A2L*-KO than in WT cells. Milder SCs extraction conditions using decreasing (4-1 mg/mg) digitonin-to-protein ratios (Figure 33), revealed no differences in the levels of SCs $I+III_2+IV_{1-n}$ between *COX7A2L*-KO and WT cells**,** but a clear decrease in the abundance of larger SCs (indicated with an asterisk) in *COX7A2L*-KO cells. Altogether, these results suggest that COX7A2L may be required for the normal assembly or stability of larger megastructures. On the contrary, the abundance and stability of monomeric and dimeric CIV were not affected by the absence of COX7A2L (Figures 32 and 33).

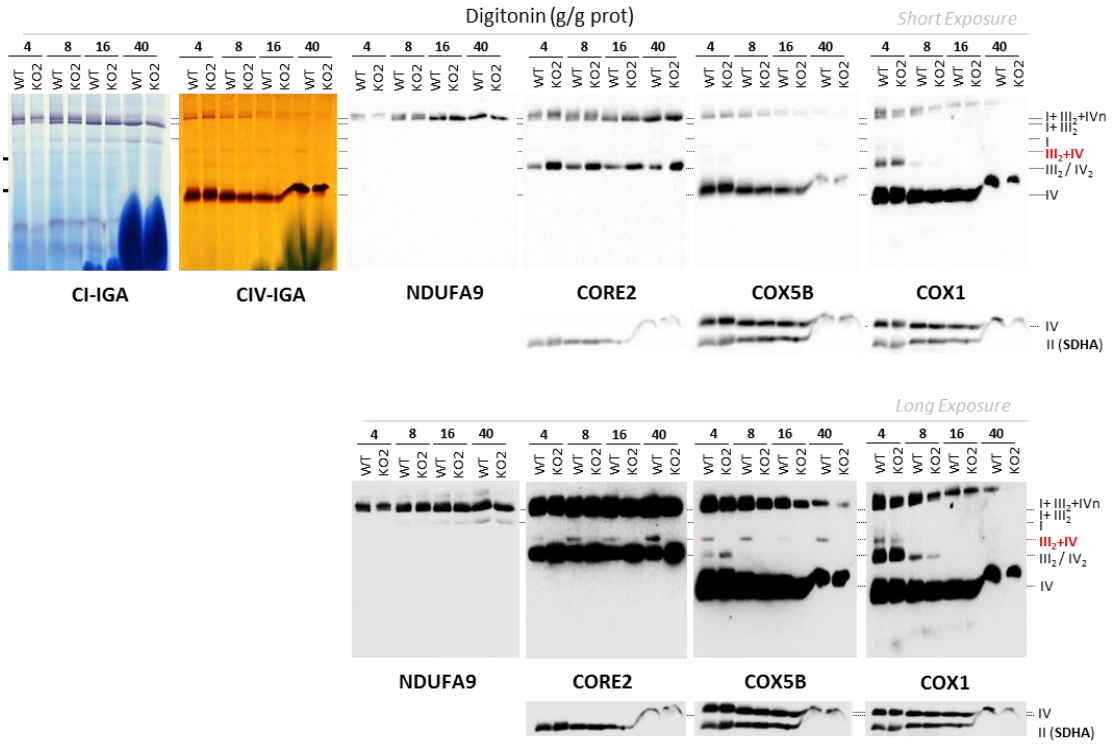

Figure 32. The absence of COX7A2L does not affect the stability of the respirasomes. Mitochondrial were extracted with increasing ratios of digitonin to mitochondrial protein (ranging from 1 to 40 g/g) and analyzed by 1D-BN-PAGE followed by CI-IGA and CIV-IGA assays. Subsequent western blot analysis was performed with antibodies for subunits NDUFA9 of CI, CORE2 of CIII and COX5B of CIV. Respirasome levels and organization are comparable between both control HEK293T (WT) cells and the *COX7A2L*-KO clone 2 (KO2) under the most stringent detergent conditions. $I+III_2+IV_n$, SC containing CI, CIII and CIV; $I+III_2$, SC containing CI and CIII; III_2+IV, SC containing CIII and CIV; III_2, complex III dimer; IV, complex IV; IV_2, complex IV dimer; II, complex II.

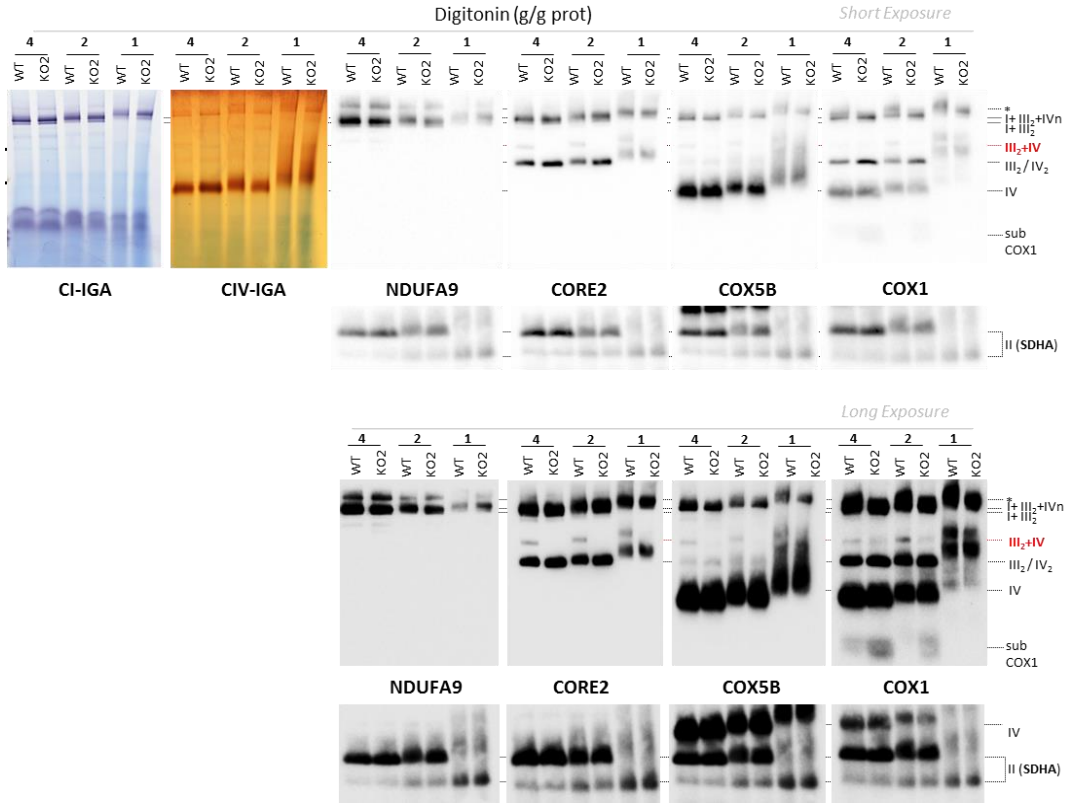

Figure 33. The absence of COX7A2L hampers the accumulation of MRC structures larger than respirasomes. Mitochondrial were extracted with decreasing ratios of digitonin to mitochondrial protein (ranging from 1 to 40 g/g) and analyzed by 1D-BN-PAGE followed by CI-IGA and CIV-IGA assays. Subsequent western blot analysis was performed with antibodies for subunits NDUFA9 of CI, CORE2 of CIII and COX5B of CIV. Respirasome levels and organization are comparable between both control HEK293T (WT) cells and the *COX7A2L*-KO clone 2 (KO2) under the low digitonin-to-protein ratios. $I+III_2+IV_n$, SC containing CI, CIII and CIV; $I+III_2$, SC containing CI and CIII; III_2+IV, SC containing CIII and CIV; III_2, complex III dimer; IV, complex IV; IV_2, complex IV dimer; II, complex II.

4. Overexpressed COX7A2L restores the wildtype phenotype in *COX7A2L*-KO cells

All the phenotypes described in *COX7A2L*-KO cells in sections 2, 3 and 4, particularly the absence of SC III_2+IV and the accumulation of $CIII_2$, were specific since they were restored by the overexpression of recombinant COX7A2L-Myc-DDK in both KOs (Figure 34), thus eliminating the possibility of off-target effects that could have arisen during the *COX7A2L* gene-disruption. Tagged-COX7A2L incorporated into the same MRC structures as the endogenous COX7A2L (Figure 34B), and its mild overexpression (2-3 fold) (Figure 34A) did not induce any aberrant phenotype (Figure 34C).

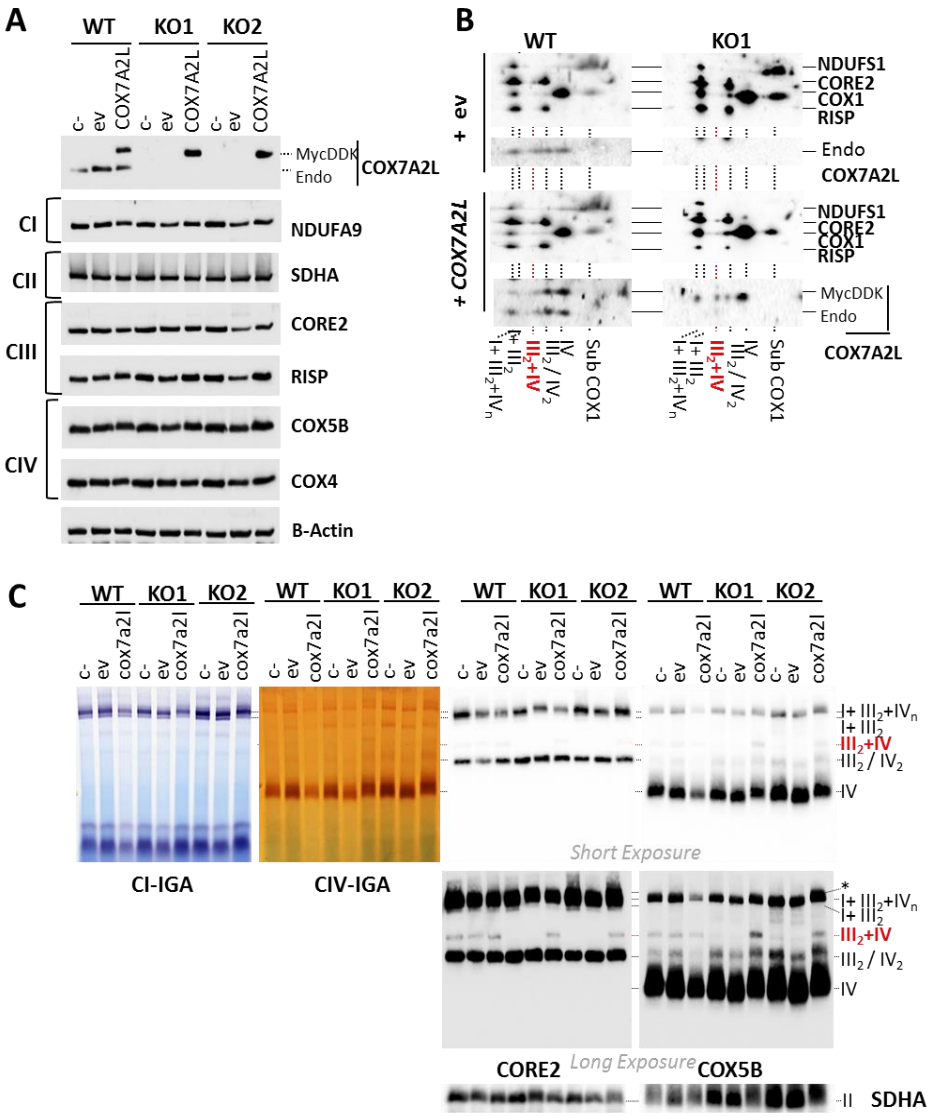

Figure 34. Tagged-COX7A2L interacts with MRC complexes and supercomplexes and restores SC III_2+IV. (A) Immunoblot analysis of the untreated (c-), empty vector (ev) or overexpressed COX7A2L-Myc-DDK (COX7A2L) constructs in control HEK293T cells (WT) and two *COX7A2L*-KO clones (KO1 and KO2). Membranes were incubated with antibodies raised against the indicated OXPHOS subunits and the antibody against COX7A2L to differentiate endogenous COX7A2L (~12.6 kDa) from exogenous COX7A2L-Myc-DDK (~16.2 kDa). **(B)** Digitonin-solubilized mitochondrial extracts (4g digitonin/1 g protein) from control HEK293T cells (WT) and *COX7A2L*-KO clone 2 (KO2) stably transfected with either the *COX7A2L*-Myc-DDK construct or with the empty vector were analyzed by 2D-BN/SDS-PAGE and immunoblotting. **(C)** 1D-BN-PAGE was followed by CI-IGA, CIV-IGA and immunoblotting with the indicated antibodies. I+III_2+IV_n, SCs containing CI, $CIII_2$ and CIV; I+III_2, SC containing CI and $CIII_2$; III_2+IV, SC containing $CIII_2$ and CIV; III_2, complex III dimer ($CIII_2$); IV, complex IV (CIV); IV_2, complex IV dimer (CIV_2); II, complex II. Subcomplexes that contain COX1 are indicated as subCOX1.

5. *COX7A2L*-KO cells display a boost in $CIII_2$ biogenesis in parallel with slower assembly kinetics of the respirasomes

The assembly kinetics of MRC complexes and SCs were next analyzed by doxycycline-induced reversible inhibition of mitochondrial translation in WT and *COX7A2L*-KO cells. Doxycycline was removed from the cell culture media after 6 days of treatment, and samples were collected at different time points (0, 6, 15, 24, 48 and 72 hours). To follow the reappearance of newly-assembled $CIII_2$, CIV, CIV_2 and SCs, digitonin-solubilized mitochondria was separated by 1D-BN-PAGE and subsequently analyzed by either CI-IGA assays (Figure 35A) or western blot using antibodies that recognize CORE2 (CIII) and COX5A (CIV) (Figure 35B). Following 6 days of doxycycline treatment (time 0h) only residual levels of CI, CIV and $CIII_2$ (5-10% of untreated cells) were detected in either control or KO cells. The treatment did not affect CII levels, as expected, since this complex lacks mtDNA-encoded subunits (Figure 35B). Once mitochondrial translation resumed (times 6-72 hours), the SC III_2+IV formed *de novo* only in the WT cells (Figures 35B and 35C). The levels of CIV and CIV_2 increased at similar rates in WT and *COX7A2L*-KO cells (Figures 35B and 35C), ruling out a possible role for COX7A2L in the biogenesis of this complex. On the contrary, the rate of $CIII_2$ biogenesis, as shown for its steady-state levels in Figure 31, was markedly higher in the KOs than in the WT cells (Figures 35B and 35C). These data suggest a dysregulation of $CIII_2$ levels in the absence of COX7A2L. Strikingly, the reappearance of the respirasomes I+III_2+IV_{1-n} was clearly delayed in the *COX7A2L*-KO cells (Figures 35A-C), but it reached levels comparable to the WT at later time-points and in the steady-state (previously shown in Figure 31). These results suggest that although the lack of COX7A2L does not prevent the formation of the respirasomes, it hampers their assembly efficiency.

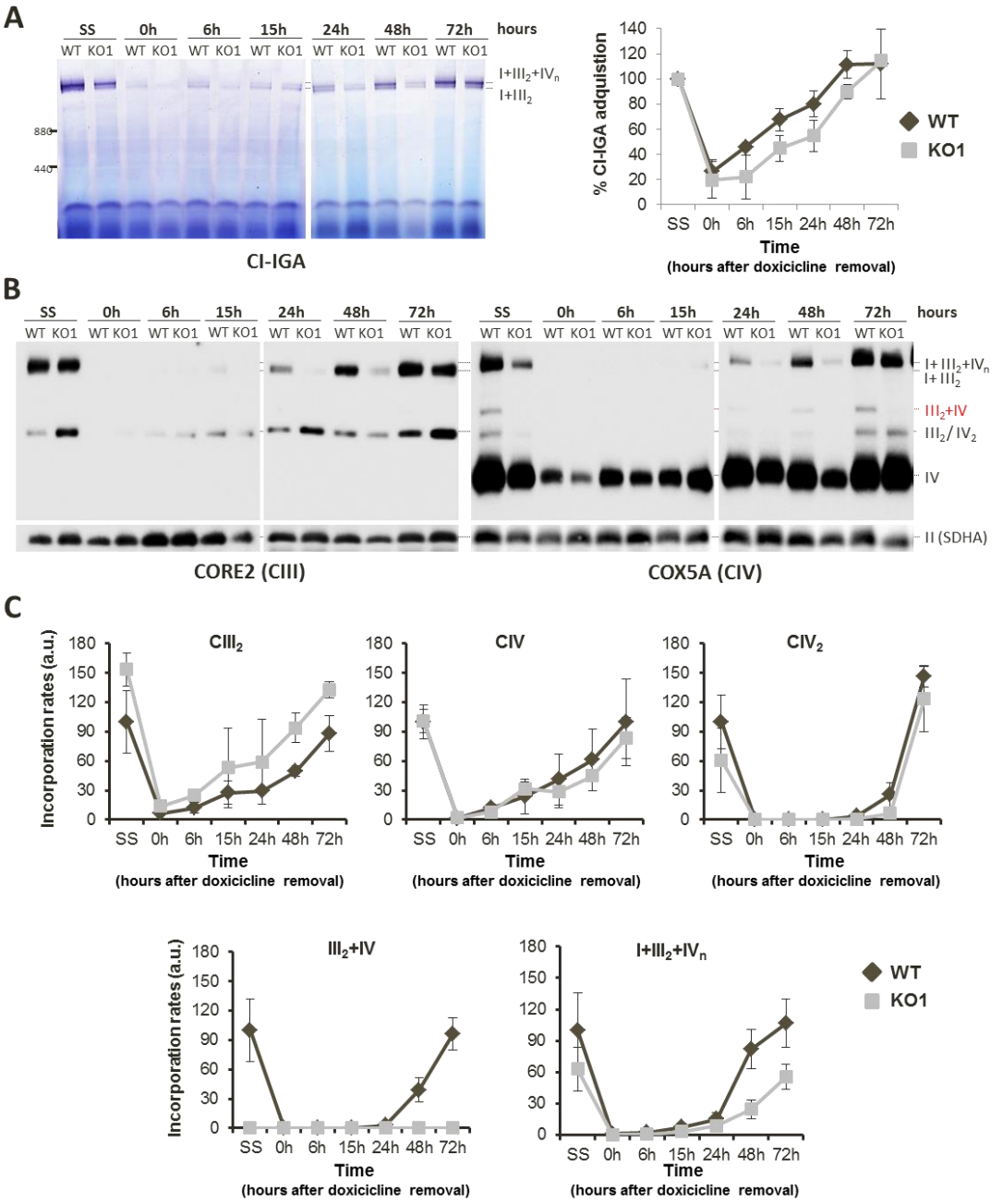

Figure 35. *COX7A2L*-KO cells have enhanced rate of *de novo* $CIII_2$ biogenesis and delayed respirasomes formation. HEK293T (WT) and *COX7A2L*-KO clone # 1 (KO1) cells were cultured for 8 days in the presence of 15 µg/ml doxycycline and collected at different time points (0, 6, 15, 24, 48, and 72h) after doxycycline removal. Mitochondria prepared from these samples were extracted with a digitonin:protein ratio of 4 g/g and analyzed by 1D-BN-PAGE in combination with **(A)** CI-IGA assays or **(B)** immunoblotting with the indicated antibodies. **(C)** Mean incorporation rates of the subunit CORE2 in $CIII_2$, and of COX5A in CIV and CIV_2 (upper panels), or their assembly kinetics in the $I+III_2+IV_{1-n}$ respirasomes (lower panels). The signals from three independent experiments for WT cells, and from two independent experiments for the KO1 clone were quantified and normalized by CII. Time point values are expressed as percentages of the untreated cells (SS), and indicated as means ± SD. $I+III_2+IV_n$, SCs containing CI, $CIII_2$ and CIV; III_2+IV, SC containing $CIII_2$ and CIV; III_2, complex III dimer ($CIII_2$); IV, complex IV; IV_2, complex IV dimer (CIV_2); II, complex II.

6. In normal cultured cell physiological conditions, COX7A2L does not have a significant impact on mitochondrial respiration

To shed light onto the functional consequences of COX7A2L and SC III_2+IV depletion, endogenous coupled cell respiration was polarographically measured in intact cells (Figure 36), by studying the co-oxidation of NADH-linked substrates (glutamate-malate) or $FADH_2$-linked substrates (succinate). First, no alterations were observed when measuring total cell respiration between the WT and *COX7A2L*-KO1. Similarly, no alterations were observed in the oxidation of glutamate-malate measured alone (Figure 36A), succinate measured alone (Figure 36B) or both substrates measured in combination (Figure 36A and 36B). Moreover, no effect on respiration resulted from COX7A2L overexpression. These results suggest that in normal cultured cell physiological conditions, neither COX7A2L nor the SC III_2+IV have an impactful functional effect on electron flow through the MRC. Examples of actual polarographic graphs are represented in Figure 37.

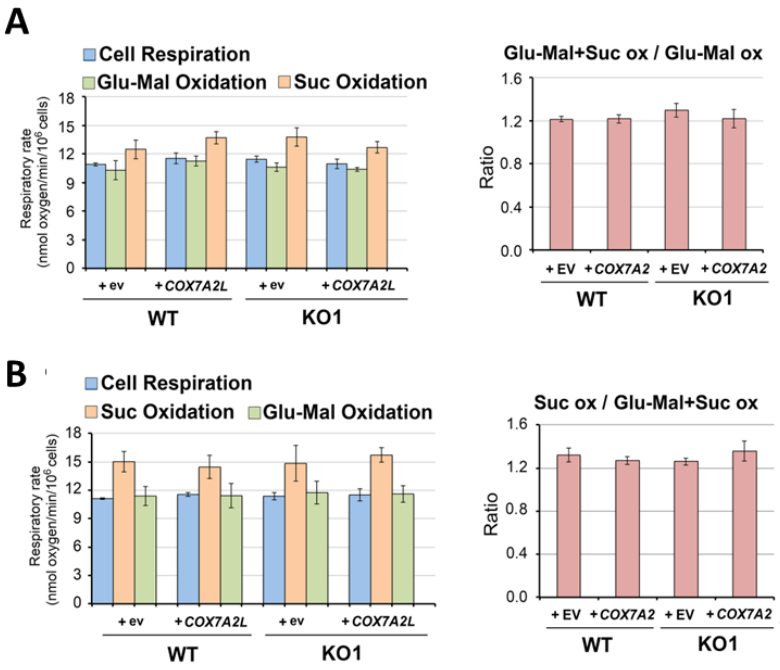

Figure 36. COX7A2L does not affect MRC function in normal cultured cell physiological conditions. Oxygen consumption rates were measured in HEK293T (WT) and *COX7A2L*-KO clone # 1 (KO1) cells grown in 4,5 g/l glucose-containing DMEM medium. Endogenous cell respiration was measured polarographically in intact cells permeabilized with 0.1% digitonin to measure substrate-driven respiration, where **(A)** glutamate+malate was followed by additional succinate co-oxidation or **(B)** succinate was followed by glutamate+malate co-oxidation. Oxygen consumption rates were calculated in nmol O_2.min^{-1}.mg protein^{-1}. Three measurements per sample were performed in three biological replicates. The left bar graphs represent the average ± SD of all replicates. The right graphs represent the ratios of oxygen consumption rates in the presence of one substrate vs the simultaneous presence of both substrates.

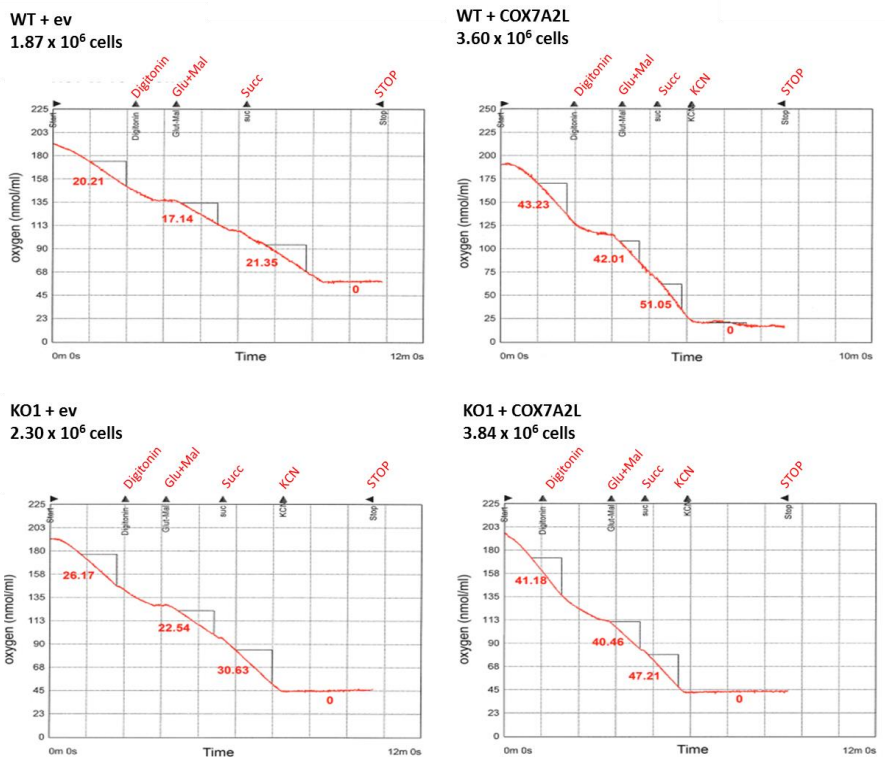

Figure 37. Examples of substrate-driven respiration polarographic graphs. Oxygen consumption rates measured in digitonin-permeabilize HEK293T control cells (WT) and *COX7A2L-KO* clone # 1 (KO1), overexpressing the empty vector (ev) or COX7A2L-Myc-DDK (COX7A2L) constructs. On each experimental setting, the cells were subsequently used to measure respiratory parameters polarographically as explained in the methods section. Endogenous cell respiration was measured in intact cells permeabilized with digitonin prior to measuring substrate-driven respiration, in which Glutamate+Malate (Glu-Mal) oxidation was followed by succinate (Succ) co-oxidation. The figure presents examples of actual polarographic graphs. Oxygen consumption rates were calculated in nmol O_2.min^{-1}.mg protein^{-1}.

7. Induction of CI deficiency significantly enhances succinate oxidation in *COX7A2L*-KO cells

Cell respiration resulted to be unaffected in the *COX7A2L*-KO clones, compared to the WT cells. Nevertheless, in human cells more than 90% of CI is present in the respirasomes and the SC III_2+IV only constitutes ~5% of the total amount of MRC structures (Moreno-Lastres et al., 2012). Taking this into account, the next step was to limit either the enzymatic activity or the amount of CI (and therefore, of the respirasomes) in order to discern whether the absence of SC III_2+IV and the accumulation of $CIII_2$ in the *COX7A2L*-KO clones affect substrate competitive oxidation. To induce a partial inhibition of CI activity, cells were first treated with either 10nM rotenone or the control vehicle (0,05% or 8,5mM ethanol) for 24h. Rotenone treatment did not significantly alter the distribution of MRC complexes and SCs in WT or KO cells (Figure

38A), but it resulted in a comparable ~40% decrease in glutamate-malate oxidation and a non-significant 10% decrease in succinate oxidation both in WT and KO digitonin-permeabilized cells (Figure 38B). By studying the co-oxidation of NADH (generated by the glutamate-malate metabolism) and succinate (an $FADH_2$-linked substrate), succinate oxidation was significantly more efficient in rotenone-treated *COX7A2L*-KO cells than in the WT cells (Figure 38B).

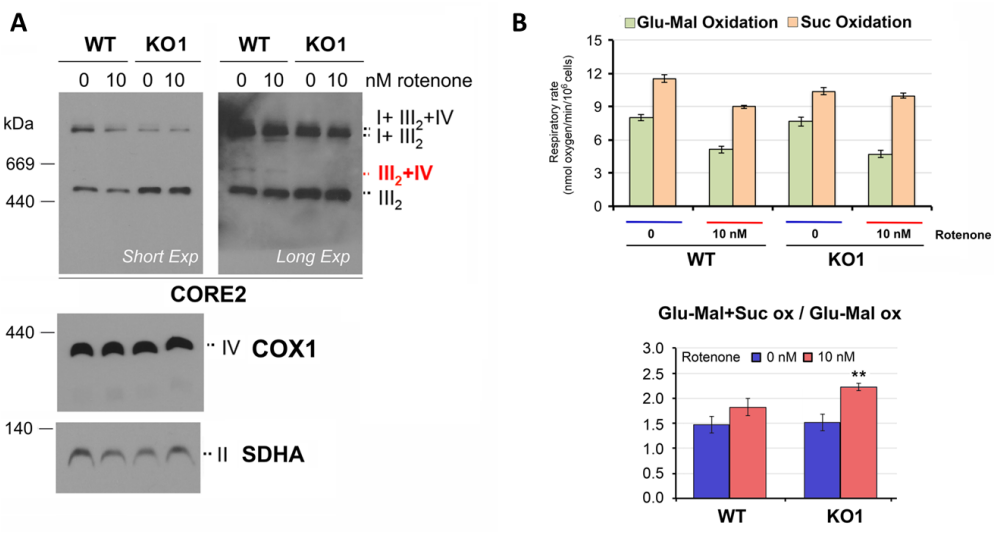

Figure 38. CI enzymatic inhibition significantly enhances succinate oxidation in *COX7A2L*-KO cells. HEK293T cells (WT) and *COX7A2L-KO* clone # 1 (KO1) were treated with the CI-inhibitor rotenone, using ethanol as a vehicle in the untreated controls. **(A)** Digitonized cell extracts from the indicated cells were analyzed by 1D-BN-PAGE and immunoblotting with the indicated antibodies. **(B)** Substrate-driven respiration was measured polarographically in digitonin-permeabilized cells. Oxidation of glutamate+malate was followed by addition of succinate to follow simultaneous oxidation. The top bar graph represents respiratory rates average ± SD of all repetitions. The bottom graph represents the ratio of oxygen consumption rates in the presence of one substrate vs the simultaneous presence of both substrates. Oxygen consumption rates were calculated in nmol O_2/min/10^6 cells. Three measurements per sample were performed in three biological replicates. Error bars represent the mean ± SD of all repetitions. $^{**}P < 0.01$.

To further confirm this observation a structural loss of CI, and therefore of the respirasomes, was induced by transfecting the WT and KO cells with siRNAs against the CI subunit *NDUFB8* mRNA, using non-targeting (NT) siRNA as a control (Figure 39B). The substantial decrease (>95%) in CI-containing respirasomes (SCs I+III_2 and I+III_2+IV_{1-n}) was accompanied by a slight accumulation of SC III_2+IV in WT cells, a mild accumulation of CIV_2 in the KO cells, and a prominent increase of $CIII_2$ in both cell types (Figure 39A). As in rotenone-treated cells, *NDUFB8* silencing lowered glutamate-malate oxidation by ~45-50% in both WT and KO digitonin-permeabilized cells, and induced a simultaneous 10% increase in succinate

oxidation in the *COX7A2L*-KO cells (Figure 39C). Overall, CI depletion resulted in NADH+$FADH_2$: NADH oxidation ratios significantly higher in the *COX7A2L*-KOs than in WT cells (Figure 39C).

Altogether, these functional data suggest that in the context of CI deficiency, the absence of COX7A2L and SC III_2+IV provokes a significant increase in CII-mediated electron flow, where electrons would preferentially flow from CII to the accumulated $CIII_2$.

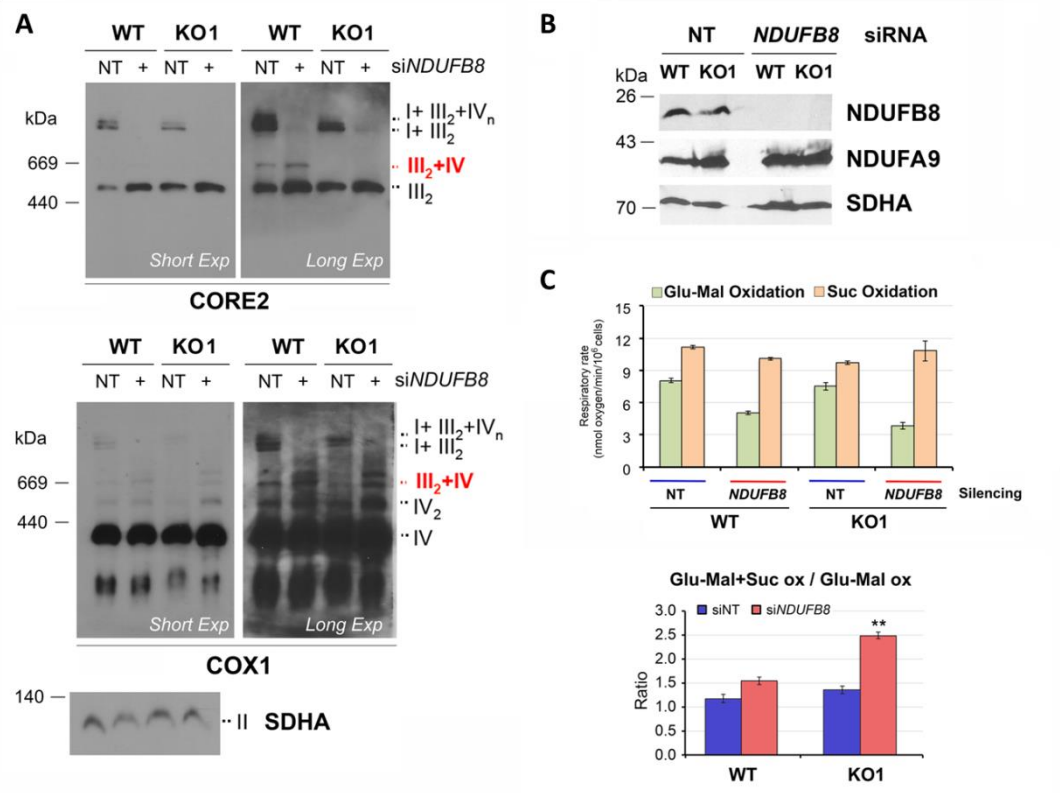

Figure 39. Complex I structural defects significantly enhance succinate oxidation in *COX7A2L*-KO cells. HEK293T cells (WT) and *COX7A2L-KO* clone # 1 (KO1) were transiently transfected with siRNAs targeted against the CI subunit *NDUFB8* mRNA. Non-targeting siRNA (NT) was used as a negative control. **(A)** Digitonized cell extracts from the indicated cells were analyzed by BN-PAGE and immunoblotting with the indicated antibodies. **(B)** SDS-PAGE followed by immunoblot analysis of NDUFB8 in silenced cells. **(C)** Substrate-driven respiration was measured polarographically in digitonin-permeabilized cells. Oxidation of glutamate+malate was followed by addition of succinate to follow simultaneous oxidation. The top bar graph represents respiratory rates average ± SD of all repetitions. The bottom graph represents the ratio of oxygen consumption rates in the presence of one substrate vs the simultaneous presence of both substrates. Oxygen consumption rates were calculated in nmol O_2/min/10^6 cells. Three measurements per sample were performed in three biological replicates. Error bars represent the mean ± SD of all repetitions. $^{**}P < 0.01$.

8. A mutant COX7A2L variant carrying a 6-base-pair deletion present in C57BL/6 mice retains the ability to bind $CIII_2$ but does not rescue SC III_2+IV assembly, in humans

To explore the functionality in human cells of the short COX7A2L isoform present in C57BL/6 and BALB/c mouse strains(Lapuente-Brun et al., 2013; Mourier, Matic, et al., 2014), constitutive cell lines were generated expressing either FLAG-tagged COX7A2L (long) or a mutant version (short) carrying a deletion of amino acids V72 and P73 of human COX7A2L (Lapuente-Brun et al., 2013). Both variants where stably expressed in both WT and *COX7A2L*-KO cells, which yielded no major differences in the steady-state levels of respiratory chain subunits, as observed in Figure 40A. MRC organization analysis by 2D-BN/SDS-PAGE revealed that the short COX7A2L variant was imported into mitochondria, where it colocalized with $CIII_2$ and SC I+III_2, but not with any CIV-containing structure (Figure 40C). In addition, whereas expression of the long COX7A2L variant in *COX7A2L*-KO cells restored normal levels of $CIII_2$ and SC III_2+IV, the short variant did not (Figure 40C and 40D). Further BN-PAGE analysis disclosed that the expression of either the long or the short COX7A2L variants did not affect the steady-state levels of the respirasomes, as observed in Figures 40B-D**.** These data suggest that the 2-amino acids deletion present in the short COX7A2L isoform prevents its association with CIV but does not affect its binding to $CIII_2$, an interaction that is not sufficient to promote the formation of the SC III_2+IV.

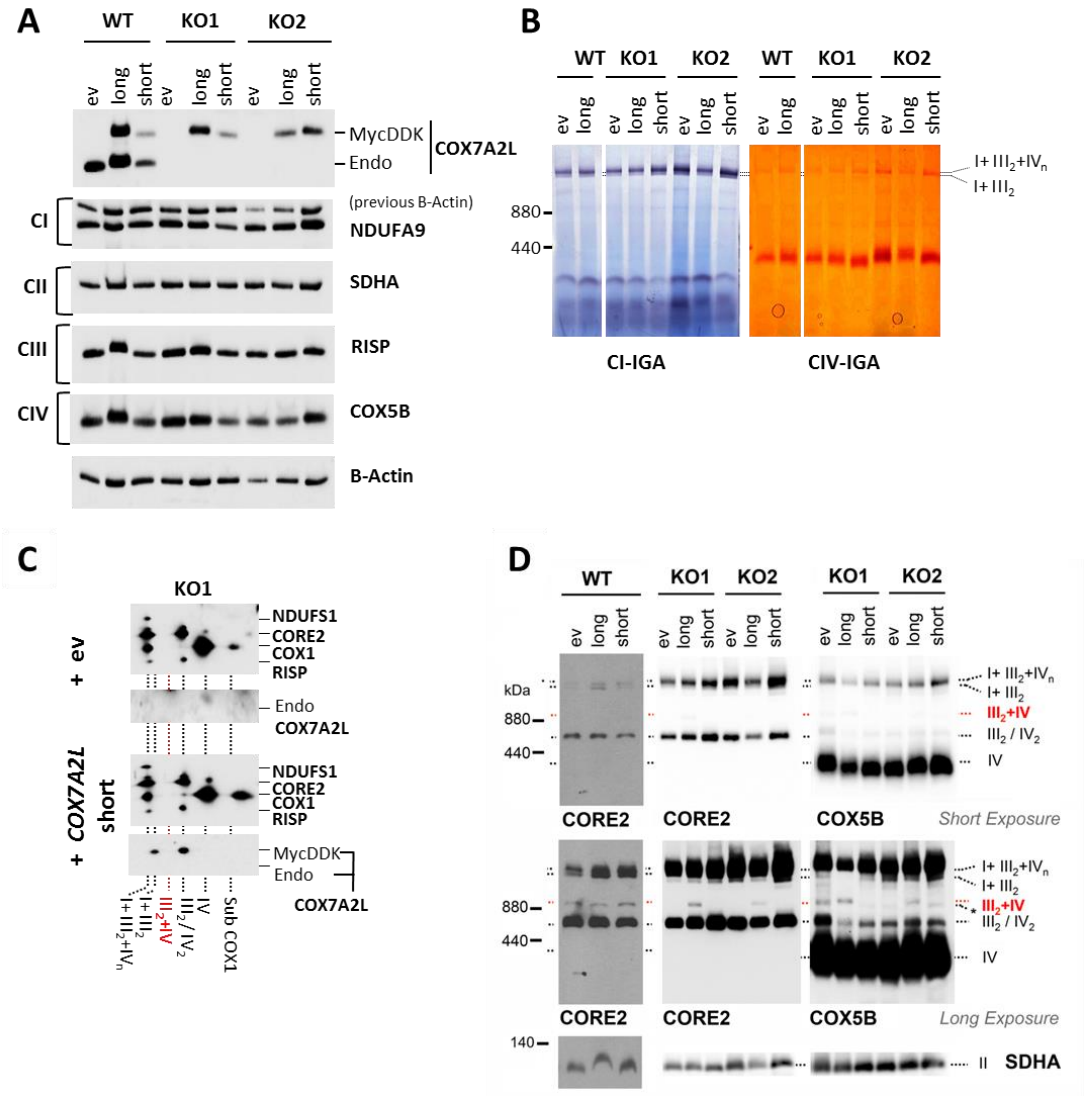

Figure 40. The short-COX7A2L variant binds to $CIII_2$ and SC $I+III_2$, but does not rescue SC III_2+IV assembly in *COX7A2L*-KO cells. Control HEK293T cells (WT) and both *COX7A2L*-KO (KO1 and KO2) clones were transfected with an empty vector (ev) or with constructs to stably overexpress COX7A2L-Myc-DDK (long) or short-COX7A2L-Myc-DDK (short). The reconstituted cells were used in the following experiments: **(A)** SDS-PAGE followed by immunoblotting to differentiate endogenous COX7A2L (~12.6 kDa) from exogenous COX7A2L-Myc-DDK (~16.2 kDa). Membranes were also incubated with antibodies that recognize the indicated OXPHOS subunits. **(B)** 1D-BN-PAGE using digitonin-solubilized mitochondrial extracts (detergent:protein ratio 4:1) followed by CI-IGA and CIV-IGA assays, or **(C)** 2D-BN/SDS-PAGE and **(D)** wester-blot, and immunoblotting with the indicated antibodies. $I+III_2+IV_n$, SCs containing CI, $CIII_2$ and CIV; $I+III_2$, SC containing CI and $CIII_2$; III_2+IV, SC containing $CIII_2$ and CIV; III_2, complex III dimer ($CIII_2$); IV, complex IV; IV_2, complex IV dimer (CIV_2); II, complex II. Subcomplexes that contain COX1 are indicated as subCOX1. In **(D)**, an unidentified band running a bit faster than the SC III_2+IV that cross-reacted with the COX5A antibody (but not with CORE2) is indicated with an asterisk.

CHAPTER 3. IN THE ABSENCE OF COMPLEX IV, COX7A2L-CONTAINING SUPERCOMPLEX I+III_2 IS STABILIZED THROUGH THE STEPWISE ASSOCIATION OF FREE COX SUBUNITS

1. Human cybrids lacking CIV form diverse SC I+III$_2$ species that contain COX7A2L and differ in their COX subunit composition

All the results presented so far suggest that COX7A2L plays a regulatory role on the biogenesis of mitochondrial CIII but no functional impact on CIV (COX). As previously observed (Figure 14), the levels of COX7A2L within all the structures were significantly decreased in the CIII-KO mutant cybrids, and only a minor residual COX7A2L signal co-migrated with free CIV. In contrast, in the CIV-KO (COX1Δ) mutant cybrids, COX7A2L clearly colocalized with SC I+III$_2$ and CIII$_2$. Interestingly, very small amounts of COX7A2L were bound to CIV in the absence of CIII, but COX7A2L appeared at normal levels within the CIII-containing structures present in the absence of CIV. To further investigate the influence of COX7A2L on the MRC structural organization, and in particular on CIII biogenesis, this study was extended to deeply examine two mutant cybrids lacking CIV (CIV-KOs) due to homoplasmic nonsense mutations in the mtDNA-encoded COX1 and COX2 subunits. First, the levels of COX7A2L and MRC subunits were examined in digitonized mitochondria (Figure 41A) and whole-cell extracts (Figure 41B) from control and CIV-KO mutant cybrids. No differences were observed in the steady-state levels of CI, CII and CIII subunits between controls and mutants. Regarding the CIV subunits, the levels of COX4 and COX5A remained unaltered in both mutants, in agreement with their stabilization in common subcomplexes at early assembly stages (McStay et al., 2013; Nijtmans et al., 1998; Stiburek et al., 2005; Vidoni et al., 2017; Williams et al., 2004). None of the remainder COX subunits were detectable in the mitochondrial fractions from the COX1 deletion mutant (COX1Δ) (Figure 41A). However, low levels of the COX5B subunit were observed in whole-cell extracts (Figure 41B), suggesting alterations in the mitochondrial import of this protein in the COX1Δ cells. In contrast, in the COX2 deletion mutant (COX2Δ) all COX subunits were detected at normal levels, except for COX2 that was undetectable, and COX6C, whose levels were markedly lower than in control cells. Regarding COX7A2L levels, no differences were observed in the absence of CIV, except for a slight increase in the COX2Δ mutant compared to its isogenic control (Figure 41A). Interestingly, spectrophotometric measurements of the MRC activities showed no functional CIV enzymatic activity in both mutants, and significantly reduced activities of complexes I and III (Figure 41C). These data suggest that in our cellular models, the absence of CIV induces alterations in the enzymatic activities of complexes I and III, despite their steady states levels remained unaltered.

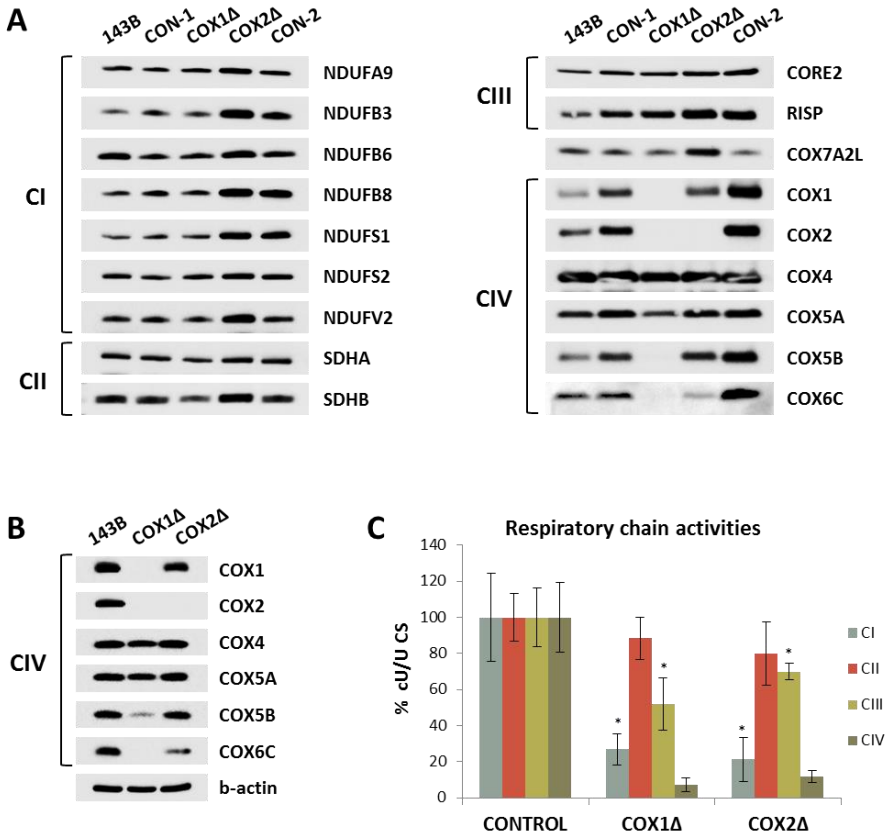

Figure 41. Steady states levels of MRC subunits and MRC enzyme activities in CV-KO cybrids. (A) Mitochondrial lysates and **(B)** whole cell extracts from control and mutant cybrids lacking CIV (CIV-KO) were analyzed by SDS-PAGE and western blot with the indicated antibodies that target COX7A2L and subunits from MRC complexes I, II, III and IV. **(C)** Spectrophotometric measurements of the enzyme activities of MRC complexes I to IV (CI-CIV) in COX1Δ and COX2Δ mutant cybrids, as well as in their respective isogenic controls and 143B cells, represented as CONTROL (n=3). Enzyme activities are expressed as the percentages of cU/U citrate synthase (CS). Error bands represent the mean ± SD of four repetitions. * p< 0.05

Subsequently, the accumulation of CI-containing SCs in the CIV-lacking mutants was analyzed by 1D-BN-PAGE in combination with CI-IGA assays (Figure 42A). As previously observed, in control 143B cells the most prominent structure corresponded to the respirasome (band 1) that contains one single copy of CIV (SC I+III_2+IV_1), followed by the respirasome containing two copies of CIV (SC I+III_2+IV_2). In the mutant cybrids, however, the absence of CIV led to the disappearance of both respirasomes, and to a differential accumulation of CI-containing SCs that displayed NADH dehydrogenase activity. The COX1Δ mutant presented a single NADH dehydrogenase-reactive band (band 2), previously demonstrated to correspond to fully-assembled SC I+III_2, which also contained COX7A2L as a CIII-interacting protein (Figure 16). The COX2Δ mutant, surprisingly, showed the accumulation of two differentiated NADH dehydrogenase-reactive bands of unknown composition (bands 3 and 4). These bands were

therefore excised from the blue native gels, and their protein composition was analyzed by high-resolution nano-LC/ESI-MS (Table 5, Appendix). The comparative proteomics analysis of the respirasome $I+III_2+IV_1$ (band 1) in control 143B cells revealed the presence of 93% of the total CI subunits, 82% of CIII subunits and 50% of CIV subunits. Parallel proteomics analyses of bands 2 to 4 identified ~89-91% of CI subunits in the three bands (including the whole catalytic NADH dehydrogenase (N) module and six mitochondrial-encoded ND subunits, except for ND4L that was neither detected in the respirasomes), together with all CIII components (including its three catalytic subunits, as well as COX7A2L), indicating that these bands contained fully-assembled SC $I+III_2$ plus COX7A2L (Figure 42B). Unexpectedly, bands 3 and 4 differed from band 2 in the presence of specific COX subunits: in band 3 only the liver isoform of the COX7A subunit (COX7A2) was detected (Figure 42B), whereas in band 4 subunits COX4, COX5B and COX7A2 were identified (Table 5, Appendix).

Further immunoblotting analyses (Figure 43) confirmed the complete loss of CIV-containing structures (monomeric and dimeric CIV, SC III_2+IV and SC $I+III_2+IV_{1-2}$) in both mutants, together with the accumulation of the CIII dimer ($CIII_2$) and the SC $I+III_2$. In agreement with the proteomics data, no COX subunits were detected in the SC $I+III_2$ from the COX1Δ mutant; however, subunit COX5B clearly colocalized with SC $I+III_2$ in the COX2Δ cybrids, as well as a fainter signal corresponding to COX4. Moreover, the COX1 subunit that was not previously identified by proteomics, was detected by immunoblotting in the SC $I+III_2$ from the COX2Δ cybrids (Figure 43A). In these cells a major proportion of the COX1 subunit colocalized in a subcomplex together with COX4, and both subunits accumulated in a second larger subcomplex together with COX5B (subIV in Figure 43B). However, subunit COX5A did not colocalize with SC $I+III_2$, but accumulated in an independent subcomplex that migrated faster than the COX1-containing subcomplex (Figure 43C), which probably corresponds to the stable association of COX4-COX5A subunits (McStay et al., 2013; Nijtmans et al., 1998; Stiburek et al., 2005; Vidoni et al., 2017; Williams et al., 2004). These results indicate that in the absence of CIV, different SC $I+III_2$ species can be formed that contain COX7A2L and differ in their COX subunit composition. Our data also suggest that the presence of the COX1 subunit is an essential requirement for the recruitment or stabilization of additional COX subunits into subcomplexes, as well as into SC $I+III_2$.

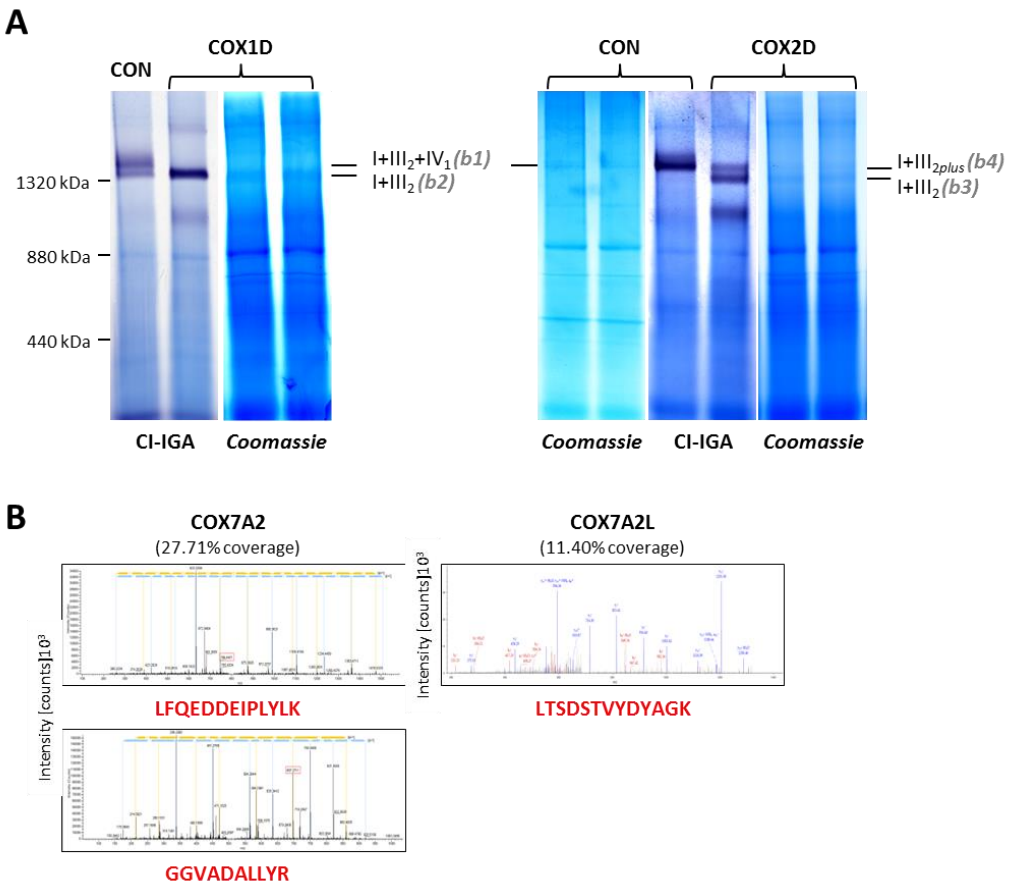

Figure 42. Identification of CI-containing SCs in control and CV-KO cybrids. (A) Digitonin-solubilized mitochondria from control (CON) and COX1Δ and COX2Δ mutants were separated by 1D-BN-PAGE. CI-containing bands *b1-b4* were identified by CI-IGA assays, excised from Coomassie-stained gels and analyzed by Nano-LC/ESI-MS. **(B)** MS/MS spectra from the doubly charged COX7A2 (left) and COX7A2L (right) peptide unambiguously detected by LC-ESI/MS in two independent experiments per sample. The amino acid sequence of the identified unique peptide is highlighted in red. The most intense signals on the MS/MS spectra correspond to the main fragmentation series (b-amino and y-carboxy). Doubly charged fragments are marked with superscript 2+. *b1*, control SC I+III_2+IV_n; *b2*, COX1Δ SC I+III_2; *b3*, COX2Δ SC I+III_2; *b4*, COX2Δ SC I+$III_{2\ plus}$; I+III_2+IV_n, SC containing CI, CIII, and CIV; I+III_2, SC containing CI and CIII; III_2+IV, SC containing CIII and CIV; III_2, CIII dimer.

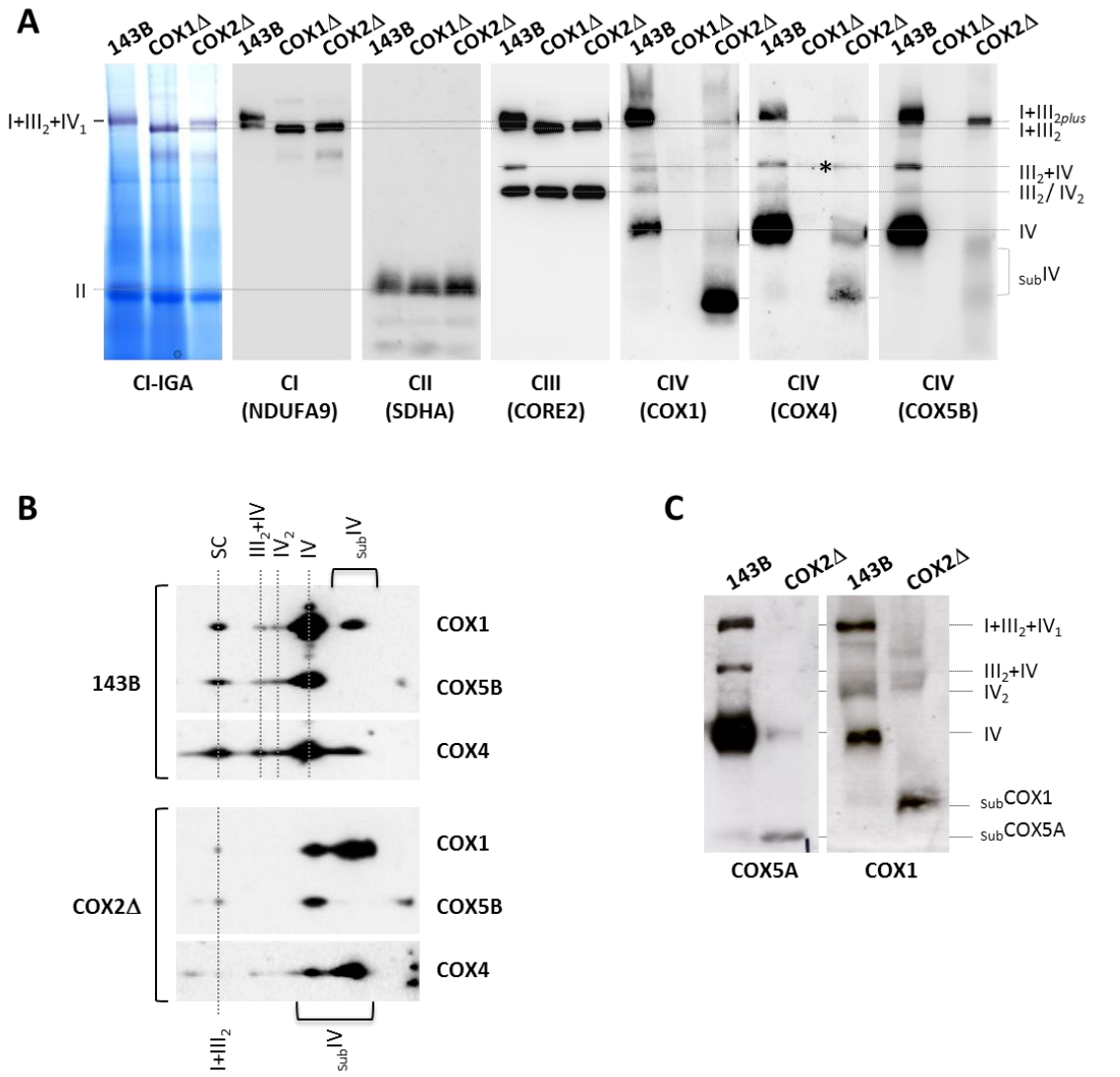

Figure 43. Identification of CIV subunits in the SC I+III$_2$. Mitochondria from control 143B cells and CIV-KO cybrids were extracted with a digitonin:protein ratio of 4 g:1 g and analyzed by **(A and C)** 1D-BN-PAGE, followed by CI *in gel* activity (IGA) assay and western-blot , or alternatively, by **(B)** 2D BN/SDS-PAGE. Gels were blotted on nitrocellulose and incubated with antibodies raised against the indicated OXPHOS subunits. I+III$_2$+IV$_1$, SC containing CI, CIII and CIV; I+III$_2$, SC containing CI and CIII; III$_2$+IV, SC containing CIII and CIV; I*, CI-containing structure; III$_2$, complex III dimer; IV, complex IV; IV$_2$, complex IV dimers; II, complex II; subIV, subcomplex containing subunits COX1, COX4 and COX5B.

2. Human cybrids lacking holo-CIV display a differential accumulation of stabilized COX subunits

Our observation that different SC I+III$_2$ species can be formed, all of which contain COX7A2L but present a differential arrangement of COX subunits was a surprising finding. Therefore, we analyzed the biogenetic dynamics of these COX subunits in SC I+III$_2$, and compared them with those of COX7A2L and selected subunits from the remainder MRC complexes in both CIV-KO

mutants and control 143B cells. To this aim, cells were cultured for 6 days in the presence of doxycycline to reversibly inhibit mitochondrial translation. Whole cell extracts were collected at different time-points (0, 6, 15, 24, 48, 72 and 96 hours) after doxycycline removal. The reappearance of MRC subunits after the reversible blockage of assembly was analyzed by SDS–PAGE and immunoblotting with a panel of twelve antibodies raised against MRC subunits and COX7A2L (Figure 44). Untreated cells (SS) were included in the panel as a positive control. No alterations were observed in the levels of the CII subunit SDHA, as expected since this complex lacks mtDNA-encoded subunits. However, there were remarkable differences in the reemergence patterns of the MRC subunits from complexes I, III and IV, which were classified in three groups. The first group included the mitochondrial-encoded subunits COX1 and COX2 (subunits colored in red), which were undetectable in the 143B cells after 6 days of doxycycline treatment (lane 0). Both subunits appeared 15-24 h after removal of the inhibitor, and gradually increased until they reached their steady-state at 96 h. Since these subunits were directly targeted by the drug, these data indicate that the inhibition of mitochondrial translation worked efficiently and that no pools of preassembled subcomplexes accumulated during doxycycline treatment. The COX1 subunit was detected in the COX2Δ mutant following a similar reappearance pattern than the control. The second group included the CI NDUFA9, the CIII CORE2, and the CIV COX4 and COX5A subunits (subunits colored in green). These subunits remained clearly visible upon mitochondrial translation inhibition (lane 0), indicating their stabilization in preassembled subcomplexes, and they reached steady-state levels at 6-15 h after doxycyline removal, in accordance with their early incorporation into their corresponding MRC complexes (Stiburek et al., 2006; Vogel et al., 2007; Zara et al., 2009b). The third group included the CI NDUFS1, the CIII RISP, and the CIV COX5B and COX6C subunits, as well as COX7A2L (subunits colored in blue). There were relatively low levels of these proteins upon doxycycline treatment (lane 0), which gradually reached their steady-states at 96 h. This result suggests that these proteins might not be fully stabilized in preassembled subcomplexes, and it is in agreement with the fact that they all enter the assembly process relatively late (Fernandez-Vizarra et al., 2007; Lazarou et al., 2007; Stiburek et al., 2006). No major differences were observed in the kinetics of reappearance of most MRC subunits between 143B cells and the CIV-lacking cybrids, except for the fact that subunits COX1, COX2 and COX6C were undetectable in the COX1Δ mutant, while only subunit COX2 was missing in the COX2Δ mutant, which also displayed a poor accumulation rate of the COX6C subunit compared with the control. These results suggest alterations in the composition and proportion of CIV subunit-containing subcomplexes in cybrids lacking holo-COX.

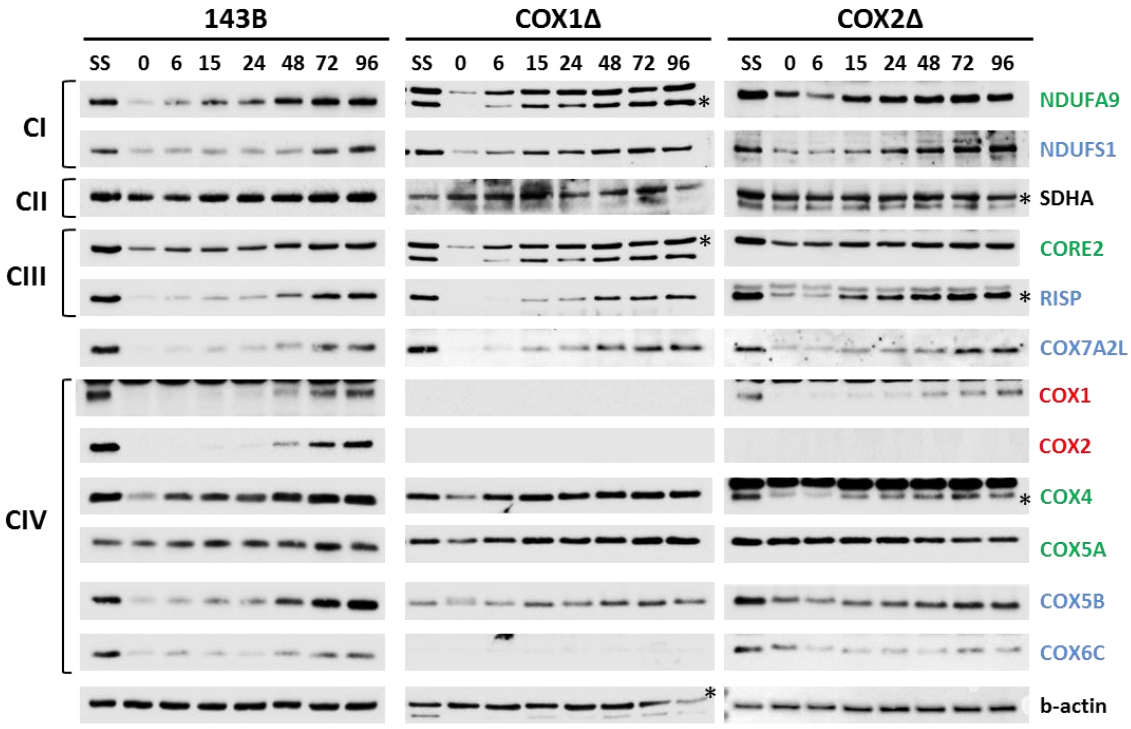

Figure 44. Dynamics of reappearance of COX7A2L and MRC subunits in control and CIV-KO cybrids reversibly treated with doxycycline. Whole cell extracts from doxycycline-treated 143B cells and COX1Δ and COX2Δ cybrids were analyzed by SDS-PAGE and western blot with the indicated antibodies. The reappearance kinetic patterns were classified in three groups indicated as red, green and blue. The subunits are coloured so that those of the same colour belong to same group. I+III_2+IV_n, SC containing CI, CIII, and CIV; III_2+IV, SC containing CIII and CIV; III_2, CIII dimer; IV, CIV; the asterisk indicate the matching subunit recognized by the antibody.

3. COX7A2L-containing SC I+III_2 is fully-assembled prior to the insertion of COX subunits

To investigate how the absence of CIV affects the biogenesis of CI-containing SCs, the assembly dynamics of the SC I+III_2 species in the CIV-KO mutant cybrids were compared with that of the respirasomes (SC I+III_2+IV_{1-2}) in control 143B cells. To this aim, the reappearance of NADH dehydrogenase-active SCs was first analyzed in digitonized mitochondria from doxycycline-treated cells by 1D-BN–PAGE in combination with CI-IGA assays (Figure 45A, upper panel). In parallel, the incorporation rates of newly-synthesized CI subunits into these structures was examined by BN-PAGE and immunoblotting with antibodies that recognize subunits NDUFA9 and NDUFS1 (Figure 45A, medium and lower panels). This two CI subunits are representative of early-intermediate and late CI assembly stages, respectively (Formosa et al., 2017; Guerrero-Castillo et al., 2017; Sanchez-Caballero et al., 2016). Signals from at least three independent experiments were quantified, normalized to CII, and expressed relative to the

steady-levels in untreated cells (SS) (Figure 45B and 45C). Significant differences were neither observed in the kinetics of incorporation of CI subunits, nor in the accumulation of active CI within the SCs from control and CIV-KO cybrids (Figure 45B). In control 143B cells, the incorporation of the NDUFS1 subunit (that belongs to the catalytic N-module) into the respirasomes was initially delayed in comparison with the NDUFA9 subunit (Figure 45C), in agreement with previous results of our group (Moreno-Lastres et al, 2012). However, in the CIV-KO cybrids both subunits first accumulated at the same rates within a ~1100 kDa band showing NADH dehydrogenase activity, compatible with fully-assembled CI (Figure 45A and 45C), and then incorporated within SC I+III_2. These data suggest that the lack of CIV promotes the integration of fully-assembled CI into SC I+III_2.

The same approach was used to subsequently analyzed the assembly kinetics of newly-synthesized CIII subunits by 2D-BN/SDS-PAGE and western-blot with antibodies that recognize CORE2 and RISP (Figure 46), representative of early and late CIII assembly stages, respectively (Fernández-Vizarra and Zeviani, 2015; Zara et al., 2009a). Following 6 days of doxycycline treatment (time 0h) only residual levels of CORE2 and RISP subunits were detected in co-localization with the CIII dimer ($CIII_2$) (Figure 46A). Upon doxycycline removal, the amounts of both subunits within $CIII_2$ increased gradually and then moved towards the position of SCs (Figure 46A). Again, no significant differences were detected in the incorporation rates of CIII subunits into SCs I+III_2 and I+III_2+IV_{1-2} between the control and COXΔ cybrids (Figure 46B). The assembly kinetics of CORE2 within SCs was similar to that of the CI subunit NDUFA9 (Figure 45A), and significantly faster than that of the RISP subunit both in control and COXΔ cybrids (Figure 46A and 46C). These results indicate that a RISP-lacking pre-SC I+III_2 is formed at an early assembly stage, to which the catalytic RISP subunit is later added to yield fully-assembled SC I+III_2, in agreement with previous observations (Fernández-Vizarra et al., 2009; Moreno-Lastres et al., 2012; Sánchez et al., 2013; Wagener et al., 2011).

Finally, the assembly kinetics of COX7A2L into SC I+III_2 was analyzed in the COX1Δ cybrids (Figure 47A). As for CIII subunits, a residual COX7A2L signal was initially detected (time 0h) only in co-localization with the CIII dimer ($CIII_2$). Upon doxycycline removal, COX7A2L accumulated gradually within $CIII_2$ and then moved towards the position of SC I+III_2 at similar assembly rates than the CORE2 subunit, as previously observed in control 143B cells (Figures 47B and 21). Altogether, these data indicate that COX7A2L-containing SC I+III_2 is normally assembled prior to the insertion of COX subunits.

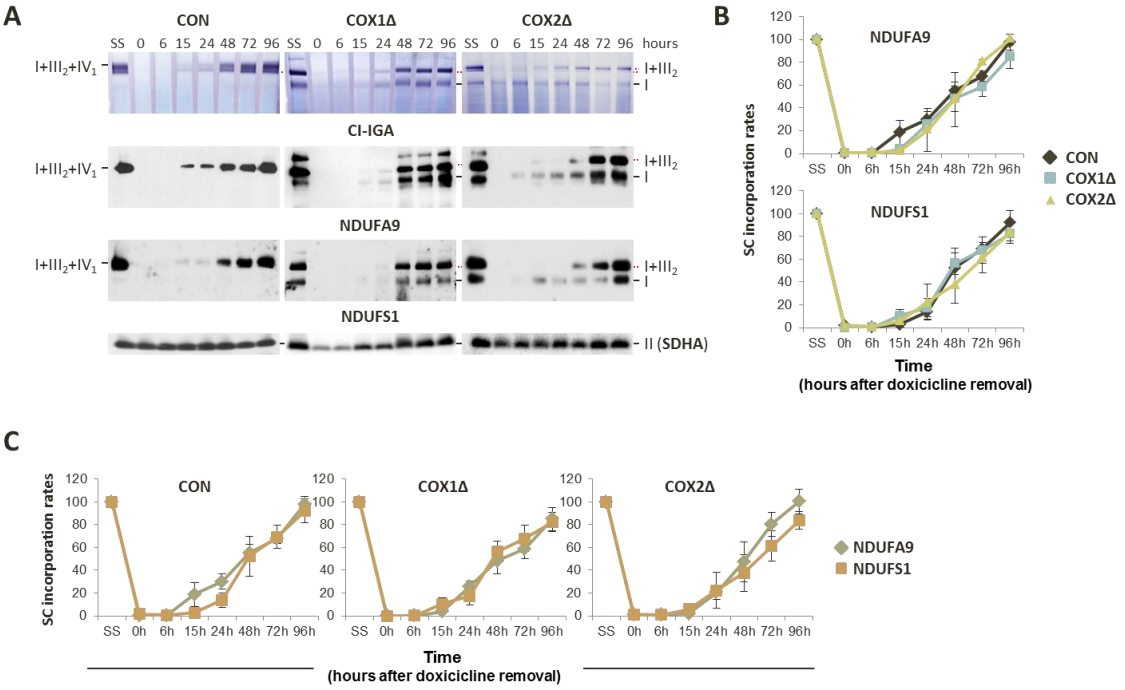

Figure 45. Assembly kinetics of CI subunits into COX7A2L-containing SC I+III$_2$. 143B (CON) cells and CIV-KO (COX1Δ and COX2Δ) cybrids were cultured for 6 days in the presence of 15 µg/ml doxycycline and collected at different time points (0, 6, 15, 24, 48, 72 and 96h) after doxycycline removal. **(A)** Mitochondria prepared from these samples were extracted with a digitonin:protein ratio of 4 g/g and analyzed by 1D-BN-PAGE in combination with CI-IGA assays and immunoblotting with the indicated antibodies. **(B)** Mean incorporation rates of subunits NDUFA9 and NDUFS1, involved in early and late steps of CI assembly respectively, in the SC I+III$_2$+IV$_{1-n}$ in control cells and in SC I+III$_2$ in CIV-KO cybrids. **(C)** The assembly dynamics of the same subunits were compared with each other in the three cell lines. The signals from three independent experiments were quantified and normalized by CII. Time point values are expressed as percentages of the untreated cells (SS), and indicated as means ± SD. I+III$_2$+IV$_1$, SCs containing CI, CIII and CIV; I+III$_2$, SC containing CI and CIII; II, complex II; I, complex I.

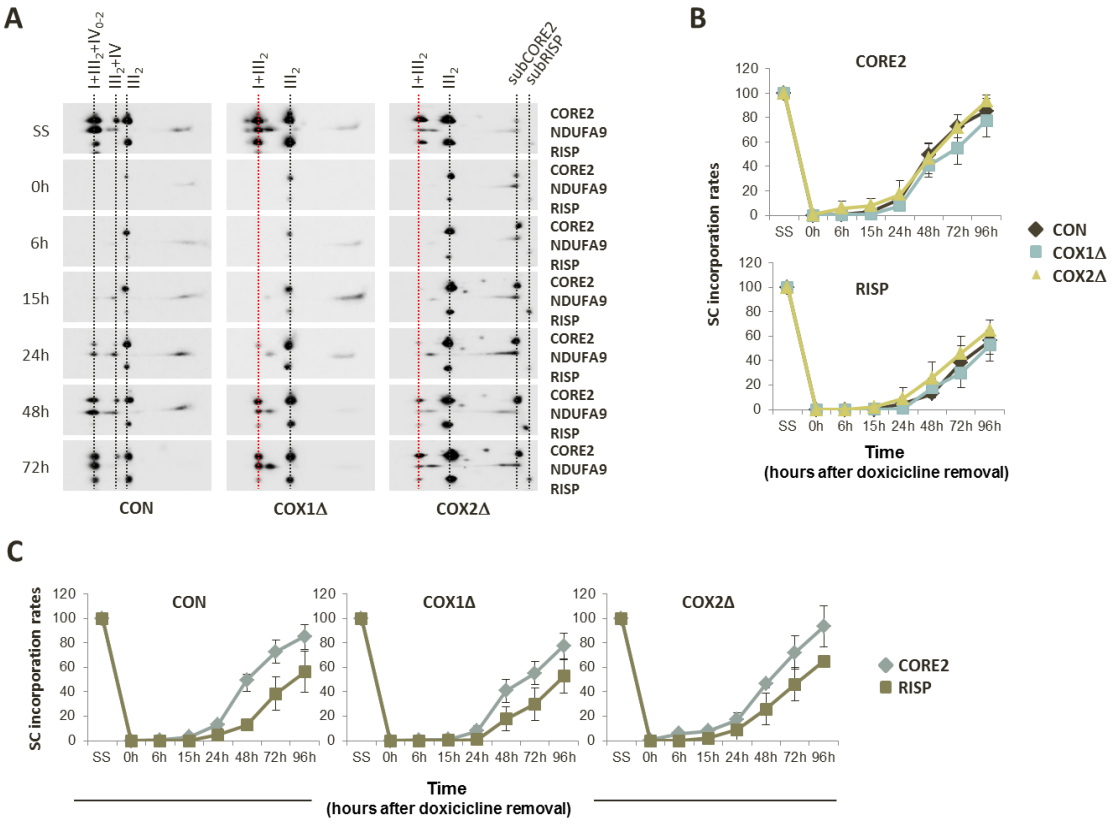

Figure 46. Assembly kinetics of CIII subunits into COX7A2L-containing SC I+III$_2$. 143B (CON) cells and CIV-KO (COX1Δ and COX2Δ) cybrids were cultured for 6 days in the presence of 15 µg/ml doxycycline and collected at different time points (0, 6, 15, 24, 48, and 72h) after doxycycline removal. **(A)** Mitochondria prepared from these samples were extracted with a digitonin:protein ratio of 4 g/g and analyzed by 2D-BN/SDS-PAGE and immunoblotting with the indicated antibodies. **(B)** Mean incorporation rates of subunits CORE2 and RISP, involved in early and late steps of CIII assembly respectively, in the SC I+III$_2$+IV$_{1-n}$ in control cells and in SC I+III$_2$ in CIV-KO cybrids. **(C)** The assembly dynamics of the same subunits were compared with each other in the three cell lines. The signals from three independent experiments were quantified and normalized by CII. Time point values are expressed as percentages of the untreated cells (SS), and indicated as means ± SD. I+III$_2$+IV$_1$, SCs containing CI, CIII and CIV; I+III$_2$, SC containing CI and CIII; III$_2$, dimeric complex III; II, complex II; I, complex I.

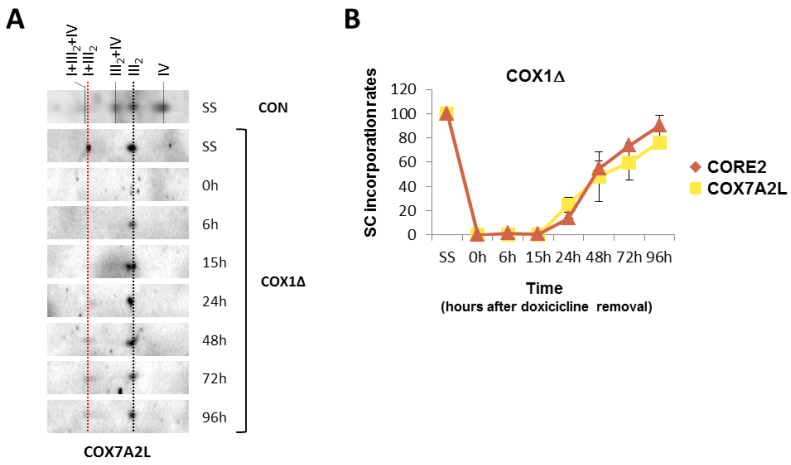

Figure 47. Assembly kinetics of COX7A2L into SC I+III$_2$ in COX1Δ cybrids. (A) COX1Δ cybrids were cultured for 6 days in the presence of 15 µg/ml doxycycline and collected at different time points (0, 6, 15, 24, 48, 72 and 96h) after doxycycline removal. Mitochondria prepared from these samples were extracted with a digitonin:protein ratio of 4 g/g and analyzed by 2D-BN/SDS-PAGE and immunoblotting with the COX7A2L antibody. 143B (CON) cells were used as control. **(B)** Mean incorporation rates of COX7A2L and CIII subunit CORE2 in the SC I+III$_2$ from COX1Δ cybrids. I+III$_2$+IV, SC containing CI, CIII and CIV; I+III$_2$, SC containing CI and CIII; III$_2$+IV, SC containing CIII and CIV; III$_2$, complex III dimer; IV, complex IV.

4. COX subunits are integrated into fully-assembled SC I+III$_2$ in a stepwise fashion

The fact that the COX1Δ mutant failed to assemble any COX subunit within SCI+III$_2$, suggests that COX1 synthesis is an essential requirement for the integration of CIV into the respirasomes. Remarkably, in the COX2Δ cybrids the colocalization of specific CIV subunits (namely COX1, COX4, COX5B and COX7A2) with SC I+III$_2$ suggested an unusual biogenetic regulatory mechanism for CIV assembly in the respirasomes. To investigate how this process takes place, the assembly kinetics of newly-synthesized CIV subunits into SC I+III$_2$ were analyzed by 2D-BN/SDS-PAGE and immunoblotting with antibodies that recognize early-assembly subunits (COX1, COX4 and COX5A) and late-assembly subunits (COX5B and COX6C) (Figure 48). Both in control 143B cells and COX2Δ mutants, subunit COX1 got incorporated into SCI+III$_2$ with the fastest assembly rates, probably representing the first CIV assembly step (Figure 48A and 48B). In control cells, COX1 incorporation was sequentially followed by subunits COX4 and COX5A, and later by COX5B and COX6C, an order that resembles the canonical CIV assembly pathway (Fontanesi et al., 2008). In the COX2Δ mutants, however, COX1 incorporation into SCI+III$_2$ occurred ahead of the incorporation of subunits COX5B and COX4. Subunits COX5A and COX6C did not get integrated into SCs despite they remained stabilized in small subcomplexes. The assembly kinetics of subunit COX4 in the SC I+III$_2$ was

slower than those of the COX1 and COX5B subunits (Figure 48B), observation that agrees with its low steady-state levels (see Figure 43) in this supercomplex. Unfortunately, due to the lack of an efficient antibody against subunit COX7A2, the assembly dynamics of this subunit was not analyzed. However, COX7A2 was the only CIV subunit detected by proteomics in the lowest SC I+III_2 band from the COX2Δ cybrids (Figure 42 and Table 5, Appendix), providing evidence that subunit COX7A2 is probably incorporated prior to the insertion of COX5B and COX4. These data therefore suggest that CIV subunits are integrated into fully-assembled SC I+III_2 in a stepwise fashion that differs between control and COX2Δ cybrids.

These observations are consistent with the structural positions of the analyzed COX subunits within the human respirasome (Guo et al., 2017). As shown in Figure 49, the COX7A2 subunit would attach COX1 to the concave surface formed by $CIII_2$ and the distal end of the CI membrane arm, an interaction that could be further stabilized by the binding of COX5B to $CIII_2$ (Letts, Fiedorczuk, et al., 2016; Wu et al., 2016). In contrast, the association of COX4 to this partially-assembled SC I+III_2+subcomplex [COX1+COX7A2+COX5B] is probably rather unstable, which is reflected in the low steady-state levels (Figure 43) and slow assembly kinetics (Figure 48) of COX4 in this SC.

5. The association of free COX subunits confers stability to SC I+III_2

The accumulation of a partially-assembled SC I+III_2 with associated COX subunits is thus an intriguing feature of cybrids lacking COX2, but not COX1. Among the possible hypotheses, the presence of these free COX subunits may confer stability to SC I+III_2. To test this hypothesis, radioactive pulse-chase analysis of the 13 mitochondrial translation products was performed, in cybrids grown in regular culture medium. The time course of their incorporation into the individual MRC complexes and SCs was subsequently analyzed by 2D-BN/SDS-PAGE and autoradiography (Figure 50). The relative positions of the labelled mtDNA-encoded subunits are indicated according to their molecular weight in control 143B cells (left panel), as well as in the COX2Δ (middle panel) and COX1Δ (right panel) mutants. After a 2 hours pulse (T0) and a chase period of 4 hours (T4), most of the signals corresponding to newly-synthesized subunits of CI (ND1-6) and CIII (cytochrome *b*, CYTB) were progressing from large subcomplexes (in the case of CI proteins) and from free $CIII_2$ (detected from the CYTB signal) to SCs. Between 4-8 hours after chase initiation (times T4-T8), in the 143B cells the COX1, COX2 and COX3 subunits were present in fully-assembled CIV, but not yet integrated in SCs. As expected, no COX subunits were detected in the COX1Δ cybrids. In the COX2Δ cybrids, however, the COX1 and COX3 subunits accumulated in low molecular weight subcomplexes incapable to reach the CIV

position. At 16 hours after chase initiation (T16), in control 143B cells most of the newly-synthesized CI subunits, >50% of CIII CYTB and ~10-15% of CIV subunits were already residing in the fully-assembled respirasomes $I+III_2+IV_1$. In the COX1Δ and COX2Δ mutants the SC $I+III_2$ was also fully-assembled at T16, although there was a larger accumulation of CI subcomplexes and SC-unbound $CIII_2$ than in control cells, in agreement with previous observations (Figures 43A and 46A). Regarding CIV subunits in the COX2Δ cybrids, at T16 the COX1 signal was still mostly accumulated in small subcomplexes while the COX3 signal disappeared, suggesting the rapid degradation of this subunit when COX2 is not present. After 24-hours chase (T24) the respirasomes $I+III_2+IV_1$ remained clearly visible in control 143B cells, as well as SC $I+III_2$ in the COX2Δ cybrids. However, in the COX1Δ cybrids the radioactive signals for CI and CIII subunits declined within SC $I+III_2$, while the relative proportion of subcomplexes increased. Therefore, these results point to the rapid turnover of SC $I+III_2$ in the absence of COX1 and strongly suggest that this SC could be stabilized in the COX2Δ mutants due to the association of free COX subunits.

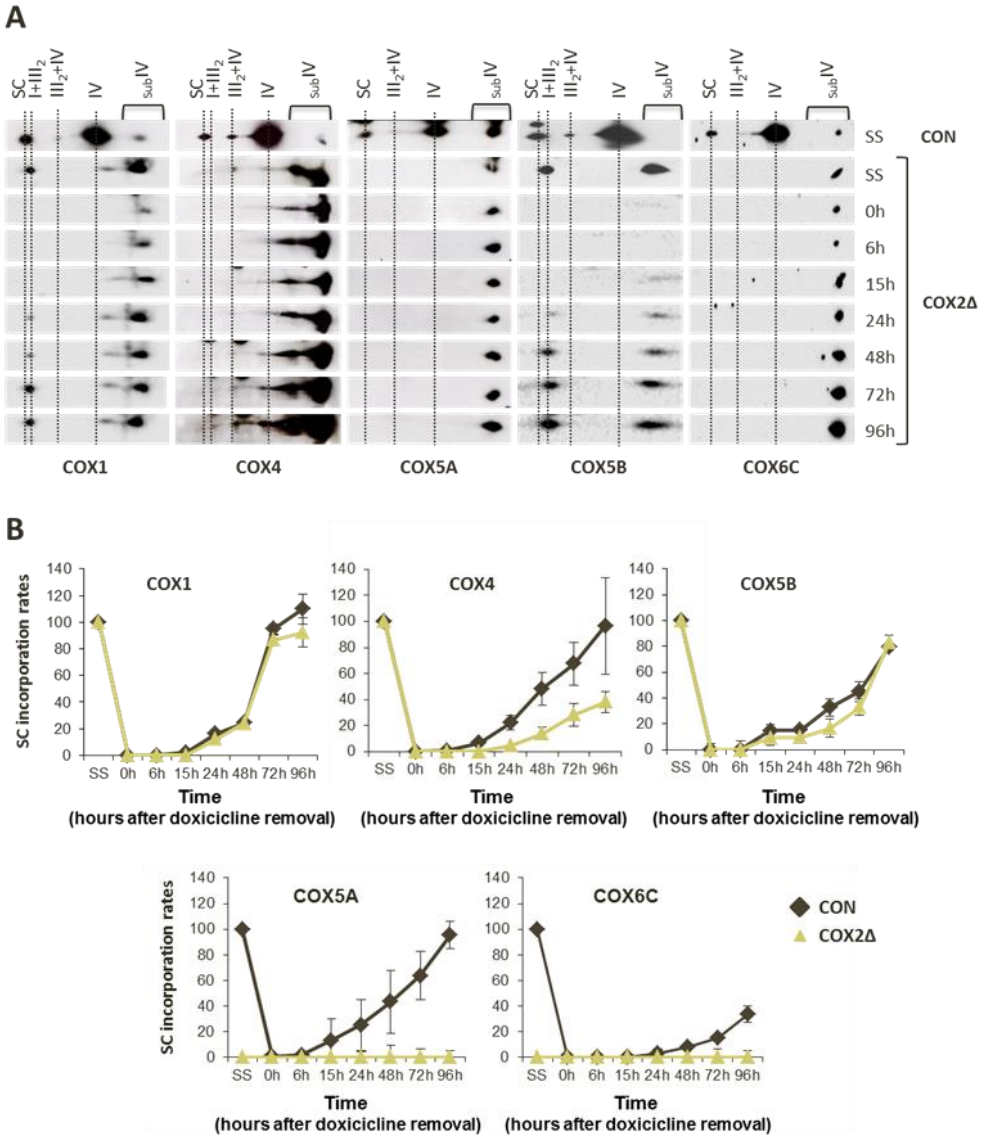

Figure 48. Assembly kinetics of COX subunits in the COX7A2L-containing SC I+III$_2$. (A) Mitochondria from doxycycline-treated COX2Δ mutant cybrids were extracted with a digitonin:protein ratio of 4 g:1 g and analyzed by 2D-BN/SDS-PAGE and western blot with the indicated antibodies. **(B)** Densitometric profiles representing the incorporation rates of COX subunits into SC I+III$_2$. The signals from three independent experiments were quantified and normalized by CII. Time point values are expressed as percentages of the untreated cells (SS) and indicated as means ± SD. Control 143B (CON) values were obtained from (Moreno-Lastres et al., 2012). SC, supercomplex containing CI, CIII and CIV in the control; I+III$_2$, SC containing CI and CIII; III$_2$+IV, SC containing CIII and CIV; IV, complex IV; subCIV, subcomplex IV.

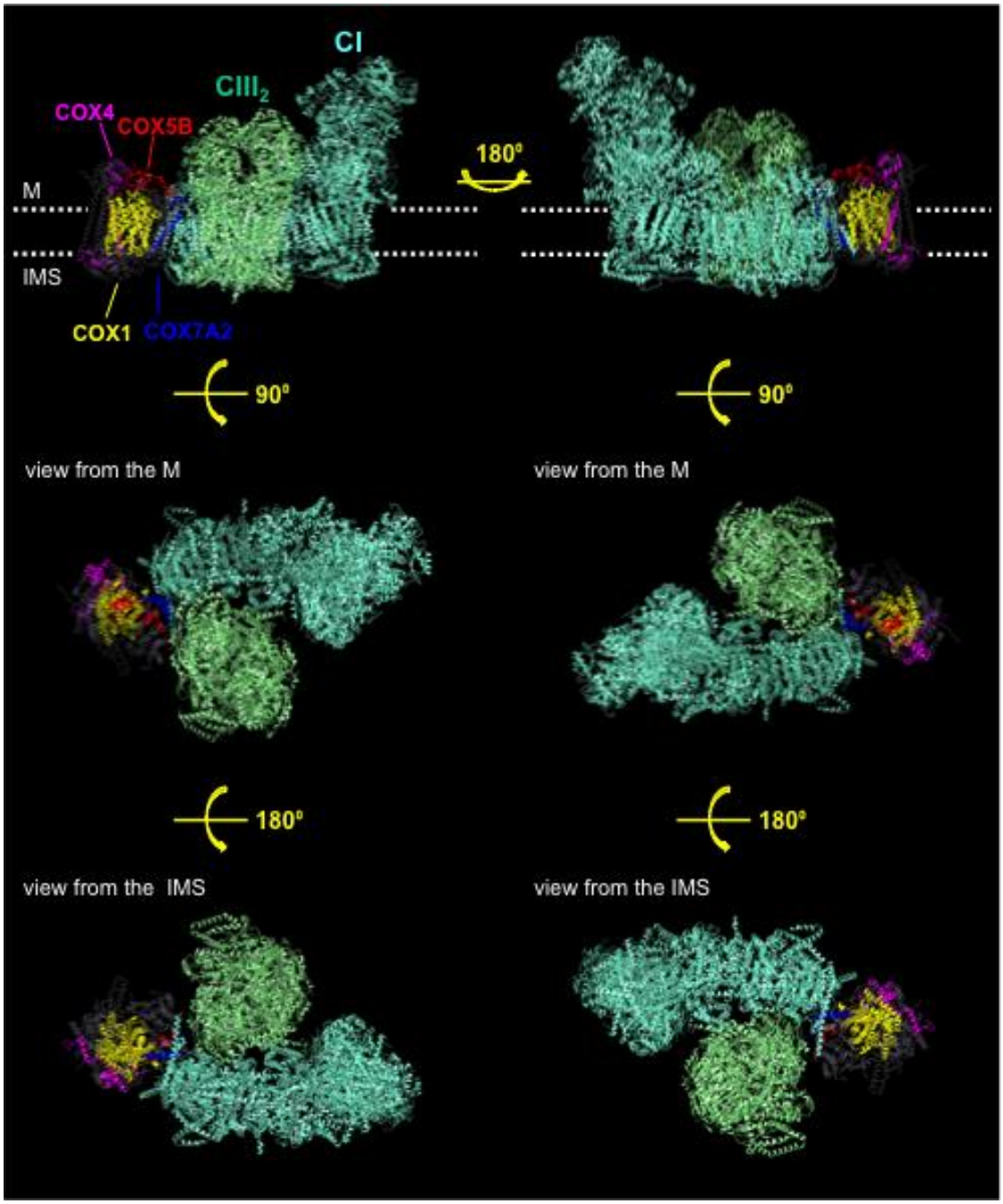

Figure 49. Arrangement of the COX subunits detected in association with SC I+III$_2$. The upper illustrations depict lateral views of human SC I+III$_2$+IV$_1$, in which CI (aquamarine) and dimeric CIII (CIII$_2$) (light green) are positioned along the inner membrane plane (dots). CIV is represented as a smooth backbone with the associated COX subunits highlightened to show their positions relative to SC I+III$_2$. The COX7A2 (blue) and COX5B (red) subunits attach COX1 (yellow) to the concave surface formed by CIII$_2$ and the CI membrane arm. COX4 (magenta) interacts with COX1 on the distal side of the CIV monomer. The same structure viewed from the matrix (M) and from the inter membrane space (IMS) is depicted in the medium and lower illustrations, respectively. The figure was created in the PDB database using the structure 5XTH (Guo et al., 2017).

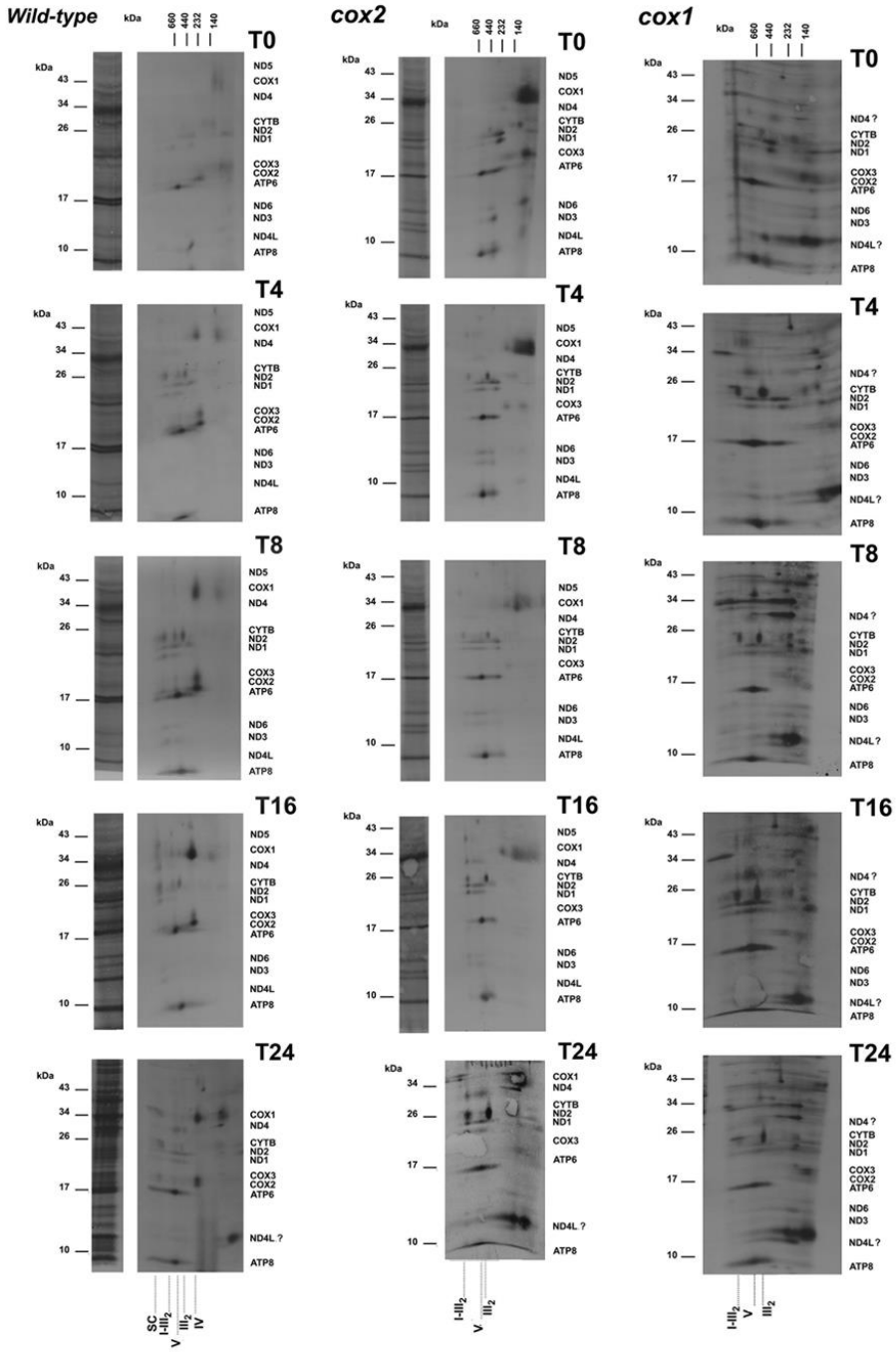

Figure 50. COX subunits-containing SC I+III$_2$ is more stable than COX free-SC I+III$_2$. Mitochondrial translation products were pulse-labeled in 143B and CIV-KO cells with [^{35}S]-methionine for 2 hours in the presence of emetine to inhibit cytosolic translation. In pulse experiments, the cells were then washed and incubated with fresh complete culture media for the indicated time points (T0- T24h). The radiolabeled mitochondrial proteins were separated by 2D-BN/SDS-PAGE and visualized by autoradiography. SC, supercomplex containing CI, CIII and CIV in the control; I+III$_2$, SC containing CI and CIII; III$_2$, dimeric CIII; IV, complex IV; V, complex V.

DISCUSSION

1. Functional characterization of human COX7A2L

The main purpose of this work has been to address how the biogenesis of human mitochondrial SCs is regulated and to clarify the role of the COX7A2L assembly factor in this process. Studies on COX7A2L function have been surrounded by conflicting results (Davoudi et al., 2016; Ikeda et al., 2013; Lapuente-Brun et al., 2013; Mourier, Ruzzenente, et al., 2014; Williams et al., 2016), mostly obtained in mouse models, which the present study is now helping to clarify. In the first chapter of the results section, we have shown that COX7A2L preferentially interacts with mitochondrial CIII and, to a minor extent, with CIV to promote the formation and stabilization of SC III_2+IV in a respirasome-independent manner in both mice and humans. In the second chapter, we have generated TALEN-based *COX7A2L* knockout (*COX7A2L*-KO) HEK293T cell lines to show that the absence of COX7A2L prevents SC III_2+IV formation without affecting *de novo* CIV biogenesis, but it enhances the assembly and accumulation of dimeric CIII ($CIII_2$) with a parallel delay in the formation of CIII-containing SCs and respirasomes that, nonetheless, are capable to reach control steady-state levels. Despite of the structural reorganization of the MRC complexes and SCs, functional substrate competition assays showed normal mitochondrial respiration in the *COX7A2L*-KO cells. However, upon enzymatic or structural induction of CI deficiency, *COX7A2L*-KO cells significantly favored electron flux through CII.

Cox7a2l was originally presented as an exclusive SC assembly factor essential for the incorporation of CIV into SCs III_2+IV and I+III_2+IV_{1-n} in mice (Lapuente-Brun et al., 2013). To investigate the functional role of human COX7A2L, we first used a combination of biochemical techniques and high-throughput proteomics to demonstrate that COX7A2L co-migrates with $CIII_2$, monomeric CIV, SC I+III_2, SC I+III_2 and the respirasomes (SC I+III_2+IV_{1-n}) in both mice and humans. Therefore, COX7A2L is not exclusively present in SCs, as previously reported (Lapuente-Brun et al., 2013; Müller et al., 2016). Moreover, the co-localization patterns of COX7A2L in control and mutant cybrids lacking one MRC complex, and the fact that the stability of COX7A2L depends on the presence of CIII suggest that COX7A2L behaves as a CIII structural component. In agreement, COX7A2L remained associated with $CIII_2$ and CIII-containing SCs in the absence of CI and CIV, and COX7A2L pull-down showed its preferential binding to CIII subunits. Furthermore, analyses of the SCs assembly rates upon reversible treatment with doxycycline showed that COX7A2L bound first to a reported CIII assembly intermediate that lacks the catalytic RISP subunit (pre-$CIII_2$) before it interacts with free CIV, SC III_2+IV or the respirasomes. In agreement with this observation, COX7A2L remained associated with pre-$CIII_2$ in HeLa cells with an impaired incorporation of RISP. In contrast, the lack of the

central CIII subunit cytochrome *b* precluded the formation of pre-$CIII_2$ and led to the disassociation of COX7A2L from CIV. Overall, our data dissent from the proposed role of COX7A2L as an assembly factor exclusive to CIV-containing SCs (Lapuente-Brun et al., 2013).

In C57BL/6 and BALB/c mouse strains, the lack of residues V72-P73 in a naturally-occurring short *Cox7a2l* variant was found to impact Cox7a2l stability and its role in the assembly of SC III_2+IV, the respirasomes, as well as on mitochondrial respiration (Ikeda et al., 2013; Lapuente-Brun et al., 2013). In contrast, our present results in heart mitochondria from different mice strains confirmed the specific loss of SC III_2+IV in the C57BL/6 mice with normal levels of respirasomes and MRC enzymatic activities. Moreover the respirasomes, but not SC III_2+IV, remained stabilized in heart mitochondria from C57BL/6 mice solubilized with increasing detergent concentrations. These data indicate that the respirasomes are stable structures that do not dependent on the *Cox7a2l* allelic variations, in accordance with previous studies (Mourier et al., 2014). Also at variance with the previous studies in fibroblasts from Cox7a2l-deprived mice (Lapuente-Brun et al., 2013), *COX7A2L* mRNA silencing in human cells led to significantly reduced levels of the COX7A2L protein, with a specific loss of SC III_2+IV but without apparent alterations in the amounts of $CIII_2$, monomeric CIV and the respirasomes, nor in the mitochondrial function. Therefore, our data contradict the hypothesis that COX7A2L is an assembly factor that regulates the respirasome formation and, on the contrary, points out a specific role in the biogenesis and stabilization of SC III_2+IV in a respirasome-independent manner. It is important to note that transient COX7A2L overexpression in human cell lines did not cause a significant increase in the levels of individual complexes III and IV, or in the SCs (including SC III_2+IV). These data suggested that COX7A2L is probably essential for the formation and stabilization of SC III_2+IV, but nonetheless it does not regulate its maximum levels.

All our previous results pointed towards the preferential interaction of COX7A2L with mitochondrial $CIII_2$ and, to a minor extent, with monomeric CIV to specifically promote SC III_2+IV biogenesis in both mice and humans. However, according to our experimental approach based on the transient silencing of *COX7A2L* mRNA expression in human cell lines, COX7A2L would neither play a determinant role in the biogenesis, stabilization and function of the free OXPHOS complexes, nor in the formation of the respirasomes I+III_2+IV_{1-n}. Since this experimental strategy still yielded low levels of the COX7A2L protein, results were not fully conclusive. Consequently, the biochemical and functional characterization of TALEN-generated *COX7A2L*-KO human cell lines presented in the second chapter of the results section aimed to provide unambiguous insights into the regulation of the MRC structural organization and respiratory metabolism by human COX7A2L. Our results showed that whereas the SC III_2+IV is

not formed in human *COX7A2L*-KO cells, the respirasomes I+III_2+IV_{1-n} are assembled at slower rates but eventually accumulate to control steady-state levels. These data are in agreement with our former observation in *COX7A2L*-silenced cells, as well as with previous studies that clearly showed the presence of respirasomes in different tissues from C57BL/6 mice, including the heart, liver, and skeletal muscle (Davoudi et al., 2014; Hatle et al., 2013; Ikeda et al., 2013; Jha et al., 2016; Milenkovic et al., 2013; Mourier et al., 2014; Williams et al., 2016), in contrast with the initial report (Lapuente-Brun et al., 2013). It is thus conceivable that *in vivo*, the effect of mouse Cox7a2l in the SCs assembly rates may vary from tissue to tissue, which could be a contributing factor to explain why respirasomes containing more than one CIV unit (I+III_2+IV_{2-n}) seem to be less abundant in liver than in heart from C57BL/6 mice (Williams et al., 2016). However, it is important to acknowledge that the observed changes in mice samples may not necessarily be a consequence of genetic *Cox7a2l* variation, but could well be explained by other types of genetic differences among mouse strains. Based on our data, we cannot exclude the possibility that the mechanisms of SC assembly are regulated in a tissue-dependent manner, as recently proposed (Jha et al., 2016; Williams et al., 2016), and that the previously reported absence of respirasomes in mouse strains with the truncated *Cox7a2l* allele (Lapuente-Brun et al., 2013) was a result from differences in the methodologies or reagents used for membrane protein solubilization. In fact, we observed variations in the intensities of different SC bands between C57BL/6J and CD1 mice strains at high detergent concentrations; however, the pattern was not constant, as specific SCs were stabilized in C57BL/6J mice but not in CD1 mice, and *vice versa*. On the same line, milder SCs extraction conditions (using digitonin at a detergent-to-protein ratio of 1-2:1) revealed no differences in the steady-state levels of SCs I+III_2+IV_{1-n} between *COX7A2L*-KO and WT cells, but a decrease in the abundance of larger SCs (I+III_2+IV_{2-n}) in *COX7A2L*-KO cells.

Regarding the functional impact of the short COX7A2L variant in human cell lines, overexpression of a short COX7A2L did not support SC III_2+IV assembly in *COX7A2L*-KO cells, as previously seen in C57BL/6 mice (Lapuente-Brun et al., 2013); but in contrast with the former report, it neither affected the steady-state levels of SCs I+III_2+IV_{1-n}. As we had observed in heart mitochondria from C57BL/6 mice, the human version of short COX7A2L retained the ability to bind both $CIII_2$ and SC I+III_2, but it did not interact with CIV or CIV-containing respirasomes. In contrast, WT (long) COX7A2L preferentially co-segregated with $CIII_2$, monomeric CIV, as well as with SCs III_2+IV and the respirasomes in human HEK293T cells, as it occurs in our mouse heart mitochondria from CD1 mice and in human 143B osteosarcoma cells. Altogether these data are consistent with our view that the formation and stabilization of SC III_2+IV relies on the association of COX7A2L with $CIII_2$ and CIV through independent protein

domains. This is in agreement with recent observations where COX7A2L binding to CIV requires the correct orientation of a histidine residue at position 73 (Cogliati et al., 2016). These results suggest that COX7A2L promotes specific interactions between $CIII_2$ and CIV that are essential for their association into SC III_2+IV, which are probably different to their interactions in the respirasomes, where CI is recruited into the macrostructure (Gu et al., 2016; Guo et al., 2017; Letts, Fiedorczuk, et al., 2016; Sousa et al., 2016; Wu et al., 2016). In this regard, it is tempting to speculate that different pathways may operate to assemble the different SCs. The fact that mammalian COX7A2L is essential to maintain SC III_2+IV stability, but it plays no critical role in the assembly or stabilization of SC I+III_2+IV_{1-n} strongly suggests that there must be independent regulatory mechanisms for the biogenesis and turnover of SC III_2+IV and the respirasomes. SC III_2+IV could be assembled by the coming-together of the individual complexes, which requires the earlier insertion of COX7A2L in the pre-$CIII_2$ (Figure 51). In contrast, SC I+III_2+IV_1 would be assembled in a COX7A2L-independent manner, compatible with the incorporation of newly-synthesized subunits/subassemblies from $CIII_2$ and CIV that accumulate once these fully-assembled complexes have reached their steady-state levels, into larger structures containing CI intermediates, as previously proposed (Moreno-Lastres et al., 2012) (Figure 51).

The total absence of COX7A2L in our *COX7A2L*-KO cells led to an unexpected significant accumulation of $CIII_2$ levels, which were restored to normal by complementation with the long-COX7A2L variant, but not with the short variant despite it retained the ability to bind the complex. Along this line, we previously mentioned that in cybrid cell lines lacking $CIII_2$, COX7A2L stability was largely compromised. Furthermore, *de novo* assembly studies in control 143B cells showed that whereas COX7A2L assembles into a pre-$CIII_2$ before the incorporation of the catalytic RISP subunit, COX7A2L only joins CIV once this complex is fully assembled. These negative genetic interactions indicate a regulatory role for COX7A2L in $CIII_2$ biogenesis, rather than an adaptation to the inability to form and utilize the SC III_2+IV. As a hypothesis, COX7A2L could establish a $CIII_2$ quality control checkpoint before the complex becomes functionally active by the incorporation of RISP, which would be reminiscent to the role played by MITRAC7 on regulating the turnover of COX1-containing intermediates during CIV assembly (Dennerlein et al., 2015). Based on our data so far, there seems to be a relationship between the deregulation in the $CIII_2$ steady-state levels provoked by the absence of COX7A2L and the delay the formation of the I+III_2+IV_1 respirasomes (Figure 52), as well as on the further incorporation of additional fully-assembled CIV units to generate I+III_2+IV_{2-n} respirasomes. Our results argue that whereas COX7A2L would be permanently associated with CIII, it would exist in association/dissociation equilibrium with CIV, which could define the fate of CIV depending

on whether COX7A2L is bound to it or not. This would provide a mechanism whereby COX7A2L-bound CIV is guided to the proximity of CIII to form and stabilize SC III_2+IV. In this aspect, COX7A2L would resemble HIG2A, the human orthologue of the yeast Rcf1 SC factor. In yeast, Rcf1 preferentially associates with CIV to mediate $SCIII_2+IV_{1-2}$ stability (Chen et al., 2012; Strogolova et al., 2012; Vukotic et al., 2012). Several human homologs of Rcf1 have been reported, whereof HIG2A is involved in the stabilization of a portion of CIV-containing SCs (Chen et al., 2012). C11ORF83 or UQCC3A, a cardiolipin-binding protein involved in the early stages of human CIII assembly, has also been reported to act as a SC III_2+IV-stabilizing factor (Desmurs et al., 2015). The similarities in modes of action between these proteins and COX7A2L make it conceivable that they could act in conjunction, having a respiratory chain ‘‘stabilizing’’ or ‘‘gluing’’ function, although further studies are required to demonstrate such functional interactions.

The impact of the MRC structural remodeling promoted by COX7A2L on mitochondrial physiology has also been a source of controversy. The fact that the formation and stabilization of a less abundant structure such as $SCIII_2$+IV is regulated by a specific protein like COX7A2L in a respirasome-independent manner may be indicative of the, yet not well-understood, physiological importance of SC III_2+IV. Originally, it was proposed that COX7A2L-dependent SCs organization remodeling would provide a mechanism for the physiological regulation of energy metabolism in mammals by providing alternate paths for electrons derived from the catabolism of specific substrates (Lapuente-Brun et al., 2013). In this model, electron flux from CI to $CIII_2$ (carried by NADH) would proceed essentially within the CI-containing SCs, whereas electron flow from CII (carried by FAD) would preferentially occur through free $CIII_2$ and SC III_2+IV (Lapuente-Brun et al., 2013). ATP production and respiration rates were found higher in mouse liver mitochondria and permeabilized fibroblasts with the unstable short-COX7A2L variant, both in the presence of pyruvate + malate (NADH-linked substrates) or succinate (FAD-linked substrate), whereas maximal respiration and ATP production in cells expressing long-COX7A2L required substrates for both electron transfer paths (Lapuente-Brun et al., 2013). However, other groups reported lower mitochondrial respiration and ATP synthesis in muscle (Ikeda et al., 2013) and liver (Shiba et al., 2017) from *COX7A2L*-KO mice, or no effect of short-COX7A2L on mouse heart mitochondrial respiration (Mourier et al., 2014). Our human *COX7A2L*-KO cellular models displayed no differences with WT cells in coupled endogenous cell respiration, or in single and combined substrate (glutamate-malate or succinate) oxidation, indicating a minor functional role of COX7A2L in normal cultured cell physiological conditions. However, the induction of CI deficiency in *COX7A2L*-KO cells had a significant effect on the simultaneous oxidation of glutamate-malate and succinate, which proceeded at rates

significantly higher than in WT cells. These data would support the idea that when CI (and hence, the respirasome) is compromised, electron flow from CII preferentially occurs through free $CIII_2$ rather than by SC III_2+IV that is absent in *COX7A2L*-KO cells. By dynamically regulating $CIII_2$ levels, the formation of SC III_2+IV, and the kinetics of respirasome assembly, COX7A2L would adjust the rate of electron flow from CII to SC-unbound $CIII_2$, which would limit $FADH_2$ oxidation when the catalytic function of CI and NADH oxidation are compromised (Figure 53). This could be a way to facilitate adaptation to varying carbon sources, as previously proposed (Lapuente-Brun et al., 2013). Alternatively, COX7A2L could be part of a metabolic response to accelerate CIII-containing SCs assembly when needed. How metabolism may compensate for CI deficiency in patients suffering from mitochondrial disorders remains intriguing (Zielinski et al., 2016), but the reported compensatory increase in CII activity is not sufficient to overcome the cellular respiratory defect (Esteitie et al., 2005). The value of this compensatory response is highlighted by the recent report that cell-permeable succinate prodrugs can bypass mitochondrial CI deficiency in cultured cells (Ehinger et al., 2016). Our data suggest that COX7A2L could be a key regulator of this adaptive process, which has vast clinical implications and could pave the way for novel *COX7A2L*-targeted gene therapy interventions.

The experimental evidence of independent regulatory mechanisms and proteins for the biogenesis of intermediate SCs and the respirasomes opens new doors for exciting future investigations of the role for these supramolecular structures in the regulation of cellular energy supply.

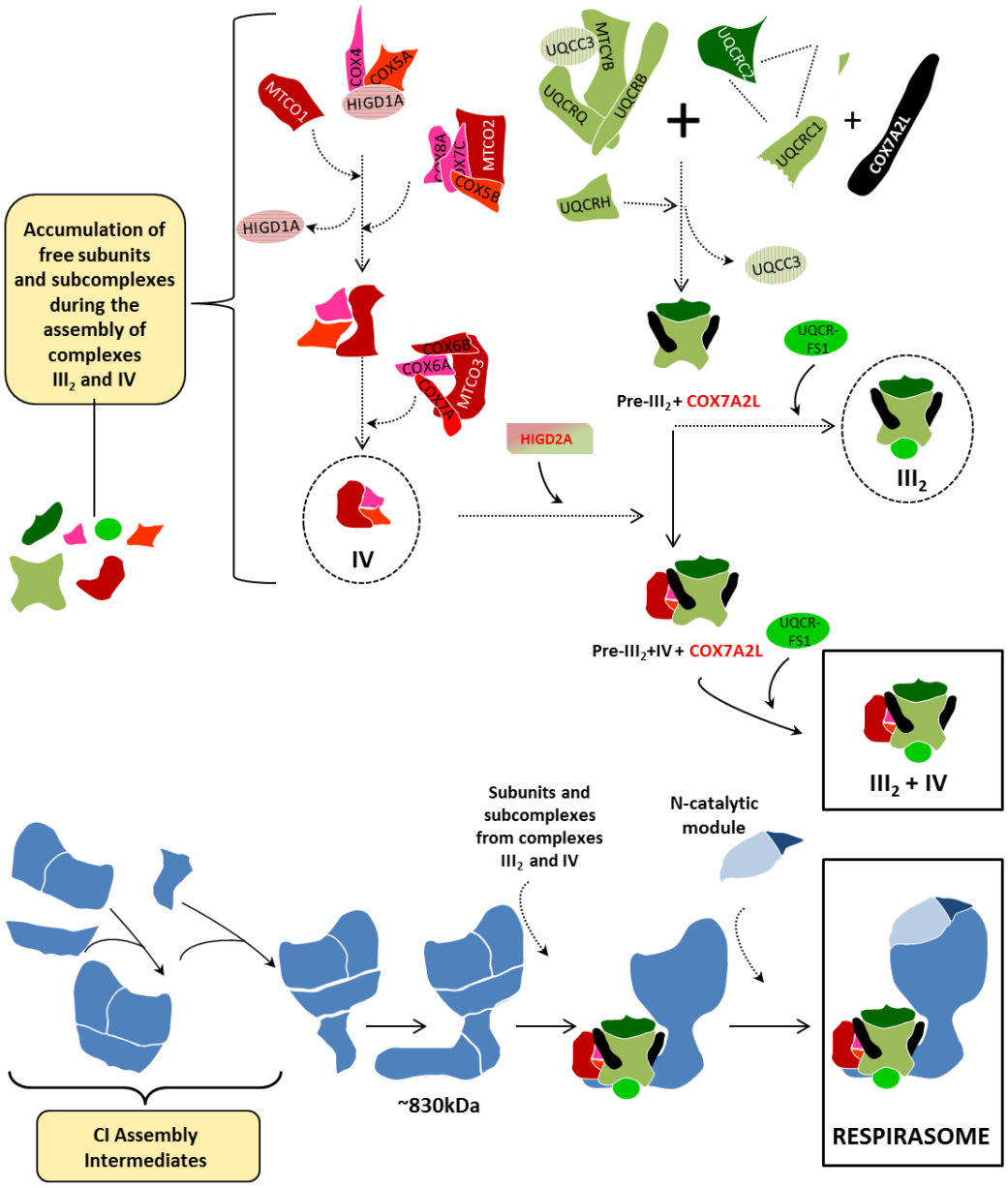

Figure 51. Human COX7A2L-mediated SC III_2+IV biogenesis is independent of respirasome assembly. COX7A2L is bound to pre-$CIII_2$ and CIV binds to COX7A2L-containing pre-III_2 prior to the incorporation of RISP (UQCRFS1). The assembly pathways of individual $CIII_2$ (green) and CIV (red), CI (blue) within the respirasome are depicted according to stablished models (Bottani et al., 2017; Moreno-Lastres et al., 2012; Vidoni et al., 2017), where SC III_2+IV is formed independently of the respirasome.

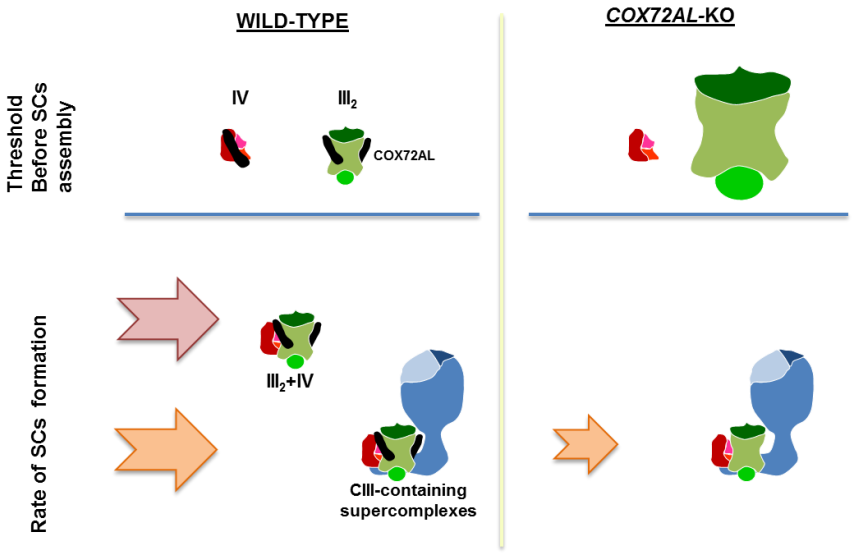

Figure 52. Structural rearrangements of the respiratory chain in the absence of COX7A2L. Fully-assembled $CIII_2$ and CIV accumulate until they reach a threshold that ignites SC III_2+IV and respirasome assembly at rates arbitrarily indicated by arrows. In the absence of COX7A2L, $CIII_2$ levels are ~3-fold, SC III_2+IV is not formed and the assembly kinetics of CIII-containing SCs is slower.

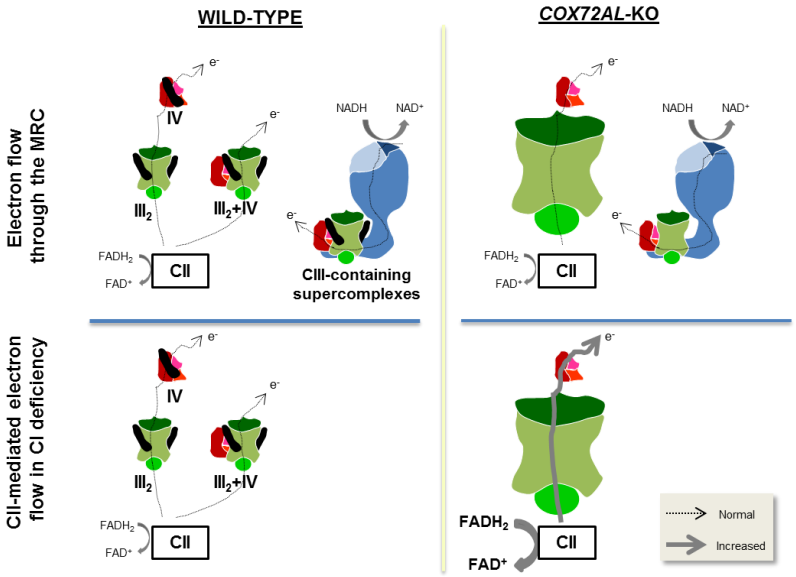

Figure 53. Functional rearrangements of the respiratory chain in the absence of COX7A2L. In physiological conditions, individual and simultaneous oxidation of NADH- and FAD-linked substrates is similar in wild-type and *COX7A2L*-KO cells. However, when CI activity in respirasomes is inhibited, succinate oxidation is enhanced in the absence of COX7A2L presumably due to the larger accumulation of $CIII_2$ and/or absence of SC III_2+IV in the KO cells. Mitochondrial CI, $CIII_2$ and CIV are represented in blue, green and red, respectively. COX7A2L is represented as a black stick.

2. COX7A2L and the structural organization of the respiratory chain in human cybrids lacking complex IV

In cellular and animal models of mitochondrial disease, mutations that generate failures in the assembly or stability of MRC complexes I, III and IV may also affect the formation, stability and activity of other OXPHOS complexes. This will probably lead to a specific accumulation of assembly intermediates that may allow us not only to elaborate a more detailed map of the biosynthetic pathway of the MRC complexes and SCs, but also to better determine the role of COX7A2L as well as of other assembly factors involved in the process. The results presented so far in this study suggest that, besides being essential for the formation and stabilization of SC III_2+IV, COX7A2L plays a regulatory role on the biogenesis of mitochondrial $CIII_2$, but has no functional impact on CIV. In the third chapter of the results section, we have further investigated the influence of COX7A2L on the structural organization of the respiratory chain, and in particular on the biogenesis of CIII-containing structures, in human cellular models of CIV deficiency. In particular, we have analyzed two mutant cybrids lacking CIV (CIV-KOs) due to homoplasmic nonsense mutations that lead to the complete loss of the mtDNA-encoded COX1 and COX2 subunits (COX1Δ and COX2Δ, respectively). As we had previously demonstrated in chapter 1, in the COX1Δ cybrids there was an accumulation of $CIII_2$ and SC I+III_2 that clearly colocalized with COX7A2L (Figure 14). Interestingly, very small amounts of COX7A2L were bound to CIV in the absence of CIII, but COX7A2L appeared at normal levels within the CIII-containing structures present in the absence of CIV. We next extended our experimental strategy to BN-PAGE in combination with proteomics, and time-course analysis of OXPHOS subunits incorporation into SCs, to show that both CIV-KO mutants lack respirasomes (SC I+III_2+IV_{1-n}), but accumulate different SC I+III_2 species that contain COX7A2L and specific COX subunits involved in both early and late steps of the canonical CIV assembly pathway. The association of individual CIV subunits takes place in a stepwise fashion once the SC I+III_2 is fully formed. This process yields a partially-assembled respirasome that remains more stable than the canonical (COX-free) SC I+III_2, indicating that COX7A2L binding is not sufficient to stabilize SC I+III_2. Our data point towards a molecular mechanism through which the binding of free CIV subunits to COX7A2L-containing SC I+III_2 is essential to stabilize CI within the respirasome.

Preceding this work, our research group reported the comigration of CIV subunits COX1 and COX4 in the SC I+III_2 from the COX2Δ mutant (Moreno-Lastres et al., 2012), and suggested that specific free COX subunits or subassemblies could bind directly to SC intermediates in the absence of holo-COX. Here we have confirmed that the absence of CIV leads to the accumulation of different SC I+III_2 species that contain COX7A2L, but surprisingly

these species differ in the presence of specific COX subunits. The fact that the COX1Δ mutant failed to assemble any of the analyzed COX subunits within SC I+III_2, suggests that either COX1 is the first CIV subunit to get incorporated into this structure in order to complete the formation of the respirasome I+III_2+IV_1, or alternatively, that its incorporation is essential to stabilize the association of COX subunits previously bound to SC I+III_2. Although the specific early steps of mammalian CIV biogenesis remains unconcluded (Timón-Gómez et al., 2017), subunit COX1 is traditionally considered as the seed around which monomeric CIV is assembled (Nijtmans et al., 1998; Stiburek et al., 2005; Vidoni et al., 2017; Williams et al., 2004). In agreement, the incorporation of nuclear-encoded COX subunits into SC I+III_2 occurred only in the COX2Δ mutant, which expressed the COX1 subunit at normal levels. Interestingly, COX1 was mainly stabilized in a number of subcomplexes in colocalization with the COX4 and COX5B subunits, but not with COX5A. Based on our observations and partially agreeing with the canonical CIV biosynthetic pathway (Dennerlein and Rehling, 2015; Fernández-Vizarra et al., 2009; Nijtmans et al., 1998; Soto et al., 2012; Stiburek et al., 2005, 2006; Vidoni et al., 2017), subunits COX4 and COX5A would form an independent submodule. In the absence of COX2, only COX4 (and not COX5A) would bind subunit COX1 in a second COX1-COX4 submodule at an early assembly step, to which subunit COX5B would be further incorporated. In addition, we cannot exclude the presence of subunit COX7A2 (also detected by proteomics) in any of these subcomplexes. Our findings partially disagree with the COX1-COX4-COX5A subassembly that is usually observed in other COX-defective cell lines, as well as in fibroblasts from patients with CIV-deficiency (Bourens and Barrientos, 2017a; Kovářová et al., 2012; Stiburek et al., 2005; Williams et al., 2004). For example, human SURF1-depleted cells accumulated the canonical COX1-COX4-COX5A subassembly (Williams et al., 2004), which was also accumulated in heart, skeletal muscle and brain of SCO2 patients (Leary et al., 2004; Stiburek et al., 2005). Both SCO2 and SURF1 play a role in COX2 maturation or assembly, either in the copper transfer to the CuA centre of COX2 (SCO2) (Richter-Dennerlein et al., 2016) or in the association of COX2 with the COX assembly intermediate composed of COX1, COX4 and COX5A (SURF1) (Williams et al., 2004). However, in none of these cases there is a full destabilization of the newly-synthesized COX2, which remains present albeit at reduced levels. Importantly, TALEN-generated *COX18*-KO and *COX20*-KO HEK293T cells, which displayed an isolated CIV deficiency due to the direct breakdown of COX2 synthesis (Bourens et al., 2014; Bourens and Barrientos, 2017a) accumulated several CIV subcomplexes that contained at least subunits COX1 and COX4. Although the authors argued that COX5A was probably present in this COX1-COX4 subassembly, this statement was based solely on the stabilization of COX5A in western-blots on SDS-PAGE gels, which is in agreement with our observations in the COX2Δ

cybrids. Furthermore, one could expect the presence of chaperones or assembly factors attending these COX1- subassemblies, in agreement with the proposed modular assembly mechanism for the cytochrome *c* oxidase in humans (Bourens et al., 2014; Bourens and Barrientos, 2017a, 2017b; Mick et al., 2012; Vidoni et al., 2017) and yeast (McStay et al., 2013), where the biogenesis of each of the three catalytic core subunits (COX1-3) proceeds by a relatively independent process with the participation of subunit-specific chaperones (McStay et al., 2013). In this regard, the well-studied biogenesis of COX1 in yeast shows a rigorous checkpoint through the so-called MITRAC (mitochondrial translation regulation assembly intermediate of COX) complex, which reduces the rate of COX1 translation under unusual conditions, e.g., a limited flux of imported subunits (Barrientos et al., 2004; Mick et al., 2007). In human, a similar regulatory cycle that links COX1 assembly to the translation of its mRNA through MITRAC has been proposed (Dennerlein and Rehling, 2015; Mick et al., 2012), indicating the importance of the evolutionarily-conserved COX1 translation regulatory mechanisms. The binding of the COX1 nascent polypeptide to COA3 (MITRAC12), COA1 (MITRAC15), COX14, CMC1 and SURF1 seems essential to promote COX1 stability, maturation and structural conformation (Bourens and Barrientos, 2017b; Dennerlein and Rehling, 2015; Mick et al., 2012). This MITRAC complex then receives newly-imported nuclear CIV subunits from the mitochondrial pre-sequence translocase (Mick et al., 2012), thus allowing COX1 to progress in the canonical assembly pathway through its interaction with the COX4-COX5A sub-module (Vidoni et al., 2017). Interestingly, an alternative MITRAC constituent, the MITRAC7 chaperone, has been identified to be dispensable for early stages of COX1 assembly but essential for the stabilization of specific COX1 submodules in human, such as COX1-COX4-COX6C (Dennerlein et al., 2015). The fact that COX6C is traditionally considered as a late-assembly subunit opens the possibility of multiple ways of COX1 stabilization in MITRAC complexes of different protein composition. Altogether, these observations suggest that, depending on the CIV subunit holding a specific pathogenic mutation, different CIV subcomplexes might be assembled to stabilize subunit COX1, which is indispensable to ignite CIV biogenesis. It is thus conceivable that in the absence of subunits COX2 and COX3 there could be a rearrangement of COX1-containinig submodules formed by specific CIV subunits, and possibly some of them in a competent state for their direct incorporation into SCs. Overall, our data indicate the accumulation of COX1-containing subassemblies in the COX2Δ cells that, due to the impossibility to form holo-CIV, would be directly integrated into SCI+III_2. Our results thus suggest different mechanisms of CIV assembly depending on whether the fate of this complex is to get associated or not with SCs.

The presence of specific COX subunits within the SC I+III_2 in the absence of fully-assembled CIV is a good indication that free COX subunits or subassemblies may associate gradually in SCs, in contrast with alternative models proposing that the respirasomes are formed by the association of fully-assembled complexes I, III and IV (Acín-Pérez et al., 2008; Guerrero-Castillo et al., 2017). Our results are in agreement with previous studies in yeast (Mick et al., 2007), where a partially assembled CIV was already competent to associate with $CIII_2$, as well as with the finding that in skin fibroblasts mitochondria from patients with severe CIV deficiency and unstable CIV, COX nuclear-encoded subunits (including COX4) were preferentially incorporated into SC I+III_2 (Lazarou et al., 2009). Moreover, in the proposed human respirasome assembly model (Moreno-Lastres et al., 2012), newly-synthesized COX subunits and subassemblies incorporated sequentially into larger structures that already contained CI and CIII assembly intermediates, therefore giving support for CIV subunits to assemble individually into the SCs in patients' mitochondria. In contrast, an extensive study on patients' fibroblasts with mutations in the assembly factor SURF1, characterized by a pronounced COX deficiency and the accumulation of CIV subcomplexes, showed that fully-assembled CIV rather than its subassemblies was preferentially associated with CI and $CIII_2$ to form SCs (Kovářová et al., 2012). Our results do not necessarily contradict previous statements (Acín-Pérez et al., 2008; Guerrero-Castillo et al., 2017; Kovářová et al., 2012), since alternative pathways for SCs biogenesis might exist in different cell lines or tissues to adjust respiratory chain function to the availability of specific MRC structural components.

Our results are consistent with the recent highly-resolved structures for the mammalian respirasomes (Gu et al., 2016; Guo et al., 2017; Letts, Fiedorczuk, et al., 2016; Sousa et al., 2016; Wu et al., 2016), except for the presence of the COX7A2L assembly factor in these structures. Noteworthy, the described respirasome structures point out an interaction between $CIII_2$ and CIV that is defined by an uncertain COX7A isoform and CIII subunits (UQCR11, UQCRC1 and UQCRB). Analysis of the loose structure of the ovine respirasome, showed that this COX7A isoform may switch contacts from $CIII_2$ to the CI subunit ND5 (Letts, Fiedorczuk, et al., 2016). Consistently, an interaction between COX7A and the CI subunit NDUFB8, which structurally is part of the ND5 module, was also observed in the porcine respirasome (Wu et al., 2016). In none of the recently described mammalian respirasomes, including the human one (Guo et al., 2017), the precise identity of the COX7A isoform responsible for these interactions has been resolved yet. Our proteomics analyses unambiguously detected both COX7A2L and the liver-isoform of COX7A (subunit COX7A2) co-existing in the respirasomes (SC I+III_2+IV) from control 143B cells, as well as in the two SC I+III_2 species from the COX2Δ mutant. According to our data, in the COX2Δ cybrids, besides

COX7A2L and subunit COX7A2, CIV subunits COX1, COX4 and COX5B were additionally incorporated into SC I+III_2. However, in the COX1Δ mutant, COX7A2L was present in SCI+III_2 without any detectable COX subunit, probably through interactions with CIII_2. These observations suggest that subunit COX7A2 would anchor COX1 to the COX7A2L-containing SC I+III_2, an interaction that could be further stabilized by the binding of COX5B and the formation of a partially-assembled respirasome, composed of SC I+III_2+subcomplex [COX1+COX7A2+COX5B]. The association of COX4 to the partially-assembled SC I+III_2+subcomplex [COX1+COX7A2+COX5B] is probably unstable due to the absence of subunit COX5A in the SC I+III_2 in the COX2Δ mutant. A striking observation is the coexistence of subunits COX5B and COX7A2 together with COX1 in the SC I+III_2, since these two subunits form part of independent CIV submodules that get incorporated in intermediate- or late-assembly steps in CV biogenesis. These observations again suggest the coexistence of alternative assembly pathways for the synthesis of free- versus SC-associated CIV, but how this is regulated at the molecular level remains unknown.

The well-known existence of CIV tissue-specific isoforms in mammalian cells and tissues, such as the liver/heart-type pairs of CIV subunits COX7A2/ COX7A1 (among others) could be an adaptation to tissue-specific metabolic demands. Heart (or muscle) isoforms are expressed in tissues that have high aerobic capacity and abundant mitochondria, whereas liver (or non-muscle) isoforms are found in tissues like brain and kidney that contain fewer mitochondria (Timón-Gómez et al., 2017). It was recently proposed in mice that the relative abundance of tissue-specific CIV subunit isoforms could vary among MRC structures in different tissues and mice strains (Cogliati et al., 2016). For instance, in liver and heart from CD1 mice expressing the long COX7A2L/SCAFI variant, the COX7A2 subunit was reported to be present almost exclusively in monomeric CIV (also slightly detected in heart respirasome), and would be preferentially replaced by COX7A2L/SCAFI in SCs that contain CIV associated with CIII_2 (the I+III_2+IV respirasomes and SC III_2+IV), and by COX7A1 in CIV dimers. In C57BL/6 mice, the COX7A2 subunit distribution appeared to be similar to that in CD1 mice; however, this subunit would be replaced by the short COX7A2L/SCAFI variant, uncapable to bind CIV and to promote associations between complexes III and IV. Therefore, the absence of functional COX7A2L/SCAFI would lead to the absence of SC III_2+IV and to looser (probably unstable) respirasomes exclusively containing subunit COX7A2 (Cogliati et al., 2016). The proteomics detection of subunit COX7A2 along with COX7A2L/SCAFI within the SC I+III_2 in our cellular models, as well as within monomeric CIV in HEK293T cells (Vidoni et al., 2017) partially disagrees with the interchange-hypothesis of COX7A subunits isoforms in different CIV-containing structures. Instead, our results support the co-existence of different CIV species,

either with COX7A2L or COX7A2 alone, or even with both proteins co-existing together within the same structure, in agreement with yeast studies showing a heterogeneous population of CIV variants with regards to their subunit composition and SCs assembly (Vukotic et al., 2012).

The presence of tissue-specific isoforms of nuclear-encoded COX subunits (Timón-Gómez et al., 2017), the heterogeneity of CIV species in both mammalian (Cogliati et al., 2016) and yeast (Chen et al., 2012; Strogolova et al., 2012; Vukotic et al., 2012), and the fact that mutations in CIV assembly factors may result in tissue-specific variations in CIV assembly into SCs (Kovářová et al., 2012; Stiburek et al., 2005) give evidence that CIV biogenesis is a heterogeneous process that remains to be fully-understood. According to our data, the binding of four specific COX subunits to SC I+III_2 yields a partially-assembled respirasome that is more stable than the canonical (COX-free) SC I+III_2. These findings gain intrigue due to the circumstance that the precise roles of the SCs and respirasomes remain unclear, and they could point out an unexpected mechanism for CI stabilization in the respirasomes. In fact, the possible role of the SCs in the stabilization of individual MRC complexes, most particularly on CI, is currently a field of intense debate. CI functional alterations are relatively infrequent to most patients presenting with $CIII_2$ or CIV enzyme deficiencies (Fernández-Vizarra and Zeviani, 2015; Rak et al., 2016), indicating that only severe structural alterations of these two complexes induce a parallel CI dysfunction. Our kinetics analyses in COX-KO cells suggest that the lack of CIV promotes the association of CI with a $CIII_2$ assembly intermediate that lacks the RISP subunit (pre-$CIII_2$), to form a partially-assembled SC (pre-SC I+III_2) that awaits RISP incorporation to complete SC I+III_2 formation (Figure 54). CI could be stabilized through its interaction with either pre-$CIII_2$ or fully-assembled $CIII_2$, consistent with experimental evidence on respiratory chain disease models, where CI is unstable if not associated with $CIII_2$ (Acín-Pérez et al., 2004; Schägger et al., 2004). Analyses in *Ndufs4*-KO mice showed that a partially-assembled CI lacking its functional NADH-binding (N) module tends to associate with $CIII_2$ in an incomplete SC (Calvaruso et al., 2012), providing further evidence that $CIII_2$ aids CI stabilization. In contrast, CI stability is mainly affected by the absence of CIV in rapidly dividing cells, as evidenced in *Cox10*-KO mouse fibroblasts (Diaz et al., 2006), in human cybrid cells (D'Aurelio et al., 2006) or in mouse cells with limited expression of subunit Cox4 (Li et al., 2007). Studies in heteroplasmic COX1 mutant cybrids also showed that small levels of fully-assembled CIV are sufficient to stabilize CI and the SCs (D'Aurelio et al., 2006), leading to the proposal that a CIV defect may only lead to combined OXPHOS deficiencies when it has surpassed a certain threshold. This is a way to reconcile different observations between patients and cellular models of CIV deficiency that showed close to normal CI activity (Tiranti et al., 2000; Valente et al., 2009). In accordance with these studies, our results argue in favour of a stabilizing role for

individual COX subunits on SC I+III_2. Alternatively, our findings may suggest the existence of a regulatory checkpoint at the level of SCs, for instance, through a mechanism for COX1 subunit stabilization within the SCs when CIV biogenesis is compromised. A previous study in cybrids with homoplasmic nonsense mutations in subunit COX1 showed that the truncated COX1 species were translated and successfully assembled into SC I+III_2, yet this SC was unstable and degraded rapidly (Hornig-Do et al. 2012). This study, as ours, suggests that the association of CI with $CIII_2$ is not sufficient to stabilize the SC I+III_2 and that CIV would function as a stabilizer.

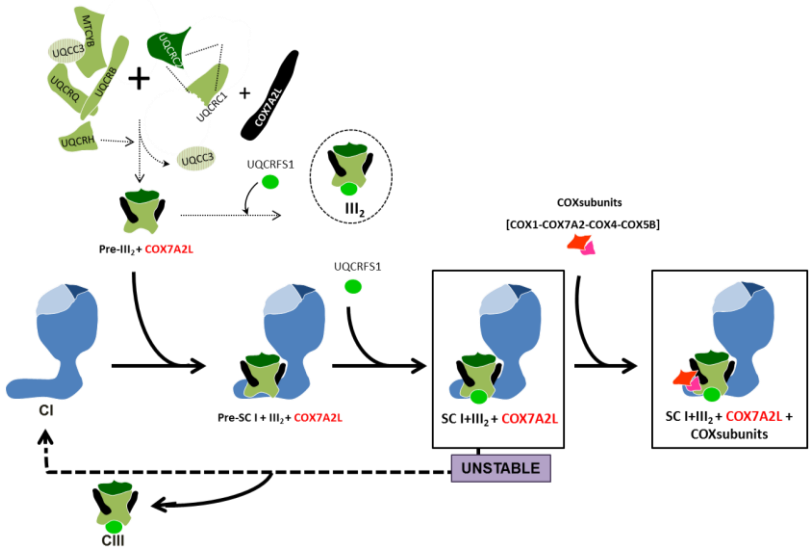

Figure 54. Biogenesis of COX7A2L-containing SC I+III_2 in CIV-deficient cybrids. COX7A2L binds a $CIII_2$ assembly intermediate that lacks the RISP subunit (pre-$CIII_2$ + COX7A2L), which joins CI to form a partially-assembled SC (pre-SC I+III_2) that awaits RISP incorporation to complete SC I+III_2 formation. The subsequent association of specific COX subunits adds stability to SC I+III_2. The assembly pathway of individual $CIII_2$ is depicted according to reported models (Bottani et al., 2017).

As a final remark, the impact of COX7A2L on the biogenesis of $CIII_2$ and SC I+III_2 remains to be clarified in cells lacking CIV. COX7A2L protein levels have been described to increase upon cellular stress conditions that stimulate energy metabolism (Zhang et al., 2016), which would enhance its binding to $CIII_2$ and CIV, and SCs formation. In agreement, our data show that COX7A2L may accelerate *di novo* SCs formation and therefore, upon *COX7A2L* silencing one would expect a delay in the SC I+III_2 assembly rates. However, since $CIII_2$ levels are already increased in CIV-KO cells, the effect of a hypothetical *COX7A2L* silencing on the structural reorganization of the MRC is unclear. The future perspectives should include the generation of a *COX7A2L*-KO in COX-deficient cell lines to detail the role of this protein when CIV is structurally and functionally compromised. Since COX7A2L could be part of a metabolic response to accelerate $CIII_2$-containing SCs assembly when needed, functional assays with different carbon sources and stress conditions, e.g., during hypoxia, may give exciting outcomes of the accurate metabolic role of COX7A2L.

CONCLUSIONS / CONCLUSIONES

1. COX7A2L is a mitochondrial protein that colocalizes with the respiratory chain complex III dimer, with monomeric complex IV, and with supercomplexes III_2+IV, I+III_2 and I+III_2 +IV_1.

2. COX7A2L preferentially associates to complex III, and with a lower affinity to complex IV. COX7A2L initially binds to a complex III assembly intermediate (named pre-complex III) prior to the incorporation of the RISP subunit, and later to fully assembled CIV.

3. Silencing of *COX7A2L* mRNA expression in human control cells displays a significant reduction of the supercomplex III_2+IV levels, without affecting the levels of the respirasomes or individual complexes III and IV.

4. Using the TALEN technology we have generated *COX7A2L-knockout* HEK293T cells (*COX7A2L*-KO). These cells exhibit a total absence of supercomplex III_2+IV, a significant increase in complex III biogenesis and a delay in the respirasome assembly rates, which nonetheless reach control steady-state levels.

5. *COX7A2L*-mutant HEK293T cells generated *in vitro* that carry an in-frame 6-base-pair deletion in the *COX7A2L* gene exhibit a total absence of supercomplex III_2+IV and control respirasome levels. In this human model the short version of COX7A2L colocalizes with respiratory chain complex III dimer and with supercomplex I+III_2, as in mouse C57BL/6 heart mitochondria.

6. Functional substrate competition assays show no significant differences in mitochondrial respiration between control and *COX7A2L*-KO cells. However, upon induction of CI deficiency, the absence of COX7A2L significantly favours succinate oxidation and electron transfer from complex II to complex III.

7. Human cybrids with homoplasmic nonsense mutations in the *MT-CO1* and *MT-CO2* genes lack mitochondrial complex IV, and accumulate different COX7A2L- containing supercomplex I+III_2 species that differ in their COX subunit composition.

8. The supercomplexes I+III_2 from mutant cybrids lacking COX2 contain subunits COX1, COX4, COX5B and COX7A2, and are more stable than the COX-free supercomplex I+III_2 present in mutant cybrids lacking COX1.

9. COX7A2 is the COX7A subunit isoform present in the respirasomes from human cybrids.

1. COX7A2L es una proteína mitocondrial que colocaliza con los complejos III y IV individuales de la cadena respiratoria mitocondrial, y con los supercomplejos III_2+IV, I+III_2 and I+III_2 +IV_1.

2. COX7A2L se asocia preferentemente al complejo III y con menor afinidad al complejo IV. Inicialmente, COX7A2L se une a un intermediario del complejo III (denominado pre-complejo III) antes de la incorporación de la subunidad RISP, y posteriormente al CIV totalmente ensamblado.

3. El silenciamiento de la expresión del mRNA de *COX7A2L* en células control de origen humano produce una reducción significativa de los niveles del supercomplejo III_2+IV, sin afectar a los niveles del respirasoma ni a los de los complejos III y IV individuales.

4. Usando la tecnología TALEN, se han generado células HEK293T carentes de COX7A2L (*COX7A2L*-KO). Estas células muestran una ausencia total del supercomplejo III_2+IV, un incremento significativo de la biogénesis del complejo III y un retraso en las cinéticas de formación del respirasoma, el cual alcanza niveles estacionarios comparables a los de células control.

5. Células HEK293T mutantes generadas *in vitro* portadoras de una delección de 6 pares de bases en el gen de *COX7A2L* muestran una ausencia total del supercomplejo III_2+IV y niveles de respirasoma comparables a los de células control. En este modelo celular humano la versión corta de COX7A2L colocaliza con el complejo III dimérico y con el supercomplejo I+III_2, como ocurre en mitocondrias de corazón del ratón C57BL/6.

6. Ensayos funcionales de competición de sustratos no muestran diferencias significativas en la respiración mitocondrial entre células HEK293T control y células *COX7A2L*-KO. Sin embargo, en ausencia de COX7A2L, la inducción de un déficit enzimático del complejo I favorece significativamente la oxidación de succinato y el flujo de electrones entre el complejo II y el complejo III.

7. Cíbridos humanos portadores de mutaciones sin sentido en los genes *MT-CO1* y *MT-CO2* carecen de CIV mitocondrial, pero acumulan diferentes especies de supercomplejo I+III_2, las cuales contienen a COX7A2L y difieren en su contenido de subunidades COX.

8. Los supercomplejos $I+III_2$ del cíbrido mutante carente de COX2 contienen a las subunidades del complejo IV COX1, COX4, COX5B y COX7A2. Estos supercomplejos son más estables que el supercomplejo $I+III_2$ (libre de subunidades COX) del cíbrido mutante carente de COX1.

9. La subunidad COX7A2 es la isoforma de COX7A presente en el respirasoma de cíbridos humanos.

BIBLIOGRAPHY

Acín-Pérez, R., Bayona-Bafaluy, M.P., Fernández-Silva, P., Moreno-Loshuertos, R., Pérez-Martos, A., Bruno, C., Moraes, C.T., et al. (2004), "Respiratory complex III is required to maintain complex I in mammalian mitochondria", *Molecular Cell*, Vol. 13 No. 6, pp. 805–815.

Acin-Perez, R. and Enriquez, J.A. (2014), "The function of the respiratory supercomplexes: The plasticity model", *Biochimica et Biophysica Acta - Bioenergetics*, Vol. 1837 No. 4, pp. 444–450.

Acín-Pérez, R., Fernández-Silva, P., Peleato, M.L., Pérez-Martos, A. and Enriquez, J.A. (2008), "Respiratory Active Mitochondrial Supercomplexes", *Molecular Cell*, Vol. 32 No. 4, pp. 529–539.

Alberts, B., Johnson, A., Lewis, J., Raff, M., Roberts, K. and Walter, P. (2007), *Molecular Biology of the Cell*, 5th ed., Garland Science, New York.

Althoff, T., Mills, D.J., Popot, J.-L. and Kühlbrandt, W. (2011), "Arrangement of electron transport chain components in bovine mitochondrial supercomplex I1III2IV1.", *The EMBO Journal*, Vol. 30 No. 22, pp. 4652–64.

Anderson, S., Bankier, A.T., Barrell, B.G., de Bruijn, M.H.L., Coulson, A.R., Drouin, J., Eperon, I.C., et al. (1981), "Sequence and organization of the human mitochondrial genome", *Nature*, Vol. 290 No. 5806, pp. 457–465.

Andrews, R.M., Kubacka, I., Chinnery, P.F., Lightowlers, R.N., Turnbull, D.M. and Howell, N. (1999), "Reanalysis and revision of the Cambridge reference sequence for human mitochondrial DNA.", *Nature Genetics*, Vol. 23 No. 2, pp. 147–147.

Antonicka, H., Ogilvie, I., Taivassalo, T., Anitori, R.P., Haller, R.G., Vissing, J., Kennaway, N.G., et al. (2003), "Identification and Characterization of a Common Set of Complex I Assembly Intermediates in Mitochondria from Patients with Complex I Deficiency", *Journal of Biological Chemistry*, Vol. 278 No. 44, pp. 43081–43088.

Aras, S., Pak, O., Sommer, N., Finley, R., Hü Ttemann, M., Weissmann, N. and Grossman, L.I. (2013), "Oxygen-dependent expression of cytochrome c oxidase subunit 4-2 gene expression is mediated by transcription factors RBPJ, CXXC5 and CHCHD2", *Nucleic Acids Research*, Vol. 41 No. 4, pp. 2255–2266.

Atkinson, A., Smith, P., Fox, J.L., Cui, T.Z., Khalimonchuk, O. and Winge, D.R. (2011), "The LYR Protein Mzm1 Functions in the Insertion of the Rieske Fe/S Protein in Yeast Mitochondria", *Mol Cell Biol*, Vol. 31 No. 19, pp. 3988–3996.

Babot, M., Birch, A., Labarbuta, P. and Galkin, A. (2014), "Characterisation of the active/de-active transition of mitochondrial complex i", *Biochimica et Biophysica Acta - Bioenergetics*, Elsevier B.V., Vol. 1837 No. 7, pp. 1083–1092.

Baradaran, R., Berrisford, J.M., Minhas, G.S. and Sazanov, L.A. (2013), "Crystal structure of the entire respiratory complex I", *Nature*, Vol. 494 No. 7438, pp. 443–448.

Barja, G. (1999), "Mitochondrial oxygen radical generation and leak: sites of production in states 4 and 3, organ specificity, and relation to aging and longevity.", *Journal of Bioenergetics and Biomembranes*, Vol. 31 No. 4, pp. 347–66.

Barrientos, A., Barros, M.H., Valnot, I., Rötig, A., Rustin, P. and Tzagoloff, A. (2002), "Cytochrome oxidase in health and disease", *Gene*, Vol. 286 No. 1, pp. 53–63.

Barrientos, A., Fontanesi, F. and Diaz, F. (2009), *Evaluation of the Mitchondrial Respiratory Chain and Oxidative Phosphorylation System Using Polarography and Spectrophotometric Enzyme Assays*, *Current Protocols in Human Genetics*, Vol. 19, available at:https://doi.org/10.1002/0471142905.hg1903s63.Evaluation.

Barrientos, A. and Ugalde, C. (2013), "I Function, therefore i am: Overcoming skepticism about mitochondrial supercomplexes", *Cell Metabolism*, Elsevier, Vol. 18 No. 2, pp. 147–149.

Barrientos, A., Zambrano, A. and Tzagoloff, A. (2004), "Mss51p and Cox14p jointly regulate mitochondrial Cox1p expression in Saccharomyces cerevisiae", *The EMBO Journal*, Vol. 23 No. 17, pp. 3472–3482.

Benard, G., Faustin, B., Galinier, A., Rocher, C., Bellance, N., Smolkova, K., Casteilla, L., et al. (2008), "Functional dynamic compartmentalization of respiratory chain intermediate substrates: Implications for the control of energy production and mitochondrial diseases", *The International Journal of Biochemistry & Cell Biology*, Vol. 40 No. 8, pp. 1543–1554.

Berrisford, J.M. and Sazanov, L.A. (2009), "Structural basis for the mechanism of respiratory complex I", *Journal of Biological Chemistry*, Vol. 284 No. 43, pp. 29773–29783.

Berry, E.A. and Trumpower, B.L. (1985), “Isolation of ubiquinol oxidase from Paracoccus denitrificans and resolution into cytochrome bc1 and cytochrome c-aa3 complexes”, *Journal of Biological Chemistry*, Vol. 260 No. 4, pp. 2458–2467.

Bezawork-Geleta, A., Dong, L., Rohlena, J. and Neuzil, J. (2016), “The Assembly Factor SDHAF2 Is Dispensable for Flavination of the Catalytic Subunit of Mitochondrial Complex II in Breast Cancer Cells”, *Journal of Biological Chemistry*, Vol. 291 No. 41, pp. 21414–21420.

Bezawork-Geleta, A., Rohlena, J., Dong, L., Pacak, K. and Neuzil, J. (2017), “Mitochondrial Complex II: At the Crossroads”, *Trends in Biochemical Sciences*, Elsevier Ltd, Vol. 42 No. 4, pp. 312–325.

Bezawork-Geleta, A., Saiyed, T., Dougan, D.A. and Truscott, K.N. (2014), “Mitochondrial matrix proteostasis is linked to hereditary paraganglioma: LON-mediated turnover of the human flavinylation factor SDH5 is regulated by its interaction with SDHA”, *The FASEB Journal*, Vol. 28 No. 4, pp. 1794–1804.

Blair, P. (1967), “Preparation and properties of repeating units of electron transfer.”, *Methods in Enzymology*, p. 10: 208-212.

Blanchi, C., Genova, M.L., Castelli, G.P. and Lenaz, G. (2004), “The mitochondrial respiratory chain is partially organized in a supercomplex assembly: Kinetic evidence using flux control analysis”, *Journal of Biological Chemistry*, Vol. 279 No. 35, pp. 36562–36569.

Blaza, J.N., Serreli, R., Jones, A.J.Y., Mohammed, K. and Hirst, J. (2014), “Kinetic evidence against partitioning of the ubiquinone pool and the catalytic relevance of respiratory-chain supercomplexes.”, *Proceedings of the National Academy of Sciences of the United States of America*, Vol. 111 No. 44, pp. 15735–40.

Blázquez, A., Arenas, J. and Martín, M.A. (2016), “Molecular Genetics of OXPHOS Disorders”, *eLS*, John Wiley & Sons, Ltd, Chichester, UK, pp. 1–10.

Boch, J., Scholze, H., Schornack, S., Landgraf, A., Hahn, S., Kay, S., Lahaye, T., et al. (2009), “Breaking the Code of DNA Binding Specificity of TAL-Type III Effectors”, *Science*, Vol. 326 No. 5959, pp. 1509–1512.

Van den Bogert, C., Dontje, B.H.J., Melis, T.E., van der Veen, C. and Kroon, A.M. (1988), “Inhibition of mitochondrial protein synthesis influences the glucocorticoid sensitivity of

lymphoid cells", *BBA - Molecular Cell Research*, Vol. 972 No. 3, pp. 302–310.

Bottani, E., Cerutti, R., Harbour, M.E., Ravaglia, S., Dogan, S.A., Giordano, C., Fearnley, I.M., et al. (2017), "TTC19 Plays a Husbandry Role on UQCRFS1 Turnover in the Biogenesis of Mitochondrial Respiratory Complex III", *Molecular Cell*, Elsevier Inc., Vol. 67 No. 1, p. 96–105.e4.

Böttinger, L., Horvath, S.E., Kleinschroth, T., Hunte, C., Daum, G., Pfanner, N. and Becker, T. (2012), "Phosphatidylethanolamine and cardiolipin differentially affect the stability of mitochondrial respiratory chain supercomplexes", *Journal of Molecular Biology*, Elsevier Ltd, Vol. 423 No. 5, pp. 677–686.

Boumans, H., Grivell, L.A. and Berden, J.A. (1998), "The respiratory chain in yeast behaves as a single functional unit", *Journal of Biological Chemistry*, Vol. 273 No. 9, pp. 4872–4877.

Bourens, M. and Barrientos, A. (2017a), "Human mitochondrial cytochrome c oxidase assembly factor COX18 acts transiently as a membrane insertase within the subunit 2 maturation module", *Journal of Biological Chemistry*, Vol. 292 No. 19, pp. 7774–7783.

Bourens, M. and Barrientos, A. (2017b), "A *CMC1* -knockout reveals translation-independent control of human mitochondrial complex IV biogenesis", *EMBO Reports*, Vol. 18 No. 3, pp. 477–494.

Bourens, M., Boulet, A., Leary, S.C. and Barrientos, A. (2014), "Human COX20 cooperates with SCO1 and SCO2 to mature COX2 and promote the assembly of cytochrome c oxidase", *Human Molecular Genetics*, Vol. 23 No. 11, pp. 2901–2913.

Bruno, C., Martinuzzi, a, Tang, Y., Andreu, a L., Pallotti, F., Bonilla, E., Shanske, S., et al. (1999), "A stop-codon mutation in the human mtDNA cytochrome c oxidase I gene disrupts the functional structure of complex IV.", *American Journal of Human Genetics*, Vol. 65 No. 3, pp. 611–620.

Bultema, J.B., Braun, H.P., Boekema, E.J. and Kouřil, R. (2009), "Megacomplex organization of the oxidative phosphorylation system by structural analysis of respiratory supercomplexes from potato", *Biochimica et Biophysica Acta - Bioenergetics*, Vol. 1787 No. 1, pp. 60–67.

Cadenas, E., Boveris, A., Ragan, C.I. and Stoppani, A.O. (1977), "Production of superoxide

radicals and hydrogen peroxide by NADH-ubiquinone reductase and ubiquinol-cytochrome c reductase from beef-heart mitochondria.", *Archives of Biochemistry and Biophysics*, Vol. 180 No. 2, pp. 248–57.

Calvaruso, M.A., Smeitink, J. and Nijtmans, L. (2008), "Electrophoresis techniques to investigate defects in oxidative phosphorylation", *Methods*, Elsevier Inc., Vol. 46 No. 4, pp. 281–287.

Calvaruso, M.A., Willems, P., Van den brand, M., Valsecchi, F., Kruse, S., Palmiter, R., Smeitink, J., et al. (2012), "Mitochondrial complex III stabilizes complex I in the absence of NDUFS4 to provide partial activity", *Human Molecular Genetics*, Vol. 21 No. 1, pp. 115–120.

Campos, Y., Garcia-Redondo, A., Fernandez-Moreno, M.A., Martinez-Pardo, M., Goda, G., Rubio, J.C., Martin, M.A., et al. (2001), "Early-onset multisystem mitochondrial disorder caused by a nonsense mutation in the mitochondrial DNA cytochrome C oxidase II gene.", *Annals of Neurology*, Vol. 50 No. 3, pp. 401–404.

Carroll, J., Fearnley, I.M., Shannon, R.J., Hirst, J. and Walker, J.E. (2003), "Analysis of the Subunit Composition of Complex I from Bovine Heart Mitochondria", *Molecular & Cellular Proteomics*, Vol. 2 No. 2, pp. 117–126.

Chaban, Y., Boekema, E.J. and Dudkina, N. V. (2014), "Structures of mitochondrial oxidative phosphorylation supercomplexes and mechanisms for their stabilisation", *Biochimica et Biophysica Acta - Bioenergetics*, Elsevier B.V., Vol. 1837 No. 4, pp. 418–426.

Chance, B. and Williams, G.R. (1955), "A method for the localization of sites for oxidative phosphorylation.", *Nature*, England, Vol. 176 No. 4475, pp. 250–254.

Chen, Y.C., Taylor, E.B., Dephoure, N., Heo, J.M., Tonhato, A., Papandreou, I., Nath, N., et al. (2012), "Identification of a protein mediating respiratory supercomplex stability", *Cell Metabolism*, Elsevier Inc., Vol. 15 No. 3, pp. 348–360.

Chomyn, A., Lai, S.T., Shakeley, R., Bresolin, N., Scarlato, G. and Attardi, G. (1994), "Platelet-mediated transformation of mtDNA-less human cells: analysis of phenotypic variability among clones from normal individuals--and complementation behavior of the tRNALys mutation causing myoclonic epilepsy and ragged red fibers.", *American Journal of Human Genetics*, Vol. 54 No. 6, pp. 966–74.

Christian, M., Cermak, T., Doyle, E.L., Schmidt, C., Zhang, F., Hummel, A., Bogdanove, A.J., et al. (2010), "Targeting DNA Double-Strand Breaks with TAL Effector Nucleases", *Genetics*, Vol. 186 No. 2, pp. 757–761.

Clayton, D.A. (1991), "Replication and transcription of vertebrate", *Annual Reviews Cell Biology*, Vol. 7, pp. 453–478.

Cogliati, S., Calvo, E., Loureiro, M., Guaras, A.M., Nieto-Arellano, R., Garcia-Poyatos, C., Ezkurdia, I., et al. (2016), "Mechanism of super-assembly of respiratory complexes III and IV.", *Nature*, Nature Publishing Group, Vol. 539 No. 7630, pp. 579–582.

Cogliati, S., Frezza, C., Soriano, M.E., Varanita, T., Quintana-Cabrera, R., Corrado, M., Cipolat, S., et al. (2013), "Mitochondrial Cristae Shape Determines Respiratory Chain Supercomplexes Assembly and Respiratory Efficiency", *Cell*, Vol. 155 No. 1, pp. 160–171.

Cruciat, C.M., Brunner, S., Baumann, F., Neupert, W. and Stuart, R.A. (2000), "The cytochrome bc1 and cytochrome c oxidase complexes associate to form a single supracomplex in yeast mitochondria", *Journal of Biological Chemistry*, Vol. 275 No. 24, pp. 18093–18098.

Cui, T.-Z., Smith, P.M., Fox, J.L., Khalimonchuk, O. and Winge, D.R. (2012), "Late-stage maturation of the Rieske Fe/S protein: Mzm1 stabilizes Rip1 but does not facilitate its translocation by the AAA ATPase Bcs1.", *Molecular and Cellular Biology*, Vol. 32 No. 21, pp. 4400–9.

D'Aurelio, M., Gajewski, C.D., Lenaz, G. and Manfredi, G. (2006), "Respiratory chain supercomplexes set the threshold for respiration defects in human mtDNA mutant cybrids", *Human Molecular Genetics*, Vol. 15 No. 13, pp. 2157–2169.

Davoudi, M., Kallijärvi, J., Marjavaara, S., Kotarsky, H., Hansson, E., Levéen, P. and Fellman, V. (2014), "A mouse model of mitochondrial complex III dysfunction induced by myxothiazol", *Biochemical and Biophysical Research Communications*, Elsevier Inc., Vol. 446 No. 4, pp. 1079–1084.

Davoudi, M., Kotarsky, H., Hansson, E., Kallijärvi, J. and Fellman, V. (2016), "COX7A2L/SCAFI and Pre-Complex III Modify Respiratory Chain Supercomplex Formation in Different Mouse Strains with a Bcs1l Mutation", *Plos One*, Vol. 11 No. 12, p. e0168774.

Dencher, N.A., Frenzel, M., Reifschneider, N.H., Sugawa, M. and Krause, F. (2007), "Proteome

Alterations in Rat Mitochondria Caused by Aging", *Annals of the New York Academy of Sciences*, Vol. 1100 No. 1, pp. 291–298.

Dennerlein, S., Oeljeklaus, S., Jans, D., Hellwig, C., Bareth, B., Jakobs, S., Deckers, M., et al. (2015), "MITRAC7 Acts as a COX1-Specific Chaperone and Reveals a Checkpoint during Cytochrome c Oxidase Assembly", *Cell Reports*, The Authors, Vol. 12 No. 10, pp. 1644–1655.

Dennerlein, S. and Rehling, P. (2015), "Human mitochondrial COX1 assembly into cytochrome c oxidase at a glance.", *Journal of Cell Science*, No. February, pp. 1–5.

Desmurs, M., Foti, M., Raemy, E., Vaz, F.M., Martinou, J.-C., Bairoch, A. and Lane, L. (2015), "C11orf83, a mitochondrial cardiolipin-binding protein involved in bc1 complex assembly and supercomplex stabilization.", *Molecular and Cellular Biology*, Vol. 35 No. 7, pp. 1139–56.

Diaz, F., Enríquez, J.A. and Moraes, C.T. (2012), "Cells lacking Rieske iron-sulfur protein have a reactive oxygen species-associated decrease in respiratory complexes I and IV.", *Molecular and Cellular Biology*, Vol. 32 No. 2, pp. 415–29.

Diaz, F., Fukui, H., Garcia, S. and Moraes, C.T. (2006), "Cytochrome c oxidase is required for the assembly/stability of respiratory complex I in mouse fibroblasts", *Molecular and Cellular Biology*, Vol. 26 No. 13, pp. 4872–4881.

Dieteren, C.E.J., Willems, P.H.G.M., Vogel, R.O., Swarts, H.G., Fransen, J., Roepman, R., Crienen, G., et al. (2008), "Subunits of mitochondrial complex I exist as part of matrix- and membrane-associated subcomplexes in living cells", *Journal of Biological Chemistry*, Vol. 283 No. 50, pp. 34753–34761.

Dröse, S., Stepanova, A. and Galkin, A. (2016), "Ischemic A/D transition of mitochondrial complex I and its role in ROS generation", *Biochimica et Biophysica Acta (BBA) - Bioenergetics*, Vol. 1857 No. 7, pp. 946–957.

Dudek, J., Cheng, I.F., Balleininger, M., Vaz, F.M., Streckfuss-Bömeke, K., Hübscher, D., Vukotic, M., et al. (2013), "Cardiolipin deficiency affects respiratory chain function and organization in an induced pluripotent stem cell model of Barth syndrome", *Stem Cell Research*, Elsevier B.V., Vol. 11 No. 2, pp. 806–819.

Dudkina, N. V, Eubel, H., Keegstra, W., Boekema, E.J. and Braun, H.-P. (2005), "Structure of a mitochondrial supercomplex formed by respiratory-chain complexes I and III.", *Proceedings of the National Academy of Sciences of the United States of America*, Vol. 102 No. 9, pp. 3225–9.

Dudkina, N. V, Kudryashev, M., Stahlberg, H. and Boekema, E.J. (2011), "Interaction of complexes I, III, and IV within the bovine respirasome by single particle cryoelectron tomography.", *Proceedings of the National Academy of Sciences of the United States of America*, Vol. 108 No. 37, pp. 15196–200.

Efremov, R.G., Baradaran, R. and Sazanov, L. a. (2010), "The architecture of respiratory complex I.", *Nature*, Nature Publishing Group, Vol. 465 No. 7297, pp. 441–445.

Efremov, R.G. and Sazanov, L.A. (2011), "Structure of the membrane domain of respiratory complex I", *Nature*, Nature Publishing Group, Vol. 476 No. 7361, pp. 414–420.

Enríquez, J.A. and Attardi, G. (1996), "Analysis of aminoacylation of human mitochondrial tRNAs.", *Methods in Enzymology*, Vol. 264, pp. 183–96.

Ferguson-Miller, S., Hochman, J. and Schindler, M. (1986), "Aggregation and diffusion in the mitochondrial electron-transfer chain: role in electron flow and energy transfer.", *Biochemical Society Transactions*, Vol. 14 No. 5, pp. 822–4.

Fernandez-Vizarra, E., Bugiani, M., Goffrini, P., Carrara, F., Farina, L., Procopio, E., Donati, A., et al. (2007), "Impaired complex III assembly associated with BCS1L gene mutations in isolated mitochondrial encephalopathy", *Human Molecular Genetics*, Vol. 16 No. 10, pp. 1241–1252.

Fernández-Vizarra, E., Tiranti, V. and Zeviani, M. (2009), "Assembly of the oxidative phosphorylation system in humans: What we have learned by studying its defects", *Biochimica et Biophysica Acta - Molecular Cell Research*, Elsevier B.V., Vol. 1793 No. 1, pp. 200–211.

Fernández-Vizarra, E. and Zeviani, M. (2015), "Nuclear gene mutations as the cause of mitochondrial complex III deficiency", *Frontiers in Genetics*, Vol. 6 No. APR, pp. 1–11.

Fiedorczuk, K., Letts, J.A., Degliesposti, G., Kaszuba, K., Skehel, M. and Sazanov, L.A. (2016), "Atomic structure of the entire mammalian mitochondrial complex I", *Nature*, Nature

Publishing Group, pp. 1–21.

Fontanesi, F., Soto, I.C. and Barrientos, A. (2008), "Cytochrome c oxidase biogenesis: New levels of regulation", *IUBMB Life*, Vol. 60 No. 9, pp. 557–568.

Formosa, L.E., Dibley, M.G., Stroud, D.A. and Ryan, M.T. (2017), "Building a complex complex: assembly of mitochondrial respiratory chain complex I", *Seminars in Cell and Developmental Biology*, Elsevier Ltd, available at:https://doi.org/10.1016/j.semcdb.2017.08.011.

Fowler, L.R. and Hatefi, Y. (1961), "Reconstitution of the electron transport system III. Reconstitution of DPNH oxidase, succinic oxidase, and DPNH, succinic oxidase", *Biochemical and Biophysical Research Communications*, Vol. 5 No. 3, pp. 203–208.

Frenzel, M., Rommelspacher, H., Sugawa, M.D. and Dencher, N.A. (2010), "Ageing alters the supramolecular architecture of OxPhos complexes in rat brain cortex", *Experimental Gerontology*, Elsevier Inc., Vol. 45 No. 7–8, pp. 563–572.

Galkin, A., Abramov, A.Y., Frakich, N., Duchen, M.R. and Moncada, S. (2009), "Lack of oxygen deactivates mitochondrial complex I: Implications for ischemic injury?", *Journal of Biological Chemistry*, Vol. 284 No. 52, pp. 36055–36061.

Galkin, A., Dröse, S. and Brandt, U. (2006), "The proton pumping stoichiometry of purified mitochondrial complex I reconstituted into proteoliposomes", *Biochimica et Biophysica Acta - Bioenergetics*, Vol. 1757 No. 12, pp. 1575–1581.

Garesse, R. and Vallejo, C.G. (2001), "Animal mitochondrial biogenesis and function : a regulatory cross-talk between two genomes", Vol. 263.

Garlich, J., Strecker, V., Wittig, I. and Stuart, R.A. (2017), "Mutational Analysis of the QRRQ Motif in the Yeast Hig1-type 2 Protein, Rcf1, Reveals a Regulatory Role for the Cytochrome c Oxidase Complex", *Journal of Biological Chemistry*, Vol. 292, pp. 5216–5226.

Genova, M.L., Ventura, B., Giuliano, G., Bovina, C., Formiggini, G., Parenti Castelli, G. and Lenaz, G. (2001), "The site of production of superoxide radical in mitochondrial Complex I is not a bound ubisemiquinone but presumably iron-sulfur cluster N2", *FEBS Letters*, Vol. 505 No. 3, pp. 364–368.

Ghezzi, D., Goffrini, P., Uziel, G., Horvath, R., Klopstock, T., Lochmüller, H., D'Adamo, P., et al. (2009), "SDHAF1, encoding a LYR complex-II specific assembly factor, is mutated in SDH-defective infantile leukoencephalopathy", *Nature Genetics*, Vol. 41 No. 6, pp. 654–656.

Greggio, C., Jha, P., Kulkarni, S.S., Lagarrigue, S., Broskey, N.T., Boutant, M., Wang, X., et al. (2017), "Enhanced Respiratory Chain Supercomplex Formation in Response to Exercise in Human Skeletal Muscle", *Cell Metabolism*, Vol. 25, pp. 1–11.

Gruschke, S., Römpler, K., Hildenbeutel, M., Kehrein, K., Kühl, I., Bonnefoy, N. and Ott, M. (2012), "The Cbp3-Cbp6 complex coordinates cytochrome b synthesis with bc1 complex assembly in yeast mitochondria", *Journal of Cell Biology*, Vol. 199 No. 1, pp. 137–150.

Gu, J., Wu, M., Guo, R., Yan, K., Lei, J., Gao, N. and Yang, M. (2016), "The architecture of the mammalian respirasome", *Nature*, Nature Publishing Group, Vol. 537 No. 7622, pp. 639–643.

Guarás, A., Perales-Clemente, E., Calvo, E., Acín-Pérez, R., Loureiro-Lopez, M., Pujol, C., Martínez-Carrascoso, I., et al. (2016), "The CoQH2/CoQ Ratio Serves as a Sensor of Respiratory Chain Efficiency", *Cell Reports*, Vol. 15 No. 1, pp. 197–209.

Guerrero-Castillo, S., Baertling, F., Kownatzki, D., Wessels, H.J., Arnold, S., Brandt, U. and Nijtmans, L. (2017), "The Assembly Pathway of Mitochondrial Respiratory Chain Complex I", *Cell Metabolism*, Elsevier Inc., Vol. 25 No. 1, pp. 128–139.

Guo, R., Zong, S., Wu, M., Gu, J. and Yang, M. (2017), "Architecture of Human Mitochondrial Respiratory Megacomplex I 2 III 2 IV 2", *Cell*, Elsevier Inc., Vol. 170 No. 6, p. 1247–1257.e12.

Gupte, S.S. and Hackenbrock, C.R. (1988), "The role of cytochrome c diffusion in mitochondrial electron transport.", *The Journal of Biological Chemistry*, Vol. 263 No. 11, pp. 5248–53.

Hao, H., Khalimonchuk, O., Schraders, M., Dephoure, N., Bayley, J., Kunst, H., Devilee, P., et al. (2009), "SDH5, a gene required for flavination of succinate dehydrogenase is mutated in paraganglioma", *Science*, Vol. 325 No. August, pp. 1139–1142.

Hatefi, Y., Haavik, A.G., Fowler, L.R. and Griffiths, D.E. (1962), "Studies on the electron transfer system. XLII. Reconstitution of the electron transfer system.", *The Journal of Biological Chemistry*, Vol. 237 No. 8, pp. 2661–2669.

Hatle, K.M., Gummadidala, P., Navasa, N., Bernardo, E., Dodge, J., Silverstrim, B., Fortner, K., et al. (2013), "MCJ/DnaJC15, an endogenous mitochondrial repressor of the respiratory chain that controls metabolic alterations.", *Molecular and Cellular Biology*, Vol. 33 No. 11, pp. 2302–2314.

Hayashi, J., Ohta, S., Kikuchi, A., Takemitsu, M., Goto, Y. and Nonaka, I. (1991), "Introduction of disease-related mitochondrial DNA deletions into HeLa cells lacking mitochondrial DNA results in mitochondrial dysfunction", *Proc Natl Acad Sci U S A*, Vol. 88 No. 23, pp. 10614–10618.

Hayashi, T., Asano, Y., Shintani, Y., Aoyama, H., Kioka, H., Tsukamoto, O., Hikita, M., et al. (2015), "Higd1a is a positive regulator of cytochrome c oxidase", *Proceedings of the National Academy of Sciences of the United States of America*, Vol. 112 No. 5, pp. 1553–1558.

Heinemeyer, J., Braun, H.P., Boekema, E.J. and Kouřil, R. (2007), "A structural model of the cytochrome c reductase/oxidase supercomplex from yeast mitochondria", *Journal of Biological Chemistry*, Vol. 282 No. 16, pp. 12240–12248.

Helbig, A.O., De Groot, M.J.L., Van Gestel, R.A., Mohammed, S., De Hulster, E.A.F., Luttik, M.A.H., Daran-Lapujade, P., et al. (2009), "A three-way proteomics strategy allows differential analysis of yeast mitochondrial membrane protein complexes under anaerobic and aerobic conditions", *Proteomics*, Vol. 9 No. 20, pp. 4787–4798.

Heron, C., Ragan, C.I. and Trumpower, B.L. (1978), "The interaction between mitochondrial NADH-ubiquinone oxidoreductase and ubiquinol-cytochrome c oxidoreductase. Restoration of ubiquinone-pool behaviour.", *The Biochemical Journal*, Vol. 174 No. 3, pp. 791–800.

Herrero, A. and Barja, G. (2000), "Localization of the site of oxygen radical generation inside the complex I of heart and nonsynaptic brain mammalian mitochondria.", *Journal of Bioenergetics and Biomembranes*, Vol. 32 No. 6, pp. 609–15.

Höchli, M. and Hackenbrock, C.R. (1976), "Fluidity in mitochondrial membranes: thermotropic lateral translational motion of intramembrane particles.", *Proceedings of the National Academy of Sciences of the United States of America*, Vol. 73 No. 5, pp. 1636–40.

Höchli, M., Höchli, L. and Hackenbrock, C.R. (1985), "Independent lateral diffusion of

cytochrome bc1 complex and cytochrome oxidase in the mitochondrial inner membrane.", *European Journal of Cell Biology*, Vol. 38 No. 1, pp. 1–5.

Hochman, J., Ferguson-Miller, S. and Schindler, M. (1985), "Mobility in the mitochondrial electron transport chain.", *Biochemistry*, Vol. 24 No. 10, pp. 2509–16.

Hochman, J.H., Schindler, M., Lee, J.G. and Ferguson-Miller, S. (1982), "Lateral mobility of cytochrome c on intact mitochondrial membranes as determined by fluorescence redistribution after photobleaching.", *Proceedings of the National Academy of Sciences of the United States of America*, Vol. 79 No. 22, pp. 6866–70.

Hornig-Do, H.-T., Tatsuta, T., Buckermann, A., Bust, M., Kollberg, G., Rötig, A., Hellmich, M., et al. (2012), "Nonsense mutations in the COX1 subunit impair the stability of respiratory chain complexes rather than their assembly.", *Embo J*, Vol. 31 No. 5, pp. 1293–1307.

Huang, L., Sun, G., Cobessi, D., Wang, A.C., Shen, J.T., Tung, E.Y., Anderson, V.E., et al. (2006), "3-Nitropropionic Acid Is a Suicide Inhibitor of Mitochondrial Respiration That, upon Oxidation by Complex II, Forms a Covalent Adduct with a Catalytic Base Arginine in the Active Site of the Enzyme", *Journal of Biological Chemistry*, Vol. 281 No. 9, pp. 5965–5972.

Huang, S., Taylor, N.L., Ströher, E., Fenske, R. and Millar, A.H. (2013), "Succinate dehydrogenase assembly factor 2 is needed for assembly and activity of mitochondrial complex II and for normal root elongation in Arabidopsis", *The Plant Journal*, Vol. 73 No. 3, pp. 429–441.

Hunte, C., Koepke, J., Lange, C., Roßmanith, T. and Michel, H. (2000), "Structure at 2.3 Å resolution of the cytochrome bc1 complex from the yeast Saccharomyces cerevisiae co-crystallized with an antibody Fv fragment", *Structure*, Vol. 8 No. 6, pp. 669–684.

Hunte, C., Zickermann, V. and Brandt, U. (2010), "Functional modules and structural basis of conformational coupling in mitochondrial complex I.", *Science (New York, N.Y.)*, Vol. 329 No. July, pp. 448–451.

Ikeda, K., Shiba, S., Horie-Inoue, K., Shimokata, K. and Inoue, S. (2013), "A stabilizing factor for mitochondrial respiratory supercomplex assembly regulates energy metabolism in muscle", *Nature Communications*, Nature Publishing Group, Vol. 4, p. 2147.

Iwata, S. (1998), “Complete Structure of the 11-Subunit Bovine Mitochondrial Cytochrome bc1 Complex”, *Science*, Vol. 281 No. 5373, pp. 64–71.

Jang, S., Lewis, T.S., Powers, C., Khuchua, Z., Baines, C.P., Wipf, P. and Javadov, S. (2017), “Elucidating Mitochondrial Electron Transport Chain Supercomplexes in the Heart During Ischemia?Reperfusion”, *Antioxidants & Redox Signaling*, Vol. 27 No. 1, pp. 57–69.

Jha, P., Wang, X. and Auwerx, J. (2016), “Analysis of Mitochondrial Respiratory Chain Supercomplexes Using Blue Native Polyacrylamide Gel Electrophoresis (BN-PAGE)”, *Current Protocols in Mouse Biology*, Vol. 6, John Wiley & Sons, Inc., Hoboken, NJ, USA, pp. 1–14.

Jones, A.J.Y., Blaza, J.N., Varghese, F. and Hirst, J. (2017), “Respiratory Complex I in Bos taurus and Paracoccus denitrificans Pumps Four Protons across the Membrane for Every NADH Oxidized”, *Journal of Biological Chemistry*, Vol. 292 No. 12, pp. 4987–4995.

King, M.P. and Attardi, G. (1989), “Human cells lacking mtDNA: repopulation with exogenous mitochondria by complementation.”, *Science (New York, N.Y.)*, Vol. 246 No. 4929, pp. 500–503.

Kounosu, A. (2014), “Analysis of covalent flavinylation using thermostable succinate dehydrogenase from Thermus thermophilus and Sulfolobus tokodaii lacking SdhE homologs”, *FEBS Letters*, Vol. 588 No. 6, pp. 1058–1063.

Kovářová, N., Čížková Vrbacká, A., Pecina, P., Stránecký, V., Pronicka, E., Kmoch, S. and Houštěk, J. (2012), “Adaptation of respiratory chain biogenesis to cytochrome c oxidase deficiency caused by SURF1 gene mutations”, *Biochimica et Biophysica Acta - Molecular Basis of Disease*, Vol. 1822 No. 7, pp. 1114–1124.

Kröger, A. and Klingenberg, M. (1973), “The Kinetics of the Redox Reactions of Ubiquinone Related to the Electron-Transport Activity in the Respiratory Chain”, *European Journal of Biochemistry*, Vol. 34 No. 2, pp. 358–368.

Kussmaul, L. and Hirst, J. (2006), “The mechanism of superoxide production by NADH:ubiquinone oxidoreductase (complex I) from bovine heart mitochondria.”, *Proceedings of the National Academy of Sciences of the United States of America*, Vol. 103 No. 20, pp. 7607–7612.

Laemmli, U.K. (1970), “Cleavage of Structural Proteins during the Assembly of the Head of Bacteriophage T4”, *Nature*, Vol. 227 No. 5259, pp. 680–685.

Lamantea, E., Carrara, F., Mariotti, C., Morandi, L., Tiranti, V. and Zeviani, M. (2002), “A novel nonsense mutation (Q352X) in the mitochondrial cytochrome b gene associated with a combined deficiency of complexes I and III”, *Neuromuscular Disorders*, Vol. 12 No. 1, pp. 49–52.

Lapuente-Brun, E., Moreno-Loshuertos, R., Acin-Perez, R., Latorre-Pellicer, A., Colas, C., Balsa, E., Perales-Clemente, E., et al. (2013), “Supercomplex Assembly Determines Electron Flux in the Mitochondrial Electron Transport Chain”, *Science*, Vol. 340 No. 6140, pp. 1567–1570.

Lazarou, M., McKenzie, M., Ohtake, A., Thorburn, D.R. and Ryan, M.T. (2007), “Analysis of the assembly profiles for mitochondrial- and nuclear-DNA-encoded subunits into complex I.”, *Molecular and Cellular Biology*, Vol. 27 No. 12, pp. 4228–4237.

Lazarou, M., Smith, S.M., Thorburn, D.R., Ryan, M.T. and McKenzie, M. (2009), “Assembly of nuclear DNA-encoded subunits into mitochondrial complex IV, and their preferential integration into supercomplex forms in patient mitochondria”, *FEBS Journal*, Vol. 276 No. 22, pp. 6701–6713.

Leary, S.C., Kaufman, B.A., Pellecchia, G., Guercin, G., Mattman, A., Jaksch, M. and Shoubr. (2004), “Human SCO1 and SCO2 have independent, cooperative functions in copper delivery to cytochrome c oxidase”, *Human Molecular Genetics*, Vol. 13 No. 17, pp. 1839–1848.

Leary, S.C. and Sasarman, F. (2009), “Oxidative Phosphorylation: Synthesis of Mitochondrially Encoded Proteins and Assembly of Individual Structural Subunits into Functional Holoenzyme Complexes”, pp. 143–162.

Lenaz, G. and Genova, M.L. (2010), “Structure and organization of mitochondrial respiratory complexes: a new understanding of an old subject.”, *Antioxidants & Redox Signaling*, Vol. 12 No. 8, pp. 961–1008.

Letts, J.A., Degliesposti, G., Fiedorczuk, K., Skehel, M. and Sazanov, L.A. (2016), “Purification of ovine respiratory complex I results in a highly active and stable preparation”, *Journal of Biological Chemistry*, Vol. 291 No. 47, pp. 24657–24675.

Letts, J.A., Fiedorczuk, K. and Sazanov, L.A. (2016), "The architecture of respiratory supercomplexes", *Nature*, Nature Publishing Group, Vol. 537 No. 7622, pp. 644–648.

Li, T., Huang, S., Zhao, X., Wright, D.A., Carpenter, S., Spalding, M.H., Weeks, D.P., et al. (2011), "Modularly assembled designer TAL effector nucleases for targeted gene knockout and gene replacement in eukaryotes", *Nucleic Acids Research*, Vol. 39 No. 14, pp. 6315–6325.

Li, Y., D'Aurelio, M., Deng, J.H., Park, J.S., Manfredi, G., Hu, P., Lu, J., et al. (2007), "An assembled complex IV maintains the stability and activity of complex I in mammalian mitochondria", *Journal of Biological Chemistry*, Vol. 282 No. 24, pp. 17557–17562.

Liu, J. and Barrientos, A. (2012), "Transcriptional Regulation of Yeast Oxidative Phosphorylation Hypoxic Genes by Oxidative Stress", *Antioxidants & Redox Signaling*, Vol. 19 No. 16, pp. 1916–1927.

Lopez-Fabuel, I., Le Douce, J., Logan, A., James, A.M., Bonvento, G., Murphy, M.P., Almeida, A., et al. (2016), "Complex I assembly into supercomplexes determines differential mitochondrial ROS production in neurons and astrocytes.", *Proceedings of the National Academy of Sciences of the United States of America*, Vol. 113 No. 46, pp. 13063–13068.

Maio, N., Ghezzi, D., Verrigni, D., Rizza, T., Bertini, E., Martinelli, D., Zeviani, M., et al. (2016), "Disease-Causing SDHAF1 Mutations Impair Transfer of Fe-S Clusters to SDHB", *Cell Metabolism*, Vol. 23 No. 2, pp. 292–302.

Mak, A.N.S., Bradley, P., Bogdanove, A.J. and Stoddard, B.L. (2013), "TAL effectors: Function, structure, engineering and applications", *Current Opinion in Structural Biology*, Elsevier Ltd, Vol. 23 No. 1, pp. 93–99.

Maranzana, E., Barbero, G., Falasca, A.I., Lenaz, G. and Genova, M.L. (2013), "Mitochondrial respiratory supercomplex association limits production of reactive oxygen species from complex I.", *Antioxidants & Redox Signaling*, Vol. 19 No. 13, pp. 1469–80.

Margoliash, E., Ferguson-Miller, S., Tulloss, J., Kang, C.H., Feinberg, B. a, Brautigan, D.L. and Morrison, M. (1973), "Separate intramolecular pathways for reduction and oxidation of cytochrome c in electron transport chain reactions.", *Proceedings of the National Academy of Sciences of the United States of America*, Vol. 70 No. 11, pp. 3245–9.

Marques, I., Dencher, N.A., Videira, A. and Krause, F. (2007), "Supramolecular organization of

the respiratory chain in Neurospora crassa mitochondria", *Eukaryotic Cell*, Vol. 6 No. 12, pp. 2391–2405.

McKenzie, M., Lazarou, M., Thorburn, D.R. and Ryan, M.T. (2006), "Mitochondrial Respiratory Chain Supercomplexes Are Destabilized in Barth Syndrome Patients", *Journal of Molecular Biology*, Vol. 361 No. 3, pp. 462–469.

McStay, G.P., Su, C.H. and Tzagoloff, A. (2013), "Modular assembly of yeast cytochrome oxidase.", *Molecular Biology of the Cell*, Vol. 24 No. 4, pp. 440–52.

Medja, F., Allouche, S., Frachon, P., Jardel, C., Malgat, M., de Camaret, B.M., Slama, A., et al. (2009), "Development and implementation of standardized respiratory chain spectrophotometric assays for clinical diagnosis", *Mitochondrion*, Vol. 9 No. 5, pp. 331–339.

Melo, A.M.P. and Teixeira, M. (2016), "Supramolecular organization of bacterial aerobic respiratory chains: From cells and back", *Biochimica et Biophysica Acta - Bioenergetics*, Elsevier B.V., Vol. 1857 No. 3, pp. 190–197.

Mick, D.U., Dennerlein, S., Wiese, H., Reinhold, R., Pacheu-Grau, D., Lorenzi, I., Sasarman, F., et al. (2012), "MITRAC links mitochondrial protein translocation to respiratory-chain assembly and translational regulation", *Cell*, Elsevier Inc., Vol. 151 No. 7, pp. 1528–1541.

Mick, D.U., Wagner, K., van der Laan, M., Frazier, A.E., Perschil, I., Pawlas, M., Meyer, H.E., et al. (2007), "Shy1 couples Cox1 translational regulation to cytochrome c oxidase assembly.", *The EMBO Journal*, Vol. 26 No. 20, pp. 4347–4358.

Milenkovic, D., Blaza, J.N., Larsson, N.-G. and Hirst, J. (2017), "The Enigma of the Respiratory Chain Supercomplex", *Cell Metabolism*, Vol. 25 No. 4, pp. 765–776.

Milenkovic, D., Matic, S., kühl, I., Ruzzenente, B., Freyer, C., Jemt, E., Park, C.B., et al. (2013), "Twinkle is an essential mitochondrial helicase required for synthesis of nascent D-loop strands and complete mtDNA replication", *Human Molecular Genetics*, Vol. 22 No. 10, pp. 1983–1993.

Mileykovskaya, E., Penczek, P.A., Fang, J., Mallampalli, V.K.P.S., Sparagna, G.C. and Dowhan, W. (2012), "Arrangement of the respiratory chain complexes in Saccharomyces cerevisiae supercomplex III2IV2 revealed by single particle cryo-electron microscopy", *Journal of*

Biological Chemistry, Vol. 287 No. 27, pp. 23095–23103.

Mitchell, P. (1975), "The protonmotive Q cycle: A general formulation", *FEBS Letters*, Vol. 59 No. 2, pp. 137–139.

Moreno-Lastres, D., Fontanesi, F., García-Consuegra, I., Martín, M.A., Arenas, J., Barrientos, A. and Ugalde, C. (2012), "Mitochondrial complex I plays an essential role in human respirasome assembly", *Cell Metabolism*, Vol. 15 No. 3, pp. 324–335.

Moscou, M.J. and Bogdanove, A.J. (2009), "A Simple Cipher Governs DNA Recognition by TAL Effectors", *Science*, Vol. 326 No. 5959, pp. 1501–1501.

Mourier, A., Matic, S., Ruzzenente, B., Larsson, N.G. and Milenkovic, D. (2014), "The respiratory Chain supercomplex organization is independent of COX7A2L isoforms", *Cell Metabolism*, Vol. 20 No. 6, pp. 1069–1075.

Mourier, A., Ruzzenente, B., Brandt, T., Kühlbrandt, W. and Larsson, N.G. (2014), "Loss of LRPPRC causes ATP synthase deficiency", *Human Molecular Genetics*, Vol. 23 No. 10, pp. 2580–2592.

Müller, C.S., Bildl, W., Haupt, A., Ellenrieder, L., Becker, T., Hunte, C., Fakler, B., et al. (2016), "Cryo-slicing Blue Native-Mass Spectrometry (csBN-MS), a Novel Technology for High Resolution Complexome Profiling.", *Molecular & Cellular Proteomics : MCP*, Vol. 15 No. 2, pp. 669–81.

Muster, B., Kohl, W., Wittig, I., Strecker, V., Joos, F., Haase, W., Bereiter-Hahn, J., et al. (2010), "Respiratory Chain Complexes in Dynamic Mitochondria Display a Patchy Distribution in Life Cells", edited by Joly, E.*PLoS ONE*, Vol. 5 No. 7, p. e11910.

Na, U., Yu, W., Cox, J., Bricker, D.K., Brockmann, K., Rutter, J., Thummel, C.S., et al. (2014), "The LYR Factors SDHAF1 and SDHAF3 Mediate Maturation of the Iron-Sulfur Subunit of Succinate Dehydrogenase", *Cell Metabolism*, Vol. 20 No. 2, pp. 253–266.

Nemudryi, A.A., Valetdinova, K.R., Medvedev, S.P. and Zakian, S.M. (2014), "TALEN and CRISPR / Cas Genome Editing Systems : Tools of Discovery", *Acta Naturae*, Vol. 6 No. 22, pp. 19–40.

Neupert, W. (2015), "A perspective on transport of proteins into mitochondria: A myriad of open questions", *Journal of Molecular Biology*, Elsevier B.V., Vol. 427 No. 6, pp. 1135–

1158.

Nijtmans, L. (2002), “Blue Native electrophoresis to study mitochondrial and other protein complexes”, *Methods*, Vol. 26 No. 4, pp. 327–334.

Nijtmans, L.G.J., Taanman, J.W., Muijsers, A.O., Speijer, D. and Van Den Bogert, C. (1998), “Assembly of cytochrome-c oxidase in cultured human cells”, *European Journal of Biochemistry*, Vol. 254 No. 2, pp. 389–394.

Nijtmans, L.G.J., Ugalde, C., Heuvel, L.P. van den and Smeitink, J.A.M. (2004), “Function and dysfunction of the oxidative phosphorylation system.”, *Mitochondrial Function and Biogenesis*, Vol. 8 No. March, pp. 115–136.

Nouws, J., Nijtmans, L.G.J., Smeitink, J.A. and Vogel, R.O. (2012), “Assembly factors as a new class of disease genes for mitochondrial complex i deficiency: Cause, pathology and treatment options”, *Brain*, Vol. 135 No. 1, pp. 12–22.

Nubel, E., Wittig, I., Kerscher, S., Brandt, U. and Schägger, H. (2009), “Two-dimensional native electrophoretic analysis of respiratory supercomplexes from Yarrowia lipolytica”, *Proteomics*, Vol. 9 No. 9, pp. 2408–2418.

Perales-Clemente, E., Fernández-Vizarra, E., Acín-Pérez, R., Movilla, N., Bayona-Bafaluy, M.P., Moreno-Loshuertos, R., Pérez-Martos, A., et al. (2010), “Five entry points of the mitochondrially encoded subunits in mammalian complex I assembly.”, *Molecular and Cellular Biology*, Vol. 30 No. 12, pp. 3038–3047.

Pfeiffer, K., Gohil, V., Stuart, R.A., Hunte, C., Brandt, U., Greenberg, M.L. and Schägger, H. (2003), “Cardiolipin Stabilizes Respiratory Chain Supercomplexes”, *Journal of Biological Chemistry*, Vol. 278 No. 52, pp. 52873–52880.

Quarato, G., Piccoli, C., Scrima, R. and Capitanio, N. (2011), “Variation of flux control coefficient of cytochrome c oxidase and of the other respiratory chain complexes at different values of protonmotive force occurs by a threshold mechanism”, *Biochimica et Biophysica Acta - Bioenergetics*, Elsevier B.V., Vol. 1807 No. 9, pp. 1114–1124.

Ragan, C.I. and Heron, C. (1978), “The interaction between mitochondrial NADH-ubiquinone oxidoreductase and ubiquinol-cytochrome c oxidoreductase. Evidence for stoicheiometric association.”, *The Biochemical Journal*, Vol. 174 No. 3, pp. 783–790.

Rak, M., Benit, P., Chretien, D., Bouchereau, J., Schiff, M., El-Khoury, R., Tzagoloff, A., et al. (2016), "Mitochondrial cytochrome c oxidase deficiency", *Clinical Science*, Vol. 130 No. 6, pp. 393–407.

Ramírez-Aguilar, S.J., Keuthe, M., Rocha, M., Fedyaev, V. V., Kramp, K., Gupta, K.J., Rasmusson, A.G., et al. (2011), "The composition of plant mitochondrial supercomplexes changes with oxygen availability", *Journal of Biological Chemistry*, Vol. 286 No. 50, pp. 43045–43053.

Rana, M., De Coo, I., Diaz, F., Smeets, H. and Moraes, C.T. (2000), "An out-of-frame cytochrome b gene deletion from a patient with parkinsonism is associated with impaired complex III assembly and an increase in free radical production", *Annals of Neurology*, Vol. 48 No. 5, pp. 774–781.

Reid, R.A., Moyle, J. and Mitchell, P. (1966), "Synthesis of Adenosine Triphosphate by a Protonmotive Force in Rat Liver Mitochondria", *Nature*, Vol. 211, pp. 1174–1175.

Richter-Dennerlein, R., Oeljeklaus, S., Lorenzi, I., Ronsör, C., Bareth, B., Schendzielorz, A.B., Wang, C., et al. (2016), "Mitochondrial Protein Synthesis Adapts to Influx of Nuclear-Encoded Protein", *Cell*, Vol. 167 No. 2, p. 471–483.e10.

Rieger, B., Shalaeva, D.N., Söhnel, A.-C., Kohl, W., Duwe, P., Mulkidjanian, A.Y. and Busch, K.B. (2017), "Lifetime imaging of GFP at CoxVIIIa reports respiratory supercomplex assembly in live cells", *Scientific Reports*, Nature Publishing Group, Vol. 7, p. 46055.

Romer, P., Hahn, S., Jordan, T., Strauss, T., Bonas, U. and Lahaye, T. (2007), "Plant Pathogen Recognition Mediated by Promoter Activation of the Pepper Bs3 Resistance Gene", *Science*, Vol. 318 No. 5850, pp. 645–648.

Römpler, K., Müller, T., Juris, L., Wissel, M., Vukotic, M., Hofmann, K. and Deckers, M. (2016), "Overlapping role of respiratory supercomplex factor Rcf2 and its N-terminal homolog Rcf3 in Saccharomyces cerevisiae", *Journal of Biological Chemistry*, Vol. 291 No. 45, pp. 23769–23778.

Rosca, M.G., Vazquez, E.J., Kerner, J., Parland, W., Chandler, M.P., Stanley, W., Sabbah, H.N., et al. (2008), "Cardiac mitochondria in heart failure: Decrease in respirasomes and oxidative phosphorylation", *Cardiovascular Research*, Vol. 80 No. 1, pp. 30–39.

Ruzzenente, B., Metodiev, M.D., Wredenberg, A., Bratic, A., Park, C.B., Cámara, Y., Milenkovic,

D., et al. (2012), “LRPPRC is necessary for polyadenylation and coordination of translation of mitochondrial mRNAs”, *The EMBO Journal*, Vol. 31 No. 2, pp. 443–456.

Sambrook, J. and Russell, D.W. (2001), *Molecular Cloning, a Laboratory Manual.*, *Cold Spring Harbor Laboratory Press*, Cold Spring Harbor, New York.

Sanchez-Caballero, L., Guerrero-Castillo, S. and Nijtmans, L. (2016), “Unraveling the complexity of mitochondrial complex i assembly: A dynamic process”, *Biochimica et Biophysica Acta - Bioenergetics*, Elsevier B.V., Vol. 1857 No. 7, pp. 980–990.

Sánchez, E., Lobo, T., Fox, J.L., Zeviani, M., Winge, D.R. and Fernández-Vizarra, E. (2013), “LYRM7/MZM1L is a UQCRFS1 chaperone involved in the last steps of mitochondrial Complex III assembly in human cells”, *Biochimica et Biophysica Acta - Bioenergetics*, Elsevier B.V., Vol. 1827 No. 3, pp. 285–293.

Sazanov, L. a and Hinchliffe, P. (2006), “Structure of the hydrophilic domain of respiratory complex I from Thermus thermophilus.”, *Science (New York, N.Y.)*, Vol. 311 No. 5766, pp. 1430–1436.

Schäfer, E., Dencher, N. a, Vonck, J. and Parcej, D.N. (2007), “Three-dimensional structure of the respiratory chain supercomplex I1III2IV1 from bovine heart mitochondria.”, *Biochemistry*, Vol. 46, pp. 12579–12585.

Schäfer, E., Seelert, H., Reifschneider, N.H., Krause, F., Dencher, N.A. and Vonck, J. (2006), “Architecture of active mammalian respiratory chain supercomplexes”, *Journal of Biological Chemistry*, Vol. 281 No. 22, pp. 15370–15375.

Schägger, H., De Coo, R., Bauer, M.F., Hofmann, S., Godino, C. and Brandt, U. (2004), “Significance of respirasomes for the assembly/stability of human respiratory chain complex I”, *Journal of Biological Chemistry*, Vol. 279 No. 35, pp. 36349–36353.

Schägger, H., Link, T.A., Engel, W.D. and von Jagow, G. (1986), “Isolation of the eleven protein subunits of the bc1 complex from beef heart.”, *Methods in Enzymology*, Vol. 126 No. 1983, pp. 224–37.

Schägger, H. and Pfeiffer, K. (2000), “Supercomplexes in the respiratory chains of yeast and mammalian mitochondria.”, *The EMBO Journal*, Vol. 19 No. 8, pp. 1777–1783.

Schägger, H. and Pfeiffer, K. (2001), “The Ratio of Oxidative Phosphorylation Complexes I-V in

Bovine Heart Mitochondria and the Composition of Respiratory Chain Supercomplexes", *Journal of Biological Chemistry*, Vol. 276 No. 41, pp. 37861–37867.

Schornack, S., Meyer, A., Römer, P., Jordan, T. and Lahaye, T. (2006), "Gene-for-gene-mediated recognition of nuclear-targeted AvrBs3-like bacterial effector proteins", *Journal of Plant Physiology*, Vol. 163 No. 3, pp. 256–272.

Sciacco, M., Bonilla, E., Schon, E.A., Dimauro, S. and Moraes, C.T. (1994), "Distribution of wild-type and common deletion forms of mtDNA in normal and respiration-deficient muscle fibers from patients with mitochondrial myopathy", *Human Molecular Genetics*, Vol. 3 No. 1, pp. 13–19.

Shiba, S., Ikeda, K., Horie-Inoue, K., Nakayama, A., Tanaka, T. and Inoue, S. (2017), "Deficiency of COX7RP, a mitochondrial supercomplex assembly promoting factor, lowers blood glucose level in mice", *Scientific Reports*, Vol. 7 No. 1, p. 7606.

Smith, P.M., Fox, J.L. and Winge, D.R. (2012), "Biogenesis of the cytochrome bc 1 complex and role of assembly factors", *Biochimica et Biophysica Acta - Bioenergetics*, Elsevier B.V., Vol. 1817 No. 2, pp. 276–286.

Sone, N., Sekimachi, M. and Kutoh, E. (1987), "Identification and properties of a quinol oxidase super-complex composed of a bc1 complex and cytochrome oxidase in the thermophilic bacterium PS3.", *Journal of Biological Chemistry*, Vol. 262 No. 32, pp. 15386–15391.

Soto, I.C., Fontanesi, F., Liu, J. and Barrientos, A. (2012), "Biogenesis and assembly of eukaryotic cytochrome c oxidase catalytic core", *Biochimica et Biophysica Acta - Bioenergetics*, Elsevier B.V., Vol. 1817 No. 6, pp. 883–897.

Sousa, J.S., Mills, D.J., Vonck, J. and Kühlbrandt, W. (2016), "Functional asymmetry and electron flow in the bovine respirasome", *eLife*, Vol. 5 No. NOVEMBER2016, pp. 1–17.

Stiburek, L., Hansikova, H., Tesarova, M., Cerna, L. and Zeman, J. (2006), "Biogenesis of Eukaryotic Cytochrome c Oxidase", *Physiotherapy Research*, Vol. 55, pp. 27–41.

Stiburek, L., Vesela, K., Hansikova, H., Pecina, P., Tesarova, M., Cerna, L., Houstek, J., et al. (2005), "Tissue-specific cytochrome c oxidase assembly defects due to mutations in SCO2 and SURF1", *Biochemical Journal*, Vol. 392 No. 3, pp. 625–632.

Strogolova, V., Furness, A., Robb-McGrath, M., Garlich, J. and Stuart, R.A. (2012), "Rcf1 and

Rcf2, members of the hypoxia-induced gene 1 protein family, are critical components of the mitochondrial cytochrome bc1-cytochrome c oxidase supercomplex", *Molecular and Cellular Biology*, Vol. 32 No. 8, pp. 1363–1373.

Stroud, D.A., Surgenor, E.E., Formosa, L.E., Reljic, B., Frazier, A.E., Dibley, M.G., Osellame, L.D., et al. (2016), "Accessory subunits are integral for assembly and function of human mitochondrial complex I", *Nature*, Nature Publishing Group, Vol. 538 No. 7623, pp. 123–126.

Sun, D., Li, B., Qiu, R., Fang, H. and Lyu, J. (2016), "Cell type-specific modulation of respiratory chain supercomplex organization SM", *International Journal of Molecular Sciences*, Vol. 17 No. 6, pp. 6–11.

Sun, F., Huo, X., Zhai, Y., Wang, A., Xu, J., Su, D., Bartlam, M., et al. (2005), "Crystal structure of mitochondrial respiratory membrane protein Complex II", *Cell*, Vol. 121 No. 7, pp. 1043–1057.

Sun, J. and Trumpower, B.L. (2003), "Superoxide anion generation by the cytochrome bc1 complex", *Archives of Biochemistry and Biophysics*, Vol. 419 No. 2, pp. 198–206.

Tasseva, G., Bai, H.D., Davidescu, M., Haromy, A., Michelakis, E. and Vance, J.E. (2013), "Phosphatidylethanolamine Deficiency in Mammalian Mitochondria Impairs Oxidative Phosphorylation and Alters Mitochondrial Morphology", *Journal of Biological Chemistry*, Vol. 288 No. 6, pp. 4158–4173.

Taylor, R.W. and Turnbull, D.M. (2005), "Mitochondrial DNA mutations in human disease", *Nat Rev Genet*, Vol. 6 No. 5, pp. 389–402.

Timón-Gómez, A., Nývltová, E., Abriata, L.A., Vila, A.J., Hosler, J. and Barrientos, A. (2017), "Mitochondrial cytochrome c oxidase biogenesis: Recent developments", *Seminars in Cell & Developmental Biology*, pp. 1–16.

Tiranti, V., Corona, P., Greco, M., Taanman, J.W., Carrara, F., Lamantea, E., Nijtmans, L., et al. (2000), "A novel frameshift mutation of the mtDNA COIII gene leads to impaired assembly of cytochrome c oxidase in a patient affected by Leigh-like syndrome.", *Human Molecular Genetics*, Vol. 9 No. 18, pp. 2733–42.

Trouillard, M., Meunier, B. and Rappaport, F. (2011), "Questioning the functional relevance of

mitochondrial supercomplexes by time-resolved analysis of the respiratory chain.", *Proceedings of the National Academy of Sciences of the United States of America*, Vol. 108 No. 45, pp. E1027-34.

Tsukihara, T., Aoyama, H., Yamashita, E., Tomizaki, T., Yamaguchi, H., Shinzawa-Itoh, K., Nakashima, R., et al. (1995), "Structures of metal sites of oxidized bovine heart cytochrome c oxidase at 2.8 A", *Science*, Vol. 269 No. 5227, pp. 1069–1074.

Ugalde, C., Hinttala, R., Timal, S., Smeets, R., Rodenburg, R.J.T., Uusimaa, J., van Heuvel, L.P., et al. (2007), "Mutated ND2 impairs mitochondrial complex I assembly and leads to Leigh Syndrome", *Molecular Genetics and Metabolism*, Vol. 90 No. 1, pp. 10–14.

Ugalde, C., Vogel, R., Huijbens, R., van der Heuvel, B., Smeitink, J. and Nijtmans, L. (2004), "Human mitochondrial complex I assembles through the combination of evolutionary conserved modules: A framework to interpret complex I deficiencies", *Human Molecular Genetics*, Vol. 13 No. 20, pp. 2461–2472.

Valente, L., Piga, D., Lamantea, E., Carrara, F., Uziel, G., Cudia, P., Zani, A., et al. (2009), "Identification of novel mutations in five patients with mitochondrial encephalomyopathy.", *Biochimica et Biophysica Acta*, Vol. 1787, pp. 491–501.

Valsecchi, F., Esseling, J.J., Koopman, W.J.H. and Willems, P.H.G.M. (2009), "Calcium and ATP handling in human NADH:Ubiquinone oxidoreductase deficiency", *Biochimica et Biophysica Acta - Molecular Basis of Disease*, Elsevier B.V., Vol. 1792 No. 12, pp. 1130–1137.

Vartak, R., Deng, J., Fang, H. and Bai, Y. (2015), "Redefining the roles of mitochondrial DNA-encoded subunits in respiratory Complex I assembly", *Biochimica et Biophysica Acta - Molecular Basis of Disease*, Elsevier B.V., Vol. 1852 No. 7, pp. 1531–1539.

Vempati, U.D., Han, X. and Moraes, C.T. (2009), "Lack of cytochrome c in mouse fibroblasts disrupts assembly/stability of respiratory complexes I and IV", *Journal of Biological Chemistry*, Vol. 284 No. 7, pp. 4383–4391.

Vidoni, S., Harbour, M.E., Guerrero-Castillo, S., Signes, A., Ding, S., Fearnley, I.M., Taylor, R.W., et al. (2017), "MR-1S Interacts with PET100 and PET117 in Module-Based Assembly of Human Cytochrome c Oxidase", *Cell Reports*, ElsevierCompany., Vol. 18 No. 7, pp. 1727–1738.

Vinothkumar, K.R., Zhu, J. and Hirst, J. (2014), “Architecture of mammalian respiratory complex I”, *Nature*, Vol. 515 No. 7525, pp. 80–84.

Vogel, R.O., Dieteren, C.E.J., Van Den Heuvel, L.P.W.J., Willems, P.H.G.M., Smeitink, J.A.M., Koopman, W.J.H. and Nijtmans, L.G.J. (2007), “Identification of mitochondrial complex I assembly intermediates by tracing tagged NDUFS3 demonstrates the entry point of mitochondrial subunits”, *Journal of Biological Chemistry*, Vol. 282 No. 10, pp. 7582–7590.

Van Vranken, J.G., Bricker, D.K., Dephoure, N., Gygi, S.P., Cox, J.E., Thummel, C.S. and Rutter, J. (2014), “SDHAF4 Promotes Mitochondrial Succinate Dehydrogenase Activity and Prevents Neurodegeneration”, *Cell Metabolism*, Vol. 20 No. 2, pp. 241–252.

Vukotic, M., Oeljeklaus, S., Wiese, S., Vögtle, F.N., Meisinger, C., Meyer, H.E., Zieseniss, A., et al. (2012), “Rcf1 mediates cytochrome oxidase assembly and respirasome formation, revealing heterogeneity of the enzyme complex”, *Cell Metabolism*, Vol. 15 No. 3, pp. 336–347.

Wagener, N., Ackermann, M., Funes, S. and Neupert, W. (2011), “A pathway of protein translocation in mitochondria mediated by the AAA-ATPase Bcs1”, *Molecular Cell*, Elsevier Inc., Vol. 44 No. 2, pp. 191–202.

Williams, E.G., Wu, Y., Jha, P., Dubuis, S., Blattmann, P., Argmann, C.A., Houten, S.M., et al. (2016), “Systems proteomics of liver mitochondria function.”, *Science (New York, N.Y.)*, Vol. 352 No. 6291, p. aad01891-aad018914.

Williams, S.L., Valnot, I., Rustin, P. and Taanman, J.W. (2004), “Cytochrome c Oxidase Subassemblies in Fibroblast Cultures from Patients Carrying Mutations in COX10, SCO1, or SURF1”, *Journal of Biological Chemistry*, Vol. 279 No. 9, pp. 7462–7469.

Wittig, I., Braun, H.-P. and Schägger, H. (2006), “Blue native PAGE”, *Nature Protocols*, Vol. 1 No. 1, pp. 418–428.

Wittig, I., Carrozzo, R., Santorelli, F.M. and Schägger, H. (2006), “Supercomplexes and subcomplexes of mitochondrial oxidative phosphorylation”, *Biochimica et Biophysica Acta - Bioenergetics*, Vol. 1757 No. 9–10, pp. 1066–1072.

Wu, M., Gu, J., Guo, R., Huang, Y. and Yang, M. (2016), “Structure of Mammalian Respiratory Supercomplex I1III2IV1”, *Cell*, Elsevier, Vol. 167 No. 6, p. 1598–1609.e10.

Xia, D., Esser, L., Tang, W.-K., Zhou, F., Zhou, Y., Yu, L. and Yu, C.-A. (2013), "Structural analysis of cytochrome bc1 complexes: Implications to the mechanism of function", *Biochimica et Biophysica Acta (BBA) - Bioenergetics*, Vol. 1827 No. 11–12, pp. 1278–1294.

Xia D, CA, Y., H, K., Xia JZ, AM, K., L, Z., L, Y., et al. (1994), "Crystal structure of the cytochrome bc1 complex from bovine heart mitochondria", *Analytical Biochemistry*, Vol. 217 No. 2, pp. 220–230.

Yankovskaya, V. (2003), "Architecture of Succinate Dehydrogenase and Reactive Oxygen Species Generation", *Science*, Vol. 299 No. 5607, pp. 700–704.

Yoshikawa, S., Shinzawa-Itoh, K. and Tsukihara, T. (1998), "Crystal Structure of Bovine Heart Cytochrome c Oxidase at 2.8 Å Resolution", *Journal of Bioenergetics and Biomembranes*, Vol. Volume 30 No. Issue 1, p. pp 7–14.

Zara, V., Conte, L. and Trumpower, B.L. (2009a), "Biogenesis of the yeast cytochrome bc1 complex.", *Biochim. Biophys. Acta*, Elsevier B.V., Vol. 1793 No. 1, pp. 89–96.

Zara, V., Conte, L. and Trumpower, B.L. (2009b), "Evidence that the assembly of the yeast cytochrome bc1 complex involves the formation of a large core structure in the inner mitochondrial membrane", *FEBS Journal*, Vol. 276 No. 7, pp. 1900–1914.

Zara, V., Palmisano, I., Conte, L. and Trumpower, B.L. (2004), "Further insights into the assembly of the yeast cytochrome bc1 complex based on analysis of single and double deletion mutants lacking supernumerary subunits and cytochrome b", *European Journal of Biochemistry*, Vol. 271 No. 6, pp. 1209–1218.

Zhang, K., Wang, G., Zhang, X., Hüttemann, P.P., Qiu, Y., Liu, J., Mitchell, A., et al. (2016), "COX7AR is a Stress-inducible Mitochondrial COX Subunit that Promotes Breast Cancer Malignancy", *Scientific Reports*, Nature Publishing Group, Vol. 6 No. July, p. 31742.

Zhang, M., Mileykovskaya, E. and Dowhan, W. (2002), "Gluing the respiratory chain together: Cardiolipin is required for supercomplex formation in the inner mitochondrial membrane", *Journal of Biological Chemistry*, Vol. 277 No. 46, pp. 43553–43556.

Zhang, Z., Huang, L., Shulmeister, V.M., Chi, Y.-I., Kim, K.K., Hung, L.-W., Crofts, A.R., et al. (1998), "Electron transfer by domain movement in cytochrome bc1", *Nature*, Vol. 392 No. 6677, pp. 677–684.

Zhu, J., King, M.S., Yu, M., Klipcan, L., Leslie, A.G.W. and Hirst, J. (2015), “Structure of subcomplex Iβ of mammalian respiratory complex I leads to new supernumerary subunit assignments.”, *Proceedings of the National Academy of Sciences of the United States of America*, Vol. 112 No. 39, pp. 12087–92.

Zhu, J., Vinothkumar, K.R. and Hirst, J. (2016), “Structure of mammalian respiratory complex I”, *Nature*, Nature Publishing Group, Vol. 536 No. 7616, pp. 354–358.

Zickermann, V., Wirth, C., Nasiri, H., Siegmund, K., Schwalbe, H., Hunte, C. and Brandt, U. (2015), “Mechanistic insight from the crystal structure of mitochondrial complex I”, *Science*, Vol. 347 No. 6217, pp. 44–49.

APPENDIX

1. Proteomics detection of MRC subunits in the SC I+III$_2$+IV from control 143B cells (Band 1), and in the SCs I+III$_2$ from COX1Δ cybrids (Band 2) and COX2Δ cybrids (Bands 3 and 4).

	SC I+III$_2$+IV	SC I+III$_2$		
COMPLEX I	Band 1	Band 2	Band 3	Band 4
NDUFA1				
NDUFA2				
NDUFA3				
NDUFA5				
NDUFA6				
NDUFA7				
NDUFA8				
NDUFA9				
NDUFA10				
NDUFA11				
NDUFA12				
NDUFA13				
NDUFAB1				
NDUFB1				
NDUFB2				
NDUFB3				
NDUFB4				
NDUFB5				
NDUFB6				
NDUFB7				
NDUFB8				
NDUFB9				
NDUFB10				
NDUFB11				
NDUFC1				
NDUFC2				
NDUFS1				
NDUFS2				
NDUFS3				
NDUFS4				
NDUFS5				
NDUFS6				
NDUFS7				
NDUFS8				
NDUFV1				
NDUFV2				
NDUFV3				
ND1				
ND2				
ND3				
ND4				
ND4L				
ND5				
ND6				

	SC I+III$_2$+IV	SC I+III$_2$		
COMPLEX III	Band 1	Band 2	Band 3	Band 4
CORE1				
CORE2				
CYTB				
CYC1				
RISP				
UQCRB				
UCRC / UQCR10				
UQCRH				
UQCR11				
UQCRQ				
COX7A2L / COX7RP				

	SC I+III$_2$+IV	SC I+III$_2$		
COMPLEX IV	Band 1	Band 2	Band 3	Band 4
COX1				
COX2				
COX3				
COX4				
COX5A				
COX5B				
COX6A				
COX6B				
COX6C				
COX7A2				
COX7B				
COX7C				
COX8				
NDUFA4				

absent

present

2. Published papers during the development of the present work

2.1. PART OF THE PRESENT THESIS

- **Lobo-Jarne, T** and Ugalde, C (2017).” Respiratory chain supercomplexes: structures, function and biogenesis” *Seminars in Cell and Developmental Biology.* pii: S1084-9521(17)30072-1. doi: 10.1016/j.semcdb.2017.07.021. [Epub ahead of print]

- Pérez-Pérez, R***.**, **Lobo-Jarne, T*.**, Milenkovic, D., Mourier, D., Bratic, A., García-Bartolomé, A., Fernández-Vizarra, E., Cadenas, S., Delmiro, A., García-Consuegra, I., Arenas, J., Martín, M.A., Larsson, N.G., Ugalde, C. (2016). “COX7A2L is a mitochondrial complex III-binding protein that stabilizes the III_2+IV supercomplex without affecting respirasome formation” *Cell Reports*, Vol.16 No.9, pp. 2387–2398.
  (* Co-first author).

2.2. PUBLISHED DURING THIS PERIOD

- García-Bartolomé , A., Peñas, A., Marín-Buera, L., **Lobo-Jarne T.**, Pérez-Pérez, R., Morán, M., Arenas, J., Martín, MA and Ugalde, C (2017). “Respiratory chain enzyme deficiency induces mitochondrial location of actin-binding gelsolin to modulate the oligomerization of VDAC complexes and cell survival” *Human Molecular Genetics* Vol. 26, No. 13, pp. 2493–2506

3. Papers under review during the development of the present work

- **Lobo-Jarne, T.**, Nývltová, E., Pérez-Pérez, R., Fontanesi, F., Ugalde, C and Barrientos, A. “Mitochondrial COX7A2L regulates the bioenergetic rates of Complex III and Complex III-containing supercomplexes to fine tune succinate oxidation”. Currently under Review in *Cell Metabolism*.

Seminars in Cell & Developmental Biology xxx (2017) xxx–xxx

Contents lists available at ScienceDirect

Seminars in Cell & Developmental Biology

journal homepage: www.elsevier.com/locate/semcdb

Review

Respiratory chain supercomplexes: Structures, function and biogenesis

Teresa Lobo-Jarne [a], Cristina Ugalde [a,b,*]

[a] Instituto de Investigación Hospital 12 de Octubre (i+12), Madrid 28041, Spain
[b] Centro de Investigación Biomédica en Red de Enfermedades Raras (CIBERER), U723, Madrid 28029, Spain

ARTICLE INFO

Article history:
Received 20 April 2017
Received in revised form 12 July 2017
Accepted 13 July 2017
Available online xxx

Keywords:
Respiratory chain function
Supercomplexes
Respirasome
Assembly factors

ABSTRACT

Over the past sixty years, researchers have made outmost efforts to clarify the structural organization and functional regulation of the complexes that configure the mitochondrial respiratory chain. As a result, the entire composition of each individual complex is practically known and, aided by notable structural advances in mammals, it is now widely accepted that these complexes stablish interactions to form higher-order supramolecular structures called supercomplexes and respirasomes. The mechanistic models and players that regulate the function and biogenesis of such superstructures are still under intense debate, and represent one of the hottest topics of the mitochondrial research field at present. Noteworthy, understanding the pathways involved in the assembly and organization of respiratory chain complexes and supercomplexes is of high biomedical relevance because molecular alterations in these pathways frequently result in severe mitochondrial disorders. The purpose of this review is to update the structural, biogenetic and functional knowledge about the respiratory chain supercomplexes and assembly factors involved in their formation, with special emphasis on their implications in mitochondrial disease. Thanks to the integrated data resulting from recent structural, biochemical and genetic approaches in diverse biological systems, the regulation of the respiratory chain function arises at multiple levels of complexity.

Contents

Abbreviations: MRC, mitochondrial respiratory chain; CoQ, coenzyme Q or ubiquinone; cyt*c*, cytochrome *c*; SC, supercomplex; CI-CIV, respiratory chain complexes I to IV; $CIII_2$, dimeric CIII; CV, ATP synthase; BN-PAGE, blue native gel electrophoresis; EM, electron microscopy.

* Corresponding author at: Instituto de Investigación Hospital 12 de Octubre (i+12), Avenida de Córdoba s/n, 28041 Madrid, Spain.
E-mail address: cugalde@h12o.es (C. Ugalde).

http://dx.doi.org/10.1016/j.semcdb.2017.07.021
1084-9521/

1. Introduction

Recent investigations have shed light into the sophistication surrounding the biogenesis of the oxidative phosphorylation (OXPHOS) system. In mammals, the OXPHOS system is formed by five multiprotein enzyme complexes and two mobile electron carriers embedded in the inner mitochondrial membrane. The first four enzyme complexes (CI-CIV) comprise the mitochondrial respiratory chain (MRC), which facilitates electron transfer from reducing equivalents to molecular oxygen coupled to the generation of a proton gradient across the inner membrane that will be used by the ATP synthase (complex V) to drive ATP synthesis. In addition to their structural subunits, the biogenesis of these five hetero-oligomeric enzymatic complexes requires an extensive number of ancillary factors to coordinate subunits maturation, incorporation of prosthetic groups and assembly into the holoenzymes. The discovery that some MRC enzymes physically interact to form a variety of supramolecular structures called supercomplexes (SCs) and respirasomes, and the existence of SC-specific assembly factors involved in their assembly, has put the spotlight on the structural and functional properties of the SCs, and on the regulatory pathways involved in their biogenesis. It is currently debated whether SCs play a relevant functional role in cellular bioenergetics, in the formation of reactive intermediates, or in the stabilization of the individual MRC complexes. Since genetic alterations in MRC subunits and assembly factors often lead to severe encephalomyopathies and neurodegenerative disorders, a full understanding of the structural organization and biosynthetic regulation of the MRC is essential to understand the molecular mechanisms underlying mitochondrial pathology. In this review we will explore the current knowledge on mammalian respiratory SCs, integrating the historical perspective with the most recent structural findings, and putting this information in the context of mitochondrial disease.

2. Mitochondrial respiratory chain, a long-lasting journey

2.1. Composition and function of the respiratory chain

The production of adenosine 5′-triphosphate (ATP), the key energy source of the cell, through aerobic substrate oxidation is the main function of the mitochondrial metabolism. In the late 50s, several redox enzymes and prosthetic groups responsible for the classic mitochondrial electron transfer chain were defined [1] followed by their reconstitution in the early 60 s [2]. The overall respiratory chain activity was postulated as a sequential transfer of electrons between four major multi-enzymatic complexes dispersed in the inner mitochondrial membrane (IMM): NADH dehydrogenase:ubiquinone oxidoreductase (complex I, CI), succinate:ubiquinone oxidoreductase (complex II, CII), ubiquinol:cytochrome *c* oxidoreductase or cytochrome *bc1* complex (complex III, CIII), and cytochrome *c* oxidase (complex IV, CIV). In addition, the electron transfer was ensured by the diffusion of two mobile components acting as co-substrates: the lipophilic ubiquinone, also designated as coenzyme Q (CoQ), embedded in the membrane lipid bilayer, and the hydrophilic heme protein cytochrome *c* (cyt*c*) located on the external surface of the IMM [3,4]. Altogether, these components form the mitochondrial respiratory chain (MRC) where cellular respiration takes place. Organic nutrients are catabolized into small electron donor molecules, $NADH_2$ and $FADH_2$, which transfer the electrons to CI and CII, respectively. CoQ uptakes the electrons from both sources, transferring them to dimeric CIII ($CIII_2$), then to cyt*c* and finally to CIV, that yields the electrons to molecular oxygen. This electron flux is coupled to a proton pump from the matrix to the intermembrane space through complexes I, III and IV, which generates an electrochemical gradient across the IMM that provides the necessary free energy for the ATP synthase (complex V, CV) to synthesize ATP through the mechanism known as oxidative phosphorylation [5].

2.2. Models for the structural organization of the respiratory chain

Despite the well-known functional relevance of the respiratory chain, the structural organization of its components remains unclear.

2.2.1. Solid-state model

The pioneering spectrophotometric studies of Chance and Williams represented the MRC as a solid state assembly of prosthetic groups that carry out sequential redox reactions in a protein matrix [1]. The evidences in favour of this “rigid” or “solid-state model” were based on the isolation of CI-CIII and CII-CIII active units in a stoichiometric molar ratio of 1:1 during intermediate purification steps of the individual enzymes, that were interpreted as secondary enzymatically active complexes [6]; and on the reconstitution of a “repeating unit of electron transfer” containing all MRC complexes from bovine heart mitochondria [7]. This model implied the notion of permanently-bound CoQ to the MRC units. Accordingly, vesicle reconstitution experiments showed stoichiometric associations between CI and $CIII_2$ at high protein concentrations with no exchange between free and bound ubiquinone, i.e., no ‘CoQ-pool’ behaviour [8]. Only when sufficient lipid was added the CoQ-pool behaviour was restored, but this was interpreted as the movement of complex-associated CoQ rather than of free CoQ [9]. Later studies in *Saccharomyces cerevisiae* provided evidence that CoQ and cyt*c* only diffused freely along the membrane upon the addition of chaotropic agents, suggesting that the respiratory chain in yeast also behaves as one functional unit that at least comprises complexes III and IV with bound CoQ and cyt*c* [10].

2.2.2. Liquid-state model

The general vision gradually evolved into a “random collision”, “fluid” or “liquid-state” model, proposed by Hackenbrock and co-workers, that pictured all membrane proteins and redox components that catalyse electron transport and ATP synthesis in constant and independent diffusional motion, where electron transfer to

Please cite this article in press as: T. Lobo-Jarne, C. Ugalde, Respiratory chain supercomplexes: Structures, function and biogenesis, Semin Cell Dev Biol (2017), http://dx.doi.org/10.1016/j.semcdb.2017.07.021

place through diffusion-based collisions among the redox partners [11]. Evidence in favour of the "liquid-state model" arose from kinetic analyses proposing not only that electron transfer in the CoQ and cytc regions obeyed a pool behaviour in mammalian mitochondria, but also that it followed saturation kinetics with regards to CoQ and cytc concentrations [3,12]. Furthermore, enzymatic activities were retained upon isolation of the individual OXPHOS complexes [2] and the use of fluorescent antibodies against $CIII_2$ and CIV caused independent aggregation of these complexes, suggesting that they diffuse laterally in the membrane plane independent of one another [13].

2.2.3. Dynamic aggregate or plasticity model

The two previous models were proposed for the way in which MRC components interact to accomplish a maximal-efficient electron transfer, representing extreme examples where intermediate modes of operation are feasible. Alternative studies by Ferguson-Miller and collaborators that analysed the role of lateral diffusion of cytc in electron transfer within native mitochondrial membranes, gave rise to the "dynamic aggregate" model [14]. In this model, a dynamic equilibrium exists between freely diffusing and associated-forms of the MRC components, all active in electron transfer. This new representation of the respiratory chain reconciled the two classical models, as it incorporated transient aggregates as well as free lateral diffusion of redox components to account for the electron transport rates. The reversible formation of specific MRC aggregates additionally offered a mechanism for localized proton flow and the possibility of regulating the direction and efficiency of electron transfer [15,16].

This idea was disregarded in favour of the "fluid" model until new data from two groups, based on the use of blue native polyacrylamide gel electrophoresis (BN-PAGE) developed by Schägger and collaborators, showed the co-existence of individual MRC complexes together with their inter-associations in supramolecular assemblies that were termed supercomplexes (SCs) [17,18]. Experimental evidences demonstrated that SCs are evolutionarily conserved stable structures in both prokaryotes and eukaryotes, and not random associations of MRC complexes [19,20], and recent high-resolution cryo-electron microscopy (cryo-EM) analyses showed the detailed structural architecture of mammalian respiratory SCs (Fig. 1) [21–23]. The coexistence of individual MRC complexes and SCs thus supports the principles of the "dynamic aggregate" model, which was lately renamed as the "plasticity" model by Enríquez and co-workers [24,25]. In its current form, this model proposes that the switch between freely moving MRC complexes to fixed SCs would optimize electron flux from different substrates (NADH and $FADH_2$), adapting the efficiency of the respiratory chain to changes in cellular metabolism via partitioned CoQ and cytc pools [26]. The catalytic relevance of this hypothesis, based on BN-PAGE and oxygen consumption analyses in mouse cells depleted of MRC complexes, was however questioned by more direct spectroscopic and kinetic experiments in yeast and bovine submitochondrial particles showing that: a) the metabolic pathways for NADH and succinate oxidation occur through a single and universally accessible CoQ-pool [27], and b) that cytc does not encounter major barriers to its free diffusion [28]. Moreover, this model was proposed on the basis of differences in the steady-state levels of respiratory chain structures on BN-PAGE gels, and therefore, the reversible and dynamic association/dissociation events –the so-called "plasticity"- between the individual complexes and the SCs remains to be proven. The prospective evolution of the "plasticity" model will thus rely on the extensive characterization of the structural, functional and kinetic properties of the SCs upon variations in physiological conditions [29,30].

3. Structural architecture of respiratory chain supercomplexes

3.1. Types of respiratory chain supercomplexes

The notion of "supercomplexes" first appeared upon the observations of preferential associations between bacterial MRC complexes [31,32]. Respiratory chain SCs of different compositions and stoichiometries were later reported by means of BN-PAGE analyses of mitochondrial fractions solubilized with the mild detergent digitonin. This method allows the retention of labile supramolecular assemblies of membrane protein complexes that would otherwise be dissociated (Fig. 2A). The solubilization of OXPHOS complexes from yeast and bovine heart mitochondria using varying digitonin-to-protein ratios and subsequent BN-PAGE allowed to separate assorted types of stoichiometric associations of complexes I, III and IV within the molecular mass range from ~750 to ~2100 kDa, in an overall 1:3:6 stoichiometry [33]. Additional BN-PAGE, single-particle electron microscopy (EM) and cryo-electron tomography studies, consistently reported specific associations between CI, $CIII_2$ and CIV in a wide range of organisms [19]. It is worth mentioning that for a long time, many researchers attributed the appearance of SCs on BN-PAGE gels to protein aggregation as a consequence of detergent solubilisation. However, the migrations of these bands in the gels are consistently reproducible, as shown by many different laboratories in the last 17 years, and well-defined structures from these bands extracted from the gels are now available.

The composition and abundance of the respiratory chain SCs may vary among organisms and tissues depending on the metabolic and physiological conditions [17,26,34–40], as well as on the lipid content of the mitochondrial inner membrane [41–44]. In most CI-containing eukaryotes, CI primarily interacts with $CIII_2$ and CIV to form the most abundant SC, $I+III_2+IV_1$, to which additional CIV monomers are added to form SCs $I+III_2+IV_{2-4}$. These structures are known as the respirasomes [17], since they contain all the components required to transfer electrons from NADH to molecular oxygen. Additionally, CI associates with $CIII_2$ to form SC $I+III_2$; and $CIII_2$ binds one to two CIV monomers to assemble SCs III_2+IV_{1-2}. In mammals, most CI, ~40-50% of $CIII_2$ and ~20-30% of CIV are localized in the largest SCs $I+III_2$ and $I+III_2+IV_{1-4}$ (Fig. 2B). $CIII_2$ and CIV may also interact to form SC III_2+IV_1 that scarcely represents 5–10% of the total MRC structures [33,45]. In higher plants mitochondria, CIV-containing SCs are barely detectable, and SC $I+III_2$ is the predominant macrostructure [46]. In *S. cerevisiae*, which lacks CI, two bands of ~750 and ~1000 kDa corresponding to SCs III_2+IV_1 and III_2+IV_2, respectively, are predominant [17,18]. These variations in the relative abundance of SCs may reflect different stoichiometries of CI, $CIII_2$ and CIV among organisms. Regarding CII and CV, these enzymes form oligomers that do not interact with complexes I, III and IV under normal physiological conditions [17,33,45,47–50].

Based on the differential solubilisation of MRC complexes and SCs on BN-PAGE, a higher organization level of SCs in "respiratory strings" was proposed for mammals and yeast [51], where respirasomes would be interconnected by CIV tetramers at regular intervals, thus generating linear assemblies of respiratory SCs. The observation of CI dimers (CI_2) in *Yarrowia lipolytica* [52] redefined this model as "respiratory patches" generated by the interactions between two CI monomers within adjacent respiratory strings. An alternative model for plants based on single-particle EM, proposed the repetition of $I_2III_2IV_2$ units into a respiratory string mediated by the interaction of two neighbouring CIV through a dimeric interface [53], which differed from the previous model by the lower abundance of CIV copies. The structural and functional characterization of SCs among different species would benefit very much from *in situ* studies without disrupting the mitochondrial mem-

Please cite this article in press as: T. Lobo-Jarne, C. Ugalde, Respiratory chain supercomplexes: Structures, function and biogenesis, Semin Cell Dev Biol (2017), http://dx.doi.org/10.1016/j.semcdb.2017.07.021

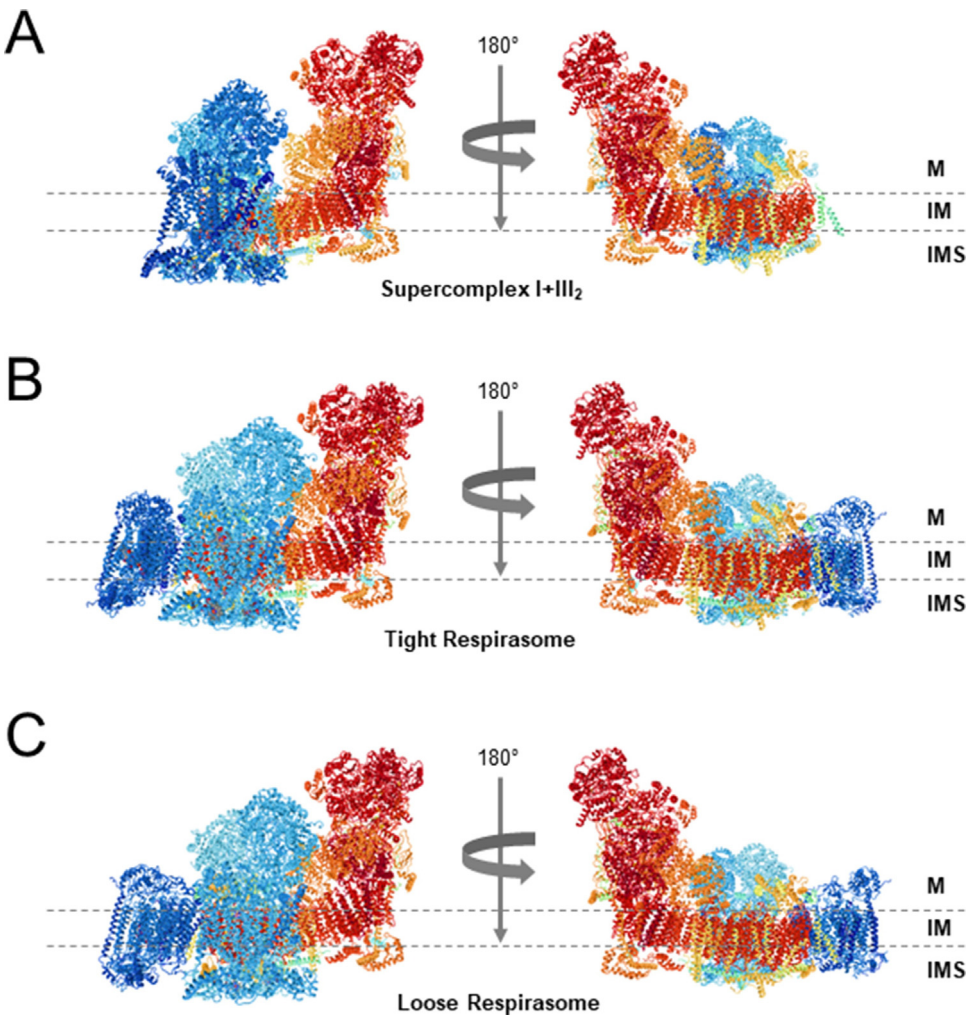

Fig. 1. Architectures of the mammalian respirasomes. Side views along the membrane from (A) Supercomplex I + III_2, (B) the tight respirasome, and (C) the loose respirasome, according to the structures proposed by Letts et al. [22]. Images were obtained from the RCSB Protein Data Bank in combination with the NGL viewer. The structural models of CI, $CIII_2$, and CIV are colored in red, turquoise, and navy blue, respectively. The transmembrane region is indicated by two dashed lines. M, matrix; IM, mitochondrial inner membrane; IMS, intermembrane space.

branes with detergents; for example, using fluorescence life-time imaging, as recently published [54].

3.2. Structural properties of respiratory chain supercomplexes

3.2.1. Supercomplexes I + III_2 and III_2 + IV_{1-2}

The first structure of SC I + III_2 from *Arabidopsis thaliana* mitochondria was determined at 18 Å resolution [46], revealing the lateral association of $CIII_2$ to the membrane-embedded distal part of CI. However, the lack of an atomic CI structure failed to decipher the precise subunit interactions within this SC. Recently, the architectures of the mammalian SC I + III_2 were resolved at high resolution in ovine (Fig. 1**A**) [22] and bovine [55]. In these structures, contacts between CI and $CIII_2$ were similar to the ones detected for SC I + III_2 + IV_1 (described in Section 3.2.2.).

A pseudo-atomic model at 15 Å resolution of yeast SCs III_2 + IV_{1-2} [56] revealed that $CIII_2$ is attached to the convex side of two CIV monomers, leaving the opposite interfaces open for CIV dimerization. Cardiolipin and phosphatidylethanolamine lipids were identified at the $CIII_2$-CIV interface. This structure also revealed cyt*c* bound to $CIII_2$, which moves and rotates within a distance of 40 Å (~4 nm) to mediate electron transfer between $CIII_2$ and CIV. Later studies based on 3D-cryo-EM maps specified the distance between the cyt*c* binding sites of $CIII_2$ and CIV as ~6 nm, considered to be sufficiently short to enable the channelling of cyt*c* between these complexes [57], although this was previously refuted [28]. The yeast $CIII_2$ subunits cytochrome *b*, cytochrome c_1, Qcr6 (Hinge protein), Qcr7, Qcr8 and Qcr9 were identified at the $CIII_2$-CIV interface, as well as the CIV subunits CoxI, CoxII, CoxIII, CoxIV, CoxVIc, CoxVIIa and CoxVIIc [56]. However, direct evidence supporting precise subunit interactions was missing. Due to its low relative abundance, SCs III_2 + IV_{1-2} from higher organisms await structural characterization.

3.2.2. Respirasome or supercomplex I + III_2 + IV_1

In mammalian mitochondria, I + III_2 + IV_1 is the most abundant SC. The first 3D maps of the bovine heart SC I + III_2 + IV_1 [47,50,58,59] revealed the lateral binding of $CIII_2$ to the middle part of the CI membrane arm, with CIV positioned in the distal tip of CI while laterally interacting with $CIII_2$, and cardiolipin molecules filling the gaps between the transmembrane domains at the interfaces between the individual complexes [47,59]. The recent characterization of the atomic structure of mammalian CI by cryo-EM [60,61] represented a major step forward that enabled to obtain high-resolution projection maps of the mammalian respirasomes [21–23,55]. Yang and collaborators solved the conformation of porcine SC I + III_2 + IV_1 [21,23], where CIV would loosely bind CI and $CIII_2$. In addition, Letts et al. [22] distinguished two archi-

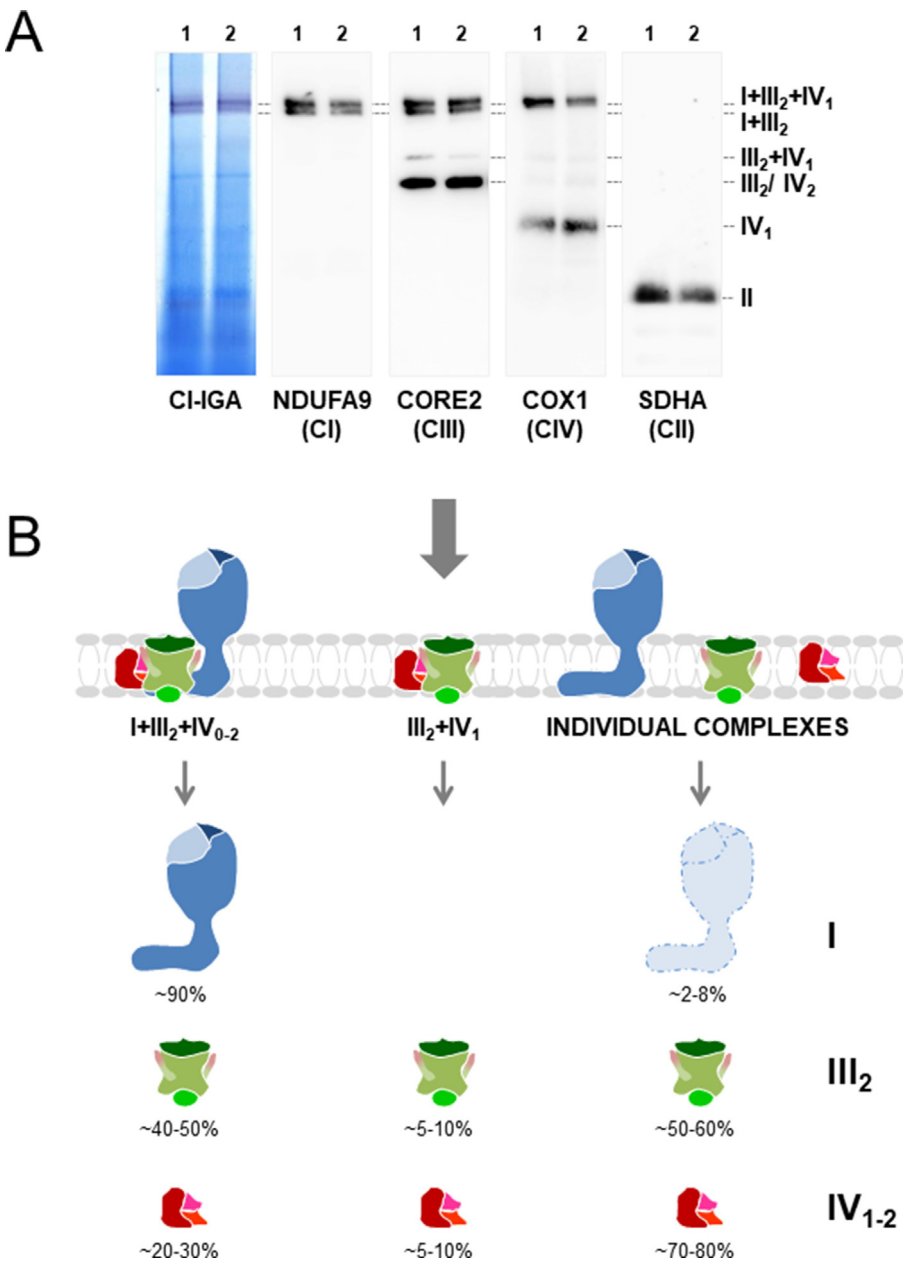

Fig. 2. Distribution of human respiratory chain complexes and supercomplexes. (A) Mitochondria isolated from cultured 143B TK- cells (1) and cybrids (2) were analysed by BN-PAGE in combination with CI *in-gel* activity (IGA) assay and western blot with antibodies against the indicated MRC subunits. (B) Most CI (blue), ~half of $CIII_2$ (green) and ~20-30% of CIV (red) are localized in the respirasome ($I+III_2+IV_{0-1}$). SC III_2+IV_1 represents ~5% of the total amount of MRC structures, as well as CIV dimers (IV_2). CII (II) is not present in SCs. Free CI (light blue) requires to be associated in supercomplexes to minimize destabilization and ROS generation [29].

tectures for the ovine respirasome, a major "tight" and a minor "loose" conformations, where CIV would contact both CI and $CIII_2$ within the tight form, but only CI within the loose form (Fig. 1B–C). Sousa et al. also resolved two classes of SC $I+III_2+IV_1$ in bovine [55]. The tight form of the ovine respirasome was essentially identical to the bovine respirasome class 1. However, the bovine respirasome class 2 differed in the conformational flexibility of $CIII_2$, as this rotates by 25° relative to CI while CIV remains unchanged. The bovine respirasome additionally showed clear density in one of the two membrane extrinsic iron-sulphur domains of $CIII_2$, suggesting that only one CIII monomer would be active [55]. The heterogeneity among these structures deserves further consideration [30], as it could reflect the existence of independent structural entities resulting from the differential association and dissociation of the MRC complexes in response to, e.g., tissue-specific phospholipid environments or ROS levels.

The respirasome-bound CI is more compact than free CI due to its associations with $CIII_2$ and CIV [60,61]. Although several interaction points exist between CI, $CIII_2$ and CIV, the most extensive and stable interactions take place between CI supernumerary subunits (absent in bacteria) and $CIII_2$ at two major points: CI subunits NDUFA11 (B14.7 in bovine) and NDUFB4 (B15) directly interact with $CIII_2$ subunit UQCRQ at the matrix and inner membrane interface, and CI subunits NDUFB4 and NDUFB9 (B22) bind $CIII_2$ subunits UQCRC1 and UQCRFS1 in the matrix [22,23]. Another important interaction occurs between CI subunit NDUFB7 (B18) and subunit UQCRH on $CIII_2$. Both subunits contain disulphide bonds, suggesting that redox regulation might modulate the interactions between MRC complexes [22]. Since the long helix of NDUFB7 is poised at

Please cite this article in press as: T. Lobo-Jarne, C. Ugalde, Respiratory chain supercomplexes: Structures, function and biogenesis, Semin Cell Dev Biol (2017), http://dx.doi.org/10.1016/j.semcdb.2017.07.021

the interface of the three complexes, it may also interact with CIV through the COX7A and COX8 B subunits at the intermembrane space and inner membrane interface [22,23]. CIV is less tightly bound to the respirasomes and major contacts differ among structures, reflecting its varying location. There is a close association of CIV subunit COX7C and ND5 on CI, as well as an interaction of COX7A on CIV with $CIII_2$ subunits UQCR11, UQCRC1 and UQCRB at the matrix and inner membrane interface [22,23]. This interaction between $CIII_2$ and CIV seems to swing away in the loose respirasome form, where only COX7A would contact CI through subunit ND5 [22]. It must be noted that the differences that exist between the structural models presented from ovine/bovine/porcine probably rely on the species-specific protein sequences of the MRC subunits. Therefore, structural variations in the SCs and respirasomes from other species, such as rodents and human, appear well possible depending on the degree of conservation of the specific protein domains and residues that promote the interactions within these structures.

3.3. Effect of cardiolipin on the stabilization of supercomplexes

Supporting the idea that phospholipids mediate protein–protein interactions in the inner mitochondrial membrane, cardiolipin molecules were detected within yeast SCs $III_2 + IV_{1-2}$ [57], where they stabilize these structures [41,42]. Moreover, studies in lymphocytes from patients with Barth syndrome, a mitochondrial disorder in which cardiolipin levels are drastically reduced due to mutations affecting Tafazzin (an enzyme involved in cardiolipin maturation), revealed the specific destabilization of SC $I + III_2 + IV_1$ [62]. A pluripotent stem cell model system of this disorder later confirmed the role of cardiolipin content for SCs stabilization [63]. Consistent with these observations, the atomic structure of the respirasome revealed clear gaps between CI, $CIII_2$ and CIV that were occupied by cardiolipin molecules to further stabilize the respirasome [23,59]. Although cardiolipin is considered to stabilize SCs, phosphatidylethanolamine, another phospholipid of the inner membrane, seems to exert the opposite effect [43]. Therefore, differences in the balance between phospholipid species may contribute to the specific reorganization of the MRC complexes and SCs.

4. Functional roles of the supercomplexes

The discovery of SCs represents a great progress in the study of the functional and structural properties of the MRC, and their existence should provide functional advantages that remain far to be fully-understood.

4.1. Catalytic enhancement of the electron flux through substrate channelling

The arrangement into SCs was initially proposed to maximize the efficiency of the electron flux across the MRC [17]. Indeed, spectrophotometric assays of the MRC activities of isolated SCs from bovine heart mitochondria showed that CI in SC $I + III_2$ displays about half the activity of that in SC $I + III_2 + IV_1$, suggesting that the full respirasome was the most active unit [50]. Substrate channelling was proposed as a possible mechanism to explain the increased rates of electron transfer within SCs based on flux control analyses of the MRC complexes in bovine heart mitochondria [64]. The authors suggested that CI and $CIII_2$ behave as a single enzymatic unit, where electron transfer through CoQ is accomplished by channelling between the two redox enzymes without following a pool behaviour, in agreement with other reports in yeast [10] and bovine mitochondria [8]. Following studies that analysed the roles of CoQ and cyt*c* in the attenuation of $CIII_2$ and CIV pharmacological inhibition on the respiratory flux supported the dynamic compartmentalization of the respiratory substrates [65], as well as studies based in the competition of substrates for NADH and succinate oxidation [26]. The proposal that SCs may provide distinct electron translocation pathways through the partition of CoQ into different pools to mediate metabolic adaptation [26], was questioned by kinetic and flux control studies showing that the metabolic pathways for NADH and succinate oxidation comprise different CoQ redox steady states, but communicate and converge on a single non-partitioned CoQ pool [27,30]. It has also been argued that the cyt*c* pool is equally compartmentalized [26], but studies monitoring the reduction potential of CIII upon addition of NADH, succinate or both [27], evidenced against cyt*c* partitioning. In agreement, time-resolved spectroscopic analysis of cyt*c* oxidation in intact yeast cells showed that cyt*c* is not trapped within SCs and, therefore, there are no restrictions that limit its diffusion [28]. Moreover, the respirasome structures showed no evidence of a protein-mediated substrate channel connecting the CoQ binding sites of CI and $CIII_2$ [22], since both active sites are open to the membrane and separated by 10 nm, as also evidenced for cyt*c*, in agreement with previous studies that questioned substrate channelling based on the distances between the substrates binding sites on SCs [47]. Therefore, the function of a direct catalytic role for mitochondrial SCs remains questionable [30].

4.2. Assembly and stability of complex I

Experimental evidence accumulated on respiratory chain disease models, suggests that the formation of mammalian SCs confers stability to their individual components, and most particularly to CI. The first description of a patient with progressive exercise intolerance due to a nonsense mutation in the $CIII_2$ subunit gene *MT-CYB* associated with a combined enzyme deficiency of complexes I and III [66], was followed by a more extensive study showing that genetic alterations leading to a loss of $CIII_2$ prevented respirasome formation and led to the secondary loss of CI [67]. Further studies confirmed that not only the structural integrity of $CIII_2$ [68], but also that of CIV [69–71], were essential to maintain the stability of mammalian CI. Despite these evidences, ostensible CI functional alterations are relatively infrequent to most patients presenting with $CIII_2$ or CIV enzyme deficiencies [72,73], indicating that only severe structural alterations of these two complexes induce a parallel CI dysfunction. On the contrary, a dramatic decrease in CI levels do not generally lead to $CIII_2$ and CIV functional defects in mammals [67]. In agreement, the depletion of 28 different CI accessory subunits in human HEK293T cells showed a loss of SCs $I + III_2$ and $I + III_2 + IV_1$ with no alterations in the steady-state levels of $CIII_2$ or CIV [74].

The specific dependence of CI stability on the respirasome biosynthesis has important repercussions for our understanding of the respiratory chain disorders. In this regard, two main hypotheses are currently debated to explain the integration and stabilization of CI into SCs (Figs. 3 and 4, see Section 5.1.). However, the fact that CI is purified and remains active in its free form adds to the debate whether CI stability may rely on additional molecular mechanisms, like alterations in the mitochondrial membrane potential [49] or ROS levels (see Section 4.3.). In accordance, the absence of respirasomes due to the lack of cyt*c* [75], $CIII_2$ or CIV induced reverse electron transport from reduced CoQ to CI, triggering local superoxide generation and CI degradation [76].

4.3. Modulation of ROS production

Because CI and $CIII_2$ constitute the main redox centres responsible for oxygen reduction to superoxide [77,78], it has been hypothesized that their arrangement into SCs could minimize ROS

Please cite this article in press as: T. Lobo-Jarne, C. Ugalde, Respiratory chain supercomplexes: Structures, function and biogenesis, Semin Cell Dev Biol (2017), http://dx.doi.org/10.1016/j.semcdb.2017.07.021

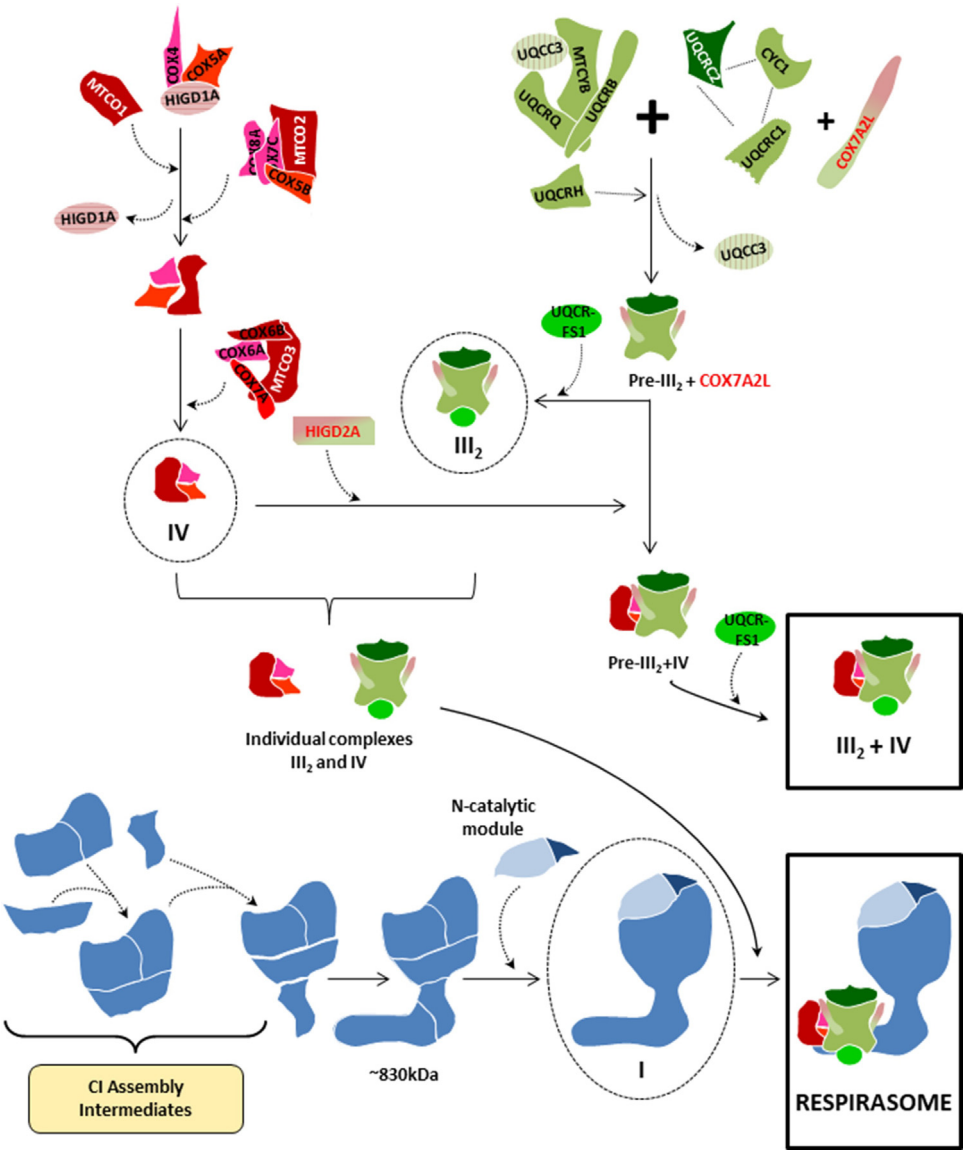

Fig. 3. Respirasome biogenesis through the direct association of fully-assembled respiratory chain complexes. This model [24,86] proposes that the mammalian respirasome ($I+III_2+IV_1$) originates by the direct association of single pre-assembled CI (blue), $CIII_2$ (green) and CIV (red). The assembly pathways of the individual MRC complexes are depicted according to stablished models [72,86,108], and SC III_2+IV_1 is formed independently of the respirasomes [98]. Supercomplex assembly factors COX7A2L and HIGD2A are marked in green/red.

production. Measurements in bovine heart mitochondria provided the first demonstration that the disruption of SC $I+III_2$ enhanced the generation of superoxide from CI [79], and a direct correlation between ROS levels and CI dissociated from SCs was established in neurons and astrocytes [80]. According to the ovine respirasome structure [22], the two CoQ binding cavities on $CIII_2$ are arranged in such way that the symmetry of $CIII_2$ is broken, and this asymmetry could limit ROS production at the expense of maximal activity.

Although decreased ROS production may be a functional consequence of SCs, oxygen levels can also modulate the assembly of these superstructures and the efficiency of mitochondrial respiration. For instance, during prolonged hypoxia, potato mitochondria showed a rearrangement of CI from SC $I+III_2$ to its free form [36]. Other studies in mouse fibroblasts lacking the Rieske Fe-S protein of $CIII_2$ showed that enhanced ROS disrupted SCs and produced a deleterious effect on the stability of complexes I and IV [81]. One way the cells adapt to hypoxic conditions is by building a more efficient respiratory chain through CIV, a key enzyme composed of oxygen-regulated subunit isoforms in yeast and mammals [82–84]. Variations in oxygen levels may thus affect the assembly state of CIV and its incorporation into respirasomes. Aging, a fundamental biological process that affects all eukaryotic lives, is generally attributed to increased oxidative damage induced by ROS, and this is usually accompanied by a decay of SCs levels [85]. Therefore, the interplay between oxygen levels, superoxide production, synthesis and turnover of SCs and impaired respiration, arises as a crucial regulatory mechanism in health, disease and ageing.

5. Biogenesis of respiratory chain supercomplexes

5.1. The respirasome assembly pathway

The precise mechanisms that regulate the biosynthesis of mammalian mitochondrial SCs remain unsolved. Two models have been proposed to explain the association of CI with complexes III and IV to form the respirasome [45,86]. The first model (Fig. 3) proposes that CI gets fully-assembled prior to its binding to SCs [86]. Time-course incorporation analyses of the 13 radiola-

Please cite this article in press as: T. Lobo-Jarne, C. Ugalde, Respiratory chain supercomplexes: Structures, function and biogenesis, Semin Cell Dev Biol (2017), http://dx.doi.org/10.1016/j.semcdb.2017.07.021

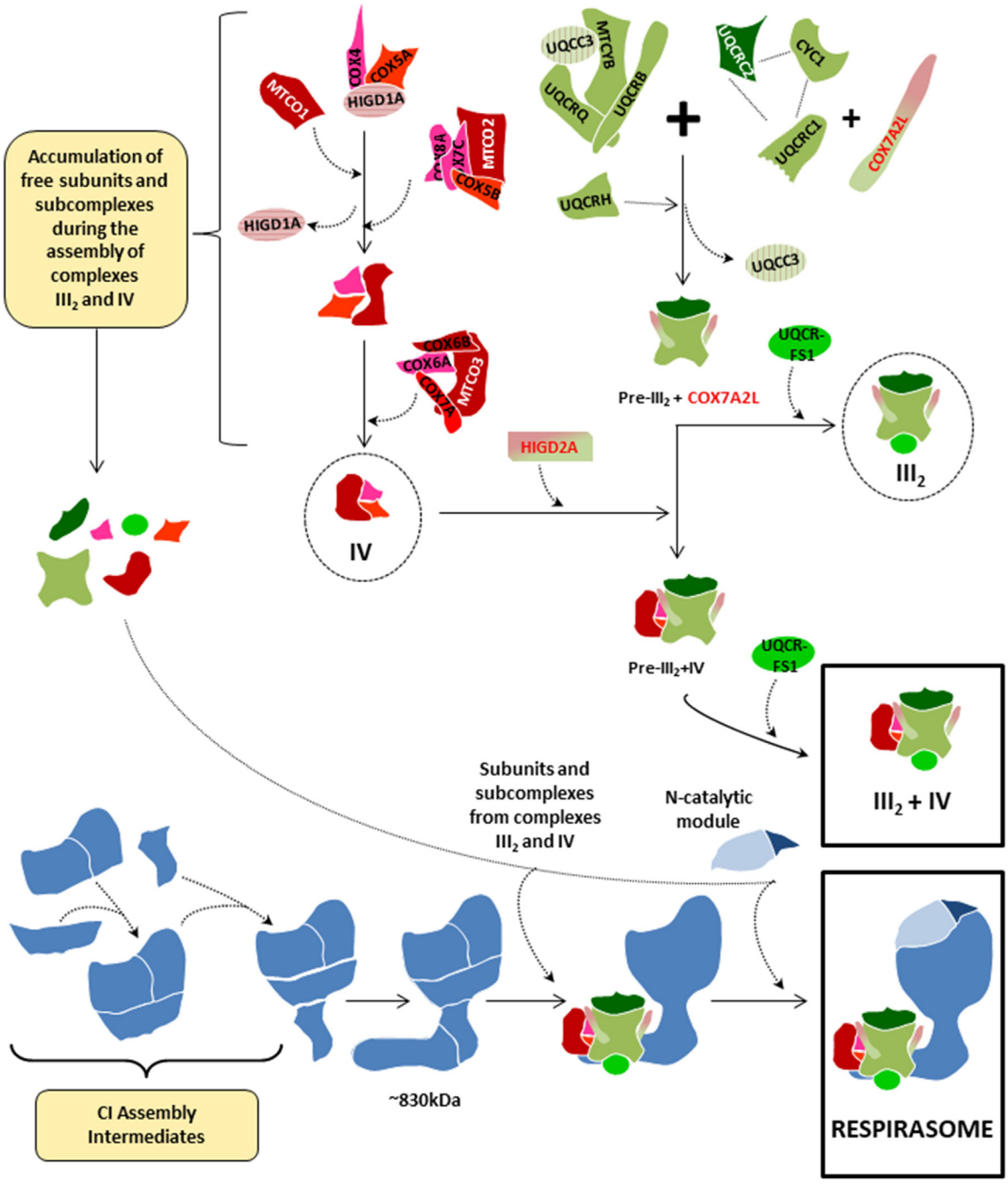

Fig. 4. Respirasome biogenesis through the stepwise association of partially- assembled respiratory chain complexes and submodules. This model [45] proposes the sequential and coordinated association of submodules and free subunits from $CIII_2$ (green) and CIV (red) to a CI-scaffold (blue) that lacks the N catalytic module, which is incorporated at the latest assembly stage to ensure respirasome activation in the presence of all the necessary structural components. The assembly pathways of individual $CIII_2$ and CIV are depicted according to stablished models [72,108], and SC $III_2 + IV_1$ is formed independently of the respirasomes [98]. Supercomplex assembly factors COX7A2L and HIGD2A are marked in green/red.

belled mitochondrial-encoded polypeptides into complexes and SCs showed the existence of a temporal gap between the formation of the complexes and their co-localization in SCs, suggesting that SCs originate by the direct association of single preassembled complexes [24]. Recent proteomics studies based on BN-PAGE and complexome profiling of CI intermediates upon mitochondrial translation inhibition with chloramphenicol, agreed that CI was independently assembled before SC formation [86]. In contrast, previous studies from the same group in *Ndufs4*-KO mice had shown that CI lacking its functional NADH-binding (N) module is associated with $CIII_2$ in a partially-assembled SC [87], suggesting that the biogenesis of SCs does not necessarily require the preassembly of individual complexes. The possibility that the formation of the respirasome could be achieved instead through a coordinated association of submodules and free subunits was supported by the observation in *Neurospora crassa* that the assembly of SC I + III_2 occurs before the individual CI is formed [88], and by studies showing that, in mitochondria from patients with chronically reduced CIV levels, newly-imported COX subunits preferentially integrate into SCs [89,90]. In accordance with this idea, we analysed

Please cite this article in press as: T. Lobo-Jarne, C. Ugalde, Respiratory chain supercomplexes: Structures, function and biogenesis, Semin Cell Dev Biol (2017), http://dx.doi.org/10.1016/j.semcdb.2017.07.021

the formation of SC assembly intermediates by reversibly depleting control cell lines of OXPHOS complexes by long treatment with doxycycline, a reversible inhibitor of mitochondrial translation. Results led us to propose a second model (Fig. 4) that involves the sequential binding of subcomplexes from $CIII_2$ and CIV to an almost complete CI scaffold that lacks the N catalytic module, which would be incorporated at the end of the assembly process to ensure the activation of the respirasome once all the essential structural components are present [45]. This model implies that the SCs constitute the structural units where CI gets fully-assembled and activated, providing a basis to explain the relevance of the respirasomes for CI stability [67] and why certain mutations in $CIII_2$ or CIV-associated genes lead to a combined enzyme deficiency of CI [45]. The differences between both CI assembly models [45,86] could be attributed to technical differences related to the use of two different mitochondrial translation inhibitors, the length of the inhibition periods, or the time gaps between the collected samples, which probably affect the balances between the synthesis of individual MRC subunits and their kinetics of incorporation into the different MRC structures. Although the first model [86] supports the dynamic exchange of CI between its free form and a SC-associated form, the fact that "free CI" is underrepresented in mammalian tissues under mild purification conditions [33] mainly agrees with our statement that SCs provide a scaffold for the full-assembly and stability of CI. Additionally, our model supports the idea that, when "unable to associate to/or once dissociated from" SCs, free CI is prone to degradation by, i.e. locally-produced superoxide [76,79]; moreover, it does not exclude the dynamic exchange of $CIII_2$ and CIV once the respirasome assembly has been completed (being compatible with the variable stoichiometry of CIV within SCs), and it allows for the dynamic replacement *on site* of specific CI reassembled modules to avoid futile continuous cycles of turnover and *de novo* synthesis of this large complex. In this regard, we agree with the previous reports where a CI intermediate lacking the N catalytic module is stably associated in SCs [55,87,91]. Extensive structural studies in cellular and animal models of respiratory chain disease are necessary to clarify the intriguing mechanisms that govern the stepwise biogenesis of the mitochondrial respirasome.

5.2. Supercomplex assembly factors

An important issue is the regulatory function that chaperones or assembly factors play on the assembly of SCs and respirasomes. Here we will discuss the roles of the two best-studied protein types currently defined as SC assembly factors: COX7A2L and the RCFs.

5.2.1. COX7A2L/COX7RP/SCAFI

An interesting debate concerns the regulatory role of the protein COX7A2L/COX7RP in the formation and stabilization of mitochondrial SCs. COX7A2L was first reported to be present in the respirasomes and SC $III_2 + IV_1$ but not in $CIII_2$ or free CIV, therefore constituting the first SC-specific assembly factor that was renamed SCAFI [26]. Enríquez and co-workers discovered that certain wild-type mouse strains widely used in biological research, e.g. C57BL/6J and BALB/c, were homozygous for a 6 bp deletion in the *Cox7a2l* gene and expressed a short, unstable COX7A2L isoform that failed to support CIV association into SCs, thereby promoting differences in mitochondrial respiration rates and ATP production. The authors proposed that COX7A2L is a SC-specific assembly factor that adapts respirasomes formation and mitochondrial function to metabolic variations [26,29]. This hypothesis was challenged by Larsson and co-workers, who demonstrated normal respirasome formation and respiratory chain function in liver and heart mitochondria from mice strains bearing the truncated COX7A2L isoform [92], which was conclusively supported by other studies [93–97]. A recent work from our laboratory showed that COX7A2L is neither essential for respirasome formation in human cell lines [98]. This protein is not uniquely found associated in SCs, since it independently interacts with both $CIII_2$ and free CIV to promote the stabilization of SC $III_2 + IV_1$, results later supported by other groups [84,96,99]. In the absence of CI and CIV, COX7A2L remains associated with $CIII_2$-containing SCs, thereby showing a preferential association for $CIII_2$ [98]. The fact that the formation/stabilization of mammalian SC $III_2 + IV_1$ is regulated by a specific protein in a respirasome-independent manner implies the co-existence of independent regulatory mechanisms for the biogenesis and turnover of different SC structures that deserve further attention.

Variations were observed among tissues in the relative distribution of BN-PAGE bands above the canonical respirasome (corresponding to SC $I + III_2 + IV_{2-4}$) in mice strains bearing the short COX7A2L isoform [94–96]. This opened the possibility that the assembly of specific SCs could be regulated in a tissue-specific manner. The high sequence similarity between COX7A2L and tissue-specific isoforms of the CIV subunit COX7A, led to speculate that COX7A2L may replace COX7A within SCs, acting as a bridge to stabilize the interaction between $CIII_2$ and CIV [22]. Mass spectrometric analyses of SCs from CD1 mice mitochondria (that express the long COX7A2L isoform), revealed that COX7A2 was present almost exclusively in CIV_{1-2}, whereas COX7A2L was present in SCs $III_2 + IV$ and $I + III_2 + IV_{1-4}$ [84]. These observations suggested that the homologous region of COX7A2L could displace COX7A from CIV to form a tight $CIII_2$-CIV interface within SCs, while in the absence of COX7A2L, respirasomes would form with a weaker $CIII_2$-CIV interface solely stabilized by interactions with CI. This possibility remains to be confirmed by higher resolution cryo-EM density maps of the "tight" and "loose" respirasome structures that allow identification of the individual residues [22].

5.2.2. Rcf 1–3

Three independent groups identified two respiratory complex factors (Rcf1 and Rcf2) that control the formation and stabilization of yeast SC $III_2 + IV_{1-2}$ [100–102]. Rcf1 and Rcf2 belong to the conserved *hypoxia induced gene 1* (Hig1) protein family, and both are CIV-binding proteins that may also interact with $CIII_2$. Regarding Rcf1, deletion mutants (*Rcf1Δ*) showed an impaired incorporation of Rcf2, and subunits Cox13 and Cox12 (Cox6a and Cox6b in mammals, respectively) into CIV [101,102], resulting in defective CIV activity, decreased SC $III_2 + IV_{1-2}$ levels and increased ROS production [100,102]. Remarkably, SC $III_2 + IV$ was detectable in the *Rcf1Δ/Rcf2Δ* double mutants, indicating that the core of CIV could still bind $CIII_2$ in the absence of these proteins [101]. These results, as well as recent kinetic and spectroscopic studies in *Rcf1Δ* and *Rcf2Δ* mutants [103], revealed the presence of at least two different enzymatically-active CIV forms, which differ in their protein composition and are independently incorporated into SCs, maybe to adapt the respiratory function to different physiological conditions. Rcf1 interacts with the Aac2 protein [101], a member of the ADP/ATP carrier protein family that facilitates the equimolar exchange of ATP for ADP across the inner membrane [104]; therefore, changes on the conformational state of the Aac2 protein could influence the binding of Rcf1 to CIV and the regulation of its activity [101]. Latest studies showed that Rcf1 interacts with CIV to regulate late stages of its assembly process [105], suggesting that it functions in the assembly of individual CIV rather than playing a direct role in SC $III_2 + IV_{1-2}$. Rcf1 eukaryotic homologs include two variants, *HIGD1A* and *HIGD2A*, that display the broadest expression pattern in mammals [100]. Silencing of *HIGD1A* in mice C2C12 cells did not induce structural alterations on mammalian SCs [100]; instead, this protein was shown to bind CIV in early assembly stages [107], and to upregulate CIV activity under hypoxic cellular stress [106]. However, *HIGD2A* knockdown caused the depletion of SC $III_2 + IV_1$ and

Please cite this article in press as: T. Lobo-Jarne, C. Ugalde, Respiratory chain supercomplexes: Structures, function and biogenesis, Semin Cell Dev Biol (2017), http://dx.doi.org/10.1016/j.semcdb.2017.07.021

of CIV-containing bands above the SC $I+III_2+IV_1$ without altering free CIV levels [100], suggestive of a true SC stabilizing role. Rcf2 is found in yeast species, and it is specifically required for CIV assembly [101,102]. Recent studies showed that Rcf2 is processed into a stable C-terminal fragment that remains associated with CIV and SCs, and a labile N-terminal fragment that displays high sequence similarity with another mitochondrial protein, Rcf3 [107]. Rcf2 and Rcf3 associate predominantly with CIV and CIV-containing SCs in the inner membrane, and in the absence of any of these proteins, CIV activity is increased. However, *Rcf2Δ*/*Rcf3Δ* double mutants displayed a decrease in CIV activity that resulted in the loss of yeast respiratory growth, indicating an overlapping function of both proteins. Whether the Rcf proteins are truly SC assembly factors is a matter of discussion, as they primarily assist CIV assembly rather than the biogenesis of SCs. However, the fact that all three Rcfs remain associated with $CIII_2$ in the absence of a functional CIV [107], open new prospects regarding their functional implications, as well as those of their human orthologues, in the assembly of SCs.

6. Conclusions and perspectives

The structural and functional organization of the respiratory chain has been long debated. Although the existence of specific associations of complexes I, III and IV into higher-order structures (i.e., respirasomes and intermediate SCs $I+III_2$ and III_2+IV_{1-2}) is generally accepted, their functional relevance remain unsolved. Recent structural advances in the composition and organization of the mammalian respirasomes represent a significant step forward to understand the functional consequences of the dynamic rearrangements between individual MRC complexes and SCs, as well as their implications in the regulation of the respiratory chain function in different physiological conditions. This is of particular importance for the understanding of the molecular mechanisms underlying respiratory chain disorders and ageing, where a general deterioration of SCs formation is commonly observed. The following research excitingly points towards the decryption of the specific interactions that govern the bindings among the individual complexes in a variety of superstructures, and to unravelling the molecular mechanisms and players that regulate SCs formation.

Acknowledgements

This work was funded by Instituto de Salud Carlos III-MINECO and European FEDER Funds (grant number PI14-00209), and by NIH-NIGMS (1R01GM105781-01).

References

[1] B. Chance, G.R. Williams, A method for the localization of sites for oxidative phosphorylation, Nature 176 (1955) 250–254.
[2] Y. Hatefi, A.G. Haavik, L.R. Fowler, D.E. Griffiths, Studies on the electron transfer system. XLII. Reconstitution of the electron transfer system, J. Biol. Chem. 237 (1962) 2661–2669.
[3] A. Kröger, M. Klingenberg, The kinetics of the redox reactions of ubiquinone related to the electron-Transport activity in the respiratory chain, Eur. J. Biochem. 34 (1973) 358–368.
[4] E. Margoliash, S. Ferguson-Miller, J. Tulloss, C.H. Kang, B. Feinberg, D.L. Brautigan, et al., Separate intramolecular pathways for reduction and oxidation of cytochrome c in electron transport chain reactions, Proc. Natl. Acad. Sci. U. S. A. 70 (1973) 3245–3249.
[5] R.A. Reid, J. Moyle, P. Mitchell, Synthesis of adenosine triphosphate by a protonmotive force in rat liver mitochondria, Nature 212 (1966) 257–258.
[6] L.R. Fowler, Y. Hatefi, Reconstitution of the electron transport system III. Reconstitution of DPNH oxidase succinic oxidase, and DPNH, succinic oxidase, Biochem. Biophys. Res. Commun. 5 (1961) 203–208.
[7] P.V. Blair, Preparation and properties of repeating units of electron transfer, Methods Enzymol. 10 (1967) 208–212.
[8] C.I. Ragan, C. Heron, The interaction between mitochondrial NADH-ubiquinone oxidoreductase and ubiquinol-cytochrome c oxidoreductase. Evidence for stoicheiometric association, Biochem. J. 174 (1978) 783–790.
[9] C. Heron, C.I. Ragan, B.L. Trumpower, The interaction between mitochondrial NADH-ubiquinone oxidoreductase and ubiquinol-cytochrome c oxidoreductase. Restoration of ubiquinone-pool behaviour, Biochem. J. 174 (1978) 791–800.
[10] H. Boumans, L.A. Grivell, J.A. Berden, The respiratory chain in yeast behaves as a single functional unit, J. Biol. Chem. 273 (1998) 4872–4877.
[11] M. Höchli, C.R. Hackenbrock, Fluidity in mitochondrial membranes: thermotropic lateral translational motion of intramembrane particles, Proc. Natl. Acad. Sci. U. S. A. 73 (1976) 1636–1640.
[12] S.S. Gupte, C.R. Hackenbrock, The role of cytochrome c diffusion in mitochondrial electron transport, J. Biol. Chem. 263 (1988) 5248–5253.
[13] M. Höchli, L. Höchli, C.R. Hackenbrock, Independent lateral diffusion of cytochrome bc1 complex and cytochrome oxidase in the mitochondrial inner membrane, Eur. J. Cell Biol. 38 (1985) 1–5.
[14] J.H. Hochman, M. Schindler, J.G. Lee, S. Ferguson-Miller, Lateral mobility of cytochrome c on intact mitochondrial membranes as determined by fluorescence redistribution after photobleaching, Proc. Natl. Acad. Sci. U. S. A. 79 (1982) 6866–6870.
[15] J. Hochman, S. Ferguson-Miller, M. Schindler, Mobility in the mitochondrial electron transport chain, Biochemistry 24 (1985) 2509–2516.
[16] S. Ferguson-Miller, J. Hochman, M. Schindler, Aggregation and diffusion in the mitochondrial electron-transfer chain: role in electron flow and energy transfer, Biochem. Soc. Trans. 14 (1986) 822–824.
[17] H. Schägger, K. Pfeiffer, Supercomplexes in the respiratory chains of yeast and mammalian mitochondria, EMBO J. 19 (2000) 1777–1783.
[18] C.M. Cruciat, S. Brunner, F. Baumann, W. Neupert, R.A. Stuart, The cytochrome bc1 and cytochrome c oxidase complexes associate to form a single supracomplex in yeast mitochondria, J. Biol. Chem. 275 (2000) 18093–18098.
[19] Y. Chaban, E.J. Boekema, N.V. Dudkina, Structures of mitochondrial oxidative phosphorylation supercomplexes and mechanisms for their stabilisation, Biochim. Biophys. Acta 1837 (2014) 418–426.
[20] A.M.P. Melo, M. Teixeira, Supramolecular organization of bacterial aerobic respiratory chains: from cells and back, Biochim. Biophys. Acta 1857 (2016) 190–197.
[21] J. Gu, M. Wu, R. Guo, K. Yan, J. Lei, N. Gao, et al., The architecture of the mammalian respirasome, Nature 537 (2016) 639–643.
[22] J.A. Letts, K. Fiedorczuk, L.A. Sazanov, The architecture of respiratory supercomplexes, Nature 537 (2016) 644–648.
[23] M. Wu, J. Gu, R. Guo, Y. Huang, M. Yang, Structure of mammalian respiratory supercomplex I1III2IV1, Cell 167 (2016) 1598–1609.
[24] R. Acín-Pérez, P. Fernández-Silva, M.L. Peleato, A. Pérez-Martos, J.A. Enriquez, Respiratory active mitochondrial supercomplexes, Mol. Cell. 32 (2008) 529–539.
[25] R. Acin-Perez, J.A. Enriquez, The function of the respiratory supercomplexes: the plasticity model, Biochim. Biophys. Acta 1837 (2014) 444–450.
[26] E. Lapuente-Brun, R. Moreno-Loshuertos, R. Acin-Perez, A. Latorre-Pellicer, C. Colas, E. Balsa, et al., Supercomplex assembly determines electron flux in the mitochondrial electron transport chain, Science 340 (2013) 1567–1570.
[27] J.N. Blaza, R. Serreli, A.J.Y. Jones, K. Mohammed, J. Hirst, Kinetic evidence against partitioning of the ubiquinone pool and the catalytic relevance of respiratory-chain supercomplexes, Proc. Natl. Acad. Sci. U. S. A. 111 (2014) 15735–15740.
[28] M. Trouillard, B. Meunier, F. Rappaport, Questioning the functional relevance of mitochondrial supercomplexes by time-resolved analysis of the respiratory chain, Proc. Natl. Acad. Sci. U. S. A. 108 (2011) E1027–E1034.
[29] A. Barrientos, C. Ugalde, I Function: therefore I am: overcoming skepticism about mitochondrial supercomplexes, Cell Metab. 18 (2013) 147–149.
[30] D. Milenkovic, J.N. Blaza, N.-G. Larrson, J. Hirst, The enigma of the respiratory chain supercomplex, Cell Metab. (2017) 765–776.
[31] N. Sone, M. Sekimachi, E. Kutoh, Identification and properties of a quinol oxidase super-complex composed of a bc1 complex and cytochrome oxidase in the thermophilic bacterium PS3, J. Biol. Chem. 262 (1987) 15386–15391.
[32] E.A. Berry, B.L. Trumpower, Isolation of ubiquinol oxidase from Paracoccus denitrificans and resolution into cytochrome bc1 and cytochrome c-aa3 complexes, J. Biol. Chem. 260 (1985) 2458–2467.
[33] H. Schägger, K. Pfeiffer, The ratio of oxidative phosphorylation complexes I-V in bovine heart mitochondria and the composition of respiratory chain supercomplexes, J. Biol. Chem. 276 (2001) 37861–37867.
[34] N.A. Dencher, M. Frenzel, N.H. Reifschneider, M. Sugawa, F. Krause, Proteome alterations in rat mitochondria caused by aging, Ann. N. Y. Acad. Sci. 1100 (2007) 291–298.
[35] A.O. Helbig, M.J.L. De Groot, R.A. van Gestel, S. Mohammed, E.A.F. de Hulster, M.A.H. Luttik, et al., A three-way proteomics strategy allows differential analysis of yeast mitochondrial membrane protein complexes under anaerobic and aerobic conditions, Proteomics 9 (2009) 4787–4798.
[36] S.J. Ramírez-Aguilar, M. Keuthe, M. Rocha, V.V. Fedyaev, K. Kramp, K.J. Gupta, et al., The composition of plant mitochondrial supercomplexes changes with oxygen availability, J. Biol. Chem. 286 (2011) 43045–43053.
[37] S. Cogliati, C. Frezza, M.E. Soriano, T. Varanita, R. Quintana-Cabrera, M. Corrado, et al., Mitochondrial cristae shape determines respiratory chain supercomplexes assembly and respiratory efficiency, Cell 155 (2013) 160–171.
[38] C. Greggio, P. Jha, S.S. Kulkarni, S. Lagarrigue, N.T. Broskey, M. Boutant, et al., Enhanced respiratory chain supercomplex formation in response to exercise in human skeletal muscle, Cell Metab. 25 (2017) 1–11.

Please cite this article in press as: T. Lobo-Jarne, C. Ugalde, Respiratory chain supercomplexes: Structures, function and biogenesis, Semin Cell Dev Biol (2017), http://dx.doi.org/10.1016/j.semcdb.2017.07.021

[39] S. Jang, T.S. Lewis, C. Powers, Z. Khuchua, C.P. Baines, P. Wipf, et al., Elucidating mitochondrial ETC supercomplexes in the heart during ischemia-reperfusion, Antioxid. Redox Signal. 27 (2017) 57–69.
[40] M.G. Rosca, E.J. Vazquez, J. Kerner, W. Parland, M.P. Chandler, W. Stanley, et al., Cardiac mitochondria in heart failure: decrease in respirasomes and oxidative phosphorylation, Cardiovasc. Res. 80 (2008) 30–39.
[41] M. Zhang, E. Mileykovskaya, W. Dowhan, Gluing the respiratory chain together: cardiolipin is required for supercomplex formation in the inner mitochondrial membrane, J. Biol. Chem. 277 (2002) 43553–43556.
[42] K. Pfeiffer, V. Gohil, R.A. Stuart, C. Hunte, U. Brandt, M.L. Greenberg, et al., Cardiolipin stabilizes respiratory chain supercomplexes, J. Biol. Chem. 278 (2003) 52873–52880.
[43] L. Böttinger, S.E. Horvath, T. Kleinschroth, C. Hunte, G. Daum, N. Pfanner, et al., Phosphatidylethanolamine and cardiolipin differentially affect the stability of mitochondrial respiratory chain supercomplexes, J. Mol. Biol. 423 (2012) 677–686.
[44] G. Tasseva, H.D. Bai, M. Davidescu, A. Haromy, E. Michelakis, J.E. Vance, Phosphatidylethanolamine deficiency in mammalian mitochondria impairs oxidative phosphorylation and alters mitochondrial morphology, J. Biol. Chem. 288 (2013) 4158–4173.
[45] D. Moreno-Lastres, F. Fontanesi, I. García-Consuegra, M.A. Martín, J. Arenas, A. Barrientos, et al., Mitochondrial complex I plays an essential role in human respirasome assembly, Cell Metab. 15 (2012) 324–335.
[46] N.V. Dudkina, H. Eubel, W. Keegstra, E.J. Boekema, H.-P. Braun, Structure of a mitochondrial supercomplex formed by respiratory-chain complexes I and III, Proc. Natl. Acad. Sci. U. S. A. 102 (2005) 3225–3229.
[47] N.V. Dudkina, M. Kudryashev, H. Stahlberg, E.J. Boekema, Interaction of complexes I III, and IV within the bovine respirasome by single particle cryoelectron tomography, Proc. Natl. Acad. Sci. U. S. A. 108 (2011) 15196–15200.
[48] B. Muster, W. Kohl, I. Wittig, V. Strecker, F. Joos, W. Haase, et al., Respiratory chain complexes in dynamic mitochondria display a patchy distribution in life cells, PLoS One 5 (2010).
[49] G. Quarato, C. Piccoli, R. Scrima, N. Capitanio, Variation of flux control coefficient of cytochrome c oxidase and of the other respiratory chain complexes at different values of protonmotive force occurs by a threshold mechanism, Biochim. Biophys. Acta 1807 (2011) 1114–1124.
[50] E. Schäfer, H. Seelert, N.H. Reifschneider, F. Krause, N.A. Dencher, J. Vonck, Architecture of active mammalian respiratory chain supercomplexes, J. Biol. Chem. 281 (2006) 15370–15375.
[51] I. Wittig, R. Carrozzo, F.M. Santorelli, H. Schägger, Supercomplexes and subcomplexes of mitochondrial oxidative phosphorylation, Biochim. Biophys. Acta 1757 (2006) 1066–1072.
[52] E. Nubel, I. Wittig, S. Kerscher, U. Brandt, H. Schägger, Two-dimensional native electrophoretic analysis of respiratory supercomplexes from Yarrowia lipolytica, Proteomics 9 (2009) 2408–2418.
[53] J.B. Bultema, H.P. Braun, E.J. Boekema, R. Kouřil, Megacomplex organization of the oxidative phosphorylation system by structural analysis of respiratory supercomplexes from potato, Biochim. Biophys. Acta 1787 (2009) 60–67.
[54] B. Rieger, D.N. Shalaeva, A.C. Söhnel, W. Kohl, P. Duwe, A.Y. Mulkidjanian, K.B. Busch, Lifetime imaging of GFP at CoxVIIIa reports respiratory supercomplex assembly in live cells, Sci. Rep. 7 (2017) 46055.
[55] J.S. Sousa, D.J. Mills, J. Vonck, W. Kühlbrandt, Functional asymmetry and electron flow in the bovine respirasome, Elife 5 (2016) 1–17.
[56] J. Heinemeyer, H.P. Braun, E.J. Boekema, R. Kouril, R. Kouřil, A structural model of the cytochrome C reductase/oxidase supercomplex from yeast mitochondria, J. Biol. Chem. 282 (2007) 12240–12248.
[57] E. Mileykovskaya, P.A. Penczek, J. Fang, V.K.P.S. Mallampalli, G.C. Sparagna, W. Dowhan, Arrangement of the respiratory chain complexes in Saccharomyces cerevisiae supercomplex III2IV2 revealed by single particle cryo-electron microscopy, J. Biol. Chem. 287 (2012) 23095–23103.
[58] E. Schäfer, N. a Dencher, J. Vonck, D.N. Parcej, Three-dimensional structure of the respiratory chain supercomplex I1III2IV1 from bovine heart mitochondria, Biochemistry 46 (2007) 12579–12585.
[59] T. Althoff, D.J. Mills, J.-L. Popot, W. Kühlbrandt, Arrangement of electron transport chain components in bovine mitochondrial supercomplex I1III2IV1, EMBO J. 30 (2011) 4652–4664.
[60] J. Zhu, K.R. Vinothkumar, J. Hirst, Structure of mammalian respiratory complex I, Nature 536 (2016) 354–358.
[61] K. Fiedorczuk, J.A. Letts, G. Degliesposti, K. Kaszuba, M. Skehel, L.A. Sazanov, Atomic structure of the entire mammalian mitochondrial complex I, Nature (2016) 1–21.
[62] M. McKenzie, M. Lazarou, D.R. Thorburn, M.T. Ryan, Mitochondrial respiratory chain supercomplexes are destabilized in barth syndrome patients, J. Mol. Biol. 361 (2006) 462–469.
[63] J. Dudek, I.F. Cheng, M. Balleininger, F.M. Vaz, K. Streckfuss-Bömeke, D. Hübscher, et al., Cardiolipin deficiency affects respiratory chain function and organization in an induced pluripotent stem cell model of Barth syndrome, Stem Cell Res. 11 (2013) 806–819.
[64] C. Blanchi, M.L. Genova, G.P. Castelli, G. Lenaz, The mitochondrial respiratory chain is partially organized in a supercomplex assembly: kinetic evidence using flux control analysis, J. Biol. Chem. 279 (2004) 36562–36569.
[65] G. Benard, B. Faustin, A. Galinier, C. Rocher, N. Bellance, K. Smolkova, et al., Functional dynamic compartmentalization of respiratory chain intermediate substrates: implications for the control of energy production and mitochondrial diseases, Int. J. Biochem. Cell Biol. 40 (2008) 1543–1554.
[66] E. Lamantea, F. Carrara, C. Mariotti, L. Morandi, V. Tiranti, M. Zeviani, A novel nonsense mutation (Q352X) in the mitochondrial cytochrome b gene associated with a combined deficiency of complexes I and III, Neuromuscul. Disord. 12 (2002) 49–52.
[67] H. Schägger, R. de Coo, M.F. Bauer, S. Hofmann, C. Godinot, U. Brandt, Significance of respirasomes for the assembly/stability of human respiratory chain complex I, J. Biol. Chem. 279 (2004) 36349–36353.
[68] R. Acín-Pérez, M.P. Bayona-Bafaluy, P. Fernández-Silva, R. Moreno-Loshuertos, A. Pérez-Martos, C. Bruno, et al., Respiratory complex III is required to maintain complex I in mammalian mitochondria, Mol. Cell. 13 (2004) 805–815.
[69] Y. Li, M. D'Aurelio, J.H. Deng, J.S. Park, G. Manfredi, P. Hu, J. Lu, Y. Bai, An assembled complex IV maintains the stability and activity of complex I in mammalian mitochondria, J. Biol. Chem. 282 (2007) 17557–17562.
[70] H.-T. Hornig-Do, T. Tatsuta, A. Buckermann, M. Bust, G. Kollberg, A. Rötig, et al., Nonsense mutations in the COX1 subunit impair the stability of respiratory chain complexes rather than their assembly, EMBO J. 31 (2012) 1293–1307.
[71] F. Diaz, H. Fukui, S. Garcia, C.T. Moraes, Cytochrome c oxidase is required for the assembly/stability of respiratory complex I in mouse fibroblasts, Mol. Cell. Biol. 26 (2006) 4872–4881.
[72] E. Fernández-Vizarra, M. Zeviani, Nuclear gene mutations as the cause of mitochondrial complex III deficiency, Front. Genet. 6 (2015) 134.
[73] M. Rak, P. Benit, D. Chretien, J. Bouchereau, M. Schiff, R. El-Khoury, et al., Mitochondrial cytochrome c oxidase deficiency, Clin. Sci. 130 (2016) 393–407.
[74] D.A. Stroud, E.E. Surgenor, L.E. Formosa, B. Reljic, A.E. Frazier, M.G. Dibley, et al., Accessory subunits are integral for assembly and function of human mitochondrial complex I, Nature (2016) 1–17.
[75] U.D. Vempati, X. Han, C.T. Moraes, Lack of cytochrome c in mouse fibroblasts disrupts assembly/stability of respiratory complexes I and IV, J. Biol. Chem. 284 (2009) 4383–4391.
[76] A. Guarás, E. Perales-Clemente, E. Calvo, R. Acín-Pérez, M. Loureiro-Lopez, C. Pujol, et al., The CoQH2/CoQ ratio serves as a sensor of respiratory chain efficiency, Cell Rep. 15 (2016) 197–209.
[77] M.L. Genova, B. Ventura, G. Giuliano, C. Bovina, G. Formiggini, G. Parenti Castelli, et al., The site of production of superoxide radical in mitochondrial Complex I is not a bound ubisemiquinone but presumably iron-sulfur cluster N2, FEBS Lett. 505 (2001) 364–368.
[78] J. Sun, B.L. Trumpower, Superoxide anion generation by the cytochrome bc1 complex, Arch. Biochem. Biophys. 419 (2003) 198–206.
[79] E. Maranzana, G. Barbero, A.I. Falasca, G. Lenaz, M.L. Genova, Mitochondrial respiratory supercomplex association limits production of reactive oxygen species from complex I, Antioxid. Redox Signal. 19 (2013) 1469–1480.
[80] I. Lopez-Fabuel, J. Le Douce, A. Logan, A.M. James, G. Bonvento, M.P. Murphy, et al., Complex I assembly into supercomplexes determines differential mitochondrial ROS production in neurons and astrocytes, Proc. Natl. Acad. Sci. U. S. A. 113 (2016) 13063–13068.
[81] F. Diaz, J.A. Enríquez, C.T. Moraes, Cells lacking Rieske iron-sulfur protein have a reactive oxygen species-associated decrease in respiratory complexes I and IV, Mol. Cell. Biol. 32 (2012) 415–429.
[82] S. Cogliati, E. Calvo, M. Loureiro, A.M. Guaras, R. Nieto-Arellano, C. Garcia-Poyatos, et al., Mechanism of super-assembly of respiratory complexes III and IV, Nature 539 (2016) 579–582.
[83] S. Aras, O. Pak, N. Sommer, R. Finley, M. Hüttemann, N. Weissmann, et al., Oxygen-dependent expression of cytochrome c oxidase subunit 4-2 gene expression is mediated by transcription factors RBPJ, CXXC5 and CHCHD2, Nucleic Acids Res. 41 (2013) 2255–2266.
[84] J. Liu, A. Barrientos, Transcriptional regulation of yeast oxidative phosphorylation hypoxic genes by oxidative stress, Antioxid. Redox Signal. 19 (2012) 1916–1927.
[85] M. Frenzel, H. Rommelspacher, M.D. Sugawa, N.A. Dencher, Ageing alters the supramolecular architecture of OxPhos complexes in rat brain cortex, Exp. Gerontol. 45 (2010) 563–572.
[86] S. Guerrero-Castillo, F. Baertling, D. Kownatzki, H.J. Wessels, S. Arnold, U. Brandt, et al., The assembly pathway of mitochondrial respiratory chain complex I, Cell Metab. (2016) 1–12.
[87] M.A. Calvaruso, P. Willems, M. den brand, F. Valsecchi, S. Kruse, R. Palmiter, et al., Mitochondrial complex III stabilizes complex I in the absence of NDUFS4 to provide partial activity, Hum. Mol. Genet. 21 (2012) 115–120.
[88] I. Marques, N.A. Dencher, A. Videira, F. Krause, Supramolecular organization of the respiratory chain in Neurospora crassa mitochondria, Eukaryot. Cell. 6 (2007) 2391–2405.
[89] N. Kovářová, A. Čížková Vrbacká, P. Pecina, V. Stránecký, E. Pronicka, S. Kmoch, et al., Adaptation of respiratory chain biogenesis to cytochrome c oxidase deficiency caused by SURF1 gene mutations, Biochim. Biophys. Acta 1822 (2012) 1114–1124.
[90] M. Lazarou, S.M. Smith, D.R. Thorburn, M.T. Ryan, M. McKenzie, Assembly of nuclear DNA-encoded subunits into mitochondrial complex IV, and their preferential integration into supercomplex forms in patient mitochondria, FEBS J. 276 (2009) 6701–6713.
[91] M. Lazarou, M. McKenzie, A. Ohtake, D.R. Thorburn, M.T. Ryan, Analysis of the assembly profiles for mitochondrial- and nuclear-DNA-encoded subunits into complex I, Mol. Cell. Biol. 27 (2007) 4228–4237.

Please cite this article in press as: T. Lobo-Jarne, C. Ugalde, Respiratory chain supercomplexes: Structures, function and biogenesis, Semin Cell Dev Biol (2017), http://dx.doi.org/10.1016/j.semcdb.2017.07.021

[92] A. Mourier, S. Matic, B. Ruzzenente, N.G. Larsson, D. Milenkovic, The respiratory Chain supercomplex organization is independent of COX7A2L isoforms, Cell Metab. 20 (2014) 1069–1075.
[93] K. Ikeda, S. Shiba, K. Horie-Inoue, K. Shimokata, S. Inoue, A stabilizing factor for mitochondrial respiratory supercomplex assembly regulates energy metabolism in muscle, Nat. Commun. 4 (2013) 2147.
[94] M. Davoudi, H. Kotarsky, E. Hansson, J. Kallijärvi, V. Fellman, COX7A2L/SCAFI and pre-complex III modify respiratory chain supercomplex formation in different mouse strains with a bcs1 l mutation, PLoS One 11 (2016) e0168774.
[95] X. P. Jha, J. Auwerx Wang, Analysis of mitochondrial respiratory chain supercomplexes using blue native polyacrylamide gel electrophoresis (BN-PAGE), in: Curr. Protoc. Mouse Biol, John Wiley & Sons Inc., Hoboken, NJ, USA, 2016, pp. 1–14.
[96] E.G. Williams, Y. Wu, P. Jha, S. Dubuis, P. Blattmann, C.A. Argmann, et al., Systems proteomics of liver mitochondria function, Science 352 (2016) aad0189–aad018914.
[97] D. Sun, B. Li, R. Qiu, H. Fang, J. Lyu, Cell type-specific modulation of respiratory chain supercomplex organization, Int. J. Mol. Sci. 17 (2016) 6–11.
[98] R. Perez-Perez, T. Lobo-Jarne, D. Milenkovic, A. Mourier, A. Bratic, A. Garcia-Bartolome, et al., COX7A2L is a mitochondrial complex III binding protein that stabilizes the III2 + IV supercomplex without affecting respirasome formation, Cell Rep. 16 (2016) 2387–2398.
[99] K. Zhang, G. Wang, X. Zhang, P.P. Hüttemann, Y. Qiu, J. Liu, et al., COX7AR is a stress-inducible mitochondrial COX subunit that promotes Breast cancer malignancy, Sci. Rep. 6 (2016) 31742.
[100] Y.C. Chen, E.B. Taylor, N. Dephoure, J.M. Heo, A. Tonhato, I. Papandreou, et al., Identification of a protein mediating respiratory supercomplex stability, Cell Metab. 15 (2012) 348–360.
[101] V. Strogolova, A. Furness, M. Robb-McGrath, J. Garlich, R.A. Stuart Rcf1, Rcf2 members of the hypoxia-induced gene 1 protein family, are critical components of the mitochondrial cytochrome bc1-cytochrome c oxidase supercomplex, Mol. Cell. Biol. 32 (2012) 1363–1373.
[102] M. Vukotic, S. Oeljeklaus, S. Wiese, F.N. Vögtle, C. Meisinger, H.E. Meyer, et al., Rcf1 mediates cytochrome oxidase assembly and respirasome formation, revealing heterogeneity of the enzyme complex, Cell Metab. 15 (2012) 336–347.
[103] C. Rydström Lundin, C. von Ballmoos, M. Ott, P. Ädelroth, Brzezinski Regulatory role of the respiratory supercomplex factors in Saccharomyces cerevisiae, Proc. Natl. Acad. Sci. U. S. A. (2016) E4475–E4485.
[104] M. Klingenberg, Molecular aspects of the adenine nucleotide carrier from mitochondria, Arch. Biochem. Biophys. 270 (1989) 1–14.
[105] J. Garlich, V. Strecker, I. Wittig, R.A. Stuart, Mutational analysis of the QRRQ motif in the yeast hig1-type 2 protein, rcf1: reveals a regulatory role for the cytochrome c oxidase complex, J. Biol. Chem. 292 (2017) 5216–5226.
[106] T. Hayashi, Y. Asano, Y. Shintani, H. Aoyama, H. Kioka, O. Tsukamoto, et al., Higd1a is a positive regulator of cytochrome c oxidase, Proc. Natl. Acad. Sci. U. S. A. 112 (2015) 1553–1558.
[107] K. Römpler, T. Müller, L. Juris, M. Wissel, M. Vukotic, K. Hofmann, et al., Overlapping role of respiratory supercomplex factor rcf2 and its N-terminal homolog rcf3 in saccharomyces cerevisiae, J. Biol. Chem. 291 (2016) 23769–23778.
[108] S. Vidoni, M.E. Harbour, S. Guerrero-Castillo, A. Signes, S. Ding, I.M. Fearnley, et al., MR-1S interacts with PET100 and PET117 in module-based assembly of human cytochrome c oxidase, Cell Rep. 18 (2017) 1727–1738.

Please cite this article in press as: T. Lobo-Jarne, C. Ugalde, Respiratory chain supercomplexes: Structures, function and biogenesis, Semin Cell Dev Biol (2017), http://dx.doi.org/10.1016/j.semcdb.2017.07.021

Article

Cell Reports

COX7A2L Is a Mitochondrial Complex III Binding Protein that Stabilizes the III_2+IV Supercomplex without Affecting Respirasome Formation

Graphical Abstract

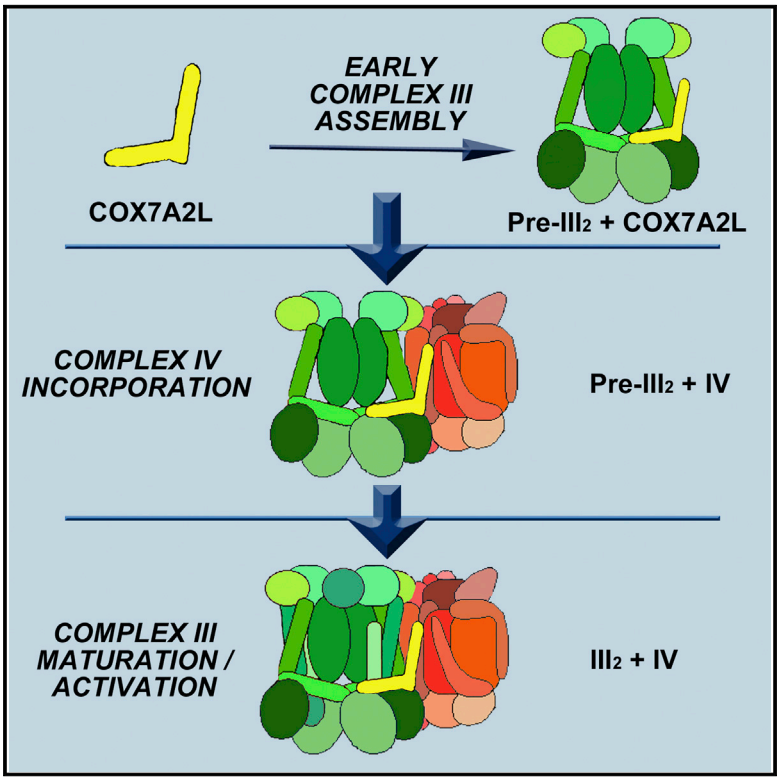

Highlights

- COX7A2L preferentially interacts with respiratory chain complex III
- COX7A2L is essential to stabilize the III_2+IV supercomplex
- COX7A2L is not necessary for biogenesis or maintenance of the respirasome
- Biogenesis of the III_2+IV supercomplex is not necessary for respirasome formation

Authors

Rafael Pérez-Pérez, Teresa Lobo-Jarne, Dusanka Milenkovic, ..., Miguel A. Martín, Nils-Göran Larsson, Cristina Ugalde

Correspondence

cugalde@h12o.es

In Brief

Previous studies highlight different roles for COX7A2L in the structural organization of the mitochondrial respiratory chain. Pérez-Pérez et al. find that mammalian COX7A2L preferentially associates with complex III to stabilize supercomplex III_2+IV in a respirasome-independent manner, indicating coexistence of independent regulatory mechanisms for the biogenesis and turnover of these structures.

Pérez-Pérez et al., 2016, Cell Reports *16*, 1–12
August 30, 2016
http://dx.doi.org/10.1016/j.celrep.2016.07.081

CellPress

Please cite this article in press as: Pérez-Pérez et al., COX7A2L Is a Mitochondrial Complex III Binding Protein that Stabilizes the III_2+IV Supercomplex without Affecting Respirasome Formation, Cell Reports (2016), http://dx.doi.org/10.1016/j.celrep.2016.07.081

Cell Reports
Article

COX7A2L Is a Mitochondrial Complex III Binding Protein that Stabilizes the III_2+IV Supercomplex without Affecting Respirasome Formation

Rafael Pérez-Pérez,[1,2,8] Teresa Lobo-Jarne,[1,2,8] Dusanka Milenkovic,[3] Arnaud Mourier,[3] Ana Bratic,[3] Alberto García-Bartolomé,[1,2] Erika Fernández-Vizarra,[4] Susana Cadenas,[5,6] Aitor Delmiro,[1,2] Inés García-Consuegra,[1,2] Joaquín Arenas,[1,2] Miguel A. Martín,[1,2] Nils-Göran Larsson,[3,7] and Cristina Ugalde[1,2,9,*]

[1]Instituto de Investigación, Hospital Universitario 12 de Octubre (i+12), Madrid 28041, Spain
[2]Centro de Investigación Biomédica en Red de Enfermedades Raras (CIBERER), U723, Madrid 28029, Spain
[3]Department of Mitochondrial Biology, Max Planck Institute for Biology of Ageing, 50931 Cologne, Germany
[4]Medical Research Council Mitochondrial Biology Unit, CB2 0XY Cambridge, UK
[5]Centro de Biología Molecular "Severo Ochoa" (CSIC-UAM) and Departamento de Biología Molecular, Universidad Autónoma de Madrid, 28049 Madrid, Spain
[6]Instituto de Investigación Sanitaria Princesa (IIS-IP), 28006 Madrid, Spain
[7]Department of Medical Biochemistry and Biophysics, Karolinska Institutet, 17177 Stockholm, Sweden
[8]Co-first author
[9]Lead Contact
*Correspondence: cugalde@h12o.es
http://dx.doi.org/10.1016/j.celrep.2016.07.081

SUMMARY

Mitochondrial respiratory chain (MRC) complexes I, III, and IV associate into a variety of supramolecular structures known as supercomplexes and respirasomes. While COX7A2L was originally described as a supercomplex-specific factor responsible for the dynamic association of complex IV into these structures to adapt MRC function to metabolic variations, this role has been disputed. Here, we further examine the functional significance of COX7A2L in the structural organization of the mammalian respiratory chain. As in the mouse, human COX7A2L binds primarily to free mitochondrial complex III and, to a minor extent, to complex IV to specifically promote the stabilization of the III_2+IV supercomplex without affecting respirasome formation. Furthermore, COX7A2L does not affect the biogenesis, stabilization, and function of the individual oxidative phosphorylation complexes. These data show that independent regulatory mechanisms for the biogenesis and turnover of different MRC supercomplex structures co-exist.

INTRODUCTION

The oxidative phosphorylation (OXPHOS) system is embedded in the lipid bilayer of the inner mitochondrial membrane and is composed of five multiprotein enzyme complexes as well as the two mobile electron carriers coenzyme Q (or Q) and cytochrome *c* (cyt *c*). The first four enzyme complexes (CI–CIV) make up the mitochondrial respiratory chain (MRC), which facilitates electron transfer from reducing equivalents to molecular oxygen. The electron translocation through the MRC is coupled to the creation of a proton gradient across the inner mitochondrial membrane that will be used by the ATP synthase (complex V) to drive ATP synthesis. In recent years, it has been widely demonstrated that MRC complexes I, III, and IV (CI, CIII, and CIV, respectively) may associate to form a diversity of supramolecular assemblies known as supercomplexes (SCs) or respirasomes (Cruciat et al., 2000; Schägger and Pfeiffer, 2000). However, the functional relevance of mitochondrial SCs is a matter of intense debate, even though they are conserved across species. In mammals, the respirasome is often referred to as SC I+III_2+IV_{1-4}. Biochemical analyses support the idea that the respirasome contains the MRC and the electron carriers and, thus, is a structural entity that can carry out respiration on its own (Acín-Pérez et al., 2008). Some authors have proposed that SCs function to confer stability to CI (Moreno-Lastres et al., 2012; Schägger et al., 2004), to reduce reactive oxygen species (ROS) production (Maranzana et al., 2013), to facilitate electron channeling (Bianchi et al., 2004), and to mediate metabolic adaptation through the partition of Q into two different pools (Lapuente-Brun et al., 2013). However, the view that SC assemblies provide distinct electron translocation pathways is currently disputed. Kinetic and spectroscopic studies have challenged the substrate channeling model by concluding that (1) cyt *c* is not trapped within the SCs, and, therefore, it does not encounter any restriction of its diffusion (Trouillard et al., 2011); and (2) the metabolic pathways for NADH and succinate oxidation impose different coenzyme Q redox steady state but communicate and converge on a single non-partitioned coenzyme Q pool (Blaza et al., 2014; Rigoulet et al., 2010). Moreover, cryo-electron microscopy analyses of the mammalian SC I+III_2+IV_1 does not support the substrate channeling model, because the distance between the binding sites for coenzyme Q on CI and CIII, as well as the distance between the binding sites for cyt *c* on CIII and CIV, is sufficiently far enough to allow free exchange (Althoff et al., 2011; Dudkina et al., 2011). Instead, it has been suggested that the relatively weak interactions between

Please cite this article in press as: Pérez-Pérez et al., COX7A2L Is a Mitochondrial Complex III Binding Protein that Stabilizes the III_2+IV Supercomplex without Affecting Respirasome Formation, Cell Reports (2016), http://dx.doi.org/10.1016/j.celrep.2016.07.081

the MRC complexes that lead to SCs formation could prevent deleterious protein aggregation in the densely packed inner mitochondrial membrane (Blaza et al., 2014). According to this latter idea, SC formation would have no direct bioenergetic role but rather be a protective mechanism that prevents tight interactions between the individual OXPHOS complexes.

In budding yeast lacking CI, the formation and stabilization of the mitochondrial SC III_2+IV_{1-2} is controlled by specific regulatory proteins called the respiratory SC factors 1 and 2 (Rcf1 and Rcf2) (Chen et al., 2012; Strogolova et al., 2012; Vukotic et al., 2012). While both proteins are preferentially associated with CIV, only Rcf1 seems to play a crucial role in SC stability, as its human ortholog HIG2A does (Chen et al., 2012). A highly controversial issue involves the potential regulatory role of the protein COX7A2L/COX7RP in the formation and stabilization of mitochondrial SCs. Mouse COX7A2L was reported to be present in SC III_2+IV and the respirasomes but not in free CIII or CIV (Lapuente-Brun et al., 2013; Müller et al., 2016), and was, therefore, renamed the SC-specific assembly factor I (SCAFI). Certain wild-type mouse strains, e.g., C57BL/6J and BALB/c, are homozygous for a 6-bp deletion in the *Cox7a2l* gene and, therefore, express a short, unstable COX7A2L variant that was reported to lead to a failure to form SC III_2+IV and respirasomes (Lapuente-Brun et al., 2013). Remarkably, the respiration rates and ATP production from CI- and CII-linked substrates were reported to be higher in tissues from mice bearing the short COX7A2L isoform. The authors suggested that COX7A2L could mediate the binding of CIV to SCs to physiologically regulate energy metabolism by providing alternate paths for electrons from different metabolic sources (NADH, FAD, or both), thus allowing optimization of respiration to substrate availability (for discussion, see Barrientos and Ugalde, 2013). Another study used *Cox7a2l* knockout (KO) mice (Ikeda et al., 2013) and reported that COX7A2L is a SC-specific factor that, in contrast to the previous model (Lapuente-Brun et al., 2013), would promote respirasome stability to gain full activity of the MRC. The KO study showed that respirasomes were present in mitochondria from skeletal muscle of C57BL/6J mice (Ikeda et al., 2013), despite previous claims that this mouse strain lacks respirasomes (Lapuente-Brun et al., 2013). In agreement, an in-depth characterization of isolated heart and liver mitochondria from control mouse strains that contained either the full-length *Cox7a2l* gene (i.e., CD1 mice) or the variant with the 6-bp deletion (i.e., C57BL/6J, C57BL/6N, and BALB/c mice) demonstrated that all mice had normal formation of respirasomes and normal respiratory chain function, thus showing that the truncated version of the *Cox7a2l* gene does not impact the bioenergetic capacity in vivo (Mourier et al., 2014a). A recent report conclusively supports the presence of respirasomes in different tissues of C57BL/6 mice (Williams et al., 2016).

The aim of the present work was to elucidate the functional importance of COX7A2L in the structural organization of the mammalian OXPHOS system. Our study demonstrates that COX7A2L preferentially interacts with mitochondrial CIII and, to a minor extent, with CIV to promote the stabilization of SC III_2+IV in both mice and humans. However, COX7A2L has no role in the biogenesis, stabilization, or function of the free OXPHOS complexes, and it has no role in the formation of the respirasomes. These data show the co-existence of alternative regulatory mechanisms for the biogenesis and turnover of different respiratory chain SC structures.

RESULTS

Mouse COX7A2L Is Essential for SC III_2+IV Formation in a Respirasome-Independent Manner

In order to shed light on these contradictory conclusions regarding COX7A2L function in murine models (Ikeda et al., 2013; Lapuente-Brun et al., 2013; Mourier et al., 2014a; Williams et al., 2016), we first analyzed the COX7A2L levels relative to OXPHOS subunits by western blots in isolated heart mitochondria from CD1 versus C57BL/6 mice (Figure S1A). The allelic variation of the *Cox7a2l* gene in nuclear DNA was previously described (Mourier et al., 2014a). The CD1 mice express high levels of a 113-amino-acid COX7A2L protein isoform, whereas C57BL/6 mice express low levels of a slightly shorter and unstable COX7A2L protein isoform of 111 amino acids. CI and CIV subunits were present at similar levels in the wild-type CD1, C57BL/6J, and C57BL/6N mouse strains. However, the levels of COX7A2L and CIII subunits were slightly increased in the CIV-deficient conditional *Lrpprc* KO mice compared with their wild-type littermates that all were maintained on the C57BL/6N background (Mourier et al., 2014b). These data suggest that COX7A2L, as well as CIII, is stabilized in the *Lrpprc* KO mice as a response to the severe CIV deficiency.

In agreement with a previous report (Mourier et al., 2014a), BN-PAGE analysis of digitonin-solubilized heart mitochondria from CD1 and C57BL/6 mice confirmed similar levels and activities of the respirasomes in all wild-type strains (Figures 1A and 1B). Analysis of COX7A2L distribution in CD1 mice (Figure 1C) showed its preferential co-segregation with free CIV, with SC III_2+IV and respirasomes, and, to a minor extent, with the CIII dimer. In the C57BL/6 mice, however, COX7A2L was mostly found in CIII-containing structures (Figure 1C). These data suggest that the two-amino-acid deletion and consequent reduction in COX7A2L levels mostly hampers the binding of COX7A2L to CIV, which, nevertheless, only provoked the disappearance of SC III_2+IV (Figures 1B and 1C) without affecting free CIV or respirasome levels and activities (Figures 1A–1C). Thus, the severely reduced COX7A2L levels in C57BL/6 mice do not hamper the association of CIV with the respirasomes, as previously proposed (Lapuente-Brun et al., 2013). To test whether the respirasome stability depends on COX7A2L levels, we exposed heart mitochondria from CD1 and C57BL/6J mice to increasing amounts of the detergent digitonin, followed by BN-PAGE analysis (Figure S1B). Respirasome levels and organization were comparable between both mouse strains at the low digitonin-to-protein ratios. Also, under the most stringent detergent conditions, respirasomes were still clearly detectable in the C57BL/6J mice, albeit at slightly lower levels than those in the CD1 mice. Noteworthy, SCs from both mouse strains reorganized in different ways upon increasing digitonin treatment, and some respirasome bands appeared to be more stable in C57BL/6J than in CD1 mice and vice versa. Next, we analyzed DDM-solubilized mouse heart mitochondria, a condition in which respirasomes are disrupted (Figure S1C), and found that

Please cite this article in press as: Pérez-Pérez et al., COX7A2L Is a Mitochondrial Complex III Binding Protein that Stabilizes the III_2+IV Supercomplex without Affecting Respirasome Formation, Cell Reports (2016), http://dx.doi.org/10.1016/j.celrep.2016.07.081

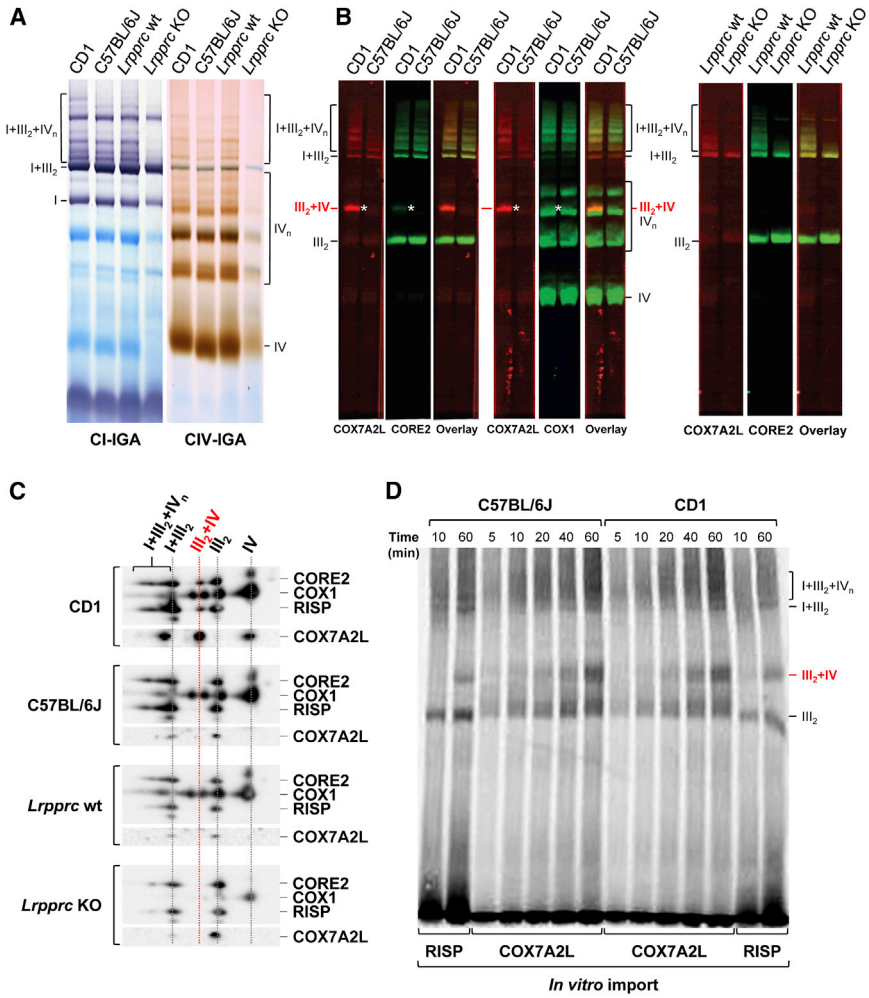

Figure 1. Mouse COX7A2L Behaves as a CIII-Binding Protein Specifically Required for SC III_2+IV Assembly

(A) Supramolecular organization of the respiratory chain in heart mitochondria from wild-type (wt) CD1, C57BL/6J, and C57BL/6N (*Lrpprc* wt) mouse strains, as well as from *Lrpprc*-deficient (KO) mice with a C57BL/6N genetic background. Mitochondria were extracted with a digitonin:protein ratio of 4 g:1 g and analyzed by BN-PAGE, followed by CI and CIV-IGA assays.

(B) Heart mitochondria were extracted with a digitonin:protein ratio of 6 g:1 g and analyzed by BN-PAGE, followed by western blot with double-fluorescent detection of CIII and CIV (anti-CORE2 or anti-COX1, green) and COX7A2L-containing complexes (anti-COX7A2L, red). White asterisks show the localization of SC III_2+IV.

(C) Heart mitochondria were extracted with a digitonin:protein ratio of 4 g:1 g and analyzed by 2D BN/SDS-PAGE, followed by western blot and immunodetection with antibodies against COX7A2L and the indicated OXPHOS subunits.

(D) Import of radiolabeled RISP and COX7A2L precursors and subsequent incorporation into CIII and SCs in intact heart mitochondria from C57BL/6J and CD1 mouse strains. After the indicated incubation times (in minutes), mitochondria were solubilized in 6 g:1 g digitonin per protein and analyzed by BN-PAGE.

$I+III_2+IV_n$, SC containing CI, CIII, and CIV; $I+III_2$, SC containing CI and CIII; III_2+IV, SC containing CIII and CIV; III_2, CIII dimer; IV, free CIV; IV_n, CIV oligomers.

See also Figure S1.

the co-segregation between COX7A2L and free CIV was totally lost, suggesting that their interaction is, indeed, labile. In CD1 mice, both COX7A2L and the CIII subunit CORE2 co-localized with the CIII dimer and SC III_2+IV, whereas in C57BL/6 mice, both proteins only were present in the CIII dimer. Altogether, these data show that COX7A2L is essential for SC III_2+IV stability, whereas it is dispensable for the respirasome formation.

Next, we assessed import and assembly of the radiolabeled 113-amino-acid COX7A2L isoform into isolated heart mitochondria from CD1, C57BL/6J, and C57BL/6N mice by BN-PAGE analyses (Figures 1D, S1D, and S1E). We used mitochondria with dissipated membrane potential as controls to ensure that the protein import and assembly depend on the membrane potential across the inner mitochondrial membrane (Figure S1D). The comparison of migration patterns and the kinetics of formed assembly intermediates after import of COX7A2L or the CIII subunit RISP showed that the long COX7A2L isoform was incorporated into CIII-containing structures in all mice strains. We observed a preferential co-segregation of the newly imported COX7A2L with the CIII dimer at early time points after import (Figure 1D), whereas COX7A2L was present in higher molecular-weight structures, such as SC III_2+V and respirasomes, at later time points. These data demonstrate that COX7A2L preferentially interacts with CIII prior to SC formation. Additional analyses of the import of COX7A2L into isolated mitochondria from *Lrpprc* wild-type and KO hearts (Figure S1E) revealed that COX7A2L associates with CIII independently of the presence of CIV.

Human COX7A2L Co-localizes with Respiratory Chain CIII and CIV and CIII-Containing SCs

In humans, only one COX7A2L protein of 114 amino acids has been reported in the NCBI Gene database ([Gene ID: 9167] http://www.ncbi.nlm.nih.gov/gene/9167) To clarify the functional role of the human COX7A2L protein, we first analyzed its distribution pattern in relation to free MRC complexes and SCs by performing BN-PAGE, followed by western blot analyses. We analyzed digitonin-solubilized mitochondria from control 143B cells and cybrids with a severe CI assembly defect (CI-KD [knockdown]), total lack of CIII (CIII-KO) or total lack of CIV (CIV-KO) (Figure 2A; Figure S2A). In controls, COX7A2L co-localized not only with SC III_2+IV and the respirasomes (SC $I+III_2+IV_n$), as previously described in murine models (Lapuente-Brun et al.,

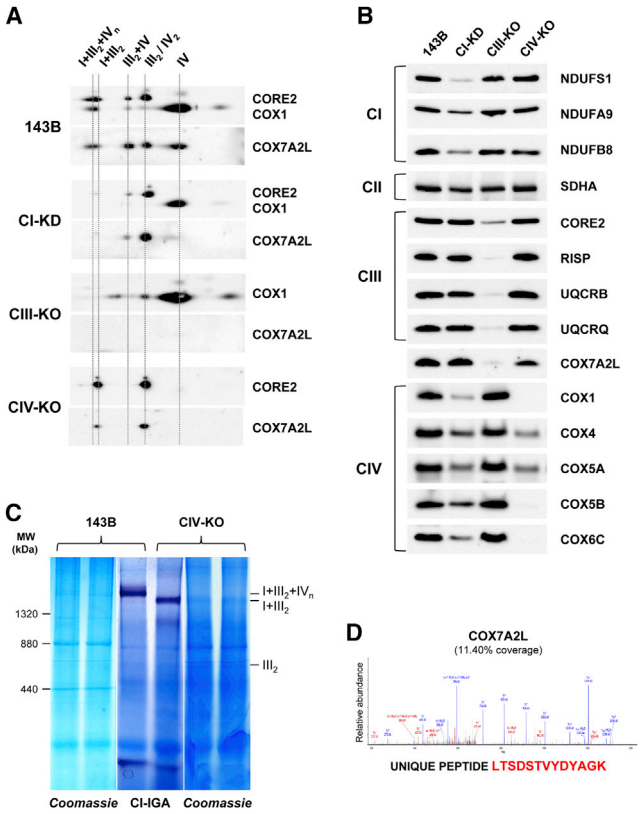

Figure 2. Human COX7A2L Co-migrates with Respiratory Chain SCs and Free CIII and CIV

(A) Mitochondria from control 143B cells and mutant cybrids defective in CI (CI-KD), CIII (CIII-KO), and CIV (CIV-KO) were extracted with a digitonin:protein ratio of 4 g:1 g and analyzed by 2D BN/SDS-PAGE and western blot with antibodies raised against COX7A2L, CORE2, and COX1.

(B) Mitochondrial lysates from control and mutant cybrids were analyzed by SDS-PAGE and western blot with the indicated antibodies.

(C) BN-PAGE and CI-IGA analysis of control 143B cells and CIV-KO mutant cybrids. After Coomassie staining, the SC $I+III_2+IV_1$ band was excised from the control lane, and the bands corresponding to SC $I+III_2$ and CIII were excised from the CIV-KO lane. Bands were subsequently analyzed by LC coupled to tandem MS (MS/MS). MW, molecular weight.

(D) MS/MS spectra from the doubly charged COX7A2L tryptic peptide unambiguously detected by LC-ESI/MS in two independent experiments per sample. The amino acid sequence of the identified COX7A2L unique peptide is highlighted in red. The most intense signals on the MS/MS spectra correspond to the main fragmentation series (b-amino and y-carboxy). Doubly charged fragments are marked with superscript 2+.

$I+III_2+IV_n$, SC containing CI, CIII, and CIV; $I+III_2$, SC containing CI and CIII; III_2+IV, SC containing CIII and CIV; III_2, CIII dimer; IV, CIV; IV_2, CIV dimer.

See also Figure S2 and Table S1.

2013; Williams et al., 2016), but also with SC $I+III_2$, the CIII dimer ($CIII_2$), and free CIV. The CI-KD cybrids, which harbored a >90% heteroplasmic mutation in the *MT-ND2* subunit gene of mtDNA (Ugalde et al., 2007), showed a strong reduction in the levels of SC $I+III_2+IV_n$, SC III_2+IV, and free CIV. Consistently, the amounts of COX7A2L within those structures were also reduced in the CI-defective cells compared with the controls. The CIII-KO cybrids lacked CIII due to a homoplasmic 4-bp deletion in the *MT-CYB* gene that encodes cytochrome *b* (Rana et al., 2000). Lack of CIII caused the complete disruption of SC $I+III_2+IV_n$ and SC III_2+-IV, accompanied by increased levels of free CIV and CIV oligomers. In addition, a dramatic reduction in COX7A2L levels, comparable to that of the CIII structural subunits, was observed (Figure 2B). Only a minor residual COX7A2L signal co-migrating with free CIV was seen at the longest exposures (Figure S2B), indicating that the lack of CIII profoundly affects the stability of COX7A2L and its binding to CIV. The CIV-KO cybrids harbor a homoplasmic nonsense mutation in *MT-CO1* (Bruno et al., 1999), leading to the disappearance of free CIV, SC III_2+IV, and SC $I+III_2+IV_n$, accompanied by an accumulation of SC $I+III_2$ and $CIII_2$. Interestingly, COX7A2L could bind SC $I+III_2$ and $CIII_2$ in the absence of CIV, whereas very small amounts were bound to CIV in the absence of CIII. Thus, in human cells, COX7A2L preferentially associates with $CIII_2$ and CIII-containing structures, and only to a minor extent with free CIV, showing that COX7A2L principally behaves as a CIII interactor rather than an assembly factor exclusive to CIV-containing SCs (Lapuente-Brun et al., 2013). The presence of COX7A2L in $CIII_2$, SC $I+III_2$, and $I+III_2+IV_n$ was further confirmed by high-resolution nano-LC/ESI-MS (nano-liquid chromatography/electrospray ionization-mass spectrometry) proteomic analysis of the blue native (BN) gel bands corresponding to SC $I+III_2+IV_n$ in 143B cells and to SCs $I+III_2$ and $CIII_2$ in the CIV-KO mutant cybrids (Figures 2C and 2D; Table S1).

Overexpressed COX7A2L Is Imported into Mitochondria and Binds CIII and CIV without Significantly Enhancing SC Formation

Next, we investigated the cellular localization of human COX7A2L by transfecting control 143B cells with a construct expressing COX7A2L with a C-terminal GFP-tag, yielding a product of ~39.3 kDa (Figure S3A). Confocal microscopy showed co-localization of COX7A2L-GFP with the ATP synthase (complex V), thus confirming mitochondrial localization of the fusion protein (Figure 3A). Next, we analyzed by BN-PAGE the mitochondrial distribution of exogenous COX7A2L and the effect of *COX7A2L* overexpression on the assembly of the OXPHOS system. To this end, we initially used 143B cells transfected either with the GFP-tagged COX7A2L construct or with a vector that expressed COX7A2L with a C-terminal MYC-DDK tag, yielding a product of ~16.2 kDa (Figures 3B and S3B). In 143B cells, COX7A2L-GFP was effectively overexpressed by ~15-fold relative to the endogenous COX7A2L (Figure S3A), while COX7A2L-MYC-DDK was overexpressed by ~2-fold (Figure S3B). BN-PAGE analyses confirmed the co-migration of exogenous COX7A2L with the CIII dimer, free CIV, SC III_2+IV, and the respirasomes in digitonin-solubilized mitochondria (Figures 3B and S3C), thus showing that COX7A2L, with both tags, is efficiently incorporated into MRC complexes and SCs. Densitometric analyses of OXPHOS subunit distribution showed that the overexpression of tagged COX7A2L induced no significant increase in the amounts of CIII- and CIV-containing structures (Figure 3C). We extended this analysis to HEK293 cells transfected with either the MYC-DDK-tagged COX7A2L construct or the MYC-DDK tag alone. In HEK293 cells, COX7A2L-MYC-DDK was effectively overexpressed by ~10-fold, relative to endogenous COX7A2L (Figure S3B), and co-migrated with the CIII dimer, free CIV, SC III_2+IV, and the respirasomes

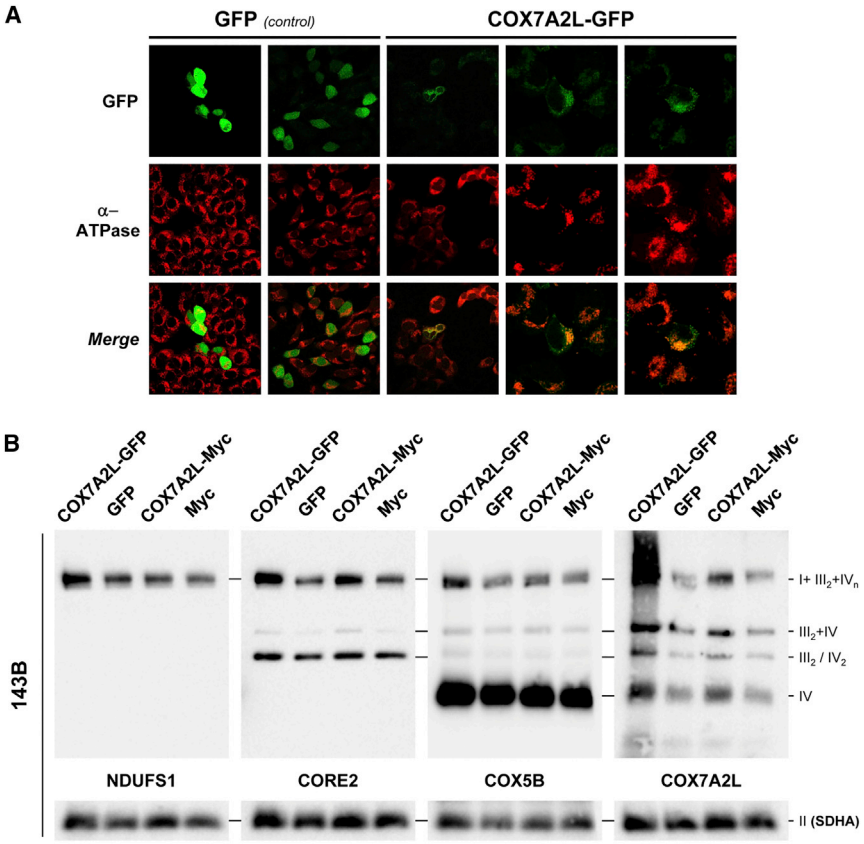

Figure 3. Overexpressed COX7A2L Localizes to Mitochondria with Minor Effects on the Respiratory Chain Complexes and SCs

(A) Confocal microscopy of 143B cells transiently transfected with the COX7A2L-GFP construct and with the empty-GFP vector as a control. Upper images show the GFP signal. Middle images show the mitochondrial network using an antibody against the ATPase α subunit. Lower images show the overlay between the two signals.

(B) BN-PAGE and western blot analyses of control 143B cells transiently transfected both with the COX7A2L-GFP or COX7A2L-MYC-DDK constructs and with their corresponding empty vectors. Membranes were incubated with antibodies raised against COX7A2L and the indicated OXPHOS subunits.

(C) Densitometric analysis of the MRC complexes and SCs in 143B cells transfected with both COX7A2L-tagged constructs. The optical densities of immunoreactive bands that had not reached saturation levels were measured with the ChemiDoc MP Image Analyzer software package (Biorad). The antibody signals within the same structures were quantified; the mean values were normalized by CII and expressed as percentages of the cells transfected with the empty vectors (horizontal bar). Values represent the means ± SD from four independent experiments.

$I+III_2+IV_n$, SC containing CI, CIII, and CIV; III_2+IV, SC containing CIII and CIV; III_2, CIII dimer; IV, CIV; IV_2, CIV dimer; II, CII.

See also Figure S3.

(Figure S3D). Tagged COX7A2L overexpression in HEK293 cells altered the levels of neither MRC complexes nor SCs.

Next, we tested whether the COX7A2L co-localization with MRC CIII and CIV was due to a direct physical interaction. We performed co-immunoprecipitation assays of digitonin-solubilized mitochondrial lysates from HEK293 cells transfected with either the COX7A2L-MYC-DDK construct or the empty vector (Figure 4A). Immunoprecipitation with an anti-DDK antibody specifically pulled down the tagged-COX7A2L protein in cells overexpressing COX7A2L-MYC-DDK. In addition, the CIII subunits CORE1, CORE2, CYC1, RISP, and UQCRQ and the CIV subunits COX1, COX4, COX5B, and COX6C were detected in the co-immunoprecipitate (coIP). The CI subunits NDUFA9 and NDUFS1 were barely detectable, and CII was not detected in the coIP samples. When reverse immunoprecipitation assays were performed using antibodies against CORE2 or COX1 proteins, both the tagged and the endogenous COX7A2L proteins were successfully pulled down (Figures 4B and 4C). Importantly, immunoprecipitation with CORE2 (but not with COX1) pulled down the endogenous COX7A2L protein in cells transfected with the empty vector. These data show that COX7A2L physically interacts with CIII and CIV but presents a higher affinity for CIII. According to the TOPCONS prediction software (http://topcons.cbr.su.se/), human COX7A2L contains one transmembrane domain that spans amino acids 86 to 107, leaving most of the N-terminal part of the protein exposed to the mitochondrial matrix, and a short C-terminal stretch of seven amino acids facing the inter membrane space. The direct association of COX7A2L with mitochondrial CIII and CIV is, therefore, compatible with its predicted topology.

Endogenous COX7A2L Associates with Respiratory Chain CIII and CIV and with SCs during Their Assembly Process

Next, we analyzed the assembly kinetics of COX7A2L into MRC complexes and SCs by doxycycline-induced reversible inhibition of mitochondrial translation in control 143B cells (Moreno-Lastres et al., 2012). Doxycycline was removed from cell-culture media after 6 days of treatment, and samples were collected at different time points (0, 6, 15, 24, 48, 72, and 96 hr). To follow the

Please cite this article in press as: Pérez-Pérez et al., COX7A2L Is a Mitochondrial Complex III Binding Protein that Stabilizes the III_2+IV Supercomplex without Affecting Respirasome Formation, Cell Reports (2016), http://dx.doi.org/10.1016/j.celrep.2016.07.081

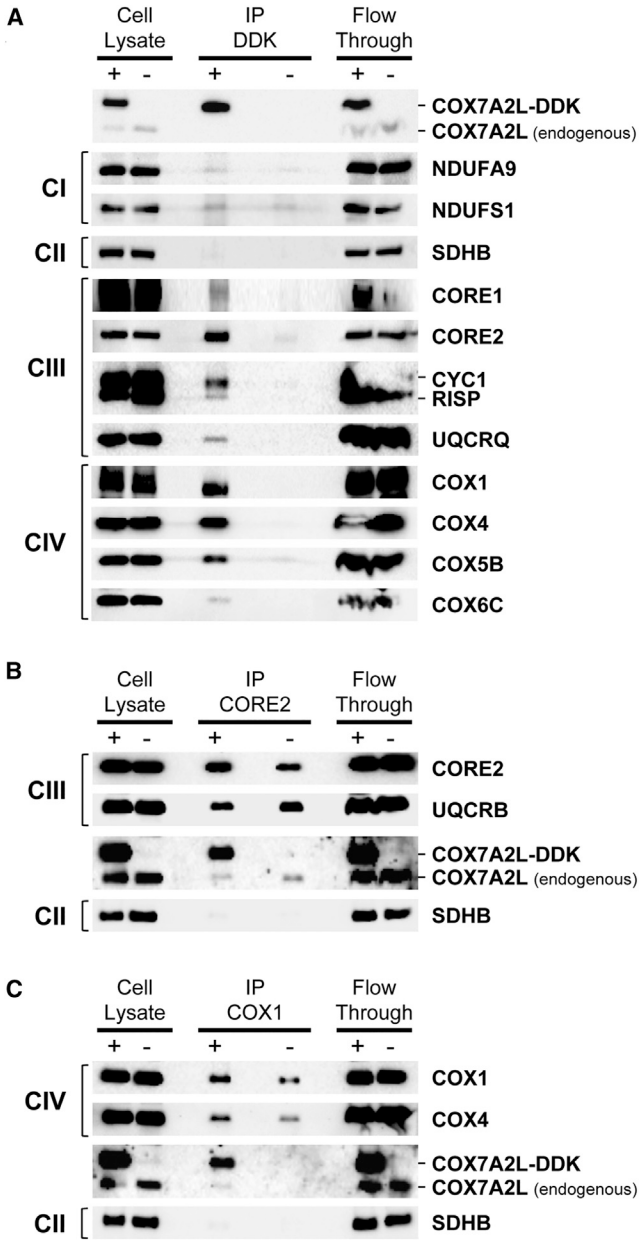

Figure 4. COX7A2L Physically Binds CIII and CIV

(A) COX7A2L co-immunoprecipitation assay. Digitonin-solubilized mitochondrial extracts (4 g digitonin/1 g protein) from HEK293 cells transiently transfected with COX7A2L-MYC-DDK (+) or the empty MYC-DDK construct (–) were immunoprecipitated using an anti-DDK antibody. IP, immunoprecipitate. (B and C) The same digitonin-solubilized mitochondrial extracts were immunoprecipitated using antibodies against (B) CORE2 or (C) COX1. Samples were subsequently analyzed by SDS-PAGE and western blot with the indicated antibodies.

integration of endogenous COX7A2L into newly assembled CIII, CIV, and SCs, digitonin-solubilized mitochondria were separated by 2D BN/SDS-PAGE and subsequently analyzed by western blot using antibodies that recognize COX7A2L, CORE2 (CIII), RISP (CIII), and COX5A (CIV) (Figure 5A). Signals from at least three independent experiments were quantified by densitometry and normalized to CII levels, and values were expressed relative to levels in untreated cells (SS in Figures 5B and 5C; Figures S4A–S4D). After 6 days of doxycycline treatment (time, 0 hr), there was a drastic decrease (80%–95%) in the levels of the CIII dimer ($CIII_2$), CIV, SC III_2+IV, and SC I+III_2+IV_n, as well as in the levels of COX7A2L that co-localizes with these structures. The CII levels remained normal after doxycycline treatment (data not shown) as expected, because this complex lacks mtDNA-encoded subunits. Once mitochondrial translation resumed (times, 6–96 hr; Figures 5B and 5C), we observed a gradual increase of the levels of COX7A2L protein that co-localized with $CIII_2$, in agreement with our previous results showing the co-localization of newly imported COX7A2L and the CIII dimer in mouse heart mitochondria (Figure 1D). The incorporation of COX7A2L into CIII occurred in parallel to the insertion of the CORE2 subunit, which gets assembled into CIII prior to the incorporation of RISP (Figure S4A). In contrast, the CIV levels increased prior to the binding of COX7A2L (Figure S4B), suggesting that COX7A2L only binds fully assembled CIV. Once COX7A2L had bound to CIV, there was a simultaneous increase of the levels of COX7A2L in CIV and SC III_2+IV (Figures 5B and 5C). Moreover, COX7A2L was incorporated into SC III_2+IV in parallel with the CORE2 and COX5A subunits but prior to the integration of RISP in this structure (Figure S4C). The incorporation of COX7A2L into respirasomes occurred concomitantly with the integration of CORE2 and COX5A, and earlier than the integration of RISP (Figure S4D), which indicates that COX7A2L is incorporated before the respirasome formation is completed.

COX7A2L Associates with CIII and SC III_2+IV prior to the Insertion of the RISP Catalytic Subunit

In the reported CIII assembly models, incorporation of CORE2 allows the formation of a non-functional intermediate called pre-CIII, which contains CORE2 and the rest of the CIII subunits except RISP and the smallest subunit (Qcr10 in yeast, UQCR11 in mammals), which are incorporated at a later assembly stage (Fernández-Vizarra and Zeviani, 2015; Smith et al., 2012). This late assembly step is promoted by LYRM7/MZM1L, an assembly factor that binds RISP to stabilize it prior to its incorporation into CIII. HeLa cells that stably overexpress hemagglutinin (HA)-tagged MZM1L showed sequestering of RISP in a small subcomplex, thereby preventing CIII maturation (Sánchez et al., 2013). Doxycycline experiments suggested that human COX7A2L could be a component of pre-CIII, as this protein gets incorporated into CIII in parallel with the CORE2 subunit but before the incorporation of RISP (Figure S4A). To confirm this hypothesis, we analyzed COX7A2L distribution by BN-PAGE of digitonin-solubilized mitochondria isolated from HeLa cells overexpressing MZM1L-HA (Figure 6). As observed by CI in-gel activity (IGA), MZM1L overexpression induced a decrease in the levels and activity of the respirasomes (SC I+III_2+IV), as well as an accumulation of CI-containing structures (Figure 6A). As expected, the levels of the RISP subunit were strongly decreased in the respirasomes, in SC III_2+IV, and in the CIII dimer, and there was a parallel accumulation of RISP in a small subcomplex that also contains MZM1L-HA (Sánchez et al., 2013) (Figure 6B). The amount of RISP remained relatively high in SC I+III_2+IV, compared with

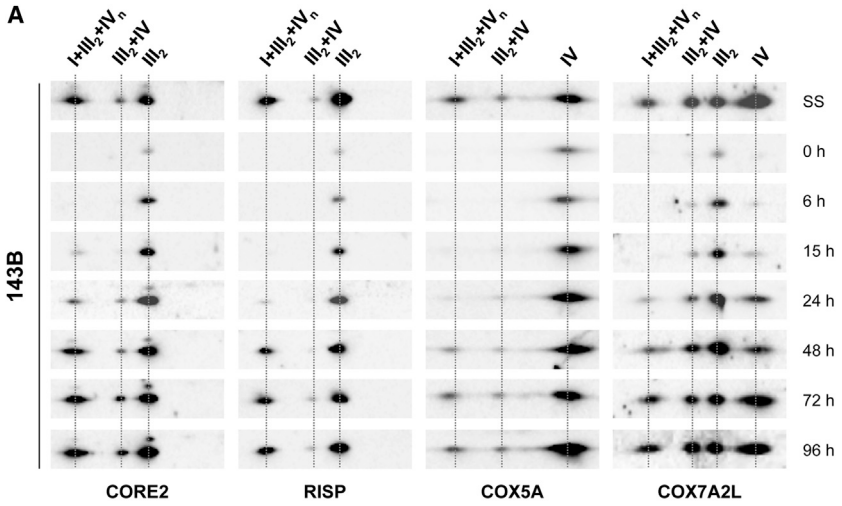

Figure 5. Assembly Kinetics of COX7A2L in Free Complexes and SCs

(A) Mitochondria from doxycycline-treated 143B cells were extracted with a digitonin:protein ratio of 4 g:1 g and analyzed by 2D BN/SDS-PAGE and western blot with the indicated antibodies.

(B) Densitometric profiles representing the assembly progress of COX7A2L in CIII- and CIV-containing structures.

(C) Mean incorporation rates of COX7A2L into CIII- and CIV-containing structures. The signals from three independent experiments were quantified and normalized by CII. Time point values are expressed as percentages of the untreated cells (SS) and indicated as means ± SD.

$I+III_2+IV_n$, SC containing CI, CIII, and CIV; III_2+IV, SC containing CIII and CIV; III_2, CIII dimer; IV, CIV; a.d.u., arbitrary densitometric units.

See also Figure S4.

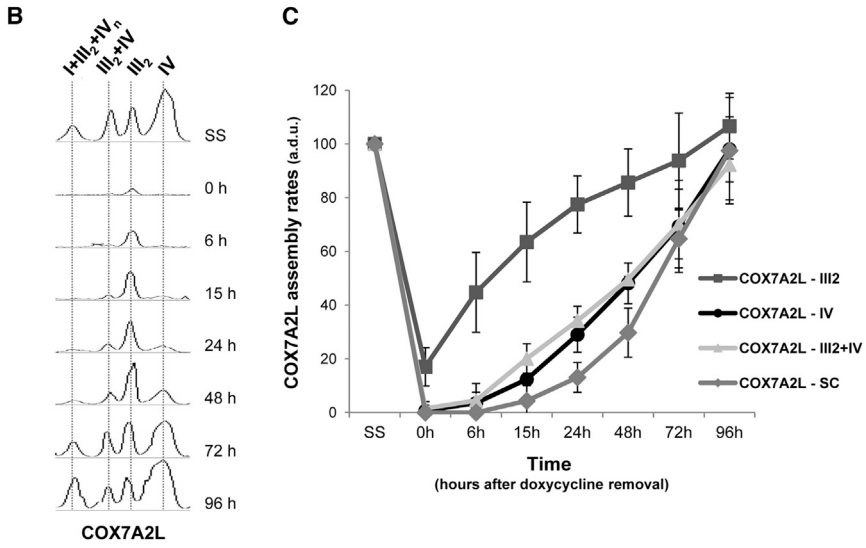

other structures, suggesting that this subunit is stably bound to the respirasomes. Upon MZM1L/LYRM7 overexpression, CORE2 and COX7A2L co-segregated with pre-SC III_2+IV and pre-CIII (Figure 6B), further supporting that COX7A2L associates with pre-CIII before the incorporation of RISP takes place (Figure S4E). All in all, our data demonstrate that, in human cells, the interaction of COX7A2L with CIV depends on the presence of pre-CIII, the formation of which is not affected by the lack of RISP (Figure 6) but is dependent on cytochrome *b* (Figure 2B).

COX7A2L Downregulation Causes SC III_2+IV Disassembly without Altering Respirasome Stability or Respiratory Chain Function

We further investigated the effect of *COX7A2L* KD on mitochondrial function by using a mix of two small interfering RNAs (siRNAs) targeting exons 2 and 3 of *COX7A2L* mRNA. The *COX7A2L* KD efficiency was analyzed by SDS-PAGE of whole-cell protein extracts from control 143B cells and CIV-KO mutant cybrids (Figures S5A and S5B). *COX7A2L* RNAi effectively knocked down the COX7A2L protein by 80% in the 143B cells and by 74% in the CIV-KO mutants, compared with cells transfected with unspecific scrambled siRNAs (C- in Figures S5A and S5B). Next, we analyzed the effects of *COX7A2L* silencing on OXPHOS system assembly by BN-PAGE in combination with CI-IGA and western blot analyses of mitochondrial-enriched fractions from 143B and CIV-KO cells (Figure 7A). Upon *COX7A2L* KD, there was a significant decrease in the signals of COX7A2L that co-localized with the CIII dimer, free CIV, and SCs III_2+IV, $I+III_2$, and $I+III_2+IV_n$. Despite the severe drop in COX7A2L levels, we only observed a specific reduction in the levels of SC III_2+IV in the 143B cells, whereas the CI activity and the levels of free OXPHOS complexes, other SCs, and respirasomes were normal.

To gain deeper insight into the nature of SC III_2+IV disruption in 143B cells, we performed 2D BN/SDS-PAGE and western blot analyses with antibodies against CORE2 (CIII), RISP (CIII), COX1 (CIV), and COX5B (CIV) (Figure 7B). Quantification of results from five independent experiments (Figure 7C; Figures S5C and S5D) showed that *COX7A2L* KD specifically led to a significant decrease in the levels of the four analyzed subunits within SC III_2+IV but not in the other CIII- and CIV-containing structures. These data indicate that COX7A2L has a specific role in the stabilization of SC III_2+IV but not in the respirasome maintenance. Moreover, *COX7A2L* silencing did not result in a clear accumulation of intermediates smaller than CIII and CIV, indicating that their assembly and/or stability are not disturbed. In agreement with these results, *COX7A2L* KD in the CIV-KO mutant cybrids produced no significant alterations in the levels of the CIII dimer or SC $I+III_2$ (Figures S6A and S6B). Altogether, our results show that the stabilization of SC III_2+IV relies on the association of COX7A2L with MRC CIII and CIV.

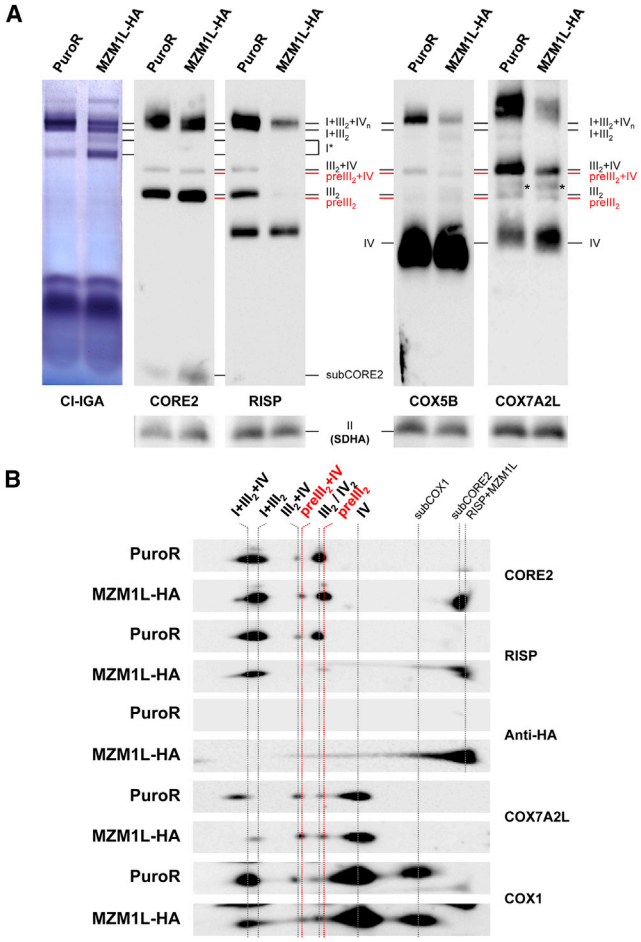

Figure 6. COX7A2L Binds to CIII Assembly Intermediates

(A) Digitonin-solubilized mitochondrial extracts (4 g digitonin/1 g protein) from HeLa cells transduced with the MZM1L-HA construct or with the empty vector (PuroR) were analyzed by BN-PAGE and CI-IGA assays or, alternatively, by western blot and immunodetection. Asterisks indicate unspecific signals that do not appear on 2D BN/SDS-PAGE gels.

(B) Subsequent 2D BN/SDS-PAGE and western blot analyses were performed with antibodies against COX7A2L, the indicated OXPHOS subunits, and the HA epitope.

$I+III_2+IV_n$, SC containing CI, CIII, and CIV; $I+III_2$, SC containing CI and CIII; I*, CI-containing structure; III_2+IV, SC containing CIII and CIV; Pre-III_2+IV, SC containing pre-CIII and CIV; III_2, CIII dimer; Pre-III_2, pre-CIII lacking the RISP subunit; IV, CIV; IV_2, CIV dimer; II, CII. SCs that contain CORE2 and COX1 are indicated as subCORE2 and subCOX1, respectively. The association of RISP and MZM1L is indicated as RISP+MZM1L.

Finally, we measured oxygen consumption rates (OCRs) in 143B cells and found no significant differences between *COX7A2L*-silenced cells and cells transfected with scrambled siRNA (Figure S6C). In contrast, mitochondrial respiration was drastically reduced in the CI-KD cybrids that retained SC III_2+IV but showed minimal levels of CI and respirasomes (Figure S6D). Respiratory chain activities measured in *COX7A2L*-silenced 143B cells were also comparable to the activities in control cells (Figure S6E). These results show that a substantial loss of COX7A2L and SC III_2+IV has no significant impact on MRC function in human cell lines.

DISCUSSION

We have investigated the role of COX7A2L/COX7RP in the structural organization of the mammalian OXPHOS system and clarified the apparent contradictions about the role of this protein in the literature (Ikeda et al., 2013; Lapuente-Brun et al., 2013; Mourier et al., 2014a; Williams et al., 2016). Our data demonstrate that COX7A2L acts as a CIII-binding protein in mitochondria from mouse heart and human cell lines. Furthermore, COX7A2L is specifically required for SC III_2+IV maintenance, and this finding strongly argues against its previously proposed function as a SC-specific assembly factor that mediates respirasome formation.

We used a combination of COX7A2L immunodetection, high-throughput proteomics, and mitochondrial in vitro import assays to demonstrate that COX7A2L co-migrates with the CIII dimer, free CIV, SC $I+III_2+IV_n$, SC $I+III_2$, and SC III_2+IV in both mice and humans. Thus, the COX7A2L protein is not exclusively present in SCs, as previously reported (Lapuente-Brun et al., 2013; Müller et al., 2016); instead, it predominantly associates with different CIII-containing structures. In mice, the long COX7A2L isoform preferentially interacts with CIII prior to SC formation. The small amount of COX7A2L that co-segregates with free CIV in the CD1 strain could reflect continuous turnover and exchange cycles between the SC-bound and free CIV states, or, alternatively, a fraction of the COX7A2L-bound CIV could be dissociated from SCs upon detergent extraction. Such dissociation cannot be observed in the C57BL/6 mice, because they have already lost the association between COX7A2L and CIV. Our data in human control and mutant cybrids lacking one MRC complex suggest that COX7A2L behaves as a structural component of CIII, because COX7A2L preferentially binds this complex, and the stability of COX7A2L depends on the presence of CIII. Accordingly, COX7A2L remains associated with the CIII dimer and CIII-containing SCs in the absence of CI and CIV. Furthermore, COX7A2L binds to a reported CIII assembly intermediate that lacks the RISP subunit (pre-CIII) before it interacts with free CIV, SC III_2+IV, or the respirasomes. In agreement with this observation, COX7A2L remained associated with pre-CIII in HeLa cells with an impaired incorporation of RISP. In contrast, lack of cytochrome *b* precludes the formation of pre-CIII and led to the disappearance of CIV-associated COX7A2L.

At variance with previous studies in fibroblasts from COX7A2L-deprived mice (Lapuente-Brun et al., 2013), COX7A2L overexpression in human cell lines did not cause a significant increase in the levels of MRC CIII, CIV, or SCs. However, reduced COX7A2L levels led to a specific loss of SC III_2+IV but did not affect the amounts of free CIII and CIV, respirasomes, or mitochondrial function. Similar to the situation in cultured human cells, the mouse COX7A2L variant of 113 amino acids is imported into mitochondria, where it preferentially associates with CIII-containing structures and plays an essential role in SC III_2+IV stabilization. These results show that mammalian COX7A2L is essential to maintain SC III_2+IV stability, but it plays no critical role in the assembly or stabilization of SC $I+III_2+IV_n$. These findings strongly suggest that there are independent regulatory mechanisms for the biogenesis and turnover of SC III_2+IV and the respirasomes. This is in accordance with previous observations suggesting that SC III_2+IV gets fully assembled after the completion of

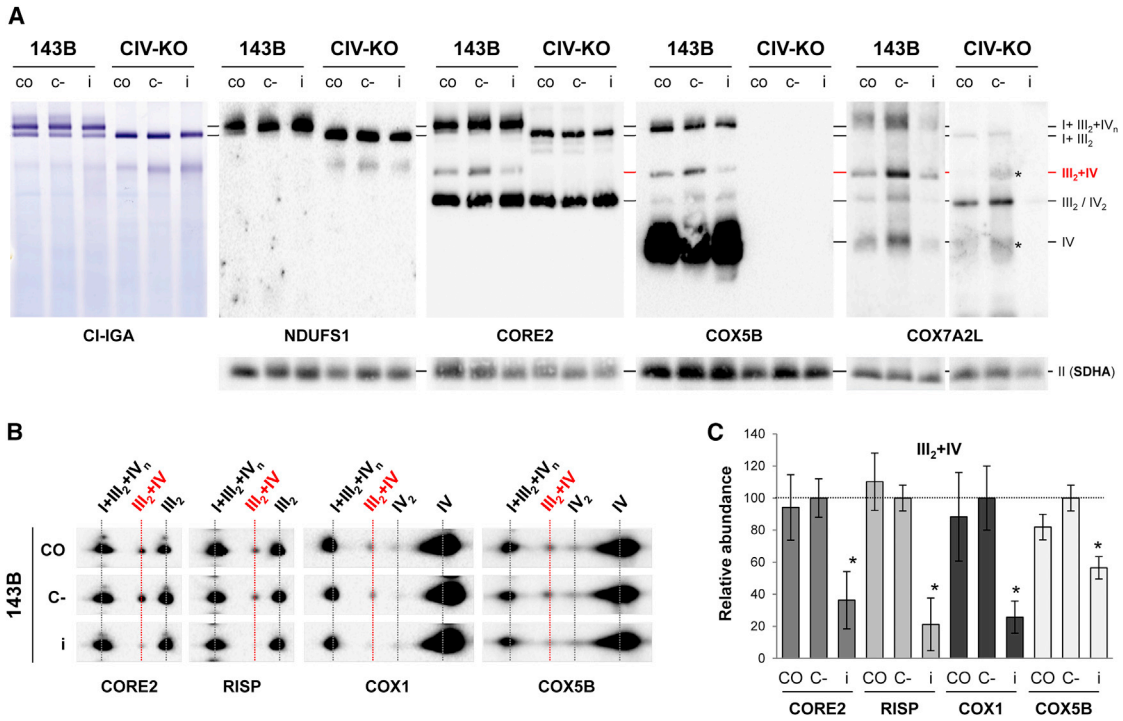

Figure 7. COX7A2L Downregulation Specifically Decreases the Levels of SC III_2+IV without Affecting Respirasome Biogenesis

The effect of COX7A2L KD on MRC complex assembly was investigated in untreated (CO), mock-transfected (C−), and *COX7A2L* siRNA-transfected (i) 143B cells and in the CIV-KO mutants.

(A) Mitochondria were extracted with a digitonin:protein ratio of 4 g:1 g and analyzed by BN-PAGE, followed by CI-IGA assays, or alternatively, by western blot and immunodetection with the indicated antibodies. Asterisks indicate unspecific signals that do not appear on 2D BN/SDS-PAGE gels.

(B) 2D BN/SDS-PAGE and western blot analyses of 143B cells upon *COX7A2L* silencing.

(C) The optical densities of immunoreactive bands that had not reached saturation levels were measured. The signals within SC III_2+IV were quantified, normalized by CII, and shown as means ± SD from five independent siRNA experiments. Values are expressed as percentages of the cells transfected with scramble RNA (C−, horizontal bar).

$I+III_2+IV_n$, SC containing CI, CIII, and CIV; $I+III_2$, SC containing CI and CIII; III_2+IV, SC containing CIII and CIV; III_2, CIII dimer; IV, CIV; IV_2, CIV dimer; II, CII. *$p < 0.05$, Mann-Whitney U test.

See also Figures S5 and S6.

respirasome formation (Moreno-Lastres et al., 2012). Our present results also confirm that the levels of respirasomes and MRC activities in mitochondria from mouse hearts are not dependent on the allelic variations of *Cox7a2l* (Mourier et al., 2014a), and they contradict the hypothesis that COX7A2L is an assembly factor that regulates respirasome formation to modulate respiration. The fact that respirasomes (but not SC III_2+IV) are present in C57BL/6J mitochondria solubilized with a variety of detergent concentrations provides additional support for a role for COX7A2L to stabilize SC III_2+IV. These data are in agreement with other reports that show the presence of respirasomes in different tissues, including the heart, liver, and skeletal muscle, of C57BL/6 mice (Hatle et al., 2013; Ikeda et al., 2013; Jha et al., 2016; Milenkovic et al., 2013; Williams et al., 2016). In this regard, the previously reported absence of respirasomes in mouse strains with the truncated *Cox7a2l* allele (Lapuente-Brun et al., 2013) could have resulted from differences in the methodologies or reagents used for membrane solubilization. Indeed, we observed some variations in the intensity of SC isoforms between C57BL/6J and CD1 mice at high detergent concentrations; however, the pattern was not constant, as specific SCs were stabilized in C57BL/6J mice but not in CD1 mice, and vice versa. Based on our data, we cannot exclude the possibility that the mechanisms of SC assembly are regulated in a tissue-dependent manner, as recently proposed (Jha et al., 2016; Williams et al., 2016). However, it is important to acknowledge that the observed changes may not necessarily be a consequence of genetic COX7A2L variation but could well be explained by other types of genetic differences among mouse strains.

Our results argue that COX7A2L is permanently associated with CIII and that it exists in an association/dissociation equilibrium with CIV, which can define the fate of CIV depending on whether COX7A2L is bound or not. This could provide a mechanism whereby COX7A2L-bound CIV is guided to the proximity of CIII to form and stabilize SC III_2+IV_n. The functional role of COX7A2L may resemble that described of HIG2A, the human ortholog of the yeast Rcf1 SC factor. In yeast, Rcf1 and Rcf2 preferentially associate with CIV to mediate SC III_2+IV_{1-2} stability (Chen et al., 2012; Strogolova et al., 2012; Vukotic et al., 2012). Whereas Rcf2 is yeast specific, several human homologs of Rcf1 have been reported, whereof HIG2A is involved in the stabilization of a proportion of CIV-containing SCs (Chen et al.,

Please cite this article in press as: Pérez-Pérez et al., COX7A2L Is a Mitochondrial Complex III Binding Protein that Stabilizes the III_2+IV Supercomplex without Affecting Respirasome Formation, Cell Reports (2016), http://dx.doi.org/10.1016/j.celrep.2016.07.081

2012). C11ORF83 or UQCC3A, a cardiolipin-binding protein involved in the early stages of human CIII assembly, has also been reported to act as a SC III_2+IV-stabilizing factor (Desmurs et al., 2015). The similarities in modes of action between these proteins and COX7A2L make it conceivable that they could act in conjunction, having a respiratory chain "stabilizing" or "gluing" function, although further studies are required to demonstrate such functional interactions.

Interestingly, the COX7A2L-mediated absence of SC III_2+IV_n does not affect respirasome formation or maintenance. In addition, the fact that the formation and stabilization of a less abundant structure such as SC III_2+IV_n is regulated by specific proteins in a respirasome-independent manner supports the existence of alternative assembly pathways for SC III_2+IV_n and the respirasomes. It may also be indicative of a specific, yet not well-understood, physiological importance of SC III_2+IV_n. Results from others have suggested that SC III_2+IV_n could provide an MRC structure to receive electrons from CII (Lapuente-Brun et al., 2013). However, given current evidence that puts in doubt the catalytic roles for mitochondrial SCs (Blaza et al., 2014; Trouillard et al., 2011), alternative non-catalytic functions should also be considered. These would include the regulation of MRC complex distribution in specific cardiolipin microdomains within the densely protein-packed mitochondrial inner membrane or a role in storage or preservation of excess MRC components to avoid futile continuous cycles of turnover and de novo synthesis. The experimental evidence of independent regulatory mechanisms and proteins for the biogenesis of intermediate SCs and the respirasomes opens new doors for exciting future investigations of the role for these supramolecular structures in the regulation of cellular energy supply.

EXPERIMENTAL PROCEDURES

Cell Cultures

The CI-deficient (CI-KD) cell line harbors a homoplasmic m.4681T > C mutation in the *MT-ND2* subunit gene that leads to a severe CI assembly defect due to a p.L71P substitution (Ugalde et al., 2007). The CIII mutant (CIII-KO) cell line contains a homoplasmic 4-bp deletion in the *MT-CYB* gene affecting the de novo synthesis of cytochrome *b* (Rana et al., 2000). The CIV mutant cell line (CIV-KO) lacks holo-COX due to the homoplasmic m.6930G > A transition in the *MT-COI* gene, which creates a stop codon that results in a predicted loss of the last 170 amino acids of the COX1 polypeptide (Bruno et al., 1999). HeLa cells, either transduced with the empty pWPXLd-ires-PuroR vector or overexpressing LYRM7-001-HA (MZM1L-HA), were generated as previously described (Sánchez et al., 2013).

Cells were cultured in high-glucose DMEM (Life Technologies), supplemented with 10% fetal calf serum (FCS), 2 mM L-glutamine, 1 mM sodium pyruvate, and antibiotics. To block mitochondrial translation, 15 μg/ml doxycycline was added for 6 days to the culture medium. Cells were grown in exponential conditions and harvested at the indicated time points.

In Vitro Import

Radiolabeled COX7A2L, COX6A, and RISP proteins were obtained by coupled transcription and translation in the presence of ^{35}S-methionine (PerkinElmer), using the TNT SP6 Quick Coupled System (Promega). Import experiments were performed on freshly isolated mitochondria from heart tissue, as described previously (Mourier et al., 2014a).

Immunoprecipitation

Mitochondrial protein (1 mg) from HEK293-transduced cells was solubilized in 600 μl of 4 g/g digitonin-to-protein buffer, as for BN electrophoresis (BNE) analyses. After centrifugation for 30 min at 13,000 rpm at 4°C, 50 μg supernatant was separated as the input fraction. The remaining supernatant was co-immunoprecipitated in resin spin columns (Pierce CoIP Kit, Thermo Scientific), in which 15 μg antibodies against DDK-tag (Oncogene), CORE2, or COX1 had been previously immobilized. The mixture was gently incubated overnight at 4°C in a rotating shaker and centrifuged at 1,000 × g for 1 min to separate the flowthrough fraction. The column was washed three times with lysis buffer containing 1% NP-40, and proteins were eluted. The immunoprecipitate was divided into three aliquots, treated with 5× loading sample buffer, and heated at 95°C for 5 min prior to loading.

BNE and IGA Assays

Isolation of mitochondrial pellets and BN analyses were performed as described previously (Moreno-Lastres et al., 2012; Mourier et al., 2014a). Native PAGE Novex 3%–12% Bis-Tris Protein Gels (Life Technologies) or self-made 4%–10% polyacrylamide gradient gels were loaded with 60–80 μg mitochondrial protein. After electrophoresis, proteins were transferred to nitrocellulose or PVDF (polyvinylidene fluoride) membranes at 40 V overnight and probed with specific antibodies.

Antibodies

Western blot was performed using primary antibodies raised against COX7A2L (ProteinTech), Myc (Origene), turbo-GFP (Origene), HA (Roche), β-actin (Sigma), and the following human OXPHOS subunits: NDUFS1 (GeneTex); NDUFA9, NDUFB8, CORE2, RISP, CYC1, UQCRB, UQCRQ, COX1, COX4, COX5A, COX6C, SDHA, and SDHB (Mitosciences); and COX5B (Santa Cruz Biotechnology). Peroxidase-conjugated anti-mouse and anti-rabbit immunoglobulin Gs (IgGs) were used as secondary antibodies (Molecular Probes). Immunoreactive bands were detected with the ECL Prime Western Blotting Detection Reagent (Amersham) in a ChemiDoc MP Imager (Biorad). Optical densities of the immunoreactive bands were measured using the ImageLab (Biorad) and ImageJ analysis softwares.

Indirect Immunofluorescence

Cells were fixed with 4% paraformaldehyde for 15 min, permeabilized for 15 min with 0.1% Triton X-100, and incubated in blocking buffer containing 10% goat serum for 1 hr. Coverslips were incubated with an antibody against monoclonal complex V α subunit and a Texas Red-conjugated anti-mouse secondary antibody (Abcam). Coverslips were rinsed and mounted in ProLong Gold antifade reagent (Molecular Probes) on glass slides, and cells were viewed with a Zeiss LSM 510 Meta confocal microscope and a 63× planapochromat oil inmersion objective (NA, 1.42). Sequential scanning of green and red channels was performed to avoid bleed-through effect. Cells were imaged randomly with 0.5- to 1.0-μm slices and 1,024- × 1,024-pixel resolution. For colocalization analysis, the "Merge channels" plugin from the ImageJ 1.48v software was used.

Statistical Data Analysis

All experiments were performed at least in triplicate, and results were presented as means ± SD. Statistical p values were obtained by application of the Friedman and Mann-Whitney U tests using the SPSS v21.0 program.

Ethics Statement

This study was performed in accordance with the guidelines of the Federation of European Laboratory Animal Science Associations. The protocol was approved by the Landesamt für Natur, Umwelt und Verbraucherschutz in Nordrhein-Westfalen in Germany.

SUPPLEMENTAL INFORMATION

Supplemental Information includes Supplemental Experimental Procedures, six figures, and one table and can be found with this article online at http://dx.doi.org/10.1016/j.celrep.2016.07.081.

AUTHOR CONTRIBUTIONS

Conceptualization, Methodology and Investigation, R.P.-P., T.L.-J., D.M., A.M., A.B., A.G.-B., E.F.-V., I.G.-C., and C.U.; Formal Analysis, A.D.; Writing, C.U.; Funding Acquisition, S.C., E.F.-V., M.A.M., N.-G.L., and C.U.; Resources, E.F.-V., J.A., and N.-G.L.; Supervision, S.C., N.-G.L., and C.U.

ACKNOWLEDGMENTS

The authors acknowledge Prof. Leo Nijtmans, Prof. Carlos Moraes, and Prof. Giovanni Manfredi for kindly providing the mutant cybrids and Prof. Antoni Barrientos and Prof. Flavia Fontanesi for manuscript revision and fruitful discussion. The proteomic analysis was carried out in the Proteomics Facility UCM-FPCM, a member of the ProteoRed network (Spain). This work was funded by Instituto de Salud Carlos III (grant number PI14-00209 to C.U., grant number PI12-01683 to M.A.M., and grant number PI12-00933 to S.C.), by Comunidad Autónoma de Madrid (P2010/BMD-2361 to C.U. and P2010/BMD-2402 to M.A.M. and S.C.), by European FEDER Funds, by Association Française contre les Myopathies (16086 to E.F.V.), by an European Research Council Advanced Investigator grant (268897), by grants from the Knut and Alice Wallenberg Foundation and the Swedish Research Council (2015-00418) to N.G.L., and by NIH-NIGMS (1R01GM105781-01) to C.U.

Received: January 28, 2016
Revised: April 28, 2016
Accepted: July 27, 2016
Published: August 18, 2016

REFERENCES

Acín-Pérez, R., Fernández-Silva, P., Peleato, M.L., Pérez-Martos, A., and Enriquez, J.A. (2008). Respiratory active mitochondrial supercomplexes. Mol. Cell *32*, 529–539.

Althoff, T., Mills, D.J., Popot, J.L., and Kühlbrandt, W. (2011). Arrangement of electron transport chain components in bovine mitochondrial supercomplex I1III2IV1. EMBO J. *30*, 4652–4664.

Barrientos, A., and Ugalde, C. (2013). I function, therefore I am: overcoming skepticism about mitochondrial supercomplexes. Cell Metab. *18*, 147–149.

Bianchi, C., Genova, M.L., Parenti Castelli, G., and Lenaz, G. (2004). The mitochondrial respiratory chain is partially organized in a supercomplex assembly: kinetic evidence using flux control analysis. J. Biol. Chem. *279*, 36562–36569.

Blaza, J.N., Serreli, R., Jones, A.J., Mohammed, K., and Hirst, J. (2014). Kinetic evidence against partitioning of the ubiquinone pool and the catalytic relevance of respiratory-chain supercomplexes. Proc. Natl. Acad. Sci. USA *111*, 15735–15740.

Bruno, C., Martinuzzi, A., Tang, Y., Andreu, A.L., Pallotti, F., Bonilla, E., Shanske, S., Fu, J., Sue, C.M., Angelini, C., et al. (1999). A stop-codon mutation in the human mtDNA cytochrome c oxidase I gene disrupts the functional structure of complex IV. Am. J. Hum. Genet. *65*, 611–620.

Chen, Y.C., Taylor, E.B., Dephoure, N., Heo, J.M., Tonhato, A., Papandreou, I., Nath, N., Denko, N.C., Gygi, S.P., and Rutter, J. (2012). Identification of a protein mediating respiratory supercomplex stability. Cell Metab. *15*, 348–360.

Cruciat, C.M., Brunner, S., Baumann, F., Neupert, W., and Stuart, R.A. (2000). The cytochrome bc1 and cytochrome c oxidase complexes associate to form a single supracomplex in yeast mitochondria. J. Biol. Chem. *275*, 18093–18098.

Desmurs, M., Foti, M., Raemy, E., Vaz, F.M., Martinou, J.C., Bairoch, A., and Lane, L. (2015). C11orf83, a mitochondrial cardiolipin-binding protein involved in bc1 complex assembly and supercomplex stabilization. Mol. Cell. Biol. *35*, 1139–1156.

Dudkina, N.V., Kudryashev, M., Stahlberg, H., and Boekema, E.J. (2011). Interaction of complexes I, III, and IV within the bovine respirasome by single particle cryoelectron tomography. Proc. Natl. Acad. Sci. USA *108*, 15196–15200.

Fernández-Vizarra, E., and Zeviani, M. (2015). Nuclear gene mutations as the cause of mitochondrial complex III deficiency. Front. Genet. *6*, 134.

Hatle, K.M., Gummadidala, P., Navasa, N., Bernardo, E., Dodge, J., Silverstrim, B., Fortner, K., Burg, E., Suratt, B.T., Hammer, J., et al. (2013). MCJ/DnaJC15, an endogenous mitochondrial repressor of the respiratory chain that controls metabolic alterations. Mol. Cell. Biol. *33*, 2302–2314.

Ikeda, K., Shiba, S., Horie-Inoue, K., Shimokata, K., and Inoue, S. (2013). A stabilizing factor for mitochondrial respiratory supercomplex assembly regulates energy metabolism in muscle. Nat. Commun. *4*, 2147.

Jha, P., Wang, X., and Auwerx, J. (2016). Analysis of mitochondrial respiratory chain supercomplexes using blue native polyacrylamide gel electrophoresis (BN-PAGE). Curr. Protoc. Mouse Biol. *6*, 1–14.

Lapuente-Brun, E., Moreno-Loshuertos, R., Acín-Pérez, R., Latorre-Pellicer, A., Colás, C., Balsa, E., Perales-Clemente, E., Quirós, P.M., Calvo, E., Rodríguez-Hernández, M.A., et al. (2013). Supercomplex assembly determines electron flux in the mitochondrial electron transport chain. Science *340*, 1567–1570.

Maranzana, E., Barbero, G., Falasca, A.I., Lenaz, G., and Genova, M.L. (2013). Mitochondrial respiratory supercomplex association limits production of reactive oxygen species from complex I. Antioxid. Redox Signal. *19*, 1469–1480.

Milenkovic, D., Matic, S., Kühl, I., Ruzzenente, B., Freyer, C., Jemt, E., Park, C.B., Falkenberg, M., and Larsson, N.G. (2013). TWINKLE is an essential mitochondrial helicase required for synthesis of nascent D-loop strands and complete mtDNA replication. Hum. Mol. Genet. *22*, 1983–1993.

Moreno-Lastres, D., Fontanesi, F., García-Consuegra, I., Martín, M.A., Arenas, J., Barrientos, A., and Ugalde, C. (2012). Mitochondrial complex I plays an essential role in human respirasome assembly. Cell Metab. *15*, 324–335.

Mourier, A., Matic, S., Ruzzenente, B., Larsson, N.G., and Milenkovic, D. (2014a). The respiratory chain supercomplex organization is independent of COX7a2l isoforms. Cell Metab. *20*, 1069–1075.

Mourier, A., Ruzzenente, B., Brandt, T., Kühlbrandt, W., and Larsson, N.G. (2014b). Loss of LRPPRC causes ATP synthase deficiency. Hum. Mol. Genet. *23*, 2580–2592.

Müller, C.S., Bildl, W., Haupt, A., Ellenrieder, L., Becker, T., Hunte, C., Fakler, B., and Schulte, U. (2016). Cryo-slicing blue native-mass spectrometry (csBN-MS), a novel technology for high-resolution complexome profiling. Mol. Cell Proteomics *15*, 669–681.

Rana, M., de Coo, I., Diaz, F., Smeets, H., and Moraes, C.T. (2000). An out-of-frame cytochrome b gene deletion from a patient with parkinsonism is associated with impaired complex III assembly and an increase in free radical production. Ann. Neurol. *48*, 774–781.

Rigoulet, M., Mourier, A., Galinier, A., Casteilla, L., and Devin, A. (2010). Electron competition process in respiratory chain: regulatory mechanisms and physiological functions. Biochim. Biophys. Acta *1797*, 671–677.

Sánchez, E., Lobo, T., Fox, J.L., Zeviani, M., Winge, D.R., and Fernández-Vizarra, E. (2013). LYRM7/MZM1L is a UQCRFS1 chaperone involved in the last steps of mitochondrial Complex III assembly in human cells. Biochim. Biophys. Acta *1827*, 285–293.

Schägger, H., and Pfeiffer, K. (2000). Supercomplexes in the respiratory chains of yeast and mammalian mitochondria. EMBO J. *19*, 1777–1783.

Schägger, H., de Coo, R., Bauer, M.F., Hofmann, S., Godinot, C., and Brandt, U. (2004). Significance of respirasomes for the assembly/stability of human respiratory chain complex I. J. Biol. Chem. *279*, 36349–36353.

Smith, P.M., Fox, J.L., and Winge, D.R. (2012). Reprint of: Biogenesis of the cytochrome bc(1) complex and role of assembly factors. Biochim. Biophys. Acta *1817*, 872–882.

Strogolova, V., Furness, A., Robb-McGrath, M., Garlich, J., and Stuart, R.A. (2012). Rcf1 and Rcf2, members of the hypoxia-induced gene 1 protein family, are critical components of the mitochondrial cytochrome bc1-cytochrome c oxidase supercomplex. Mol. Cell. Biol. *32*, 1363–1373.

Trouillard, M., Meunier, B., and Rappaport, F. (2011). Questioning the functional relevance of mitochondrial supercomplexes by time-resolved analysis of the respiratory chain. Proc. Natl. Acad. Sci. USA *108*, E1027–E1034.

Please cite this article in press as: Pérez-Pérez et al., COX7A2L Is a Mitochondrial Complex III Binding Protein that Stabilizes the III_2+IV Supercomplex without Affecting Respirasome Formation, Cell Reports (2016), http://dx.doi.org/10.1016/j.celrep.2016.07.081

Ugalde, C., Hinttala, R., Timal, S., Smeets, R., Rodenburg, R.J., Uusimaa, J., van Heuvel, L.P., Nijtmans, L.G., Majamaa, K., and Smeitink, J.A. (2007). Mutated ND2 impairs mitochondrial complex I assembly and leads to Leigh syndrome. Mol. Genet. Metab. *90*, 10–14.

Vukotic, M., Oeljeklaus, S., Wiese, S., Vögtle, F.N., Meisinger, C., Meyer, H.E., Zieseniss, A., Katschinski, D.M., Jans, D.C., Jakobs, S., et al. (2012). Rcf1 mediates cytochrome oxidase assembly and respirasome formation, revealing heterogeneity of the enzyme complex. Cell Metab. *15*, 336–347.

Williams, E.G., Wu, Y., Jha, P., Dubuis, S., Blattmann, P., Argmann, C.A., Houten, S.M., Amariuta, T., Wolski, W., Zamboni, N., et al. (2016). Systems proteomics of liver mitochondria function. Science *352*, aad0189.

Cell Reports, Volume *16*

Supplemental Information

COX7A2L Is a Mitochondrial Complex III Binding Protein that Stabilizes the III_2+IV Supercomplex without Affecting Respirasome Formation

Rafael Pérez-Pérez, Teresa Lobo-Jarne, Dusanka Milenkovic, Arnaud Mourier, Ana Bratic, Alberto García-Bartolomé, Erika Fernández-Vizarra, Susana Cadenas, Aitor Delmiro, Inés García-Consuegra, Joaquín Arenas, Miguel A. Martín, Nils-Göran Larsson, and Cristina Ugalde

SUPPLEMENTAL TABLE

Table S1. Proteomic features of COX7A2L and complex III subunits identified by nano LC-ESI-MS analysis in mitochondrial complex III-containing structures.

CIII SUBUNITS IN $CIII_2$	Accession[a]	Coverage (%)[b]	# PSMs[c]	# Peptides[d]	Score[e]
Cytochrome b	P00156	2,37	2	1	49,72
UQCRC1 - CORE1	P31930	35,83	50	13	1339,01
UQCRC2 - CORE2	P22695	48,34	52	14	1442,20
CYC1 - Cytochrome c1	P08574	20,62	52	5	710,57
UQCRFS1 - Rieske FeS*	P47985	23,36	15	5	469,24
UQCRH - Subunit 6	P07919	19,78	2	1	61,11
UQCRB - Subunit 7	P14927	30,63	19	4	518,81
UQCRQ - Subunit 8	O14949	12,20	4	2	77,07
UQCR10 - Subunit 9	Q9UDW1	65,08	9	3	189,97
UQCR11 - Subunit 10	O14957	21,43	3	1	64,81
COX7A2L	O14548	11,40	4	1	149,43

CIII SUBUNITS IN $SCI+III_2$	Accession[a]	Coverage (%)[b]	# PSMs[c]	# Peptides[d]	Score[e]
Cytochrome b	P00156	2,37	1	1	45,50
UQCRC1 - CORE1	P31930	19,58	26	9	551,53
UQCRC2 - CORE2	P22695	31,13	29	8	780,09
CYC1 - Cytochrome c1	P08574	15,69	9	4	159,24
UQCRFS1 - Rieske FeS*	P47985	13,87	3	3	68,83
UQCRH - Subunit 6	P07919	7,69	1	1	26,45
UQCRB - Subunit 7	P14927	30,63	12	4	298,03
UQCRQ - Subunit 8	O14949	12,20	4	2	57,61
UQCR10 - Subunit 9	Q9UDW1	38,10	5	2	171,68
UQCR11 - Subunit 10	O14957	21,43	1	1	32,11
COX7A2L	O14548	11,40	2	1	106,86

CIII SUBUNITS IN SCI+III$_2$+IV$_n$	Accession[a]	Coverage (%)[b]	# PSMs[c]	# Peptides[d]	Score[e]
Cytochrome b	P00156	2,37	4	1	56,95
UQCRC1 - CORE1	P31930	50,21	74	18	1692,75
UQCRC2 - CORE2	P22695	41,28	70	14	1891,05
CYC1 - Cytochrome c1	P08574	27,08	21	6	448,78
UQCRFS1 - Rieske FeS*	P47985	32,85	21	6	546,23
UQCRH - Subunit 6	P07919	n.d.	n.d.	n.d.	n.d.
UQCRB - Subunit 7	P14927	43,24	21	6	451,96
UQCRQ - Subunit 8	O14949	15,85	2	1	68,39
UQCR10 - Subunit 9	Q9UDW1	38,10	6	2	99,73
UQCR11 - Subunit 10	O14957	n.d.	n.d.	n.d.	n.d.
COX7A2L	O14548	19,30	4	2	140,64

[a]Protein accession numbers according to the Uniprot/Swiss-Prot/TrEMBL database.
[b]Amino acid sequence coverage for the matched peptides in identified proteins.
[c] Number of peptide spectrum matches.
[d]Number of distinct peptide sequences identified in MS/MS MASCOT results. The confidence ion was high (>95%) for all matches.
[e]Mascot protein score, obtained from LTQ-OrbiTRAP MS/MS spectra. In all cases, a probability score <0.05 was obtained.
n.d., not detected.

SUPPLEMENTAL FIGURES AND LEGENDS

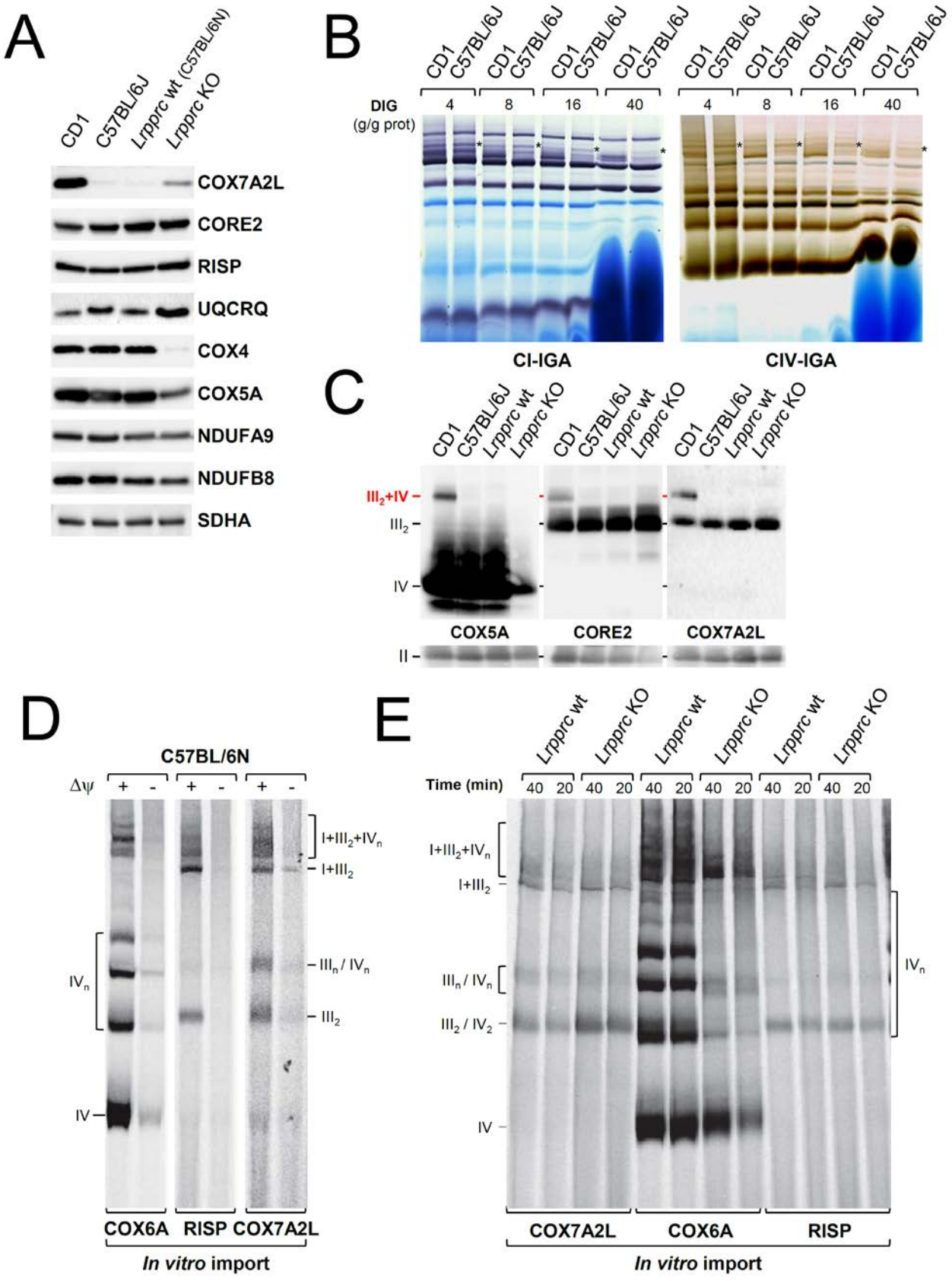

Figure S1

Figure S1. Mouse COX7A2L behaves as a complex III-binding protein specifically required for supercomplex III_2+IV assembly. (A) Heart mitochondrial extracts from CD1 and C57BL/6J mouse strains, and from control littermates (*Lrpprc* wt) and *Lrpprc* deficient mice with a C57BL/6N genetic background, were analyzed by western blot with antibodies raised against COX7A2L and the indicated OXPHOS subunits. **(B)** Heart mitochondria from CD1 and C57BL/6J mouse strains were extracted with increasing ratios of digitonin to mitochondrial protein (ranging from 4 to 40 g/g) and analyzed by BN-PAGE followed by CI-IGA or CIV-IGA assays. Asterisks indicate the presence of respirasome bands that are more stable in mitochondria from the C57BL/6J mice. **(C)** Mitochondrial samples were solubilized with 2% DDM, which disrupts respirasomes and CIV oligomers but maintains SC III_2+IV and free complexes, and were next analyzed by BN-PAGE followed by western blot and immunodetection with the indicated antibodies. **(D)** Import of radiolabeled COX6A, RISP and COX7A2L precursors and subsequent incorporation into complexes III, IV and SC in intact heart mitochondria from wild type mice with C57BL/6N genetic background. After 60 minutes of incubation, mitochondria were solubilized in 6 g/g digitonin per protein and analyzed by BN-PAGE. Import experiments were performed in the presence or absence of the mitochondrial membrane potential (Δψ). **(E)** Assembly of the radiolabeled COX7A2L, COX6A and RISP into complexes and SC in intact heart mitochondria from wild type and *Lrpprc* knockout mice. After the indicated times of incubation (in minutes), mitochondria were solubilized in digitonin (6 g/g mitochondrial protein) and analyzed by BN-PAGE. I+III_2+IV_n, SC containing CI, CIII and CIV. I+III_2, SC containing CI and CIII. III_2+IV, SC containing CIII and CIV. III_2, complex III dimer; IV, complex IV; IV_n, complex IV oligomers. II, complex II.

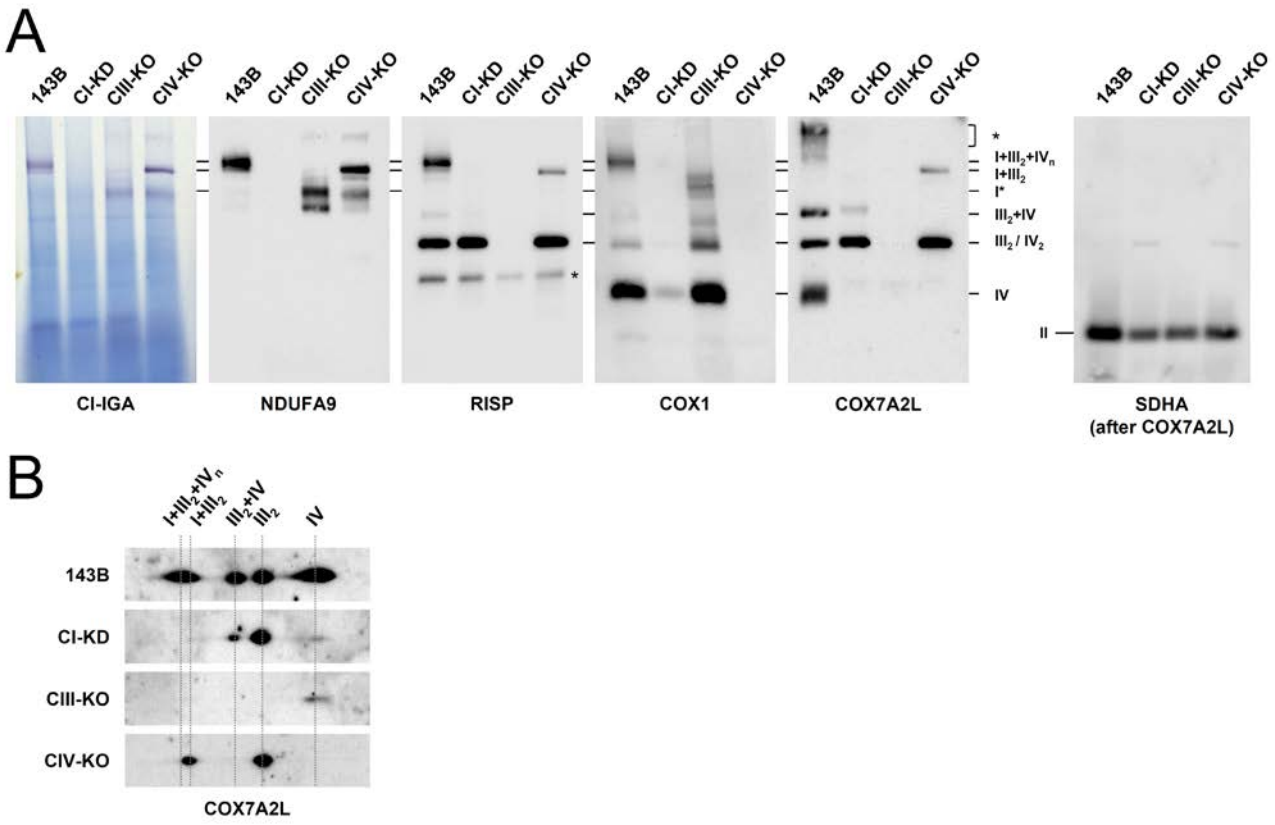

Figure S2

Figure S2. COX7A2L comigrates with respiratory chain supercomplexes and free complexes III and IV. (A) Mitochondria from control 143B cells and from three mutant cybrids respectively defective in complexes I (CI-KD), III (CIII-KO) and IV (CIV-KO) were analyzed by BN-PAGE, followed by CI *in gel* activity (IGA) assay, or alternatively, blotted on nitrocellulose and incubated with antibodies raised against human COX7A2L and the indicated OXPHOS subunits. Asterisks indicate unspecific signals that do not appear on 2D-BN/SDS-PAGE gels. **(B)** 2D-BN/SDS-PAGE and western-blot analyses of COX7A2L distribution in control and mutant cybrids at long exposure times. $I+III_2+IV_n$, SC containing CI, CIII and CIV. $I+III_2$, SC containing CI and CIII. III_2+IV, SC containing CIII and CIV. I*, complex I-containing structure. III_2, complex III dimer; IV, complex IV; IV_2, complex IV dimers. II, complex II.

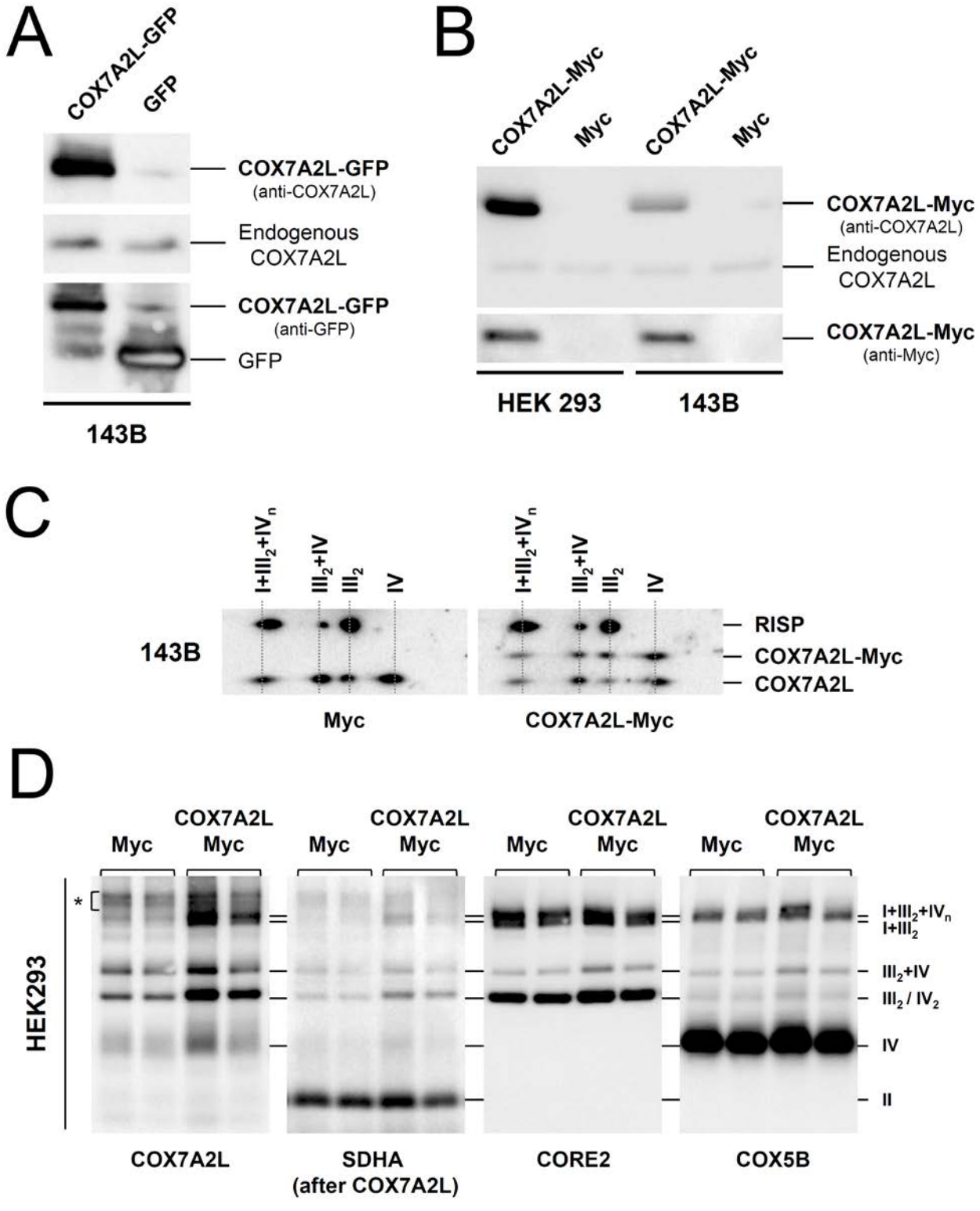
A
COX7A2L-GFP
GFP
COX7A2L-GFP
(anti-COX7A2L)
Endogenous
COX7A2L
COX7A2L-GFP
(anti-GFP)
GFP
143B
B
COX7A2L-Myc
Myc
COX7A2L-Myc
Myc
COX7A2L-Myc
(anti-COX7A2L)
Endogenous
COX7A2L
COX7A2L-Myc
(anti-Myc)
HEK 293
143B
C
I+III2+IVn
III2+IV
III2
IV
143B
RISP
COX7A2L-Myc
COX7A2L
Myc
COX7A2L-Myc
D
COX7A2L
Myc
Myc
HEK293
*
I+III2+IVn
I+III2
III2+IV
III2 / IV2
IV
II
COX7A2L
SDHA
(after COX7A2L)
CORE2
COX5B

Figure S3

Figure S3. Tagged-COX7A2L is efficiently overexpressed and imported into mitochondrial respiratory chain complexes and supercomplexes. (A) Western blot analysis of the over expressed COX7A2L-GFP or GFP-empty constructs in 143B cells, and **(B)** of the COX7A2L-MYC-DDK construct and its corresponding empty vector (Myc) in 143B and HEK293 cells. Lanes were immunodecorated with an antibody against COX7A2L to differentiate endogenous COX7A2L (~12.6 kDa) from either exogenous COX7A2L-GFP (~39.3 kDa) or COX7A2L-MYC-DDK (~16.2 kDa). Membranes were further incubated with antibodies against the GFP and MYC epitopes. **(C)** 2D-BN/SDS-PAGE analysis of control 143B cells transiently transfected with the COX7A2L-MYC-DDK construct, and with the MYC-empty vector. Membranes were incubated with antibodies raised against COX7A2L and the CIII RISP subunit. **(D)** BN-PAGE followed by western-blot analyses of control HEK293 cells transiently transfected either with the COX7A2L-MYC-DDK construct, or with the MYC-empty vector. Membranes were incubated with antibodies raised against COX7A2L and the indicated OXPHOS subunits. Two independent transfection experiments per experimental condition are shown on the same gel. Asterisks indicate unspecific signals that do not appear on 2D-BN/SDS-PAGE gels. $I+III_2+IV_n$, SC containing CI, CIII and CIV. $I+III_2$, SC containing CI and CIII. III_2+IV, SC containing CIII and CIV. III_2, complex III dimer; IV, complex IV; IV_2, complex IV dimer. II, complex II.

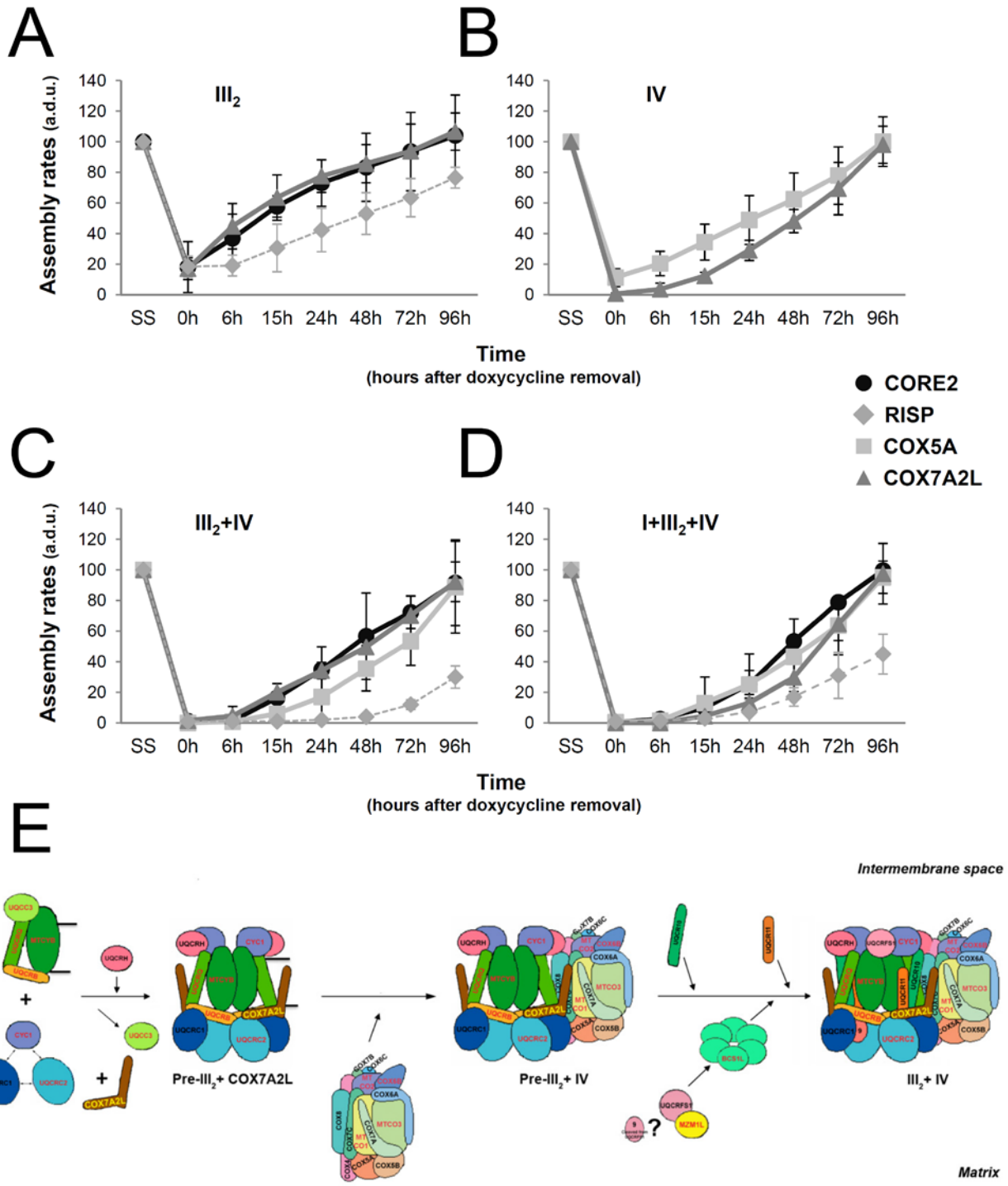
A
B
III_2
IV
Assembly rates (a.d.u.)
140
120
100
80
60
40
20
0
SS 0h 6h 15h 24h 48h 72h 96h
Time
(hours after doxycycline removal)
CORE2
RISP
COX5A
COX7A2L
C
D
III_2+IV
I+III_2+IV
E
Intermembrane space
Matrix
Pre-III_2+ COX7A2L
Pre-III_2+ IV
III_2+ IV

Figure S4

Figure S4. Assembly of COX7A2L, CORE2, RISP and COX5A in complex III- and complex IV- containing structures. (A) Incorporation rates of COX7A2L into the CIII dimer relative to the RISP and CORE2 subunits. **(B)** Incorporation rates of COX7A2L and COX5A into free CIV. **(C)** Assembly rates of COX7A2L, RISP, CORE2 and COX5A in SC III_2+IV. **(D)** Incorporation rates of COX7A2L, RISP, CORE2 and COX5A into SC I+III_2+IV. The COX7A2L signals from three independent experiments, and the CORE2, RISP and COX5A signals from at least ten independent experiments were quantified and normalized by the signal corresponding to the CII subunit SDHA. Time point values are expressed as percentages of the untreated cells (SS), and indicated as means ± SD. I+III_2+IV_n, SC containing CI, CIII and CIV. III_2+IV, SC containing CIII and CIV. III_2, complex III dimer. IV, complex IV. **(E)** Human COX7A2L-mediated SC III_2+IV assembly steps. Model based on (Fernandez-Vizarra and Zeviani, 2015). The UQCRB and UQCRQ subunits first bind to MT-CYB, to form the early-stage CIII intermediary MT-CYB+UQCRB+UQCRQ. Additional subunits, i.e., UQCRC1, UQCRC2 and CYC1 are incorporated in a second step, followed by UQCRH and later UQCR10, to form pre-complex III. At this point, the complex is already dimeric (pre-III_2) and COX7A2L is bound to it. According to the incorporation kinetics, CIV binds to COX7A2L-containing pre-III_2 prior to the incorporation of RISP (UQCRFS1). RISP is bound and stabilized by MZM1L in the mitochondrial matrix, from where it is translocated into the inner membrane through the action of BCS1L, and gets incorporated into pre-III_2+IV to allow the formation of mature SC III_2+IV. If SC III_2+IV followed the same pathway as described for $CIII_2$, the last assembly step would include the incorporation of subunit UQCR11 to complete the nascent supercomplex.

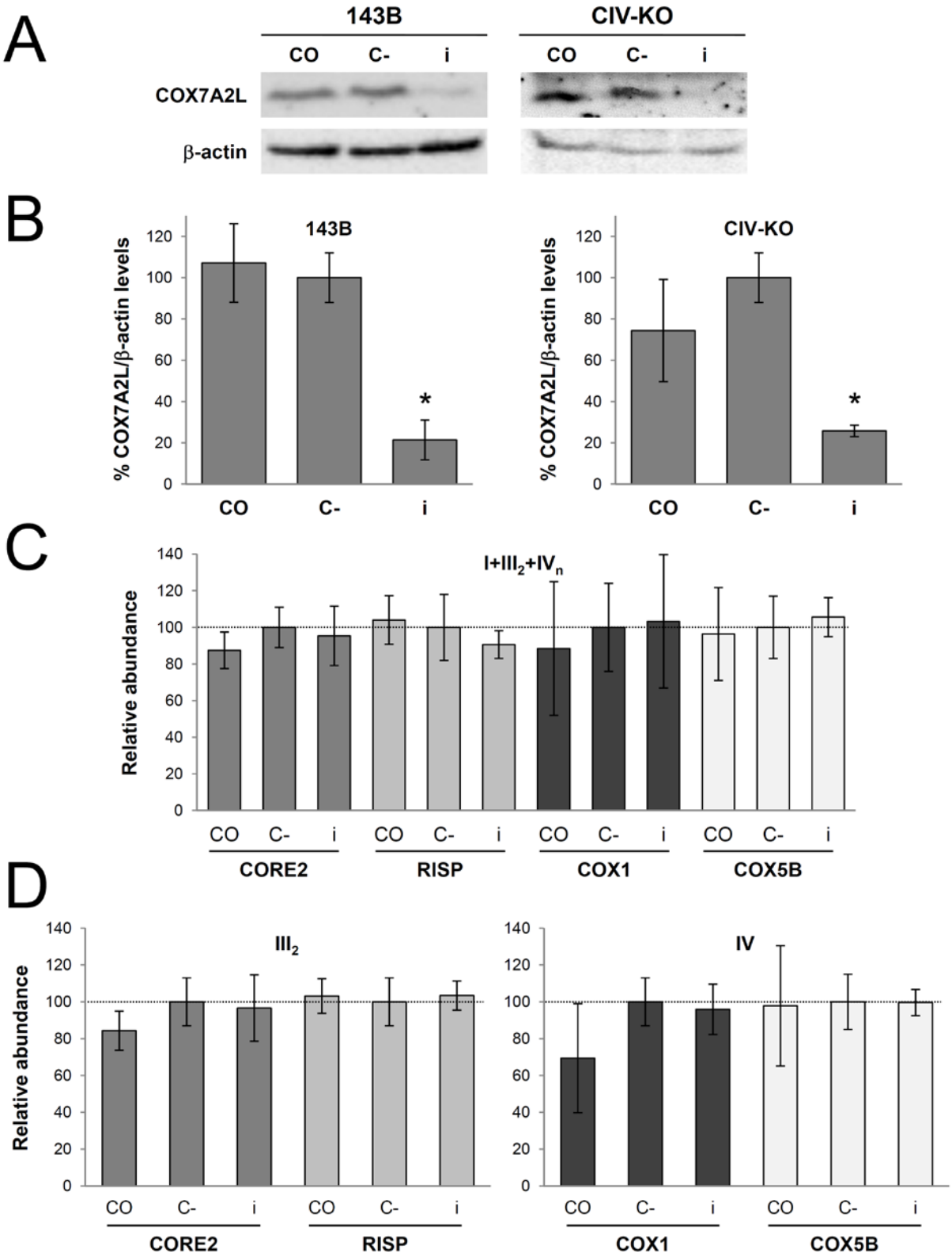
A
143B
CIV-KO
CO
C-
i
COX7A2L
β-actin
B
143B
CIV-KO
% COX7A2L/β-actin levels
120
100
80
60
40
20
0
*
CO
C-
i
C
Relative abundance
I+III2+IVn
140
120
100
80
60
40
20
0
CO
C-
i
CORE2
RISP
COX1
COX5B
D
III2
IV
Relative abundance
CORE2
RISP
COX1
COX5B

Figure S5

Figure S5. *COX7A2L* knock-down efficiency. (A) To characterize the functional role of COX7A2L in the OXPHOS system, silencing assays were performed with a mix of two *COX7A2L* siRNAs in control 143B cells as well as in mutant cybrids lacking complex IV (CIV-KO). Upon two rounds of transfection and silencing for 48 hours, cells were collected and whole cell extracts were analyzed by SDS-PAGE and western blot using antibodies targeted against COX7A2L and β-actin as a loading control. **(B)** The COX7A2L signals from five independent siRNA silencing experiments were quantified, normalized by β-actin and expressed as the percentages relative to the cells transfected with the scramble siRNA (C-). **(C)** To address the relative amounts of SC I+III_2+IV, and **(D)** of complexes III and IV in 143B cells after *COX7A2L* silencing, we measured the optical densities of immunoreactive bands that had not reached saturation levels with the ImageLab™ software of the ChemiDoc™ MP Image Analyzer (Biorad). The signals from each antibody within the different structures were quantified, normalized by CII, and indicated as means ± SD from five independent siRNA experiments. Numerical values are expressed as percentages of the signals obtained for each antibody in cells transfected with the scramble siRNA (C-, represented as a horizontal bar). I+III_2+IV_n, SC containing CI, CIII and CIV. III_2, complex III dimer. IV, complex IV. CO, cells only treated with the transfection reagent; C-, cells transfected with a scrambled siRNA; i, cells transfected with a combination of two specific *COX7A2L* siRNAs.

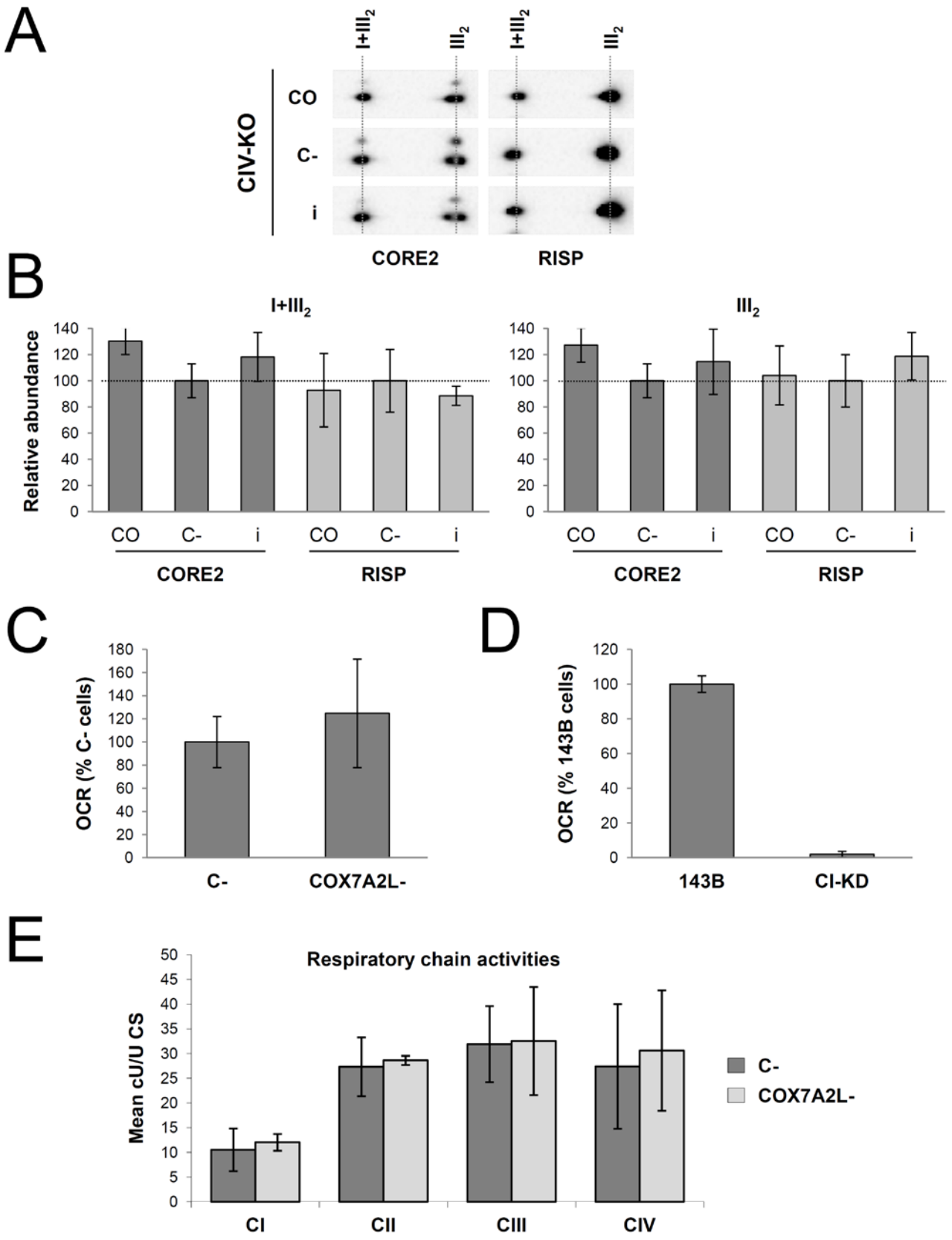
A
I+III2
III2
I+III2
III2
CIV-KO
CO
C-
i
CORE2
RISP
B
I+III2
III2
Relative abundance
140
120
100
80
60
40
20
0
CO
C-
i
CO
C-
i
CORE2
RISP
CO
C-
i
CO
C-
i
CORE2
RISP
C
OCR (% C- cells)
180
160
140
120
100
80
60
40
20
0
C-
COX7A2L-
D
OCR (% 143B cells)
120
100
80
60
40
20
0
143B
CI-KD
E
Respiratory chain activities
Mean cU/U CS
50
45
40
35
30
25
20
15
10
5
0
CI
CII
CIII
CIV
C-
COX7A2L-

Figure S6

Figure S6. COX7A2L down regulation neither alters the biogenesis of OXPHOS structures nor affects mitochondrial function. (A) Representative 2D-BN/SDS-PAGE analysis of the CIV-KO mutant cybrids analyzed in Figure 7A. Shown are the immunodetections of CIII subunits CORE2 and RISP in untreated (CO), mock-transfected (C-), and *COX7A2L* siRNA-transfected (i) cybrids lacking CIV (CIV-KO). **(B)** To address the relative amounts of III_2 and SC $I+III_2$ in the CIV-KO mutants after *COX7A2L* silencing, the signals from each antibody within these structures were quantified, normalized by CII, and indicated as means ± SD from three independent siRNA experiments. Numerical values are expressed as percentages of the signals obtained for each antibody in cells transfected with the scramble RNA (C-, represented as a horizontal bar). $I+III_2$, SC containing CI and CIII. III_2, complex III dimer. **(C)** Oxygen consumption rates (OCR) measured in 143B cells respiring in 1 g/l glucose-containing medium that were previously transfected either with a scrambled siRNA (C-, negative control), or with a combination of two specific *COX7A2L* siRNAs (COX7A2L-). Ten measurements per sample were performed each time in three independent experiments. Data are expressed as the mean± standard deviation of the percentages of the negative control. **(D)** Oxygen consumption rates (OCR) measured in control 143B cells and CI-defective mutant cybrids (CI-KD) respiring in 1 g/l glucose-containing medium. Five measurements per sample were performed each time in two independent experiments. Data are expressed as the mean± range of the percentages of the control 143B cells. OCR values were calculated in pmol $O_2.min^{-1}.\mu g\ protein^{-1}$ in all experiments. **(E)** Spectrophotometric measurements of the individual activities of MRC complexes I to IV (CI-CIV) in 143B cells transfected either with a scrambled siRNA (C-), or with a mix of two specific *COX7A2L* siRNAs (COX7A2L-). Enzyme activities are expressed as cU/U citrate synthase (CS).

SUPPLEMENTAL EXPERIMENTAL PROCEDURES

Protein identification by liquid chromatography coupled to tandem mass spectrometry

Gel bands of interest were excised from blue native gels. All samples were reduced by adding 10 mM DTT for 30 min at 37ºC and alkylated with 55 mM iodacetamide during 20 min in the dark. Next, digestion was performed by adding recombinant sequencing grade Trypsin (Roche) 1:20 (w/w) overnight at 37ºC. The produced peptides were cleaned up with Omix tips (Agilent technologies), eluted with 80% ACN in 0.1% TFA, dried in a Speed-vac and resuspended in 0.1% formic acid.

To identify proteins, the resulting tryptic peptide mixtures were analyzed by nano-liquid chromatography coupled to mass spectrometry. Peptides were loaded onto a C18-A1 ASY-Column 2 cm precolumn (Thermo Fisher Scientific) and then eluted onto a Biosphere C18 analytic column (C18, inner diameter 75 μm, 15 cm long, 3 μm particle size) (NanoSeparations) and separated using a 150 min gradient from 0-45% Buffer B (Buffer A: 0.1% formic acid/2% ACN; Buffer B: 0.1% formic acid in ACN) at a flow-rate of 250 nL/min on a nanoEasy HPLC (Proxeon) coupled to a nanoelectrospay ion source (Proxeon). Mass spectra were acquired on the LTQ-Orbitrap Velos (Thermo Scientific) in the positive ion mode. Full-scan MS spectra (m/z 400-1800) were acquired in the Orbitrap at a resolution of 60,000 at m/z 400 and the 15 most intense ions were selected for collision induced dissociation (CID) fragmentation in the LTQ with a normalized collision energy of 35%. Precursor ion charge state screening and monoisotopic precursor selection were enabled. Singly charged ions and unassigned charge states were rejected. Dynamic exclusion was enabled with a repeat count of 1 and exclusion duration of 45s.

Peptide identification from raw data (MS/MS spectra) was carried out using a licensed version of search engine MASCOT 2.3.0 through Proteome Discoverer Software 1.2.0.208 (Thermo Fisher Scientific). Database search was performed against

a Uniprot- SwissProt with taxonomy restriction to Human (date 2012/12/11; 20233 sequences). The following parameters were used for the searches: tryptic cleavage after Arg and Lys, up to two missed cleavage sites allowed, tolerances of 10 ppm for precursor ions and 0.8 Da for MS/MS fragment ions. Oxidation of Methionine was selected as dynamic modification and carbamidomethylation of Cysteine as fixed modification. Search against decoy database (integrated decoy approach in MASCOT) was used for FDR calculation and this filter was applied to MASCOT results. The acceptance criteria for proteins identification were FDR < 1% and at least one peptide identified with high confidence (CI>95%). These results were filtered and annotated with R (www.R-project.org) and biomaRt package (Durinck et al., 2009).

Plasmids and COX7A2L Over expression

Vectors pCMV6-Entry (C-terminal Myc-DDK-tagged), pCMV6-COX7A2L-Myc-DDK, pCMV6-AC-GFP and pCMV6-AC-COX7A2L-GFP were purchased from Origene (catalog numbers PS100001, RC202697, PS100010 and RG202697, respectively) and amplified using PureLink^{TM} HiPure Plasmid Filter Midiprep Kit (Invitrogen). For DNA transfection, 143B cells cultured in serum-free medium were transfected for 48 h with 10 μg of plasmid DNA using 40 μl of FuGENE® HD Transfection Reagent (Promega), and alternatively, HEK293 cells were transfected with Lipofectamin^{TM} (Thermo Fisher) according to the manufacturer's instructions.

COX7A2L siRNA Transfection

For siRNA transfection, 143B cells and CIV-KO mutant cybrids were plated in 10 ml of DMEM supplemented with 10% FBS in 10-cm dishes with a cell density of $7.8x10^5$ cells per plate. The next day, cells were transfected with two mixed *COX7A2L* siRNAs (references SASI_Hs01_00081409 and SASI_Hs02_00338185, Sigma Aldrich) in the presence of 52 μl X-treme GENE siRNA Transfection Reagent (Roche) to achieve a final concentration of 0.15 μM siRNA in a total volume of 10 ml per plate. The negative

control used was MISSION® siRNA Universal Negative Control (Sigma Aldrich). Cells were incubated at 37 ºC in a CO_2 incubator for 48 hours prior to experimental analyses.

Cell respiration

Oxygen consumption rates were measured in 143B cells and transmitochondrial cybrids using an XF24 Extracellular Flux Analyzer (Seahorse Bioscience). The day before the experiment, around 9.0×10^4 143B cells per well were plated in order to obtain a total amount of 150-200 µg protein per well on the day of the experiment. The cells were previously incubated with either scrambled or specific COX7A2L siRNAs for 24 h. As controls for the oxygen consumption measurements in siRNA-treated cells, around 5.0×10^3 143B cells and 1.0×10^4 CI-KD cells (CI defective mutant cybrids) per well were plated two days before the experiment, from which 150-200 µg protein per well were obtained on the day of the experiment. The cells were then incubated for 1 h in unbuffered DMEM supplemented with 1 g/l glucose, 1 mM sodium pyruvate and 2 mM glutamine at 37ºC in a CO_2-free incubator. Respiration was calculated after the addition of mitochondrial inhibitors rotenone and antimycin at 1 µM final concentration. In all experiments, the protein concentration in each well was determined using the Pierce BCA Protein Assay Kit (Thermo Scientific) after cell lysis in extraction buffer, and was used to calibrate the oxygen consumption data.

Respiratory Chain Enzyme Activities

Mitochondrial respiratory chain enzyme activities were performed according to established methods (Medja et al., 2009).

SUPPLEMENTAL REFERENCES

Durinck, S., Spellman, P.T., Birney, E., and Huber, W. (2009). Mapping identifiers for the integration of genomic datasets with the R/Bioconductor package biomaRt. Nat. Protoc. *4*, 1184-1191.

Medja, F., Allouche, S., Frachon, P., Jardel, C., Malgat, M., Mousson de Camaret, B., Slama, A., Lunardi, J., Mazat, J.P., and Lombès, A. (2009) Development and implementation of standardized respiratory chain spectrophotometric assays for clinical diagnosis. Mitochondrion *9*, 331-339.